NON-LINEAR FRICTION BEHAVIOUR BETWEEN PLAIN CAST IRON SLIDEWAYS TRAVELLING AT SLOW SPEEDS

A thesis submitted to

THE UNIVERSITY OF ASTON IN BIRMINGHAM

as partial requirement for the degree of

DOCTOR OF PHILOSOPHY

by

David G. Fox. M.Sc. C.Eng. M.I.Mech.E. M.I.Prod.E.

Department of Production Engineering

November 1975

THIS THESIS IS DEDICATED TO THE HOSPITAL STAFF

of

THE MIDLAND CENTRE FOR NEUROSURGERY

whose skill saved my life in October 1969

CONTENTS

ACKNOWLEDGEMENTS

I would like to thank:-

My colleague and friend, Mr.Neville Williams, whose help and encouragement has never been lacking throughout the supervision of this work.

Professor Eric Downham, of the Department of Mechanical Engineering, who was advisor to this research work.

Professor Robert Thornley, Head of the Department of Production Engineering, for the support given to me and other colleagues pursuing various research topics.

Dr.David Tabor, F.R.S., Cavendish Laboratory, Cambridge, for his interesting comments during discussions on various aspects of this work.

H.W.Ward & Co., who assisted in many ways, especially during the work carried out on surface replication, at their factory at Worcester.

Mrs.Audrey Brereton, who has typed the thesis in her usual efficient way and never once complained.

My wife, Christine, whose love and patience has always been encouraging, especially during the months of writing when jobs around the house have been left undone.

DECLARATION

No part of the work described in this thesis has been submitted in support of an application for another degree or qualification of this or any other University or other institute of learning

David C Fox.

SUMMARY

Non-linear friction behaviour between cast iron slideways has been studied with particular reference to low sliding speeds, (0 - 5 cm/s). The reduction in friction force with increasing velocity gives rise to oscillatory motion in the form of 'stick-slip' or quasi-harmonic motion. A complete friction system has been analysed and an attempt has been made to describe it in terms of mathematical equations.

This has led to the simulation of such a system using the Analogue Computer. Results have been obtained and made comparable with those recorded experimentally by the adjustment of system variables. These are not always easy to determine within the physical system.

Mathematical expressions concerning surface topography, surface penetration and separation, lubricant and rheological effects have been set up. These have led to a method of determining slideway behaviour from the shape of the steady state friction characteristic. Further, it has been possible to formulate an expression for the critical velocity above which oscillatory motion ceases. The system dynamics is also analysed, using the Describing Function approach.

Wherever possible mathematical models have been tested against known experimental data and pertinent theories, to strengthen and support the relationships between the friction variables and slideway oscillatory motion.

In order to achieve the final results a control systems approach has been adopted as it provides a basic philosophy by which the many disciplines involved can be linked together.

It has been borne in mind, throughout this work, that although some of the mathematical expressions are complex the purpose of the investigation has been to provide data, in acceptable terms, useful to the design engineer faced with friction problems on machine tool slideways.

NOMENCLATURE *

A_a – contact area between two crossed ridges

A_c – contact area for asperity range

A_A – apparent contact area

A_{cL} – leading contact area

A_{cLv} – leading contact area at some sliding velocity

α – E_v/E_o in the dry condition; – $\frac{P_w}{(P_w - P_L)}$ in lubricated condition

α' – reciprocal of real part of rationalised equation for α (dry case)

α'' – complex part of rationalised equation for α (dry case)

a – force due to viscous friction

B – asperity ridge base width

β – cross angle of asperity ridges

b – $\frac{B}{Z}.h$, an asperity width

b(E) – out of phase component of Describing Function

C_ε – normal surface damping coefficient per cm^2

Cn – gradient of solid friction characteristic

Cv – correction factor

E – Modulus of Elasticity

E_o – Modulus of Elasticity at zero velocity

E_v – Modulus of Elasticity at some sliding velocity

$E\sin\theta$ – Describing Function input signal

e – amplitude of positional error signal

F – Friction force

F_s – Static friction force

F_v – Friction force at some sliding velocity

f – linear viscous damping coefficient

G – Shear modulus

G(s) – Linear system Transfer Function expressed in Laplace

g(E) – In phase component of Describing Function

H – oil film thickness between two solid surfaces

H_o – minimum equivalent oil film thickness between two surfaces at rest

h_d – total surface penetration at rest

h_{dv} – total penetration at some velocity

* Units are normally designated within the text

$\dot{h}_d$ – normal velocity related to h_d

$\dot{h}_{dv}$ – normal velocity related to h_{dv}

hf – a normal displacement between contacting surfaces $(= \frac{x}{\sin\theta})$

hf(max) – $\frac{x_m}{\sin\theta}$

he – equivalent film thickness over apparent contact area

hs – surface separation from rest condition

ho – oil film thickness

h – normal movement between surfaces

K – System drive stiffness

Ka – normal stiffness term for asperity junction $(\frac{dW_T}{dh_d})$

K_d – coefficient related to changes in Ac with h_d

K_E – normal surface stiffness per cm^2

K_{EV} – normal surface stiffness per cm^2, at some sliding velocity

Kf – coefficient related to fluid friction equation

K_{LP} – surface coefficient

Ko – oil film coefficient

Kp – coefficient related to fluid pressure equation

Ks – ℓ.Kp – constant for fluid pressure equation

K_T – $K_L = \frac{Ka}{2}$

ko – oil film coefficient

L – characteristic length of contact area in direction of sliding

ℓ – distance between centres of asperity ranges

M – system sliding mass

m – hydrodynamic variable

N – Non-linear friction term at zero sliding condition

Nc – number of contact areas established between two asperity ranges

N_E – Describing Function term for a non-linear element

n – amplitude of solid friction sinusoid

Pa – average pressure over contact area

P_L – Fluid pressure generated in hydrodynamic condition – per cm^2

P_{OL} – "Yield pressure" of oil film

Pm – Yield pressure of metal

Pw – Average pressure (equal to W_T) for an asperity range occupying one square centimetre

P_x – Maximum pressure acting on contact area

S_{OL} – Shear strength of oil film

S_s – shear strength of metallic junction

T – Time constant

T_c – Time constant related to simulation work

T_L – Time constant of simple Voigt model

U_A – "dynamic viscosity" coefficient of surface asperities, per cm^2

U_m – a "dynamic viscosity" coefficient

V – sliding velocity

V_c – critical velocity

V_{CL} – velocity at which minimum solid friction level is reached

V_m – sliding velocity to cause minimum friction

v – amplitude of velocity oscillation

V_B – bias voltage (Analogue simulation)

V_I – input voltage " "

V_o – output voltage " "

V_F – scaled voltage for Fs "

W – Sliding load

W_T – Load on an asperity range

X_i – input displacement to friction system

$\dot{X}_i$ – input velocity

X_o – output displacement

$\dot{X}_o$ – output velocity

$\ddot{X}_o$ – output acceleration

x – movement between contacting surfaces, tangential to friction plane

x_m – maximum movement between contacting surfaces, tangential to friction plane

Z – Asperity ridge height

γ – Phase angle related to Describing Function

β – Linear system damping ratio

ζ – Oil dynamic viscosity

θ – angle between plane of contact area and horizontal friction plane

θ_n – angular quantity related to Describing Function equations

μ - coefficient of friction
μ_s - static coefficient of friction
μ_k - kinetic coefficient of friction - due to metallic contact
μ_o - kinetic coefficient of friction - due to lubricant film
μ_T - kinetic coefficient of friction for lubricated surfaces

ν - Poissons Ratio

ρ - Oil density

ϕ - linear system phase angle

ω - frequency
ω_n - undamped natural frequency
ω_d - damped natural frequency

LIST OF ILLUSTRATIONS

Photograph No.

Fig. No.

CHAPTER 1

INTRODUCTION

Over the centuries man has inevitably been concerned with the natural phenomenon of friction. Although there would be problems if it were not universally present, the greater part of man's interest has been with reducing its effect. However, it was not until the time of Leonardo da Vinci (1)*, (1452-1515), that some physical relationships were propounded through his experimental work. Since then the basic laws of friction have been established and used by many researchers and engineers up to the present day.

These basic laws represent a justified concensus of opinion relating the force required to move one body over the surface of another, to the weight of the moving body and the coefficient of friction.

$$F = \mu W$$

As man has advanced technologically and our study of engineering problems has become more intense, the pursuance of information regarding friction phenomena has grown rapidly. Today these activities are grouped under the general heading of Tribology. Experimentation in this field increased our understanding of the role friction plays within the sphere of engineering, but it can be stated that the Basic Laws still maintain their validity. The area covered by tribology is vast, and several empirical relationships and theories have been put forward for many aspects and conditions required through technological demand.

This thesis has its own particular reference within the engineering context, namely machine tool slideways. A study is made of the non-linear friction behaviour which occurs when a body slides over another at slow speeds. This phenomenon has commonly been given the descriptive title of "stick-slip". Although occurring in many areas associated with tribology, stick-slip is most pertinent to machine tool slideways as it is well known that it does affect the static and dynamic behaviour of the machine tool.

*Please see the bibliography

In order to study and hence analyse non-linear friction behaviour a basic philosophy of approach is required, and in this case a Control Theory approach has been adopted to formulate a describable model. (This philosophy is detailed in chapter 3). It is sufficient to state here that the philosophy is one in which the observed and some unobserved phenomena that occur are related to the physical nature of all the parts of the whole. All the elements together comprise the system. The control theory concept is mathematically based thus demanding that all constituent parts of a system have a mathematical description related to their physical nature.

To enable successful analysis to be completed, especially for complex systems, the computer is utilised. In this thesis a great deal of use was made of the Analogue computer to simulate the interaction between elements of a machine tool drive system and the effects which contribute to stick-slip phenomena.

It is hoped that the simulation together with other observed experimental data will enable a mathematical description of non-linear behaviour to be formulated, which relates to the actual physical variables in such a system.

One of the difficulties in using this philosophy is that empirical relationships must be replaced by actual physical relationships and it is expected that this work will produce an insight, if not a direct transposition, for some of the system variables.

Finally, it must be stressed that the engineer relies heavily on the use of simple formulae whose variables are easily observed and quantified. Complex equations will not easily help to solve the day to day problems the engineer faces in his work. Any mathematical relationships with regard to stick-slip, its prediction and reduction or elimination will be simplified where possible and the phenomena expressed in physical terms easily understood by the engineer in industry. In this context the observations made by Leonardo da Vinci and others leading to the basic laws of friction are surely an example to follow.

CHAPTER 2

LITERATURE SURVEY

2.1) INTRODUCTION

This survey has been conducted to examine and bring together the ideas and theories of many researchers. In general, the investigations into friction phenomena have been carried out using experimental apparatus and it is most important to appreciate the results in their proper context in order to provide some basic ground rules. Although the results are most useful there is no implication that the related theories and empirical formulae can be used per se.

It is hoped to show that, although friction experiments were carried out under many varying conditions, e.g. size of experimental test rig, some of the recorded data and observations are common. This means that it is possible to establish a basis on which this thesis is built.

A comprehensive survey is required into friction phenomena in order to uncover as many facts as possible, bearing in mind that some of these will ultimately be used to resolve the problems of non-linear friction behaviour between cast iron slideways travelling at slow speeds. It should be stressed that, although this work is a study of particular friction behaviour, there is a very important relationship between friction and wear, and where one occurs so will the other. The relationship between them is complex and has not been overlooked, although the wear phenomenon is mentioned only briefly throughout the thesis.

This survey has been set out in four parts to show the chronological progression of work in the friction field and to avoid complicated cross-referencing.

2.2) HISTORICAL REVIEW ON THE NATURE OF SLIDING FRICTION

Since studies began there has been a continual growth in investigations into friction. Fig. 2.1 illustrates this point and the curve is based upon the literature reviewed by the author. It is felt that the same curve would also indicate the changes in educational progress and

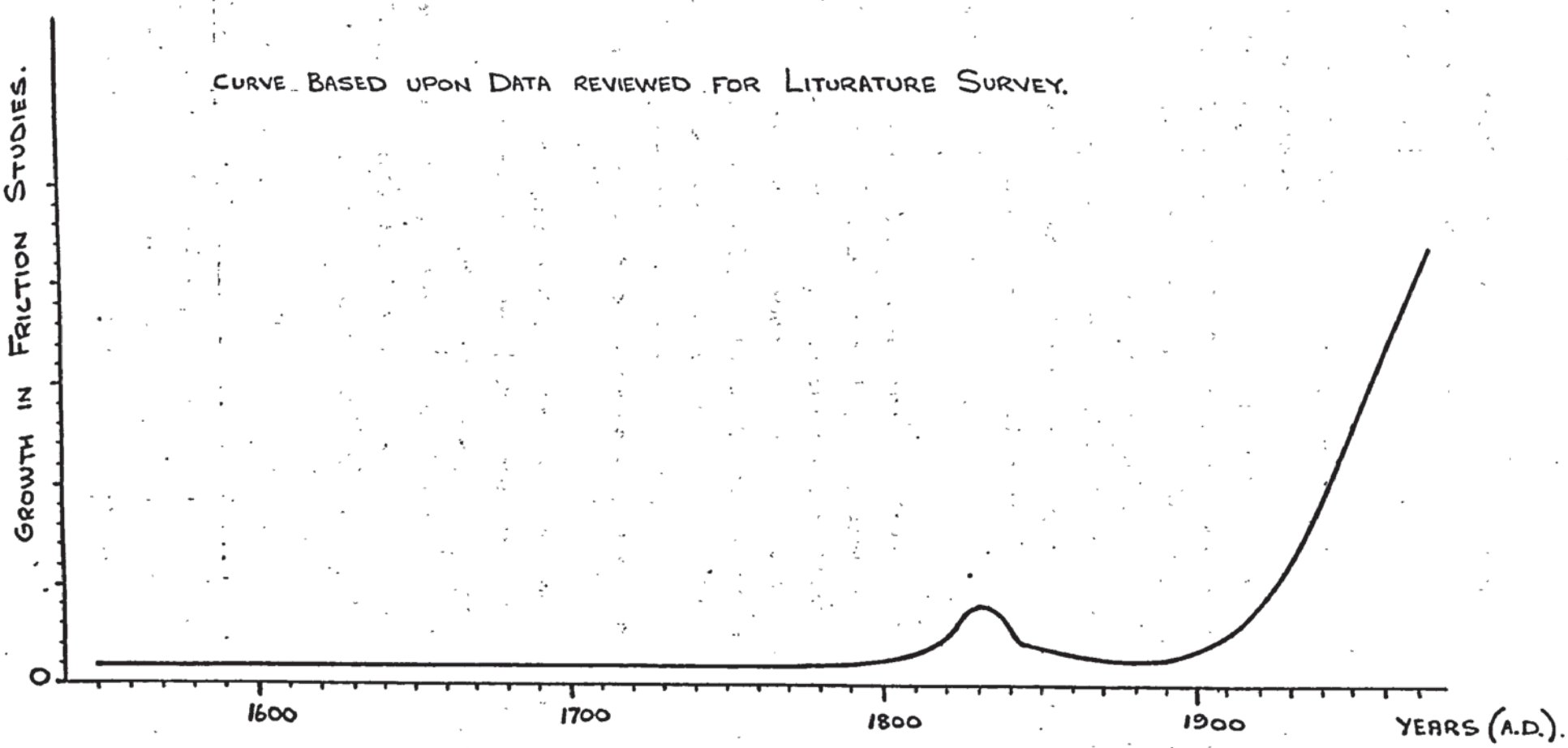

FIG. 2·1 GROWTH IN FRICTION STUDIES.

more importantly the growth of science and technology through developing instrumentation. Unfortunately this has led to the discovery of more problems to solve.

The "father of friction", Leonardo da Vinci (1) was the first experimenter to study and document his work about the forces required to slide one body over another. He noted that the force required was proportional to the weight of the sliding member and independent of the contact area. By using a block resting on a platform, he found that by changing the inclination of the platform until the block moved smoothly, the angular displacement was constant. By smoothing the contact surfaces this angle was reduced. Although he did state that the force required to move a sliding block was equal to one quarter of its weight, there appears to be no application of his findings.

It was not until G.Amontons (1) (1699), attempted to analyse the problems of friction, and tried to relate them to solving difficulties with machines of the time, that any serious attention was taken. He was unaware of the work of Leonardo da Vinci but did come to the same conclusions. These being that the friction force was independent of the contact area but proportional to load and that friction force was one third of the load weight. He did intimate that he thought the friction force may be dependent upon the velocity of movement.

The significance of resting a block on an inclined platform, and changing the angle until the block started to move, was rediscovered by A. Parent (1) (1704), and called the angle of repose. This work was elaborated upon by L. Euler (1) (1748), who stated for the first time that the force of static friction is greater than that of kinetic friction and gave an equation for each in terms of the angle of repose.

In 1785 C.A.Coulomb (1) (2) conducted similar experiments and obtained the same results, but added that the force of kinetic friction was independent of velocity. His experimental apparatus did not show this to be true as the friction force did vary slightly but he came to this conclusion by taking an average friction value. He proposed that friction

force was due to the meshing of asperities and inferred that smooth surfaces produced less friction force. At the same time S.Vince (1) came to a similar conclusion in that friction force would be proportional to load if the roughness of the sliding surfaces was the predominant feature. He and Coulomb argued that if molecular attraction was the principal cause of friction then the force should be proportional to the area of the contact surfaces. (This is apparent area).

The experimental work of Coulomb was criticised by A.Morin (1) in 1831. His work on friction was extensive, covering a period of four years. He took great care when operating his equipment and recording data,and confirmed the "basic" laws of friction; stating that the kinetic friction was definitely independent of sliding velocity. The friction data he collected has been the only source quoted in the Handbook of Chemistry and Physics up to as late as 1954 (3).

Nearly all of the friction studies that have been mentioned were carried out using unlubricated surfaces, but it was Hirn (2) in 1854 who first distinguished between lubricated and unlubricated surfaces, observing that the effect of velocity, surface area and load differed in both cases. It can be stated that up to this time few precautions were taken by any of these experimenters to obtain "clean" and reproducable surfaces.

The main theory for the generation of friction was the interlocking of surface asperities. This argument wascounteracted by a molecular theory of friction proposed by Ewin (1892), G.A.Tomlinson (1929) and Derjaguin, (1934), (4) (5).

The paper by Tomlinson (6) although speculative did highlight some ideas which are still considered to-day. Although the friction was due to the reaction of molecular forces, following molecular displacements, he suggested relating the coefficient of friction to the material elastic constants and the bulk properties of the materials.

$$\mu = 1.07 \times 10^4 . (A_1 + A_2)^{\frac{2}{3}} \qquad - 1.2$$

where A_1 and A_2 are constants for each material,

and $$A = \frac{3E - 4G}{G(3E + G)} \qquad - 2.2$$

These researches indicated that there was a movement away from proving the empirical "laws" to the understanding of the mechanism of friction of sliding bodies. This changing situation produced a paper by Bowden and Leben (7) in 1939 which stated that the 'classic laws' were a crude approximation. The major part of their work was conducted with unlubricated surfaces using various combinations of metallic sliding pairs. It was noted that friction was greatly affected by surface contamination such as oxide films, molecular absorption of gases and water vapour at the sliding surfaces. They suggested that the contact points of the surface asperities produced local welding and the formation of metallic junctions; the breaking away of these junctions caused the friction. This implied that the actual area in contact was much smaller than the apparent area. The relative movement produced surface scratches which indicated some damage and surface wear. More importantly they demonstrated that when the sliding is at low velocities (e.g. 0.06 mm/s) jerking motion took place and stated "the sliding process is not a continuous one, the motion proceeds in jerks - the metallic surfaces 'stick' together until as a result of gradual increasing force there is a sudden break with a consequent very rapid slip". It was noted that even with a lubricant such as mineral oil "stick-slip" could still occur under boundary lubrication conditions and they related the magnitude of the slip to the melting point of the material which was slid over a steel plate. It was also concluded that the friction effect was not confined to the surface but extended well below and was dependent on the bulk properties of the solids in contact.

The phenomenon of "stick-slip" was first mentioned in a paper by Kaidanvosky and Haykin (8) (9) in 1933 who pointed out that jerky motion was due to 'relaxation oscillations' and that the friction characteristic should be non-linear, containing a falling section at low velocities before rising again from a minimum value. The sliding system will be unstable and oscillations will occur until the friction minimum is reached and the friction characteristic takes on a positive gradient.

Blok (5) commented in a 1940 paper that he found that stick-slip could be obviated by careful consideration to the rigidity of the driving mechanism and the damping and intertia of the moving parts.

In 1942 Schmurman and Warlow-Davies (9) presented a paper on the 'electrostatic component of friction', describing again the stick-slip process related to the steady-state friction/velocity curve. Their interpretation of this process is different from that of Bowden and Leben (7) in that they suggest that local welding does not take place, as the temperature rise at the junction is likely to be small, surface damage could be negligible and the jerky motion was due to the characteristics of sliding and not to scoring. Thus, when the conditions are such that the electrostatic component of the force of sliding motion is appreciable and varies as sliding proceeds, jerky motion will arise. They also deduced that the limiting value of static friction was reached by elastic asperity deformation, together with a slight actual displacement at the contact area of the two bodies.

This non-linear motion was again studied by Sampson, Morgan, Musket and Reed, (10), (1943), with unlubricated surfaces. For the first time they do describe part of the sliding motion mathematically, with due regard to the mechanics of their equipment. They also confirmed that the bulk properties of the material are of primary importance and that the frictional mechanism involves plastic deformation. It was found to be difficult to obtain reproducable results due to a number of individual factors, e.g. surface contamination. With the mathematical model they calculated the slip distance against time and produced a friction coefficient/velocity curve. The analysis shows friction behaviour during 'slip' and that dependence on velocity is not simple and reversible. In general friction is less at the end of a slip than at the beginning. They assume for calculation that the friction force drops rapidly from static to a constant kinetic friction force as slip commences. When the slider comes to rest there is a gradual build-up of friction force during 'stick'. This depends upon the condition of the surface, the mechanical properties of the surface material and the previous history of sliding motion on the surface. They conclude that high friction at the beginning of sliding means that shearing takes place as well as ploughing of the surface asperities. Kinetic friction due to sliding is mainly due to the ploughing component. The kinetic value does not return to its static value unless the surfaces remain at rest long enough for new adhesive junctions to be formed. Therefore they were intimating that the coefficient of static friction is time dependent.

During the time period covered by this section of the review, the study of friction can be broken down into two main parts. It is suggested that the first part, covering a period up to the Industrial Revolution, led experimenters

to relate empirically the force of friction to basic known parameters (e.g. weight of slider, surface roughness). The validity of the equation,

$$F = \mu W \qquad - 3.2$$

is still maintained to-day and is one of the classical laws.

The second part is concerned with developments since the Industrial Revolution when it became quite obvious that a study of friction between sliding metal surfaces was of utmost importance. Experiemental equipment became quite sophisticated and, as there was some knowledge with regard to the properties of metals, studies began to try to obtain an understanding of the nature of sliding friction. This led to the proposal of several friction models which would obey the classic friction laws. Some of the earlier model concepts have been rejected and the 'laws' are being questioned. The remaining friction models are concerned basically with the mechanical properties of the surface and the bulk properties of the material. Much of the fundamental friction work since 1945 has been connected with the properties of materials under various physical conditions. This has meant that most of the work has been carried out by physicists and chemists and because of the lack of communications the engineers, concerned with technological problems, have had to rely heavily on the basic laws.

2.3) RECENT CONCEPTS OF THE NATURE OF SLIDING FRICTION

It is probably time to say that the foundations of modern experimental and theoretical work were laid by F.P.Bowden and D.Tabor (2) with the publication of their book "The friction and lubrication of solids" in 1950 . It has influenced many researchers and is often quoted as a reference work, even to-day. They have attempted to explain and maintain the 'classic' friction laws by logically developed arguments based upon the chemical and physical nature of the contacting surfaces.

The dry friction force was a product of two effects, one due to the shearing of the metallic junctions and the other to the ploughing of grooves on the surface of the material. In this way it was possible to obtain an approximate expression for the friction in terms of the bulk properties of the metals. Thus,

$$F = A.Ss + a.p. \qquad - 4.2$$

where A – actual contact area on sliding plane

Ss – shear stress of these metallic junctions

a – contact area normal to sliding plane, the ploughing area of submerged asperities

p – mean pressure to displace the metal, acting on area(a)

Tests indicated that the term S_s was of the same order of magnitude as the shear stress of the softer material of the sliding pair and that (p) was of the same order of magnitude as the yield pressure of the same material. If the force due to the ploughing term was small and could be neglected, with small load pressures, the area of contact could be expressed as

$$A = \frac{W}{P_m} \qquad - 5.2$$

where P_m – yield pressure of softer material

Thus

$$F = AS_s = \frac{WS_s}{P_m} \qquad - 6.2$$

and it was established that the friction force was proportional to the load W, but the coefficient of friction virtually independent of the load since from eqn. 6.2,

$$\mu = \frac{S_s}{P_m} \qquad - 7.2$$

They go on to point out that the relationship between S_s and P_m can become very complex, especially with the ability of the metal to work-harden. There will be an increase in the static friction force when a tangential force is applied due to an increase in the contact area as a result of some deformation.

If the contacting areas are contaminated with a surface film such as oxide or lubricant, the frictional force can be expressed as

$$F = A\left(S_{s_1} + (1 - \alpha).S_{s_2} \right) \qquad - 8.2$$

where α is the fraction of contact area which is truly metallic having a shear strength S_{s_1} and $A(1 - \alpha)$ is the remaining area of contact, where the adhesion will be weaker, thus producing an average shear strength S_{s_2} for the contaminated film. As the variables S_s and P_m change so will the friction force, which gives an explanation for the difference between the static and kinetic friction forces.

If the static force is greater than the kinetic then during sliding motion 'stick-slip' can occur. The tests carried out were at slow sliding speeds in order to maintain a temperature independence for S_s and P_m. Their results show that the change in friction force during 'slip' reduced as the sliding speed increased and that the 'slip' time was equal to π/ω, where ω was the natural frequency (Rad/s) of the drive system. The 'stick' time and hence the static friction force was reduced as the sliding speed increased, thus intimating a relationship between the static friction force and time at rest (or time of 'stick').

They maintain that when the 'static' and kinetic forces become equal intermittent motion ceases. The 'stick-slip' phenomenon was also used to demonstrate the effectiveness of lubricant films and they suggested that lubricants containing fatty acids are much more likely to provide smooth sliding than lubricants containing only paraffins or alcohols.

The friction theories mentioned above cover only a part of their total experimental work, but it was apparent to friction researchers that two features needed further investigation. These were related to establishing a measure of the area of intimate contact between metal surfaces, and the time dependence of static friction.

Ernst and Merchant (5) proposed that under dry, sliding conditions the friction force was the resultant of the force necessary to shear the metallic junctions (Fs) and the force necessary to lift the asperities of one surface over the asperities of the other (Fa). Thus,

$$F = Fs + Fa \qquad - 8.2$$

and

$$\mu = \frac{Fs}{W} + \frac{Fa}{W} \qquad - 9.2$$

$$= \frac{ASs}{W} + \frac{Fa}{W}$$

$$\mu = \frac{Ss}{Pm} + \frac{Fa}{W} \qquad - 10.2$$

The term Fa/W was expressed in the form of the mean asperity angle between its slide and base (Θ) in the direction of motion, thus

$$\mu = \frac{Ss}{Pm} + \operatorname{Tan}\Theta \qquad - 11.2$$

This equation introduces a new term based upon a description of the surface asperities contained on the sliding surfaces.

The work of E.Rabinowicz (11) (12) (13) enabled him to develop two theories, one known as the critical distance concept and the other being the surface energy criterion.

His experiments related to static and kinetic friction indicated that the static friction force between two dry metal surfaces was maintained for a certain sliding distance before falling to a kinetic level. He developed a friction / displacement curve and considered that the size of the metallic junctions could be estimated from this curve by examining the distance at

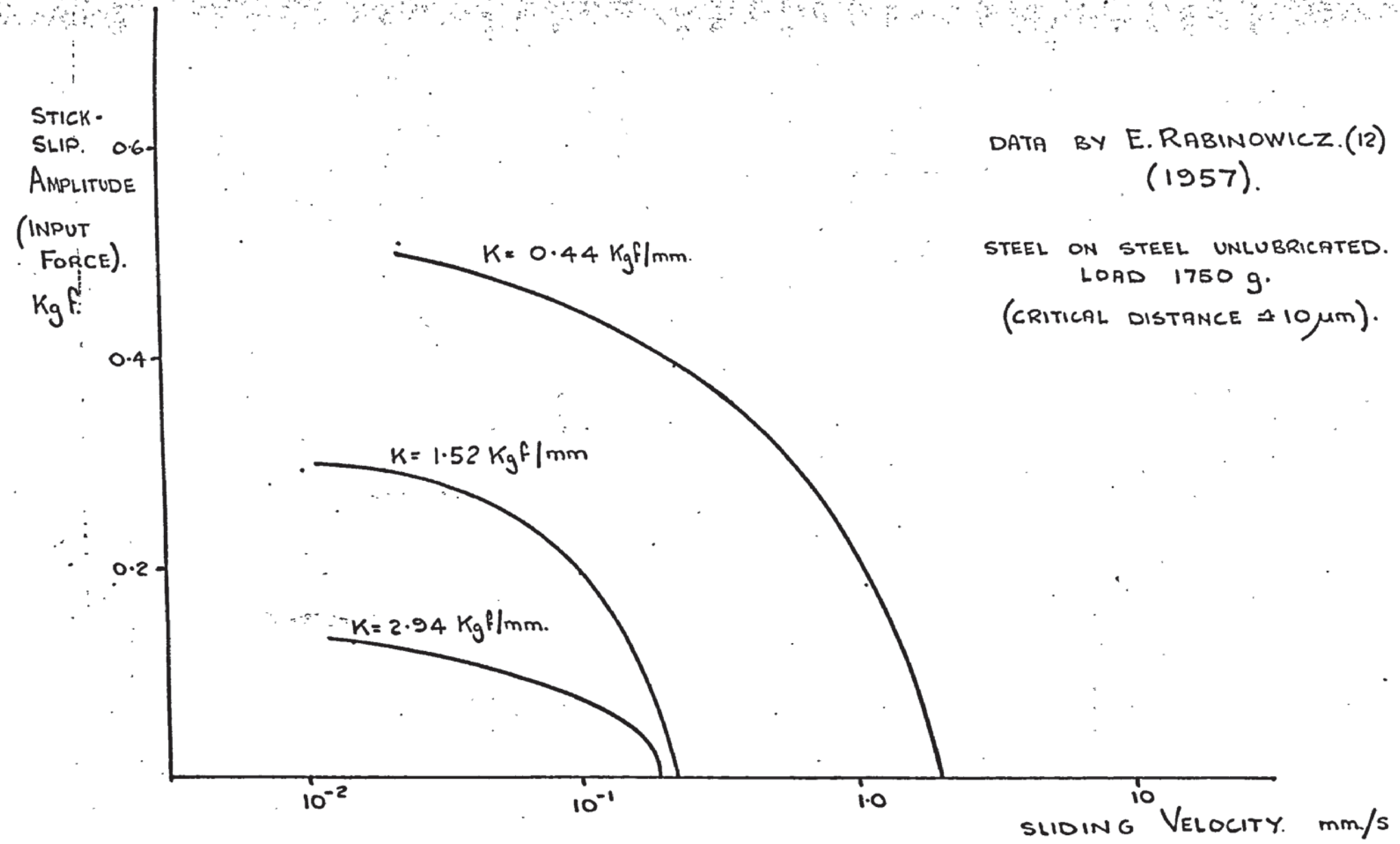

FIG. 2·2. STICK-SLIP AMPLITUDE VERSUS SLIDING VELOCITY.

which the actual friction first became equal to the kinetic force. This displacement was termed the critical distance. Using the 'stick-slip' technique he measured the 'static' friction force level and the time of 'stick' to produce a static friction/time curve, for various metal pairs. This plot enabled him to determine the amplitude of the friction force for various drive stiffnesses and input velocities. These correlated very well with experimental data and this interesting relationship is shown in Fig 2.2 from information taken from his paper (12) . It was argued that oscillatory motion would cease when the displacement amplitude was equivalent to the critical distance. Thus by increasing the drive stiffness the friction force amplitudes decreased in magnitude and oscillations terminated at a lower sliding velocity.

He also suggested that as the kinetic friction varies with sliding speed it was possible to find a relationship between the static friction/time curve and the kinetic friction/velocity curve. If the static force after a certain time was known then, by dividing the critical distance by this time to produce a 'velocity' term, the static force is the kinetic force at that 'velocity'. This technique for producing the friction/velocity curve was shown to compare reasonably well with his experimental results.

The general behaviour of two sliding surfaces is influenced by the surface energy (W) and Rabinowicz states that expressions for friction and wear phenomena are related to the function (W/p), where p is the hardness of the softer material. He suggests that the diameter of wear particles (d), for most metals, is related to the function,

$$d \geqslant 60{,}000 \frac{W}{p} \quad \text{cm}$$

where W and p have c. g. s. units.

It is intimated that as two surfaces are rubbed together there will be a steady state interfacial condition for wear rate, debris size and surface finish, all of which are related to the ratio (W/p), especially when light loads are applied.

In 1957 the Conference on Lubrication and Wear (14) was held in London. As far as friction was concerned, very little progress had been made since the ideas and concepts of Bowden and Tabor (2) in 1950. It was shown

that the effect of lubricants did modify the friction conditions by weakening some of the parameters established for the dry friction conditions. This point was illustrated by K.L.Johnson (15) who stated that the presence of a lubricant on a metal surface did not affect the deformation process for tangential forces less than those required to cause surface slip. The lubricant weakened the surface interaction so that the maximum static friction force was lowered.

In his conference review Bowden (14) stated that it was generally accepted that an appreciable part of the resistance to sliding may be due to the plastic deformation of the asperities, even under lubricated conditions. The shearing of the asperities gave rise to wear and consequent surface debris.

It was pointed out by Kraghelskii (16) that the 'classic' friction laws were valid when the surface contact was in a plastic condition. His equation for the dry friction force was given by a 'binomial' form,

$$F = \alpha Aa + \beta W \qquad - 12.2$$

where α and β are coefficients for a particular metal pair. Under conditions of ideal plasticity

$$Aa = \frac{W}{\upsilon . \sigma s} \qquad - 13.2$$

where σs is theyield stress and υ is a factor dependent upon the boundary conditions of the contact thus,

$$\frac{F}{W} = \mu = \frac{\alpha}{\upsilon . \sigma s} + \beta \qquad - 14.2$$

and μ is a constant.

During the discussion related to the friction papers (Session 3), Archard (17) stated that in a practical situation the rubbed surfaces involved much elastic deformation of the asperities, without wear. He suggested that an asperity may be deformed plastically at its first encounter with the other surface but it would relax elastically and at subsequent encounters bear the same load without plastic flow. This point indicated an elastic-plastic regime at the sliding surfaces, and although for a single contact the area involved was not proportional to the load, for multiple contacts his

surface model (18) suggested that the contact area became very nearly proportional to the load.

Most of the conference papers described experimental work which in essence substantiated many of the previously published ideas. One of the few analytical papers presented by Derjaguin, Tolstoi and Push (19) concerned a theory of stick-slip related to sliding solids. This was the first comprehensive study and attempted to take into account some of the modern, experimentally derived, concepts. The equation of motion of the slider on a uniformly driven platform was,

$$M\ddot{x}o + f\dot{x}o + Kxo \pm Fs - n(\dot{x}o - \dot{x}i) = 0 \qquad - 15.2$$

where n is a coefficient describing the rate of decrease of friction force with increased relative sliding speed. It was considered that a linear relationship between friction force and velocity was in order, so that the equation could be simplified and the friction at any velocity was given by

$$F = Fs - n(\dot{x}o - \dot{x}i) \qquad - 16.2$$

The equation of motion above only applied to the slip portion of the stick-slip condition and the solution of the equation enabled the slip time and the maximum slider velocity to be calculated. It was decided to consider the initial conditions at the instant that slip occured and in particular that there would be an instantaneous change of friction force ΔF giving rise to an instantaneous change in acceleration from zero to $\Delta F/M$. The solution is similar to that for the standard second order linear system (20) but did introduce a negative damping coefficient ϕ where

$$\phi = \frac{\Delta F}{\dot{x}i\sqrt{K.M}} \qquad - 17.2$$

and thus

$$\frac{V}{\dot{x}i} = 1 - e^{-\theta\omega t}\left(\text{Cos}\omega t + \frac{\zeta - \phi}{\sqrt{1-\zeta^2}}\,\text{Sin}\omega t\right) \qquad - 18.2$$

where V = velocity difference between the two surfaces $(\dot{X}i - \dot{X}o)$.

$$\theta = \frac{\zeta}{\sqrt{1-\zeta^2}}$$

and

$$\omega = \sqrt{K/M}\cdot\sqrt{1-\zeta^2}$$

$$\zeta = \frac{(f-n)}{2\sqrt{KM}} = \text{an equivalent linear damping ratio}$$

Further analysis indicated that if ζ was small the critical velocity (Vc) was given by the equation,

$$Vc = \frac{\Delta F}{\sqrt{4\pi.\zeta.MK.}} \qquad - 19.2$$

The velocity profile could be plotted during slip and the time interval for slip was governed by the boundary condition at start and finish when V was zero. The velocity wave form was sinusoidal and changed with increasing input velocity. A condition was possible where the term V would be constant ($\dot{V} = 0$) and equal to $\dot{x}_i$. The input velocity, to bring about this condition, was called the critical Velocity and further increases in velocity also resulted in stable motion. That is to say the critical velocity produced a condition in the system of zero 'stick' time.

It was possible to reduce oscillatory motion by increasing ζ which means increasing f or decreasing n and hence ΔF. The equations show that changing the drive stiffness also affects Vc.

Although the friction/velocity characteristic was linearised the analysis did relate very well to experimental observations and theories with regard to sliding friction phenomena. Their analysis depended upon some intimate knowledge of three variables, the static coefficient of friction (Fs), the damping term (f) and the friction/velocity coefficient (n). These terms may be difficult to ascertain experimentally but if they were available the analysis could be used. The authors considered the variation of static friction with time of 'stick', which made their analysis complex. The critical velocity condition could then only be found by an unwieldy graphical technique. Nevertheless, this paper made a major contributionto the overall understanding of stick-slip in mechanical systems.

Friction analysis since 1957 has been dominated by the investigations into the stick-slip condition as the work of Brockley et al (21) (22) (23) (24) demonstrates. His experimental work has been influenced by Rabinowicz and Tabor and has resulted in an attempt to express mathematically the relationship between the static friction force and time. Thus,

$$\mu s - \mu k = Y.t^{\beta} \qquad - 20.2$$

where μs becomes equal to μk when t is zero. The constants Y and β are dependent upon surface parameters and the applied load. There were found, for dry sliding surfaces using various metal pairs, by first plotting the static friction/time curve and then replotting this data as log $(\mu s - \mu k)$

against log (t). This produced a straight line relationship and hence Y and β could be estimated. His analytical work was influenced by Derjaguin et al (19), but the methods used involved the application of phase - plane techniques, developed by Lienard (25). It is interesting to note that the phase plane plots did serve to illustrate the oscillatory motion in a new way by plotting system positional error against sliding output velocity.

His experimental observations confirmed previously expressed views that vibrations are reduced by having

a) A small mass and a large drive stiffness
b) A small difference between μs and μk
c) Large damping coefficient - ζ
d) A small value of β (eqn. 20.2) which is termed the static friction growth constant

Further experimental work (23) revealed that another type of oscillatory motion occured where the output velocity waveform was nearly sinusoidal and the minimum velocity was not zero, this was termed quasi-harmonic motion, which would result in a closed circular form of phase-plane. Frictional quantities also varied this type of motion, whichdied away at some "critical" velocity. He plotted the friction force/velocity curve using a technique developed by Bell and Burdekin (26). This involved measuring slider acceleration and displacement in order to produce a signal quantity equal to

$$\left(M\ddot{x}o - K\,(x_i - x_o)\right)$$

The magnitude of this signal was the total friction term and was called the system dynamic friction. A phase plane of the dynamic friction force against velocity, under stick-slip conditions, was recorded directly by his instrumentation and is very similar to the characteristic laboriously produced by Sampson et al (10) nearly twenty eight years earlier.

The consideration of a dynamic friction force was a new concept in analytical work as it relates

$$\left(M\ddot{x}o - K\,(x_i - x_o)\right) \text{ to } \dot{x}_o$$

whereas previous analysis relied upon the relationship

$$K\,(x_i - x_o) \text{ to } \dot{x}_o$$

which was normally used to produce the steady state friction/velocity characteristic. It suggested that oscillatory motion should be investigated from a system dynamics point of view and that due consideration should be

given to the part played by the slider acceleration forces.

Another interesting paper by Johannes, Brockley and Green (27) concerned with static friction was published in 1973. The experimental work considered the rate of application of the tangential driving force and its affect on the static coefficient of friction. It was observed that the static friction force reduced as the rate of application of tangential force increased. The work intimated that the growth of actual contact area was also sensitive to the rate of force applied by the system drive.

A recent analysis by Takano and Ishibashi (28) of oscillatory motion, again using phase-plane techniques, indicated that the type of motion either quasi-harmonic or stick-slip was dependent upon the shape of the steady state friction/velocity curve. Their experimental work showed these effects to be dependent upon surface contamination and surface finish. This point was also made by Pavelescu et al (29) (30) who investigated the relationship between stick-slip motion and wear. In this case sliding was between flat surfaces of cast iron. The surfaces were lubricated and their results indicated that stick-slip diminished if the surface roughness was reduced and lubricant viscosity increased. The wear rate increased during stick-slip motion and was also governed by lubricant viscosity, applied load and surface finish. The experimental conditions approximated to those found in general engineering practice and it was suggested that the most favourable wear conditions may exist if the surfaces are machined with different finishes, i.e. one surface fine milled and the other lapped.

The variation of friction force is related to the changes in topographical surface conditions which govern the amount of intimate metallic contact. This contact area has been extremely difficult to express mathematically because of the many variables involved. Attempts have been made by Peklenik (31) and Kimura (32) using statistical techniques to express the geometric nature of metallic surfaces. These have not been successfully applied in the friction field although they do indicate the complexities involved in trying to describe machined surfaces.

In order to attempt a friction analysis many researchers have assumed certain surface profile conditions and most of the recent papers have been presented by Japanese authors. Tsukizoe and Hisakado (33) considered contacting surfaces whose asperities were cones interacting under dry sliding conditions.

Their analysis produced the following equations for a rough hard metal surface resting on a smooth soft surface.

1) The coefficient of friction due to the shearing of metallic junctions μ_{sm} is

$$\mu_{sm} = \frac{Ss}{Pm} \times \frac{1}{\sqrt{1 - \alpha \left(\frac{Ss}{Pm}\right)^2}} \qquad - 21.2$$

where α – the junction growth constant

Ss – shear stress of the contact area

Pm – yield pressure of softer material

2) The static coefficient of friction is,

$$\mu_s = \frac{2/\pi \, \mathrm{Tan}\Theta. + 1/2 \, \mu \left(1/\mathrm{Cos}\Theta + 1\right)}{1 + 2/\pi \, \mu \, \mathrm{Tan}\Theta.} \qquad - 22.2$$

where Θ – base angle of the asperities

$$\mathrm{Tan}\,\Theta = \frac{H}{3.12H + 15.5} \qquad - 23.2$$

and H – height of the asperities.

Experimental verification was carried out using copper and steel specimens with ground surfaces. The time effect for the friction force was neglected as the specimens were at rest for a period of two minutes before a tangential force was applied. The results enabled the variable α (eqn. 21.2) to be established. It was noted that the surface roughness had a marked effect on the coefficient of static friction and that the maximum tangential displacement before 'slip' occurred was in the range of three to five times as large as the average radius of the contact points.

Similar observations were made by Gupta and Cook (34) who used spherical asperities for their model. They assumed constant interfacial shear stress and thus maintained that the friction force was proportional to the contact area. Their relationship for actual contact area between surfaces of the same material and their physical properties was given by

$$\left(\frac{2}{3}\right) \cdot \frac{A}{W} = 0.31 \cdot \left(\frac{2}{Y}\right) \qquad - 24.2$$

where Y – material tensile yield stress

W – applied load

A – actual contact area

hence the friction force is of the form

$$F = A \times \text{shear stress}$$

$$F = 0.47\, W. \left(\frac{2}{Y}\right) \times S. \qquad - 25.2$$

and

$$\frac{F}{W} = \mu = 0.93 . \left(\frac{S}{Y}\right) \qquad - 26.2$$

(This is a very similar to the result given by eqn. 7.2)

In 1974 comparable results were obtained by Chivers et al (35) using a surface model which consisted of a uniform array of wedges with a distribution of peak and valley heights. The analysis indicated that the compression characteristics of the real surface could not be deduced from the C.L.A. value alone. The use of a ratio $\left(\frac{d}{\sigma}\right)$ was suggested as a meaningful parameter, (d) being the separation of the mean valley and mean peak level and (σ) the standard deviation of the distribution. For a given contact pressure it was calculated that the real contact area was small, for low values of the $\left(\frac{d}{\sigma}\right)$ ratio. Their results show that there was a linear relationship between the actual contact area (A) and the load (W), when this was small, of the form

$$A = \alpha . \frac{W}{Y} . 0.87 \qquad - 27.2$$

where α is a coefficient related to a material pair. This relationship is very similar to that produced by Gupta and Cook (34).

A very interesting analysis, using a wedge profile description for ground surfaces, was produced by Tsukada and Anno (36). They investigated the elastic and plastic deformation of the surfaces, experimentally, using flat steel specimens. The mathematical model had both surfaces covered with an array of wedges which cross at an arbitrary angle, when placed together. There was a very good correlation between experimental results and theoretical analysis which indicated a linear relationship between the logarithm of load and logarithm of normal deformation, when expressed in non-dimensional form. Thus,

$$\frac{\log P}{\log he'} = \text{constant} \qquad 28.2$$

where

$$P = \frac{W}{Aa \cdot Pm} \qquad - 29.2$$

Aa – actual contact area

Pm – plastic flow pressure

and

$$he' = \frac{he}{\sigma e} \qquad - 30.2$$

he = elastic deformation, normal to asperity plane

σe = equivalent standard deviation of the surfaces.

Similar expressions were shown to exist for plastic deformation and it should be noted that the terms for he' are very similar in nature to the ratio (d/σ) suggested by Chivers et al (35) as being a useful expression.

The work carried out by Tsukada and Anno has produced complex expressions of which the significance is the inclusion of physical parameters of the materials together with quantities describing the surface topography.

Hisakado (37) has also produced very similar mathematical relationships using a surface distribution of asperities having varying radii of curvature of the peaks and his analysis, as does Tsukada's, shows that the real area of contact increases with decreasing surface roughness.

This review has attempted to develop modern friction concepts since 1950 and the general areas of study undertaken by researchers can be summarised as follows:

a) Friction force associated with actual contact area
b) Actual contact area related to surface topography, material properties and applied load – the two contacting surfaces being at rest
c) The dependence of friction force on sliding velocity
d) The dependence of static friction force on time and the rate of applied tangential force
e) The variations in friction force with surface contamination

There are basically two groupings, one of which is the friction and sliding velocity and the other friction and contact area. Therefore it can be assumed that another relationship must exist between sliding velocity and surface

contact area. This interesting point is taken up in a paper by D. Tolstoi (38) published in 1967.

His experiments demonstrated the changes in friction force with corresponding changes in small movements normal to the sliding plane. In particular the friction force reduces as the normal movement increases, separating the surfaces.

Observations indicated that surface separation would occur and increase, with sliding velocity. Thus the contact area and friction force would decrease. This effect was used to explain oscillatory sliding motion, in that a 'slip' displacement along the sliding plane was accompanied by a normal displacement. As stick-slip motion occured the slider was also oscillating in a vertical manner. Thus for oscillatory motion,

$$\frac{df}{d\dot{x}o} \equiv \frac{\partial f}{\partial H} \cdot \frac{dH}{d\dot{x}o} + \frac{\partial f}{d\dot{x}o} < 0 \qquad - 31.2$$

(a negative friction characteristic)

or

$$S. \frac{\partial Ac}{\partial H} \cdot \frac{dH}{d\dot{x}o} + Ac\frac{\partial S}{\partial \dot{x}o} < 0 \qquad - 32.2$$

$(S. \partial Ac = Ac.\partial S = \partial f)$

where H – normal displacement (from rest condition)

S – average shear stress of material in contact

In the stick-slip condition then the term $\frac{\partial f}{\partial H}$ is always negative, whilst $\frac{dH}{d\dot{x}o}$ is always positive (or zero). It follows that if H is kept constant then $\frac{df}{d\dot{x}o}$ will be positive and smooth sliding will exist. Tolstoi demonstrates that there can be two velocity boundary conditions for H to remain constant, at very low velocities (lower critical velocity) and at a higher velocity (upper critical velocity). Between these two velocities self-excited vibrations will occur. The effect of surface lubricant is to control H, thus reducing the upper critical velocity and slightly increasing the lower critical velocity.

It is interesting to note that the ideas presented in Tolstoi's paper have never been investigated by other friction researchers. Takahashi et al (39), using an electron microscope to study intermittent motion,

illustrate grooves in stainless steel made by a diamond stylus. Although plastic deformation has occured the track width did vary during 'slip' and indicated that the maximum width was produced during 'stick', just before 'slip' took place. This suggests that there was some normal movement of the stylus as sliding motion took place.

Finally in reviewing the papers included in this section some comments must be made on the general approaches made by the researchers.

1) Most experimental test rigs were small and the configuration of the sliding pair varied. (Types of sliding pairs are well documented by Pavalescu (29)).

2) Most of the metals used were homogeneous in structure. Cast Iron gave very unpredicatable results and consequently little attention has been paid to this material.

3) It has been possible to use many sophisticated measuring techniques and instrumentation due to small specimen size. An interesting review of some equipment is given by Quinn (40).

4) Many of the experimental results have led to derivationsof empirical formulae, coefficients included having no relationship with physical laws. This has meant that the results cannot be generally applied in engineering practice.

2.4 FRICTION STUDIES ON MACHINE TOOL SLIDEWAYS

The analysis of friction phenomena on machine tool cast iron slideways has generally been undertaken by mechanical engineers. This fact alone has produced experimentaldata and theories which are very much related to the

mechanics of the overall system and the friction ideas of the physicists have never been fully exploited. This does not mean to say that the general observations detailed by engineers differ from those of other friction researchers.

Major studies into slideway friction started in the early 1960's and have been largely confined to investigations into oscillatory motion at low sliding speeds. As the experimental equipment was large, there were restrictions on the types of instrumentation useful for recording and analysis. This has meant that mathematical descriptions have been orientated towards basic mechanical analysis and the establishing of empirical relationships. Nevertheless new ideas have emerged which are pertinent, not only to this thesis work, but to machine tool slideway studies in general.

Matsuzaki et al (41) (42) made an analysis of stick-slip motion on an hydraulically driven slideway mechanism. They recorded the position and velocity of the moving slide and also the positional error between the input command and the output. Subsequent analysis similar to that of Brockley (21) led to the conclusion that the oscillatory motion was characterised primarily by the drive stiffness and the steady-static friction/velocity relationship of the sliding surfaces. Similar findings were reported by Steward and Hunt (43) who made an extensive study of stick-slip. Some of their graphical data resembles that by Rabinowicz (12). In developing their analysis they state that friction force is very much related to the slideway lubrication conditions. The variation of friction with time and velocity is related to a squeezing action of the lubricant between the rough surfaces. Lubricant polar additives are shown to reduce the friction forces by supporting part of the load and a squeeze film time constant is suggested; this being dependent upon the amount of these additives, load pressures

and surface topography. It was noted that the critical velocity was determined as the velocity which made the 'stick' time zero (as Derjaguin et al (19)).

A precise definition of critical velocity was not forthcoming until the publications by Bell and Burdekin (44) (45) (46) of experimental works on slideways. Again the slideway was hydraulically driven but the drive stiffness was dependent upon the size of a mechanical spring, which could easily be varied. A very interesting instrumentation arrangement (26) enabled the term ($M\ddot{x}_o + K(x_i - x_o)$) to be extracted and was called the dynamic friction force; which represented the friction in the system at any particular instant of time during sliding motion. A recorded phase-plane of dynamic friction force against table velocity was used to determine a dynamic damping coefficient (Cs) where

$$Cs = \frac{\text{Max. friction force} - \text{friction force at max. velocity}}{\text{Maximum velocity} - \text{velocity at max. friction force}} \quad - 33.2$$

Cs was determined for various input velocities, enabling a graph to be constructed. This was done for various values of drive stiffness. It was suggested that stable motion occurs when the value of Cs is positive and the critical velocity was defined as the value of input when (Cs + Cd) was zero. (The term Cd was defined as the equivalent linear damping term, which is always positive). For negative values of (Cs + Cd) oscillations will occur. Their curves indicate that, at certain drive frequencies, Cs is initially positive and becomes negative over some small range of velocities. This suggests that by using the same criterion as above, a lower critical velocity could be established and therefore oscillations would occur between two intermediate sliding speeds. It is stated that Cs is dependent upon the system natural frequency and the viscosity of the lubricant.

Further experimental work attempted to relate the friction force at zero velocity to the separation of the sliding surface and their results do correspond to the work carried out under very different conditions, by Tolstoi (38). As the surface separation increases the friction force reduces. It is assumed that this reduction is attributed to the decrease in actual contact area and it is argued that as the steady state friction falls with increased velocity the contact area, causing 'solid' friction, also reduces. Thus total friction force was made up of two components, one related to metallic interaction and the other to the shearing of the boundary and viscous films. The steady-state friction/velocity characteristics were influenced by lubricant viscosity and the addition of polar hydrocarbons.

In general, the work of Bell and Burdekin suggests that the dynamic conditions should be studied in order to obtain meaningful solutions to friction problems.

Britton and Bell (47) investigated several machine tool drive parameters in order to establish design criteria for the stability of sliding motion. They were interested in relating these parameters (mass, stiffness and lubricant viscosity) to the magnitude of the critical velocity. An original display technique was used, by plotting table velocity against the ramp command velocity signal. This velocity profile illustrated the complete history of oscillatory motion and a typical plot is shown in Fig.2.3 The profiles do depend upon the parameter combinations, and do show that both 'stick-slip' and quasi-harmonic conditions exist on machine tool slideways.

A number of researchers have suggested that stable sliding conditions can be accomplished by the correct selection of the system parameters. Other authors have attempted to prevent stick-slip by other means. Matsuzaki (48) used acceleration feedback effectively in a hydraulic drive system and Lenkiewicz (49) has experimented with external vibrations forced

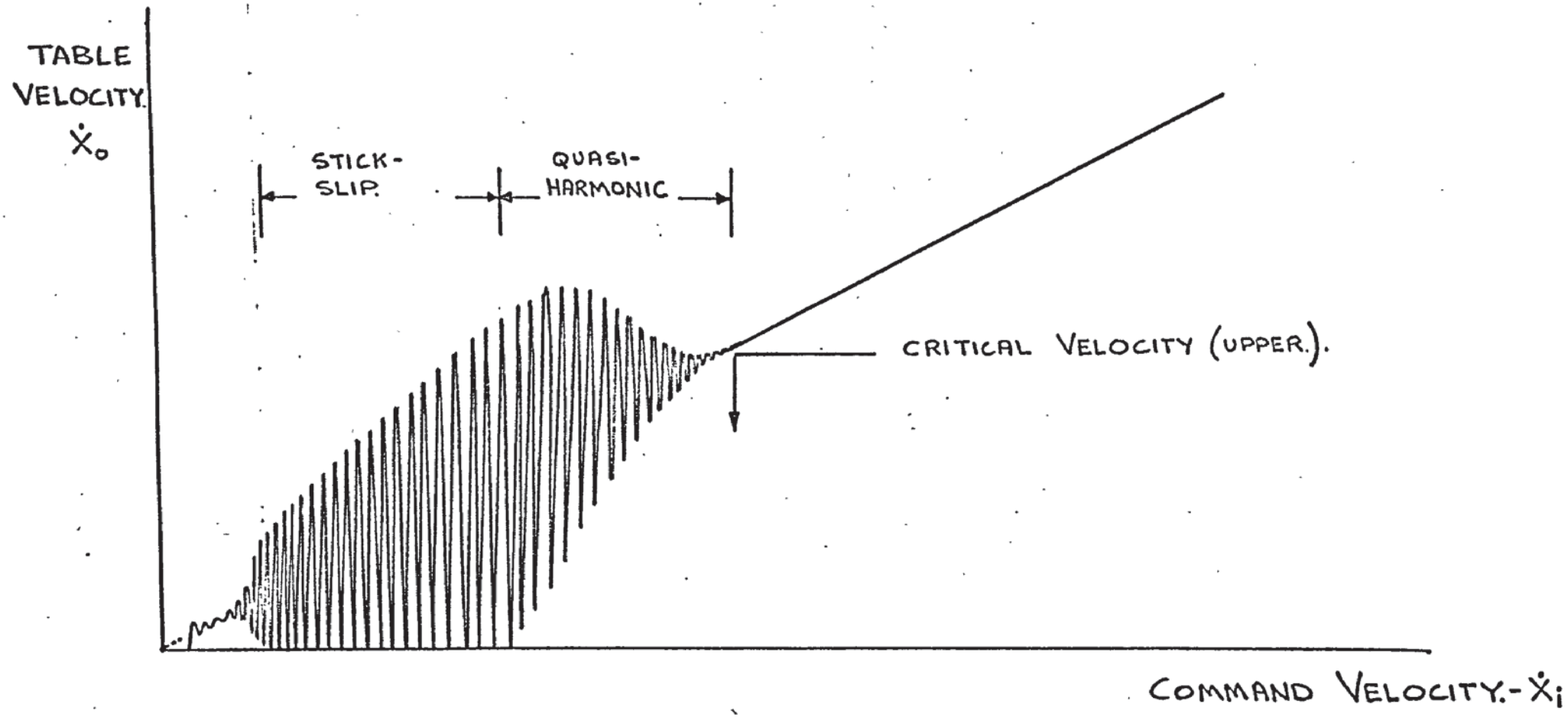

FIG. 2·3. A SYSTEM VELOCITY PROFILE.

normal to the sliding plane. These vibrations were more effective at low sliding speeds when only small amplitudes and low powers were required to effect quite dramatic reductions in friction force. (Similar observations were made by Tolstoi (38))It was suggested that a frequency of 100 H_z gave optimum conditions.

A paper by Kato, Yamaguchi and Matsubayashi (50) shows a very similar philosophy of approach tothat of Bell et al. (44) in that during 'slip' the equation of motion for the table was,

$$M\ddot{x}o = K(x_i - x_o) - F \qquad - 34.2$$

hence

$$F = K(x_i - x_o) - M\ddot{x}o \qquad - 35.2$$

and is the total system friction force. By obtaining plots of table displacement, velocity and acceleration against time, they were able to use the above relationship to obtain the friction coefficient/velocity curve. Their equation for the critical velocity was given by,

$$Vc = \frac{2W}{\pi\sqrt{KM}}.(\mu_s - \mu_d).\left(1 - e^{-a\left(\frac{\pi}{\omega n}\right)^m}\right).\left(1 - e^{-b\left(\frac{\pi}{\omega n}\right)^n}\right) \qquad - 36.2$$

where μ_d = the static friction coefficient when 'stick' time tends to zero, and a, b, m and n are coefficient dependent upon the surface lubricant.

It can be seen from the above equation that as the drive natural frequency increases the critical velocity reduces. Many other factors are involved but these are obscured by the empirical relationships, especially those appertaining to the lubricant.

A following paper by Kato et al (51) makes a very good attempt to bring together the ideas and theories of friction researchers (section 2.3 of this chapter) and their own experimental results. Unfortunately the presentation of so many empirical relationships has rather confused their

findings and conclusions, and as a result no fresh arguments are proposed.

It can be seen from this review that very little analytical work has been put forward which will aid the engineer. The following general comments can however be made.

a) Most of the friction theories used by the authors were propounded at least six years earlier, (by physicists), indicating a large time lag between the work of the physicist and the engineer.

b) In order to calculate the critical velocities for a particular system, the system itself must exhibit oscillatory motion in order to provide the necessary data required to establish these velocities.

c) The work of Bell et al (44 - 46) has provided the most useful information, but it would require a very long time to collect data related to all known parameters that effect the friction and the stability of sliding motion.

d) The effects of surface topography, its changes and other surface contaminants such as debris and oxide have not been fully considered.

e) Only simple instrumentation has been used to record basic experimental data, such as velocity, acceleration and displacement. This is due to the large size of the test apparatus. Sophisticated techniques have been attempted by Bell and Burdekin (44) but have required extreme care in setting-up and interpretation of the results. This makes them unsuitable for use in a general engineering enviroment.

f) Most friction problems have been partially solved, by engineers, using empirical formulae. In the majority of cases these have proved satisfactory.

2.5 COMPUTER SIMULATIONS OF FRICTION BEHAVIOUR

The engineers had great difficulties in analysing and predicting slideway performance due to the large number of parameters affecting the

friction conditions. In carrying out experimental studies it was virtually impossible to separate and analyse individually these known variables.

The use of small mechanical models by friction researchers were, in effect, simulations of more practical systems, and they had the advantage of being able to demonstrate the influence of individual parameters. In a practical situation the interaction of these variables is a most important factor. Therefore, with the advent of the electronic computer engineers found a tool that could simulate a more viable,realistic model of a practical system. The greatest difficulty in using analogue or digital simulation is the ability to describe a system in mathematical terms. Several authors have attempted this, mainly using the analogue computer.

Singh (52) made a study of stick-slip motion and particularly the influence of friction variables on the critical velocity of sliding. His mathematical model was that originally developed by Derjaguin et al (19). Experimental results were compared with the simulation values and those obtained from an analysis of the system equation of motion. As expected the theoretical and simulation results gave very good correlation and both indicated the same trends as the experimental values when subject to various parameter changes. Unfortunately, the analogue simulation circuit was not a very good representation of the physical system. This is partially due to the interpretation given of the mathemetical equation and a lack of understanding of the operation and use of the computer system itself. The simulation was incapable of exhibiting the usual oscillatory trends with respect to displacement, velocity and acceleration, which have been recorded on many physical systems.

The digital computer was used to obtain a numerical solution by Banerjee (53) for a similar study of stick-slip. His equation of motion was similar to that of Singh (52) but modified to include a mathematical

description of the friction force/velocity plot. His approach was influenced by the work of Brockley et al (21). The analytical procedures led to the generation of two equations relating the critical velocity to the system variables. As they needed to be simultaneously satisfied a programme was developed. Using an iterative technique, changes in the critical velocity were computed. The results indicated that the shape of the friction/velocity characteristic affected the value of the critical velocity, which reduced as the characteristic became shallower. It was intimated that this characteristic change would be brought about by using lubricants containing polar additives.

The most interesting computer simulation was carried out by Nakashima, Takata and Morita (54) again using the analogue computer. Their general equation of a machine tool slideway is of the form,

$$M\ddot{x} + K(x - vt) = -F \qquad - 37.2$$

where,

M = sliding mass
K = drive stiffness
v = command velocity
x = slider displacement
F = Friction force

The expression for the friction force (F) was based on a good understanding of modern experimental results obtained from slideway analysis. Consideration was taken of surface topography, asperity deformation and the squeeze film effect created by the lubricant. The friction/velocity relationship was of the form,

$$\Delta F = W.\frac{a.bo}{s + bo} \times \Delta\dot{x} + To.\Delta\dot{x} \qquad - 38.2$$

where W = weight of slider

$\frac{a.bo}{s + bo}$ = a first order Laplace equation (in operator s) which governs the rate of change of friction force to velocity, and load. The coefficients a and bo are related to elastic deformation of asperities and the lubricant squeeze - film effect for a given contact area.

To = equivalent linear friction coefficient dependent on the shearing of lubricant and asperity junctions

ΔF = small change in friction force

$\Delta \dot{x}$ = small change in slider velocity

They suggest that the main physical factors in formulating a friction/velocity relationship are the properties of the lubricant, characteristics of the surfaces and the slider weight.

This simulation included the generation of several non-linearities related to their friction/velocity characteristic. An interesting decomposition of this characteristic was undertaken in order to use the available computer generating functions. A complete simulation circuit was produced which, although rather complex, did appear to be a very good representation of the physical system. This point is emphasised since the various recordings taken from the simulation are in very good agreement with some produced experimentally by Bell and Burdekin (46). It is acknowledged by the authors that as some empirical formulae have, by necessity, been used, their coefficients can be given some satisfactory values. It is stated that these coefficient values have, as yet, no clear relationship with the physical factors of their slideway system.

One of the most interesting and new observations made by Nakashima et al was that stable motion occurred in the range of the falling steady-state friction/velocity curve. It is suggested that this is due to a change in friction regimes, one being dynamic when stick-slip takes place and the other being steady state when stable motion exists.

This paper is very encouraging and suggests some basic principles which may need consideration by other researchers when contemplating a simulation analysis. These could be summarized as follows,

1) A thorough understanding of the computer system, especially with regard to its facilities and its programming capabilities.

s) A clear insight into the working of the physical system and the effect of known parameters on its steady state and dynamic performance.

3) The physical system must be capable of being described by relevant mathematical equations which are suitable for the purpose of simulation.

2.6 CONCLUSIONS.

This survey has reviewed the studies into the nature of sliding friction and its affects on the performance of slideway motion.

The experimental work on friction has increased enormously over the past thirty years and this is due to the following factors,

a) A desire to understand the nature of friction and the influencing effect of single variables.

b) The demands of the engineering industry for basic facts in order to solve their friction problems.

c) Rapid advances in the growth of suitable instrumentation.

It is interesting to note that the basic ideas conceived by Amontons, Coulomb and Morin (1) have not been totally neglected and still form part of the foundation upon which friction concepts have been later developed. The relationship $F = \mu W$, although regarded as a 'classic' law, still remains valid. The coefficient μ has received much attention in modern times and its variation with physical quantities forms the basis of advanced experimental study.

It is unfortunate that this simple law has only two measurable quantities, the friction force (F) and the sliding weight (W), so that the experimental apparatus was always designed to measure (F), the weight or load being a predetermined measured value. In most cases the measurement of (F) was done indirectly, by measuring the deflection of a calibrated mechanical spring, which was connected to the slider.

This spring force was equivalent to the friction force, under stable system regimes, i.e. static and smooth sliding conditions. When the slider exhibited oscillatory motion the equilibrium equation of forces included an acceleration term thus,

Spring force = Friction force + acceleration force

Therefore the measurement of (F) was rather more complicated in a dynamic system regime and called for other measuring techniques.

The friction force (F) is influenced by many physical parameters and several theories have been proposed, the most widely accepted basic concepts stemming from the work of Bowden and Tabor (2).

In friction experiments stick-slip provided a useful, inherent, condition within most systems which enabled studies of changes in friction force to be carried out. On the other hand, it is a phenomenon that the engineering industry felt must be eliminated, in particular with regard to the sliding motions in sophisticated machine tools.

Experimental analysis of machine tool slideways has revealed similar results to those carried out on small friction rigs. In particular that stick-slip or other oscillatory motion is governed by the changes in friction force, especially with sliding velocity. As most of the parameters that affected friction force had been established, theories regarding the reduction and elimination of stick-slip were produced, together with relationships between the critical velocity and the system's mechanical properties.

Complete theoretical analysis of oscillatory motion has not been satisfactory due to the complexities of the mathematical equations, which contain non-linear descriptions for some of the variables. The analysis that has been done made use of linearised equations and did indicate the same general trends as established experimentally.

The technique of using these non-linear equations, as a basis for computer simulation, is still in its infancy. Analogue computers have been used for most simulation work because the generating of non-linear relationships is easier. The most encouraging work was produced by Hakashima et al (54) and a good correlation was indicated between the recordings taken from a physical system and those produced by the electronic analogue. This also gave rise to new ideas and fresh thoughts concerning the nature of sliding friction.

CHAPTER 3

A PHILOSOPHY FOR AN ANALYTICAL STUDY OF NON-LINEAR FRICTION BEHAVIOUR (BETWEEN PLAIN C.I. SLIDEWAYS).

3.1 THE DEVELOPMENT OF A SYSTEM

An engineer usually studies one discipline within the field of engineering. This is done not only with a view to analysing the various ideas embraced by the discipline, but to develop his understanding of their interelationships and cultivate his ability to accurately assess and consequently solve engineering problems. The question of assessing a problem is of prime importance, and through industrial practice the engineer will develop his own individual techniques for doing this. In general it can be said that he may use different methods of assessment for different problems encountered within his discipline, and this may lead to an unawareness of relationships between seemingly unrelated problems. This fact can be overcome by adopting a basic philosophy. A framework for such a philosophy lies within the fundamental concepts of Control Engineering.

The study of control systems has developed over the last forty years and started with the analysis of electrical circuitry. The methodology created by these electrical engineers was quickly taken up by mechanical engineers as an aid to solving military problems during the Second World War. Since that time most technological disciplines have adopted and modified the concept which has continued to spread into management, science and medical fields, where the study is generally known as cybernetics. This indicates that control concepts have an underlying philosophy which can be readily understood and appreciated by everyone and enhances the solvability of problems.

The key to the philosophy is the word 'system'. Any two or more items capable of maintaining a relationship can be classed as a system and interaction between any of these items will give rise to a system response. This means that the size of a system is wide ranging, from atomic to galactic and beyond. In assessing a problem, prior to an attempted solution, it must be related to a system. It is most important that all the items or parts of a system are taken into account, which means that some parts themselves may be classed as sub-systems. Each part will have a unique description and, from an analytical point of view, must be capable of mathematical expression.

The control methodology entails arranging all the items in an order governed by their inter relationships. This is usually done illustratively in the form of a flow diagram or block diagram. It can be very difficult to establish the flow diagram since it requires an intimate knowledge of the physical system; but once achieved, analysis can be attempted using control theory. The general concept itself can be expressed as a flow diagram as shown in Fig 3.1

This diagram illustrates a fundamental philosophy which can be applied to any study and it should be noted that it is a continuous closed loop. It is suggested that most experimental and analytical studies that are carried out conform to only part of the whole and hence can be classed as open-loop. This means that the complete understanding of a particular problem can never be achieved.

It can be said that a control system philosophy provides an understanding of the behaviour of things and leads to a better appreciation and utilisation of the fundamental laws of nature. It makes us look into the working of a problem in such a way as to make us recognise those workings.

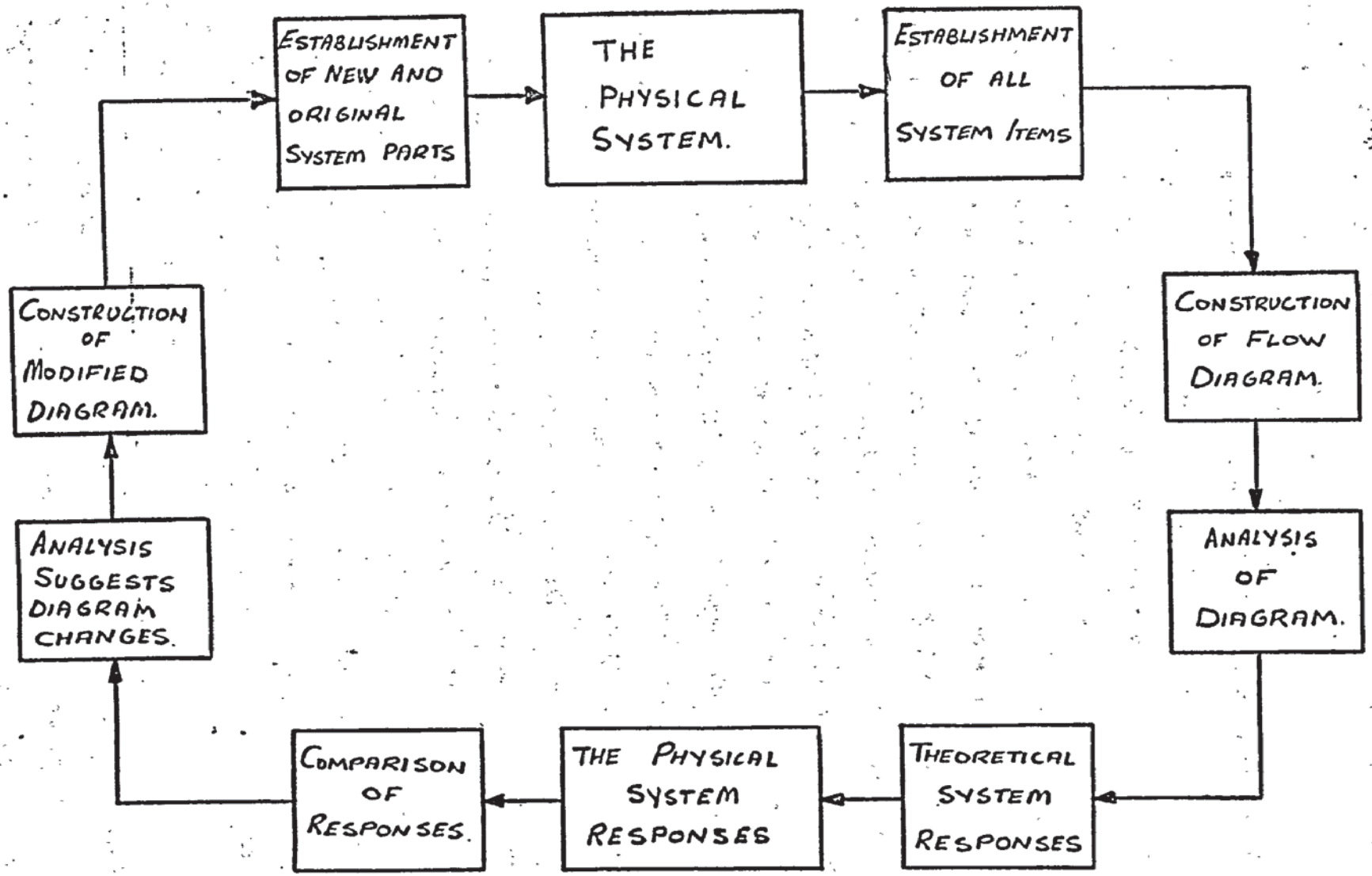

FIG. 3·1. A FUNDAMENTAL SYSTEM OF ANALYSIS.

In this thesis, the development of a system is based upon the concepts outlined above. As Wittgenstein (55) pointed out, problems can be solved, not by giving new information but by arranging in some logical manner what we have always known.

The starting point in this study is the requirement for good and reliable recorded data of non-linear friction behaviour, not necessarily related to machine tool slideways. Fortunately a great deal of material has been published. The exact known behaviour of a particular system is reproduced by an artificially created one, which will then be the analogue of the physical system. This is most easily done using an Analogue Computer where the analogue simulation is a collection of electronic circuits. An attempt is then made to relate parts of the circuitry to the known items within the actual systems. The cross-correlation will provide the build up of a picture, indicating the necessary inter-relationships required in order to produce the physical behaviour patterns. A mathematical description of the various unique activities can be attributed to certain collections of the items within the actual system, and compared with information gained by other researches. This continual inter-change will lead to the development of an analogue system which is truly consistent with its physical counterpart. An analytical study is then made of this simulation, using control theory techniques, which should reveal the best possible solutions to this thesis problem. A simulation of this sort often suggests new ideas for further experimental study, which will not only provide some verification of a particular theory, but enable the simulation to be up-dated.

The ultimate solution to any problem requires continual perseverance, and the ability to perceive fresh avenues of research is one of the rewards obtainable by using the control system concept.

3.2 A SIMULATION OF THE SYSTEM

The simulation provides ideas useful for an analytical study. The results of this depend upon the modelling concepts of the items within the system. These concepts are derived from initial studies of the simulation and subsequent experimental work, they are tested for their validity and then used to produce a better simulation. The question of validity is very subjective and is entirely dependent upon the considered judgement of the researcher, who has some knowledge and experience of the problem.

The remaining chapters of this research then follow a logical sequence of model concepts, construction of simulation circuits and theoretical analysis. It is felt that mention should be made of the system simulation since it is part of the basic philosophy and needs an initial introduction.

The overall system is that of a machine tool slideway, within which certain sliding phenomena occur that have been attributed to the variations of friction. An initial premise is made that, within this system, an equilibrium of forces is always maintained during static and dynamic conditions. A basic flow diagram can be constructed and is shown in Fig. 3.2 and from this a simulation circuit suitable for construction on an analogue computer is derived. Subsequent recordings of changes in some system variables are compared with the same variable changes recorded on an actual physical system. (The experimental work of Bell et al (45) (47) has proved most useful). This of course is an acid test which is demanded and accepted by all engineers.

The author is of the opinion that the best illustrative record of sliding velocity changes is that produced by plotting the output

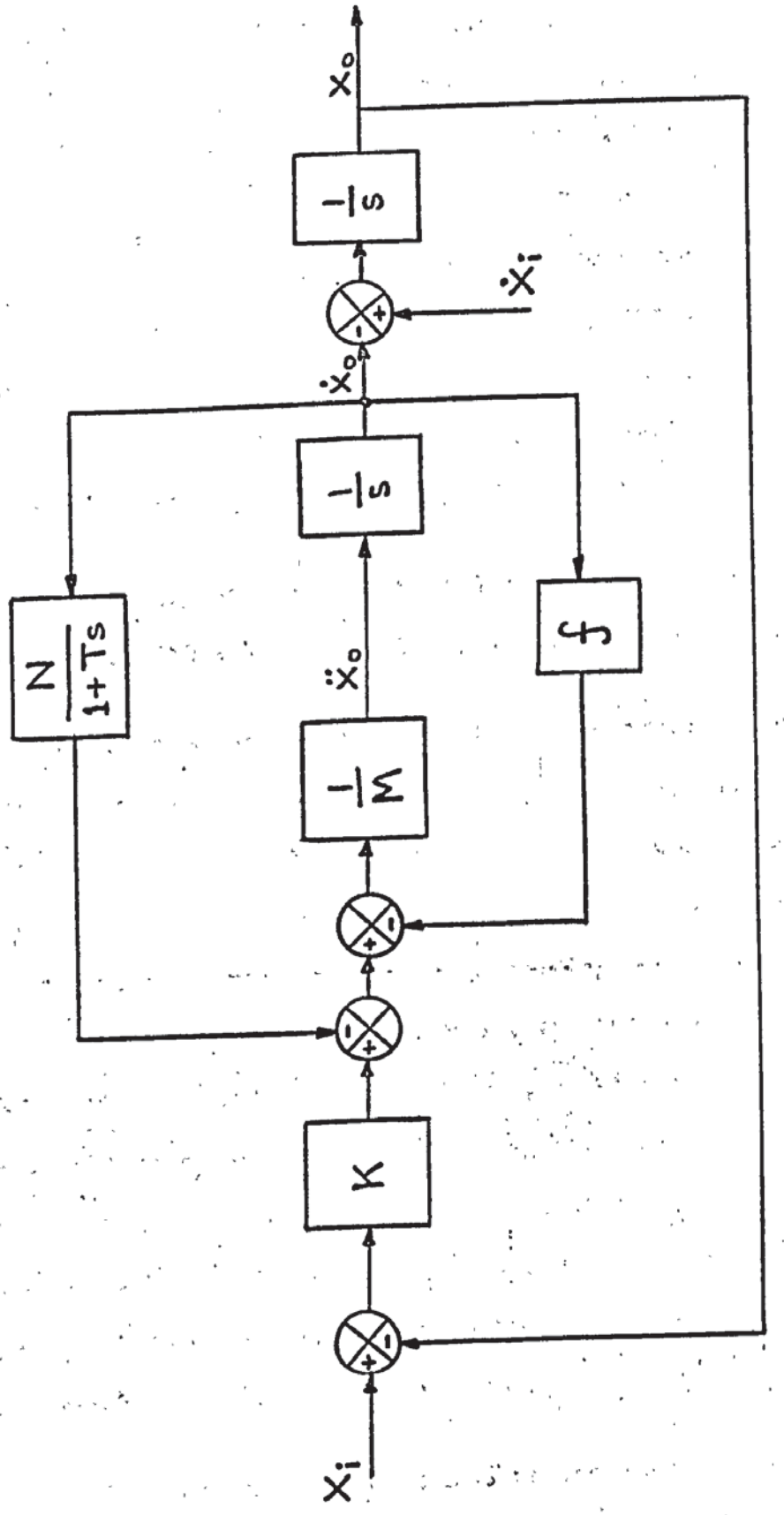

FIG. 3.2. A SIMULATION BLOCK DIAGRAM.

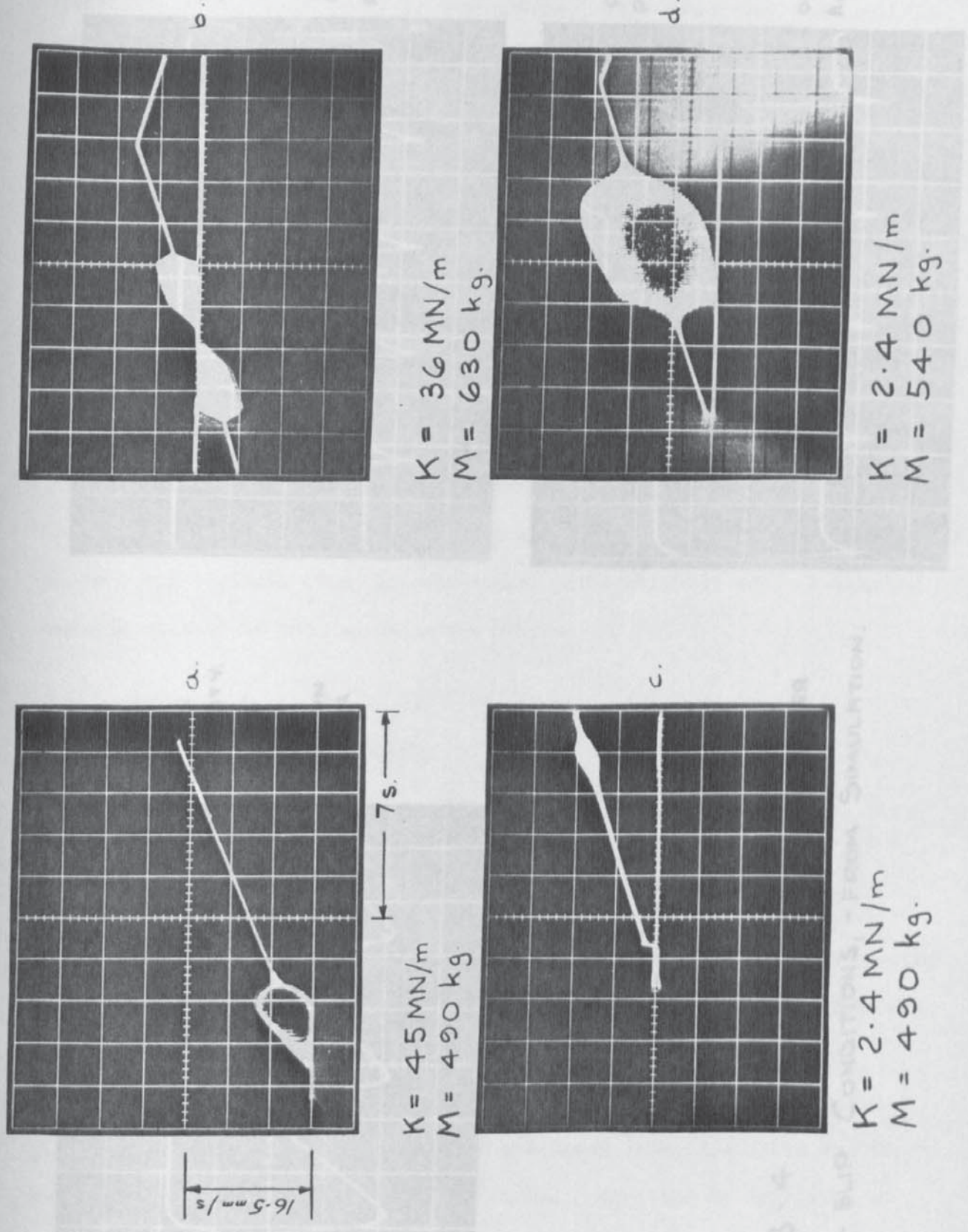

FIG. 3·3 SIMULATION RECORDINGS OF S.V.P.

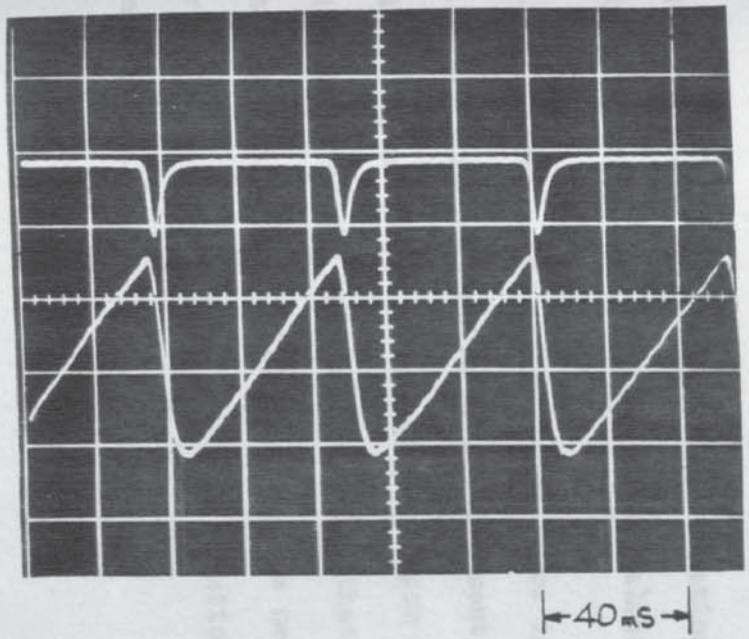

$K = 45 MN/m$
$M = 490 kg.$
$\dot{x}_i = 0.127 \ mm/s.$

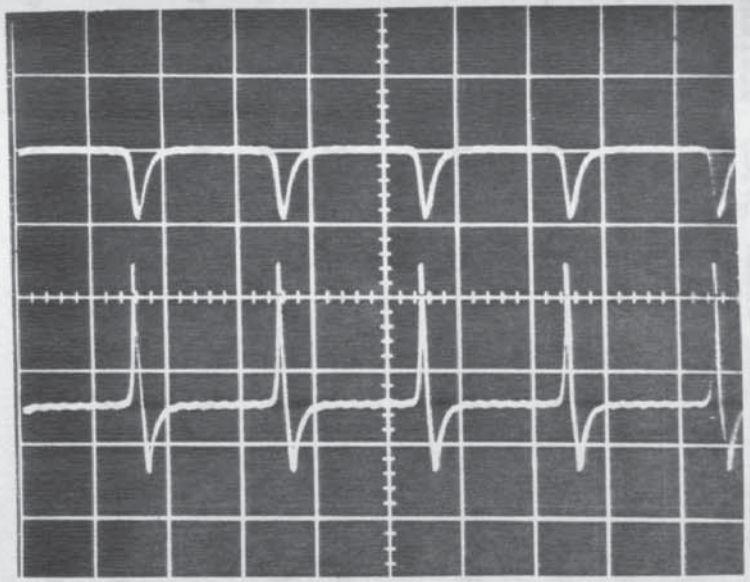

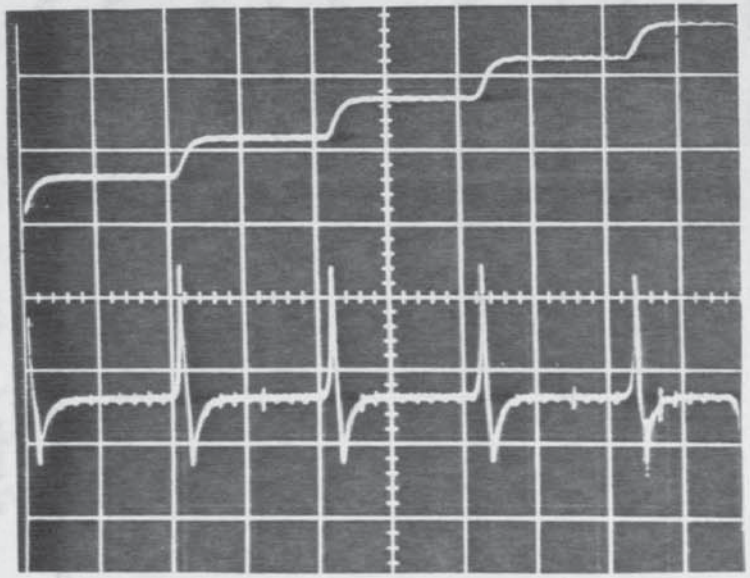

FIG. 3·4 SYSTEM RESPONSES UNDER STICK-SLIP CONDITIONS, - FROM SIMULATION.

philosophy, throughout this work, to reduce this circuitry as much as possible using basic computer components. This has meant that modifications, through constant surveillance, have been carefully undertaken in order to produce the desired, final circuit. An approach such as this can be easily neglected when one becomes involved in simulation studies.

3.3 SIMULATION REQUIREMENTS IN ORDER TO FULFILL AN ANALYTICAL CONCEPT.

It is fortunate that simulation work can, in itself, be regarded as a reversible process. It is part of a closed loop analytical system, the flow diagram of which is shown in Fig. 3.5

It is usual practice to establish a simulation circuit based upon mathematical expressions for the system. These equations may contain parts which indicate time dependence and parts which do not. A simple example related to this study is as follows,

$$\text{Friction Force } (F) = \mu W \qquad - 1.3$$

$$\text{Friction Force } (F) = \frac{Md^2x}{dt^2} + Kx \qquad - 2.3$$

Equation 1.3 is a 'steady state' relationship whilst equation 2.3 is a 'dynamic' relationship. For fixed values of weight (W), mass (M) and drive stiffness (K) the friction force is dependent upon μ from equation 1.3, and some derivative of displacement (x) in equation 2.3. Therefore it is logical that μ is dependent upon some derivative of (x). A simulation of the above equations, that can also reproduce established physical phenomena, will indicate the necessary interdependence and thus provide an insight into the real relationship that can be expressed mathematically.

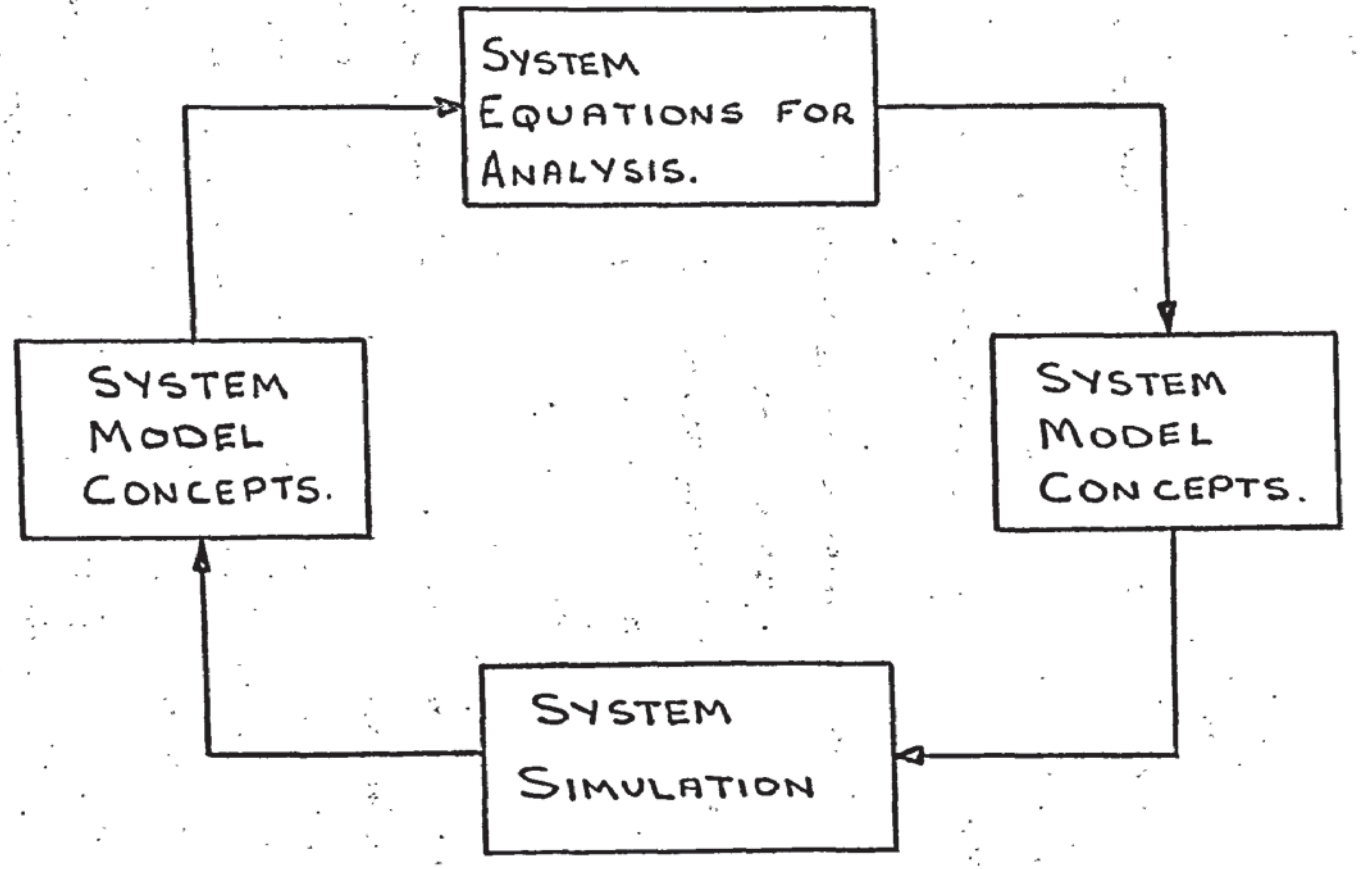

FIG. 3·5. AN ANALYTICAL SYSTEM USING SIMULATION.

This example shows that the logical entry into the closed loop system shown in Fig. (3.5) is by having some physical model concepts, based upon an understanding of the real situation. It means that a simulation will require some initial data, in order to be created. This should be kept as simple as possible until a useful man-machine relationship is established. Further information and modifications can then be undertaken as required by the simulation.

In this work, the simulation requirements have been fully developed but their basic forms can be listed in the following order,

1) An understanding of the workings of a slideway system in order to establish the main physical quantities which govern its normal linear behaviour.

2) A mathematical expression relating these physical quantities. In this case, a system characteristic equation which is linear, time dependent and governed by an equilibrium force condition.

3) The production of a flow diagram designed to illustrate the mathematical equation. From such, the simulation circuit layout can be made.

It is very important to note that in order to start and consequently pursue a system analysis an initial decision must be made as to the nature of the equilibrium quantity. (In the limiting condition it is thought that this will be either force or energy). This quantity must be maintained throughtout an investigation. Subsequent comparisons between actual and theoretical results may decide the validity of this initial selection.

4) Variances within comparable results will indicate that the linear equation is not complete. Consequently, modification to the simulation will be required, thus changing the form of the system equation.

5) Other known factors considered likely to affect the system behaviour are reviewed. They must have some relationship to the physical quantities already embodied within the simulation in order to make the circuit changes possible.

The analogue simulation is modified, using these other factors, in order to produce a closer correlation between the theoretical and actual results. If this is achieved a mathematical representation of the circuit can be attempted and subsequently related to the physical system. Therefore, the overall system concepts can be evaluated.

If discrepancies are still apparent and judged to warrant further analysis, still further variations in the computer circuitry could be made.

6) The researcher must have confidence in the computer and his own philosophy, which will enable him to make logical, intuitive modification to the simulation. He is part of the simulation system.

This point is important to understand since a man-machine relationship through experience, familiarity and respect, can produce a creative unit. Once the researcher understands that creative thoughts can be interpreted through simulation work, he will be able to analyse the true nature of the problem.

CHAPTER 4

MACHINE TOOL SLIDEWAYS

4.1 INTRODUCTION

Man has always developed and used tools to try and improve his living standards and his skills. He invented machines in order to provide extra power that was anatomically lacking. The demand for his skills created the machine tool which further used this power, enabling him to maintain a supply of manufactured goods.

The foundations for a machine tool industry were laid during the Industrial Revolution, and it grew to be an important factor in our national economy. To-day, machine tools make nearly everything we materially possess. They are worked extremely hard and now embody a great deal of research and development work. This has meant that sophisticated machines now have the skills we ourselves once possessed, and have led us to an age of automation.

This thesis is associated with machine tools that are intended to produce durable useful goods and in particular those used to shape metal by means of a cutting process. All these machines have parts which move relative to one another, either by rolling or sliding, and an important group are classed as slideways. They are usually designed to have unidirectional movement and facilitate the transportation of either the cutting tools, the work piece or both. These sliding joints affect the overall performance of a machine, that is, its ability to produce the desired components. It is not possible to eliminate slideways on metal cutting machine tools.

Friction and wear have always been considered as being two of the several factors involved in the design of slideways. With the advent of totally automated machines these factors need a more serious appraisal in order to ensure that satisfactory machine operations can be predicted and controlled. In this context, it is considered that friction is the overriding factor as it can affect the slideway performance and cause the machine tool to exhibit undesirable behaviour at any time throughout its working life.

4.2 THE CONFIGURATION OF SLIDING SURFACES

The design of slideways has developed slowly; the main considerations being those of a mechanical nature. Some of these are listed below.

1) The ability to produce single degree of freedom movement.

2) To adequately support the moving load.

3) To ensure correct alignment between tool and workpiece.

4) The provision of sufficient movement in the direction of motion.

5) To allow the operator adequate access for cleaning, maintenance and setting up operations.

6) To ensure economic use of space and materials.

In the author's experience, little regard was paid to friction and wear. This can be explained by the following observations,

a) Most machine tools were hand operated.

b) The slideway surfaces were made of cast iron.

c) A skilled toolsetter could ensure correct manufacture of a product, compensating for any small misalignments due to wear by his knowledge of the machine.

d) Refurbishing of machine slideways occurred after many years of service.

e) The power available to the slideways via a drive system, e.g. lead screws, was very generous.

f) Many components were made using jigs and fixtures, depressing the effect of machine discrepancies.

It was not until the advent of numerically controlled machines and later sequence control machines that due consideration was given to the effects of friction and wear. These sophisticated machines incorporated the operator skills and their control systems needed to ensure the correct manufacture of components. Therefore, the designer needed to look deeply into the workings of the machine and to have an understanding, which once belonged to the operator. This has not meant great changes in slideway configuration, although manufacturing tolerances have been reduced.

A typical layout is shown in Fig. 4.1 and illustrates a section through a lathe slideway.

The table is mounted on the bed and contact is made between two plain flat surfaces. To ensure no vertical movement 'keep' strips are located beneath each side of the table and effectively sandwich the lathe bed slide. To prevent horizontal movement, normal to the axis of motion, a gib strip (sometimes more than one) is used. This is a long narrow wedge, normally screw adjusted, and is driven between the side of bed and the table. Once satisfactory sliding movement is accomplished all the strips are securely fixed. Small clearances remain between the bed and these strips, nominally in the order of 0.01 mm, and prevent seizure. They require adjustments throughout the working life of the machine.

The assembly and fitting of such a slideway arrangement does require skill and it is important to ensure a good surface contact between the table and bed and a high degree of flatness for all parts. This type of mechanical assembly is very popular with machine tool makers, mainly for economical reasons. The selection and design of sliding bearings has been studied in some detail over the past ten years, (56), (57), (58), (59),

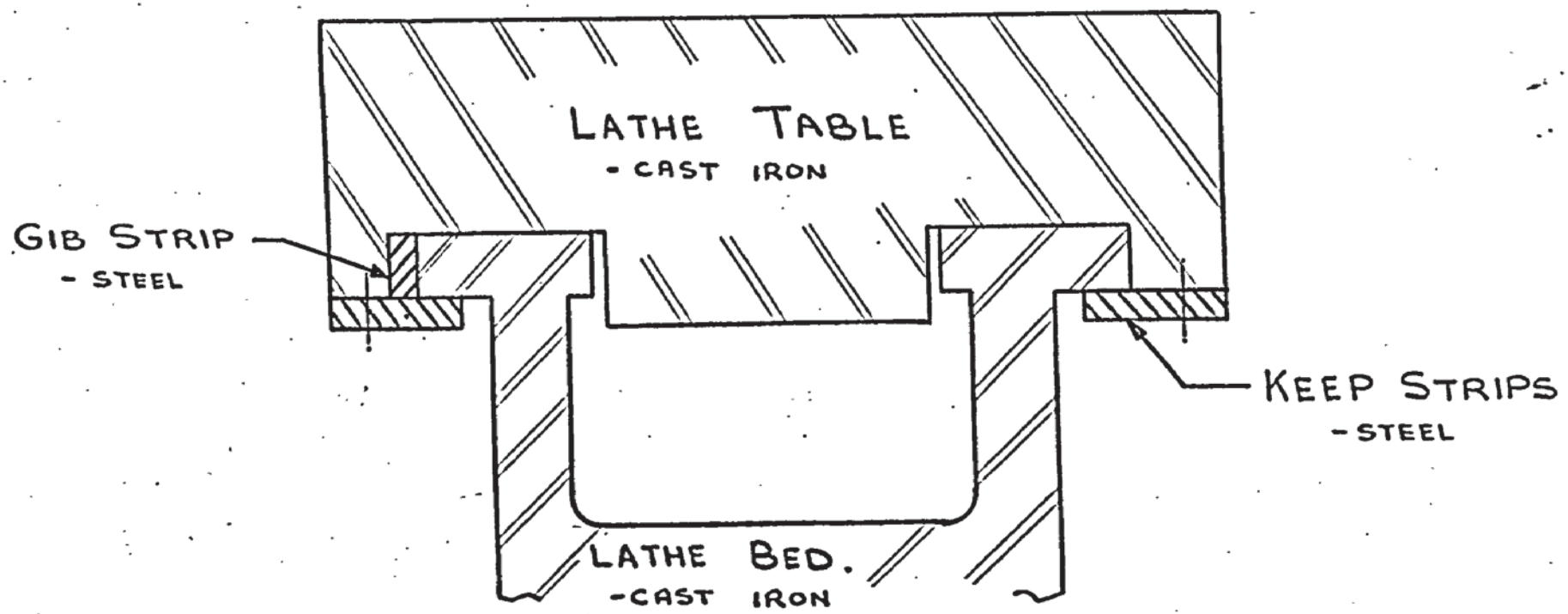

FIG. 4·1 A LATHE SLIDEWAY CONFIGURATION.

It is agreed that the best design can be proposed only after considering the particular working conditions under which the slideway has to perform, and making use of all relevant information and possible design aids.

Since 1964 other studies on this type of slideway have been undertaken (59) in areas such as frictional damping, wear and surface treatment and dynamic characteristics. (Friction studies are reviewed in chapter 2). This information can be used to obtain improved performance for automated machines, and to a lesser degree manual machines. The implementation is in the hands of the machine tool makers.

An important point to establish is that plain slideways are intended to have one axis of major movement, thus they are often described as having a single degree of freedom. In fact they have all six degrees of freedom, five being substantially restricted, in order to maintain some machine accuracy. These very small movements affect the static and dynamic behaviour of the sliding system. Therefore the term "normal degree of freedom" must be applied to a specific 'contacting' surface plane, which is parallel to the direction of the primary table movement. In most cases, researchers have considered a horizontal contacting plane between the lathe bed and table. Therefore any normal movement would be in a vertical direction. This, one other "degree of freedom" analysis does not produce a complete picture of possible table movement. An interesting paper by Kato et al (60) does investigate the pitching and yawing motion of a slideway table during sliding conditions which exhibit stick-slip.

This study shows that the table movements are dependent upon several factors.

a) Slideway configuration.

b) The flatness of contacting surfaces.

c) Clearances between nominally contacting surfaces.

d) Friction between sliding surfaces.

e) The position of the point of application of table driving force.

f) Viscosity of slideway lubricant.

These factors are considered relevant to this thesis and furthermore it is proposed that the nature of these small displacements arises from the accumulative effect of three possible inter-related movements due to

1) The slideway kinematics.

2) The result of slideway friction.

e) The stiffness between contacting surfaces.

This means that it would be difficult to measure the magnitude of normal displacements associated solely with changes in slideway friction. (The friction studies by Tolstoi (38) would not show satisfactory correlation using machine tool slideways).

Kato et al (60) illustrate clearly that although there is an optimum table driving position which substantially reduces pitching and yawing motion, the amplitude and frequency of friction force oscillations during stick-slip do not appear to be affected by a particular drive position requirement. This would indicate that the main displacement contribution, on their slideway arrangement, is attributable to the slideway kinematics.

For the purposes of this work a slideway configuration as shown in Fig. 4.1 will be considered. In doing so, the following comments should be made,

a) The sliding motion of the table is along the two horizontal bed guideways.

b) The major contacting surface is the horizontal plane between the table and the bed.

c) The greatest normal movement of the table is in a vertical direction.

d) The contacting surfaces constitute boundaries of cast iron bodies and are described as geometrically plain.

e) The weight of the table constitutes the primary loading force responsible for contact between sliding surfaces.

f) The keep strips, and particularly the gib strip, do not move relative to the table once they are set.

g) Slideway kinematics and table drive position are such as to prevent them contributing to table pitching and yawing.

4.3 LUBRICATION, FRICTION AND SURFACE TREATMENT

Economic considerations have influenced and sustained the use of cast iron as the major material for machine tool construction. Automatic controls have made demands for greater utilisation and work output in order to ensure cost effectiveness of machines. This has meant that for a given time period, greater sliding distances, faster sliding speeds and increased cutting forces are necessary in most cases. Therefore cast iron slideways must be made capable of coping with these developments. Studies into lubrication, friction and surface treatment of slideways have been undertaken with the main underlying purpose of maintaining cast iron as the basic construction material.

The introduction of a slideway lubricant does reduce both frictionand wear under given load conditions (5) (29) (45). In order to sustain this effect the oil must remain as a surface separating agent and be continually supplied. Additives within the base oil improve its capabilities of maintaining separation, even under thin film conditions (61) (62). Debris, such as cast iron particles and airborne contaminants, does affect the wear process (63) (64) and generally machine guideways

are cleaned by slideway wipers mounted on the moving table (65) or by covering the exposed areas (66). Entrained particles between the sliding surfaces can be difficult to remove unless sufficient oil supplies are maintained to provide a cleansing action (67). The drained lubricant requires filtering to remove any debris and some work has been carried out to develop a method of monitoring the amount of ferrous particles within a lubricating oil (68) to predict the wear condition between moving surfaces.

It has been shown that wear can be reduced by the hardening of the sliding surfaces (69). This is done by induction or flame hardening processes (70) giving hardening depths in the range of 0.5 to 2.0 mm. These are considered satisfactory for most applications and give hardness values of 400 - 500 Brinell as opposed to 200 Brinell for unhardened cast iron (71). Surface defects can arise with these processes in the form of surface pitting, cracking and deformation due to overheating of the surface. Even so, this process has become accepted by machine tool makers and is often highlighted in their sales literature (72).

In order to separate cast iron surfaces completely studies have been made into covering one of the slideway surfaces with a non-metallic material, usually plastic based. Reports (69) (73) indicate certain materials, which reduce both wear and friction, and are suitable for machine tools. It is stated that they do accommodate a certain amount of abuse, in that surface debris and irregularities can be absorbed by the softer plastic surface. Several manufacturers make use of slideways covered with bonded plastic material. These machines are usually bigger in size and handling capacity (74). The reduced friction level means that less power is used in moving the heavy slides about the machine.

Plastic covered slides usually require minimal lubrication and can be run in a dry condition.* Therefore their use on large machines can be further justified as complex lubrication systems will not be required. In situations where lubrication is difficult, such as vertical slideways and certain shaft bearings, a plastic interface can be used to effect. There are advantages in design, construction and cost.

Most machine tool makers favour hardened slides as against plastic covering and the following points are suggested as possible reasons for this.

1) Most machine tools are small, (would stand in a floor area of approximately 12 m^2).

2) Slideway lubrication systems have been developed and used for many years and are an accepted feature of the machine tool design.

3) Tolerable wear and friction characteristics can be maintained.

4) The working life of a cast iron slideway is satisfactory and the reclamation of such has always been possible.

5) Production methods, including processes of slideway renovation have been developed and standardised.

6) Manufacturers are reluctant to make changes since, over the years, customer satisfaction has been maintained (with regard to slideway design and function).

Further, the cost effectiveness of plastic coatings and other low friction devices for slideways and their consequential sales potential could be questioned in the light of the above comments.

It can be concluded that the increase in use of plastics on slideways will be very slow and limited to very large machines. This means that cast iron sliding surfaces will be a predominant feature of slideways for the forseeable future. Therefore the importance of lubricants and their interaction on sliding surfaces, to reduce friction and wear is a factor which requires constant attention.

* Lubrication is preferred

In order to introduce a friction concept into the slideway model, it is initially assumed that the friction force (F) is linearly related to sliding velocity (v) as shown in Fig. 4.2 a. The slope of this line will be the damping coefficient (f) and will be used in the basic slideway system transfer function for the purpose of the simulation This steady state linear description shows a positive quantity which is the resistance to motion. The literature survey indicates a more complex friction/velocity relationship in which this force always opposes motion and is therefore a positive resistance. It is important to note, especially for clarification, that the resistance or damping is always positive and therefore opposes the driving force. Within this overall concept it is known that the resistance can fall as sliding velocity increases and so the rate of change of resistance to motion can be negative. Thus,

$\frac{F}{v}$ - always positive

$\frac{dF}{dv}$ - can be positive, zero or negative

Therefore if a friction/velocity curve possesses a falling gradient portion, as shown in Fig. 4.2 b, it is not implied that the system has negative damping. If such a curve is differentiated as in Fig. 4.2 c then it is accepted that the rate of change of the damping quantity can be negative.

The reasons for this negative rate and its magnitude are key factors in the answer to non-linear friction behaviour and slideway system instability.

4.4 THE DRIVE SYSTEM

In order to move a sliding member along its guideways a driving force needs to be supplied. This input force is required to overcome

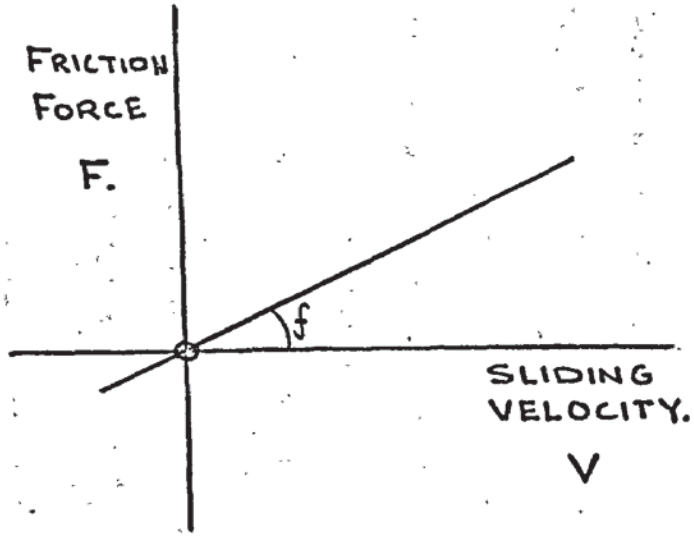

a) LINEAR FRICTION.

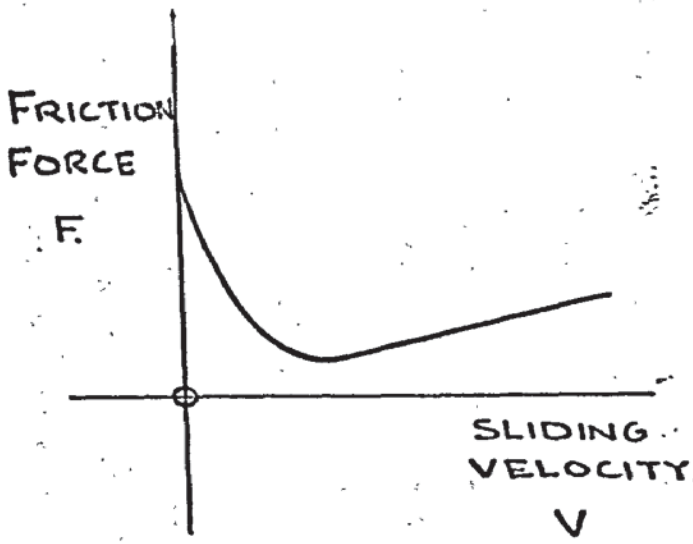

b) NON-LINEAR FRICTION

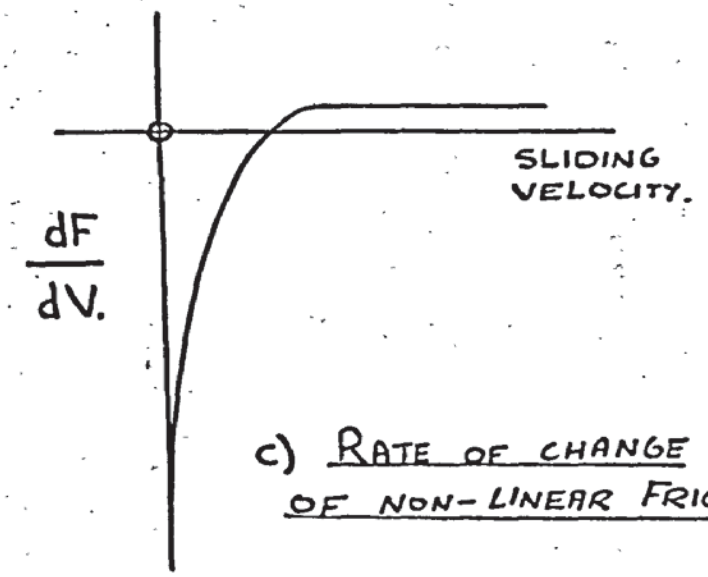

c) RATE OF CHANGE OF NON-LINEAR FRICTION.

FIG. 4·2. SOME SLIDEWAY FRICTION CHARACTERISTICS.

friction and cutting forces and provide accelerating/decelerating forces. The most popular types of mechanical drive involve the use of either a lead screw or an hydraulic cylinder. Typical arrangements of both are shown in Fig. 4.3

The lead screw is mounted along the bed of a slideway and is rotated by either electrical or hydraulic power usually via a gearbox. A nut on the lead screw is mounted in the sliding member and provides the transmission from rotary to linear force.

The hydraulic cylinder does not have such a complex machanical arrangement as it provides linear motion and force directly. The cylinder body can be mounted along the bed and the piston rod directly coupled to the slide. In order to conserve space it is sometimes convenient to mount the cylinder on the slide and therefore fix the piston rod to the machine bed.

It is important to note that the drive system function is primarily to supply a force to the slide table and is not intended to guide the table. This is done by the kinematics of the table and guide-way as shown in Fig. 4.1 . The drive system must supply a force which is precisely in the same direction as the sliding motion.

Although manual power has not been overlooked it is felt that it can be neglected here for the following reasons.

a) High forces are required by the table.

b) The increased use of automation has relieved the operator of this task .

c) Controlled feedrates need to be maintained .

d) There are positional demands placed upon the drive system as a consequence of automation .

A drive system is the mechanical link between the bed and the

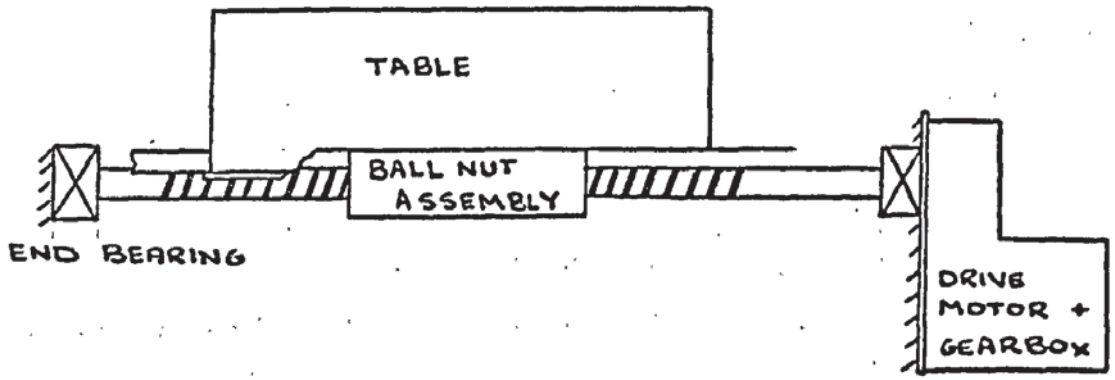

a) LEADSCREW DRIVE.

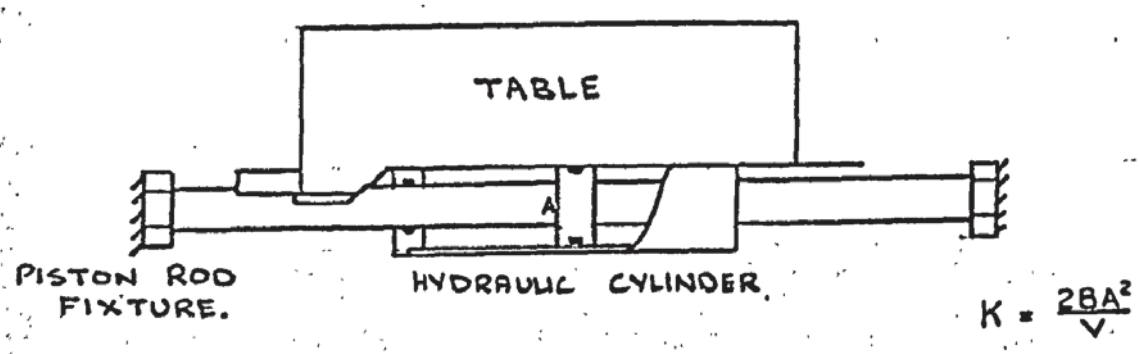

b) HYDRAULIC CYLINDER DRIVE.

FIG. 4·3. TABLE DRIVE CONFIGURATIONS.

sliding table. It has certain mechanical requirements to fulfill in order to maintain precise table motion, especially under working load conditions. These are listed below,

1) High stiffness or resistance to deflection under load.

2) Lost motion in this link must be eliminated as far as possible.

3) Friction and wear within the drive need to be held at a very low level .

On numerically controlled machines due care and attention must be given to these points in order to ease theoretical design analysis and prevent machine instability. Modern drive systems do perform satisfactorily.

The prime mechanical requirement of the drive is that of stiffness and although a simplified approach will be taken here, a great deal of work has been carried out with regard to the stiffness properties and requirements of many elements within a machine tool. (47) (75)

The hydraulic drive shown in Fig. 4.3 b has a basic stiffness that is related to cylinder dimensions and the bulk modulus of the hydraulic fluid, thus,

$$\text{stiffness} \qquad K = \frac{2BA^2}{V} \qquad 1-4$$

The force produced by the cylinder is dependent upon system oil pressure and piston area (A). In most drives the oil pressure is greater than 6.9 MN/m^2 and in this case the bulk modulus (B) is not unduly affected by entrained air. This can be a problem in low pressure systems (76), it reduces the stiffness quite drastically.

A disadvantage of hydraulic cylinder drives is that the working stroke must be limited and in order to obtain a useful stiffness magnitude, a compomise has to be made between piston area and cylinder stroke.

The main advantages of this type of drive are lower component costs, flexibility in assembly and location and the potential to supply

high traverse speeds to the table. Compliance of the piston rod, cylinder wall and location joints has been neglected in this model since the main argument is the simple concept of drive stiffness in the mechanical link. In general, the range of stiffnesses on all types of slideway drive fall into the range of 10 - 50 MN/m and undamped natural frequencies of slideway systems in the range of 10 - 50 Hz, depending upon table mass.

The fact that this mechanical link may form part of a control system loop in an automated drive can mean that the steady state relationship between system force and system error will be dependent upon the effect of the other components within the control loop. Nevertheless, it is the stiffness of the mechanical link which is the dominant factor and together with the mass of the sliding table and a linear damping coefficient will produce the fundamental resonant frequency condition in the dynamic state of the system. Therefore it is only relevant, in this work, to consider the drive system as a simple link analogous to a mechanical spring.

The location of the connection between the sliding table and the drive will be the point of application of the driving force. As pointed out by S.Kato et al (60) this position may result in some pitching and yawing of the table under sliding conditions. The effect will not be considered in the subsequent slideway model but it is felt necessary, at this point, to describe briefly how this will occur if the connection is not sited correctly.

Some assumptions have been made and are as follows,

1) The points of contact between the table and the guideways are spread evenly across the interface and there is an even contact pressure .

2) The weight of the table acts through its centre of gravity and the centre of the guideways .

3) The friction contribution is the same for each guideway/table interface and remains constant throughout .

4) The direction of the applied force, to the table, is parallel to the direction of desired table motion .

5) The normal stiffness of the sliding interface is constant and elastic .

6) The friction force is considered to act at a point in the centre of each contact area .

The illustration in Fig. 4.4 shows a basic model for consideration.

The pitching and yawing motions are illustrated in Fig. 4.5 Briefly the yawing of the table takes place around the centre of the table through which the weight acts and the pitching is centred around the mid-point of the table length on the interface friction plane.

It is considered that,

a) The table yaw is made possible by the clearance between the gib strips and the sides of the guideway (see Fig.4.1) although a small contribution may be made due to the interface deflection of this part of the sliding joint .

b) The table pitch is due to the deflections on the main friction plane although this may be accentuated by small clearances brought about by a general waviness of the surfaces .

When the table is moving at a steady velocity the pitch angle is,

$$\theta p = \mathrm{Tan}^{-1} \frac{9\ La\ F_A}{K_S\ (L_T)^2} \qquad 2-4$$

and

$$\Delta Z = \frac{9\ La\ F_A}{2\ K_S\ L_T} \qquad 3-4$$

where K_s is the surface contact stiffness

If La = 150mm, L_T = 450mm, Fa = 50 kgf and $K_S = 1 \times 10^5$ kgf/mm

then $\Delta Z = 0.75\ \mu m$.

Therefore, the leading edge of the table, as shown in Fig. 4.5 b will drop and the table inclination will be termed negative in the direction of motion. Although this value is low if compared with the experimental measurements (60) (77) (by approximately a factor of 5) due to the simplification, the analysis does indicate that the dimension La should be zero. This means that the line of action of the driving force should be on the friction plane. The effect of surface waviness

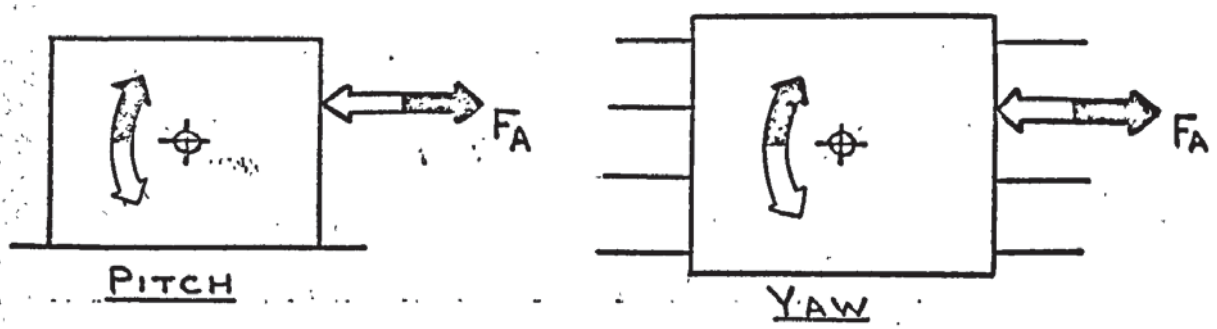

a) PITCH AND YAW WITH DIRECTION OF DRIVING FORCE.

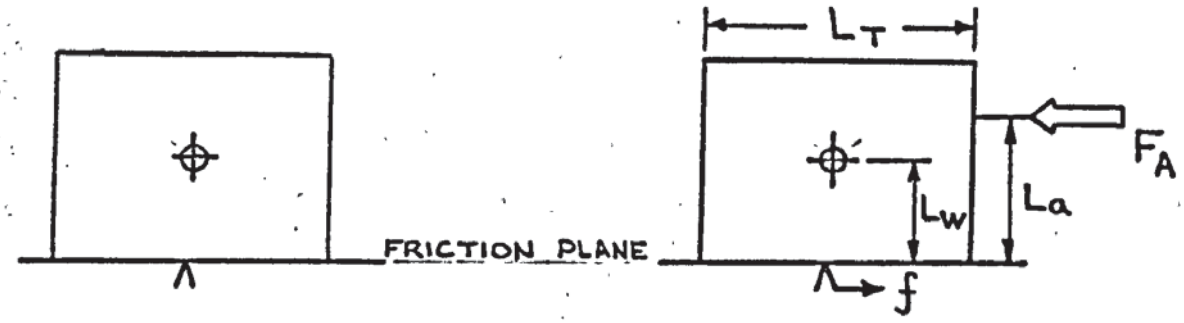

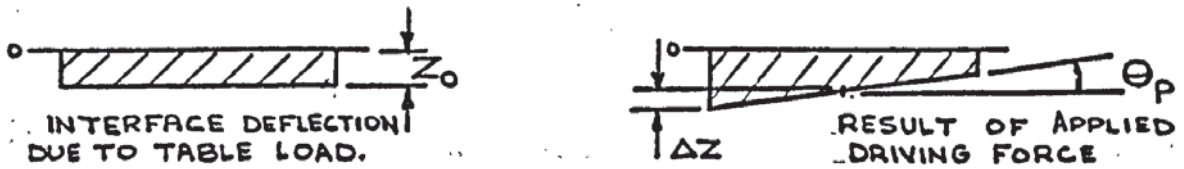

$$Z_o = \frac{W}{K_S}$$

b) TABLE PITCH

$$\Delta Z = \frac{9 . L_a . F_A}{2 K_S L_T}$$

$$\text{Tan}\,\theta_p = \frac{\Delta Z . 2}{L_T}$$

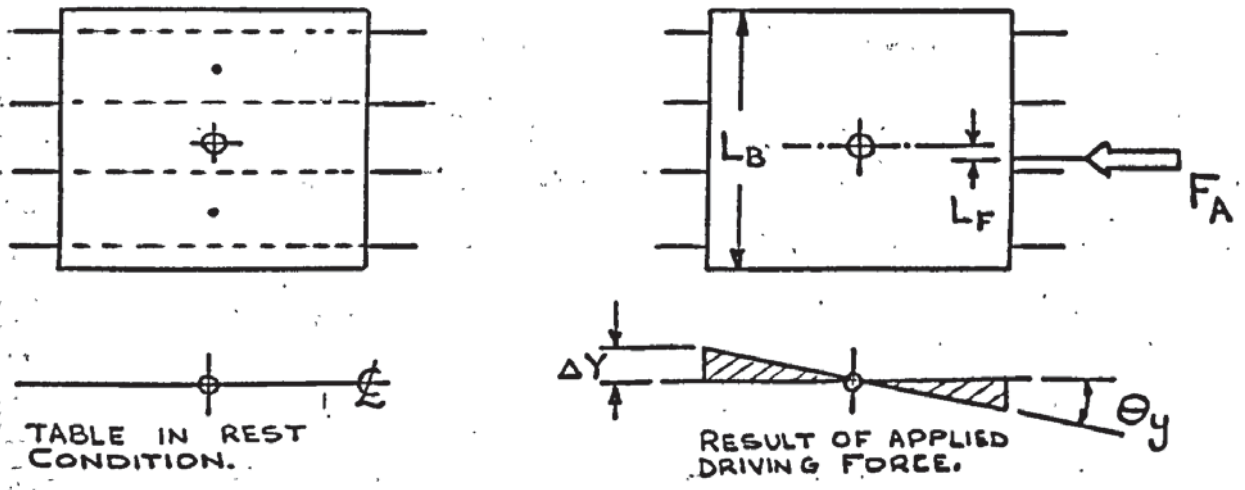

c) TABLE YAW

$$\Delta Y = \frac{9 L_F F_A}{2 K_S L_T} + Y_c$$

$$\text{Tan}\,\theta_y = \frac{\Delta Y . 2}{L_T}$$

FIG. 4·5. TABLE PITCH AND YAW.

and the force due to the moment of inertia of the table mass under oscillatory conditions will lead to an accentuation of table pitch.

The table yaw will depend upon clearance but the equations will be similar to those above, thus

$$\Delta Y = \frac{9\, L_F\, F_a}{2\, K_S\, L_T} + Y_c \qquad 4-4$$

where Yc is the gib to guide clearance

and therefore the yaw angle will be,

$$\theta_y = \text{Tan.}^{-1} \frac{\Delta Y}{2L_T} \qquad 5-4$$

The clearance Yc will only be taken up if a twisting motion is initiated by the presence of an 'offset' force, and therefore the table yaw can be considered to be zero if the dimension L_F is zero. Therefore, in this example, the driving force must act through the centre position between the guideways.

On a practical system it has been shown (76) that an offset driving force will cause the table to yaw (or "crab") which can bring about severe wear of the leading and trailing edges of the gib strips.

In conclusion it should be noted that a machine tool slideway will not have the constraints that have been imposed on the above model. The positioning of the point of application will be difficult to calculate in the design stage, to cover all contingencies. In order to reduce table pitching and yawing the following points should be considered,

1) Mechanical construction and tolerances of the slideway assembly.
2) Friction levels between sliding surfaces.
3) Cutting forces applied to the table.
4) The stiffness of the sliding joints.

It is proposed that these table movements are accentuated and manifested

by non-linear frictional behaviour, but are not the cause of such behaviour. A fundamental understanding and analysis of the non-linear friction, causing oscillatory table motion, can only be undertaken if table pitching and yawing are considered to be eliminated from the simulated slideway model.

4.5 NON-LINEAR FRICTION BETWEEN CAST IRON SLIDEWAYS

The steady state friction force/velocity characteristics of a sliding joint can be illustrated by the curves shown in Fig. 4.6

Curve (a) indicates the linear concept of friction behaviour and it is this form that lends itself readily to the adoption of a damping term suitable for a system equation of motion. This ideal condition ensures that when the table is driven at any constant velocity, oscillatory motion will not exist. In practice, slideway friction is actually of the form shown in curves (b) and (c).

These curves are non-linear. The relationship between force and velocity have a complex arrangement and in particular the friction level is not zero when the table is stationary.

The analytical study of the equation of motion is impeded and the transient and dynamic behaviour can only be established theoretically using complex control theory mathematics. In doing so, the exactness of the solution is open to question, although some useful information and general conclusions can be drawn.

The plotting of curves (b) and (c) can be hampered by oscillations on the velocity signal, especially at low velocities, brought about by 'stick-slip' motion of the table. This occurs when the slope of the force/velocity characteristic is negative and it is general practice to draw this steady state section of the curve by taking a mean line through the velocity excursions.

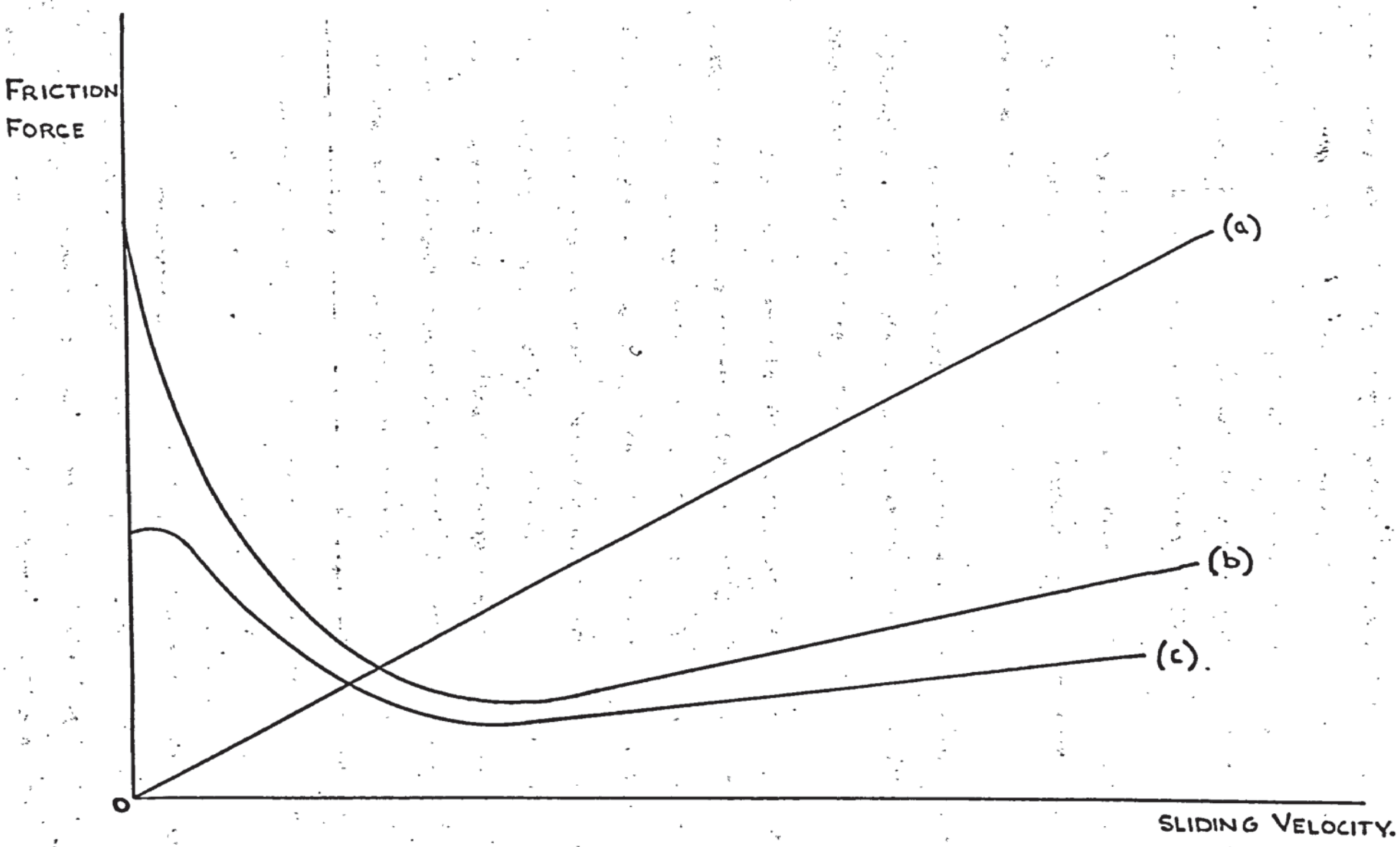

FIG. 4·6. STEADY STATE FRICTION CHARACTERISTICS.

It is thought most important to question why such characteristics as shown in Fig. 4.6 are brought about. The designer of machine tool slideway systems would be more willing to accept such physical detail than rely on empirical relationships. To this end, the experimental work of Bell et al (45) (47) is useful to the industry although overall theoretical concepts have not been developed.

A system velocity profile is drawn for all the curves in Fig. 4.6 assuming exactly the same mechanical system parameters. These are shown in Fig. 4.7

These profiles are suggested to be the likely result of their slideway friction characteristics and at this point in the thesis, are only intended for illustrative purposes.

For the linear friction characteristic the output velocity is always the same as the commanded input velocity. The profiles (b) and (c) show oscillatory motion of the table taking place over some part of the falling friction characteristic. They indicate that their pattern is dependent upon the friction/velocity characteristic. It is suggested that there will be a unique profile for each slideway system, and that they are a more sensitive indicator of parameter changes than the friction curve. Their reproduction requires little instrumentation, a suitably positioned velocity transducer and storage oscilloscope would be adequate. As these profiles have not been generally used their interpretation and relation to slideway friction does require some explanation in order that the designer or service engineer may gain meaningful information.

If we assume that the friction/velocity curve does not exist and that only the profile recording is available then it is logical to make an initial observation that curve (a) in Fig. 4.7 is the ideal requirement for a sliding system. (This does mean that the drive system

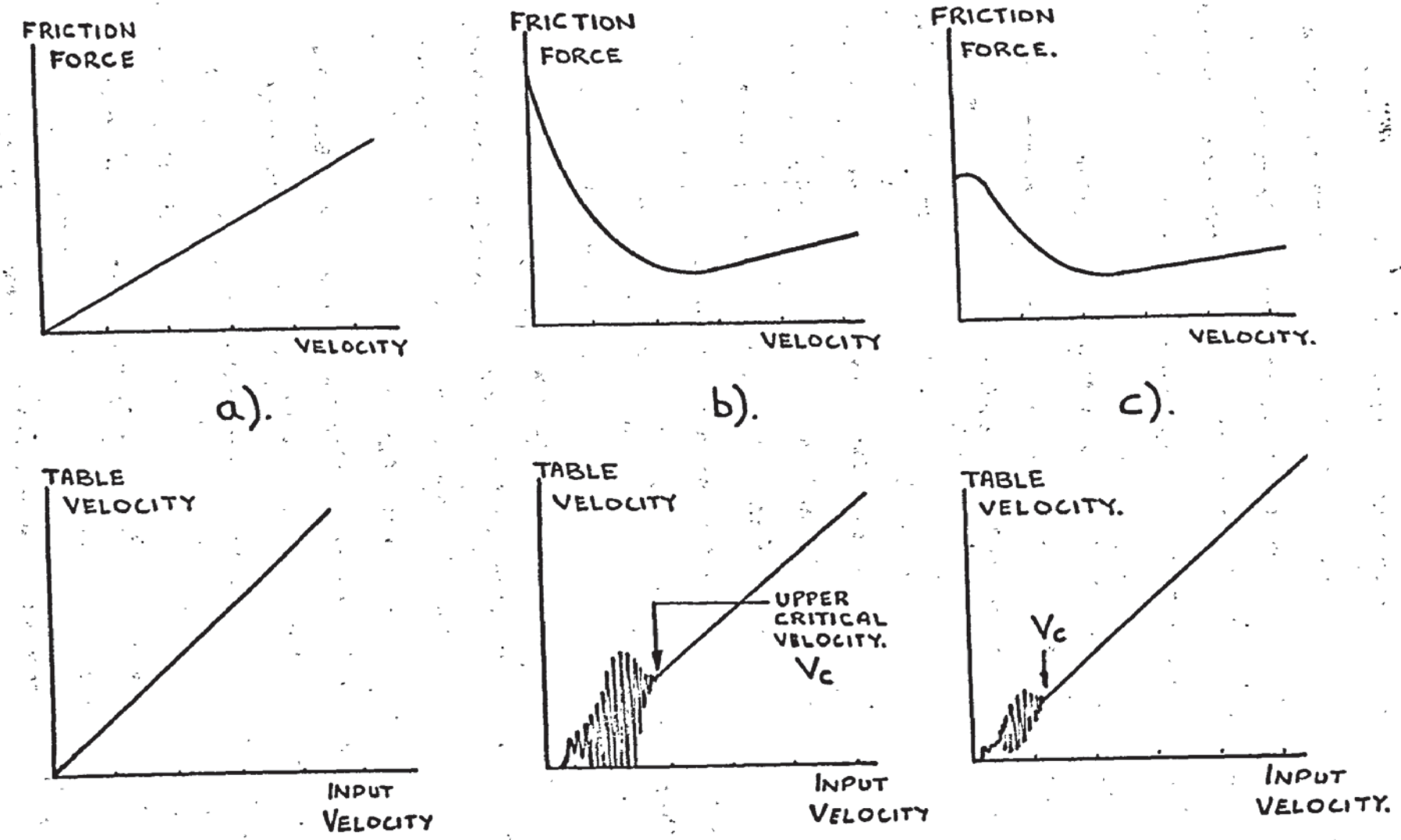

FIG. 4-7. SYSTEM VELOCITY PROFILES FOR FRICTION CHARACTERISTICS.

will need to supply high forces to the table at high velocity). Any indigenous oscillations must be eliminated or reduced to such a magnitude that system stability and slideway performance are not degraded. This means that the upper critical velocity and the amplitude of any preceding oscillations should be very small. For a particular system this can be achieved to some degree in practice by using a high viscosity lubricant or one with polar additives, as demonstrated by Britton et al (47).

In order to highlight some of the profile characteristics the curve illustrated in Fig. 4.8 has been drawn, this is an amalgam of many characteristics. The curve does indicate the many salient features which are listed below.

Point 1. The initial jump in table velocity. This indicates the presence of static friction and the time delay before movement. The height of the jump will increase with friction level.

Section A. The transient and subsequent smooth rise mean a positive rise in the force with velocity. This portion may be suppressed and become indistinguishable.

Point 2. This is the lower critical velocity and the commencement of table oscillations. The friction level will now be falling with increased velocity. This point may coincide with point 1.

Section B. The oscillations will increase in amplitude with rising velocity and depending upon the system parameters may lead into a stick-slip condition. The rate at which this occurs will be parameter dependent.

Point 3. The start of 'stick-slip' motion. This point can be very close to point 1.

Section C. The amplitude of stick-slip motion will continue to rise to a maximum. The magnitude is again dependent upon the parameters of the system, but it is generally associated with low system natural frequency,

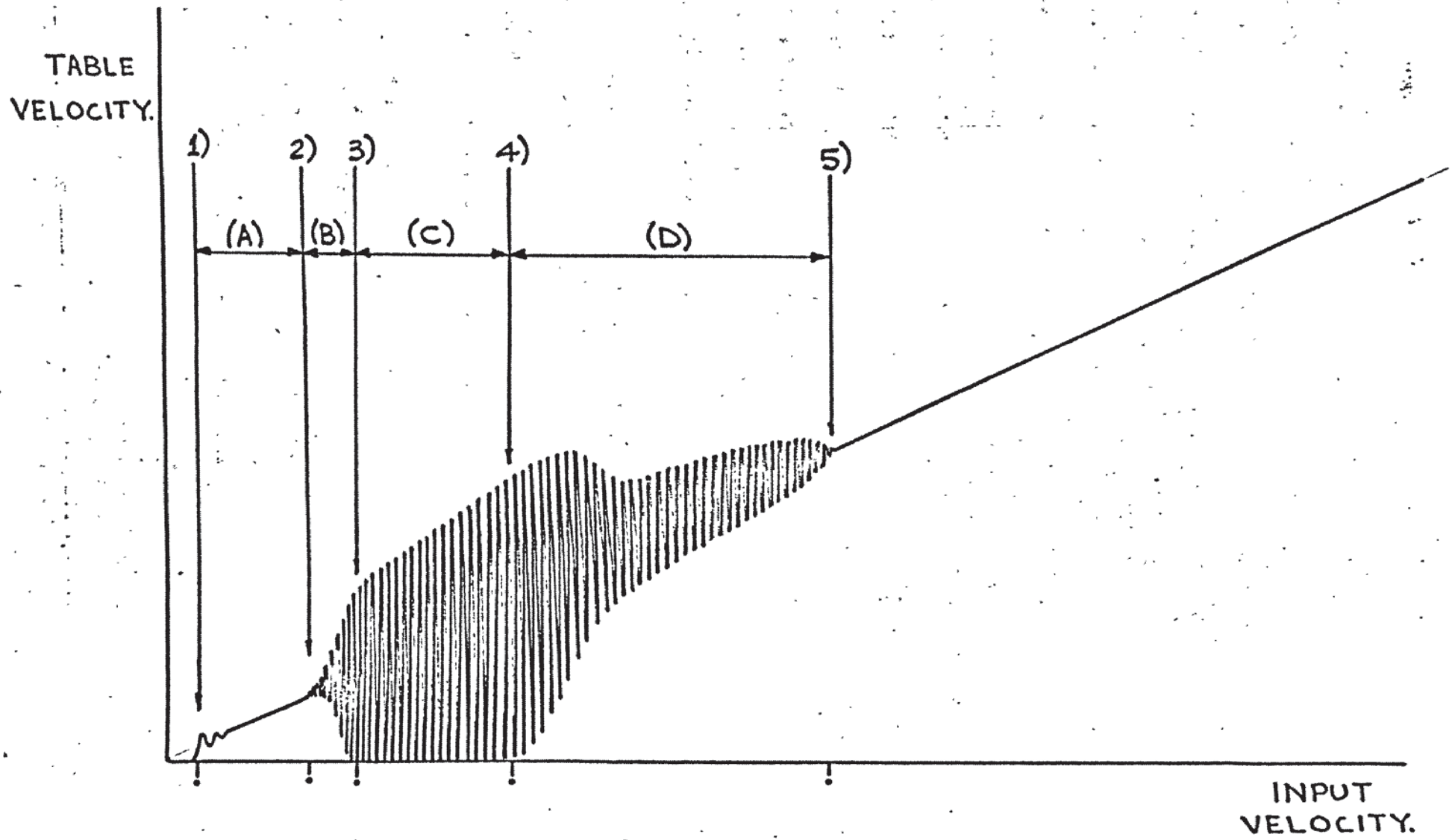

FIG. 4·8. A GENERAL S. V. P.

steep negative friction/velocity gradient, high general friction levels over this velocity range, and low lubricant viscosity.

Point 4. The termination of 'stick-slip' and the start of a decay in the amplitude of oscillations. The velocity at this point has been referred to as the critical velocity by earlier researchers (19) (43)

Section D. The table oscillations will reduce in amplitude as the velocity increases. The main parameter affecting the system over this section is the lubricant viscosity. The slideway lubricant, coupled with the interface velocity, is attempting to quench these oscillations. The friction force is still falling with increased speed but at a lower rate than over section C. These oscillations are termed quasi-harmonic and tend to be sinusoidal in shape as the velocity increases.

Point 5. This is the upper critical velocity and oscillatory motion is terminated completely. The friction/velocity gradient will still be negative but it is suggested that the nearer point 5 is to point 4, the closer will be the critical velocity to the velocity at which the gradient of the friction curve assumes a positive gradient.

At some velocity beyond point 5, the slideway lubricant will provide sufficient support, to the table, to eliminate all metallic contact between the sliding surfaces and the friction level will only gradually rise with further increases in velocity.

The simulation of a slideway system with non-linear friction, is discussed in chapter 8, but it is relevant, at this point, to include some further profile observations. These are,

1) The frequency of the oscillations is approximately the same as the system undamped natural frequency (especially over section D of the profile. This suggests a fairly low friction level and consequent system damping coefficient.

2) The shape or signature of the profile varies with the rate of change of command velocity. High rates of increase in velocity tend to show higher critical velocities. This is due to the system natural oscillatory decay which increasingly overruns

the point of actual critical velocity.

3) The profile signature is modified if the command velocity is reduced from an initially high level down to zero. In general, point 1, sections A and B, are not distinguishable and the overall shape tends to be smaller with a lower critical velocity at point 5. It is felt that this feature is again principally due to the effect of the slideway lubricant, since at high velocities a fluid film is generated and as the velocity falls this film is maintained until a breakdown sliding speed is reached. If very high rates of velocity decrease were possible, on a physical system, the oscillatory motion may be completely suppressed, but if the terminal velocity was not zero then the system would revert into an oscillatory condition after a small time interval. (Necessary for film breakdown).

It is generally accepted that oscillatory table motion at low sliding speeds is affected by the negative gradient of the friction/velocity curve and therefore the curve shown in Fig. 4.6 b will be used as the general shape for the system simulation. A theory will be propounded which will explain necessary system requirements in order to bring about the shape of this friction curve.

The analysis of the nature of this system phenomenon is the object of this thesis, bearing in mind the physical parameters of the system. The friction/velocity curve and the S.V.P. will change as a consequence of other external forces. such as those contributed by the cutting action on a machine tool. They will also be modified by external velocity vibrations applied to the system. This observation follows the experimental work of Yokoyama et al (78)(who applied harmonic vibrations in the direction of sliding motion to reduce kinetic friction) and the experimental work of Tolstoi (38)

All external forces have been excluded from the subsequent analysis in order to obtain a meaningful basic understanding of the system behaviour as outlined above.

4.6 A BASIC SLIDEWAY SYSTEM - FOR THE PURPOSES OF SIMULATION

The main factors involved in a slideway system have been outlined. Some irregularities have been excluded in order to maintain the necessary clarity.

The basic model is shown in Fig. 4.9 as a simple spring - mass - damping system.

If the friction force F is a linear viscous term $f\dot{x}_o$ then the force equation of motion will be

$$M\ddot{x}_o + f\dot{x}_o + Kx_o = Kx_i \qquad 6 - 4$$

and the system behaviour can be explained mathematically using linear control theory (20)

But the friction force term will be non-linear and the basic equation will have the form,

$$M\ddot{x}_o + \frac{\dot{x}o}{|\dot{x}o|}.F + Kx_o = Kx_i \qquad 7 - 4$$

A decomposed friction/velocity curve is shown in Fig. 4.10, the entire curve being the summation of curves (A) and (B)

Curve (A) has the equation,

$$(A) = N(V_{cL} - \dot{x}_o)^2 \qquad 8 - 4$$

and is only operative until $\dot{x}_o = V_{cL}$

If $\dot{x}_o = 0$ then

$$(A) = N(V_{cL})^2 = Fs \qquad 9 - 4$$

If $\dot{x}_o \gg V_{cL}$

(A) = Zero

Curve (B) has the equation,

$$(B) = f\dot{x}_o \qquad 10 - 4$$

where f is the apparent viscous damping coefficient.

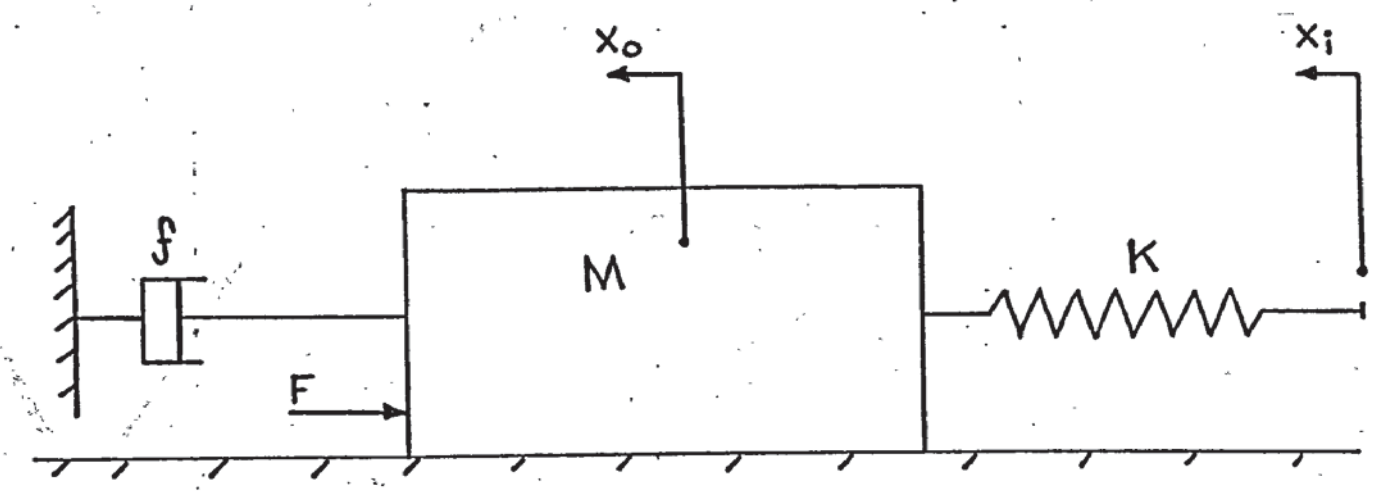

$$M.\ddot{x}_o + \frac{\dot{x}_o}{|\dot{x}_o|}.F + f.\dot{x}_o + K.x_o = K.x_i$$

FIG. 4·9. A SIMPLE SLIDEWAY MODEL SYSTEM.

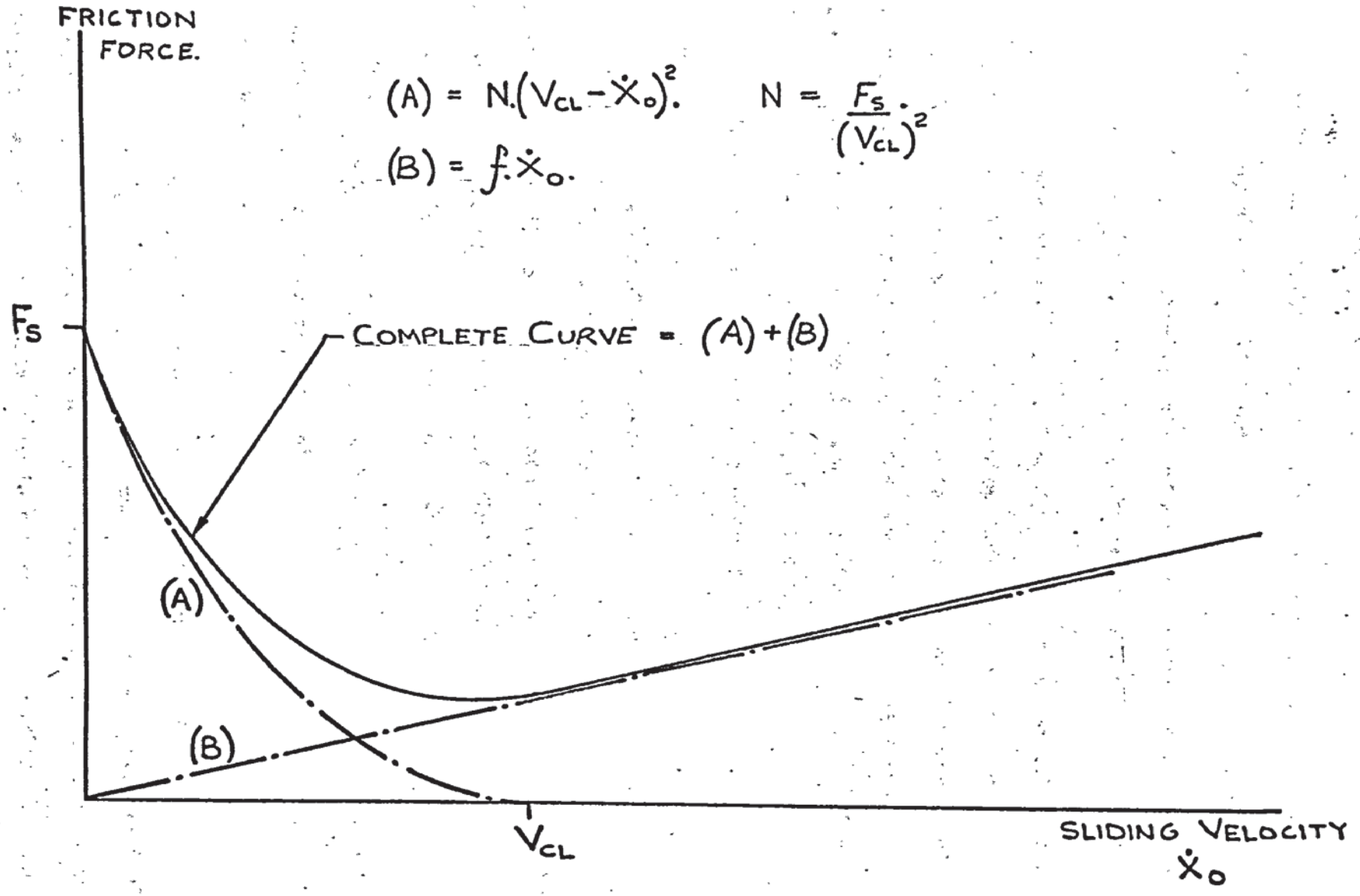

FIG. 4·10. A DECOMPOSED FRICTION CHARACTERISTIC.

Thus for positive values of output velocity,

$$F = (A) + (B)$$

$$F = N(V_{ct} - \dot{x}_o)^2 + f\dot{x}_o \qquad 11 - 4$$

A square law relationship has been used for curve (A), which is felt to be quite acceptable at this stage.

Thus, the basic equation of motion for the non-linear system is

$$M\ddot{x}_o + \frac{\dot{x}_o}{|\dot{x}_o|} N. (V_{ct} - \dot{x}_o)^2 + f\dot{x}_o + Kx_o = Kx_i \qquad 12 - 4$$

A complete mathematical analysis of such an equation is not possible unless some form of piecewise linearisation is attempted initially and it is certainly not clear that the sliding mass could maintain an oscillatory status if the command input was a velocity i.e. $x_i \equiv \dot{x}_i.t.$ Therefore the analogue simulation will be of equation 12 - 4 in order to obtain further understanding.

Two steady state conditions are considered when

a) $\dot{x}_o = 0$

Then equation 12 - 4 becomes

$$N(V_{ct})^2 = K(x_i - x_o) = Fs \qquad 13 - 4$$

and the system will not have the capacity to move the table until the error force overcomes the static friction force.

b) $\dot{x}_o = V < V_{ct}$, (a steady state table sliding velocity)

then

$$N(V_{ct} - \dot{x}_o)^2 + f\dot{x}_o = K(\dot{x}_i - x_o) \qquad 14 - 4$$

and the steady state error force will be smaller than that for equation 13 - 4.

Finally, two further points need to be mentioned,

1) Equation 11 - 4 is an attempt to fit a simple mathematical description to the friction/velocity relationship. The manner in which friction varies with velocity is to be discussed in detail. An alternative equation will be developed in which it is hoped to eliminate any empirical

relationships and thus provide analytical answers in terms of physical parameter quantities.

2) The simulation studies have shown that equation 8 - 4 is a time dependent equality and this greatly affects the S.V.P. This dependence is related to some of the system parameters and the equation will have the form,

$$(A) = (1 - e^{-\alpha t}) N (V_{CL} - \dot{x}_o)^2 \qquad 15 - 4$$

and equation 11 - 4 becomes,

$$F = (1 - e^{-\alpha t}) N (V_{CL} - \dot{x}_o)^2 + f\dot{x}_o \qquad 16 - 4$$

The simulation suggests that there is a first order form for the time dependence as subsequent results compare most favourably with past experimental results, as noted in chapter 3.

CHAPTER 5

AN ANALYSIS OF CAST IRON SLIDEWAY SURFACES

5.1 INTRODUCTION

Machining processes leave the surface of a workpiece with characteristic patterns of hills and valleys known as texture. This texture will usually have components of roughness and waviness which may be superimposed on further deviations from the intended geometric form, for example, flatness.

As R.E.Reason (79) has pointed out, the optimum surface specification may become a highly complex matter, depending upon the service conditions of the mating surfaces. In particular, it can be said that a friction system is dependent upon the physical activities that take place between the sliding surfaces.

A relationship illustrating the interdependence of these activities and friction is shown in Fig. 5.1 This diagram expresses objectively the views of an engineer and use has been made of factors which are judged to be readily appreciated and understood in an industrial environment. It can be seen in this figure (5.1) that the friction 'family' has been divided in four identifiable parts, or sub-systems, each having its own group of activities. In every case some factors are common and can be collectively described as "metallic interface characteristics". (M.I.C.)

This chapter is concerned with obtaining some understanding of these characteristics as applied to machine tool slideways so that subsequently a friction/velocity relationship can be developed and expressed mathematically in terms of physical quantities.

Experimental work has been carried out under 'dry' sliding

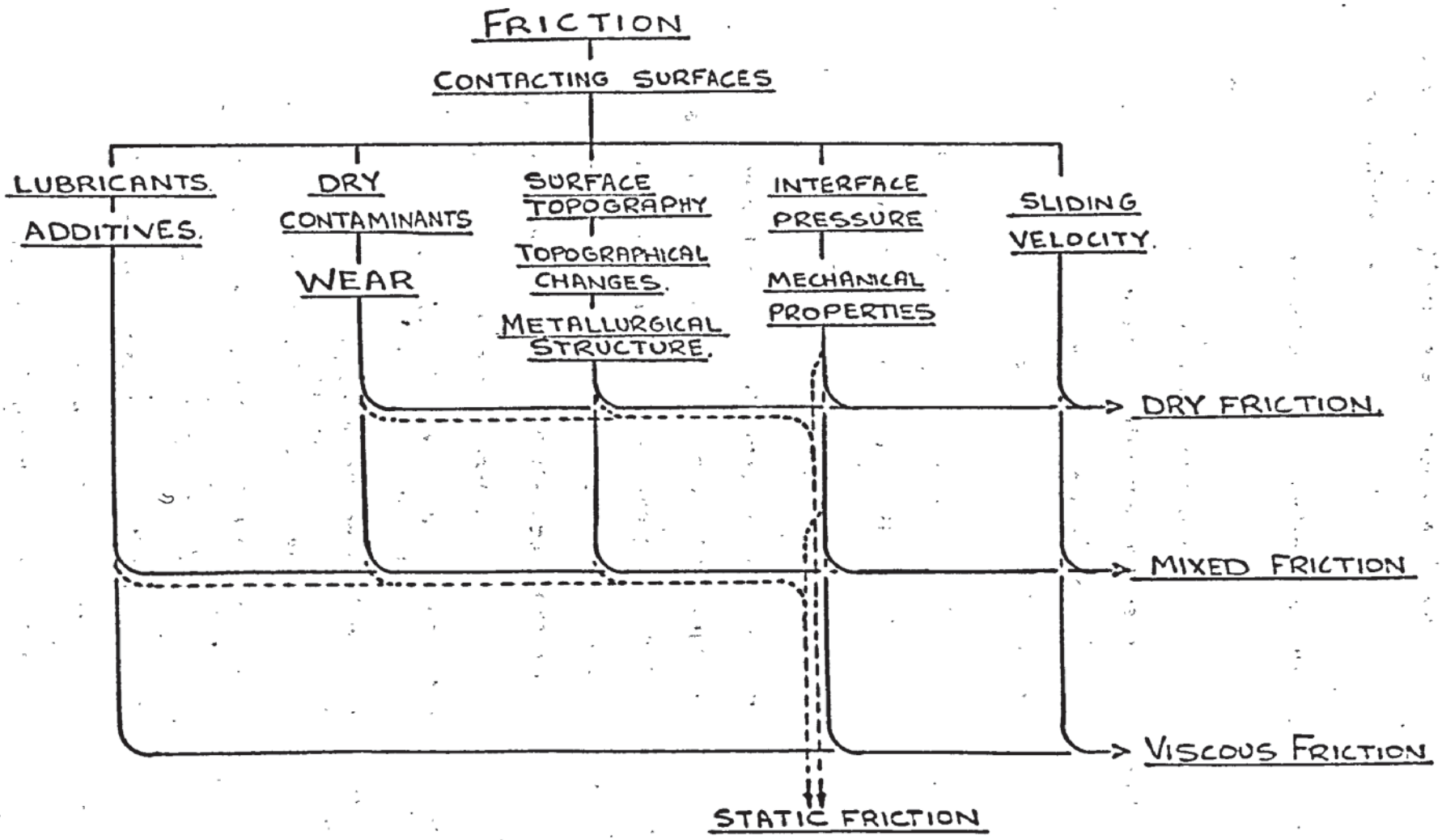

FIG. 5·1. THE FRICTION SYSTEM.

conditions using a small model. The topographical changes that occured on cast iron test pieces are compared with studies of changes on actual cast iron slideways.

The methods of studying surface topography, in varying detail, include

1) The ordinary microscope

2) The scanning electron microscope (S.E.M.)

3) Optical - interference methods

4) Stylus methods using a profilometer

The S.E.M. has been used by Frey et al (80) and Quinn (40) in their studies of changes in surface topography with particular reference to wear characteristics.

A recent paper by Grieve, Kalizer and Rowe (81) discusses the measurement and examination of surface topography using a stylus instrument to record close, parallel surface profiles for later analysis on a computer. In these studies extensive use has been made of the scanning electron microscope in favour of the profilometer. The stylus method was not used for the following reasons,

a) The instrument records only a measure of the surface profile along a line of fixed length .

b) To produce a record of the surface topology of a specific area would have meant the collecting and processing of information from many lines .

c) The precise location of such an array of lines would have been extremely difficult, especially as the exercise needed to be repeated many times .

d) Surface damage caused by the stylus would have affected the recordings, but more importantly, would have upset a particular state of the surface. This damage has been outlined by Dennis and Fuggle (82) and its effect dealt with in an interesting paper by Guerrero and Black (83). In both cases the researchers used the S.E.M. for experimental verification .

e) It was felt that surface debris may not have registered because of its interaction with the stylus. Disturbance of any debris would mean changes in the surface topography .

5.2 EXPERIMENTAL STUDY OF TOPOGRAPHICAL CHANGES ON DRY SLIDING SURFACES

The majority of machine tools use grey cast iron structures, whose grades are specified by BS.1452:1961. These structures fall in the range between grade 14 and grade 20. Small items are made with grade 14 , and this number generally increases with component size. The grade number corresponds to the minimum tensile strength in Tonf./in^2 for a 1.2 in. diameter test bar. General engineering data on grey cast irons can be found in a very useful publication by B.C.I.R.A. (71) and much relevant information has been taken and used in this work. It should be noted that the actual mechanical properties of cast iron will depend upon the mould cooling rate and component section thickness.

Following discussions with a machine tool manufacturer H.W.Ward (72), grade 17 grey cast iron was selected as the material for the small specimens. This material was supplied by the company and described as "surplus bed iron", having been taken from the slideway section of the bed casting. By doing this it was hoped to ensure that the specimens would have the same metallurgical properties as an actual slideway. The actual machine beds are cast in such a position that the slideway section is at the bottom of the mould and the slower cooling in this region should produce a fully pearlitic structure. This should give good wear resistance in comparison with a structure containing austenite. (Eyre (84) (85)).

A micro structure of this material is shown in Fig. 5.2 and indicates graphite flakes, with a small amount of manganese sulphide, (usually rectangular in shape), in a pearlitic matrix. The relative coarse structure is caused by the slow cooling rate of the casting. A finer distribution of graphite flakes would indicate a faster rate of cooling.

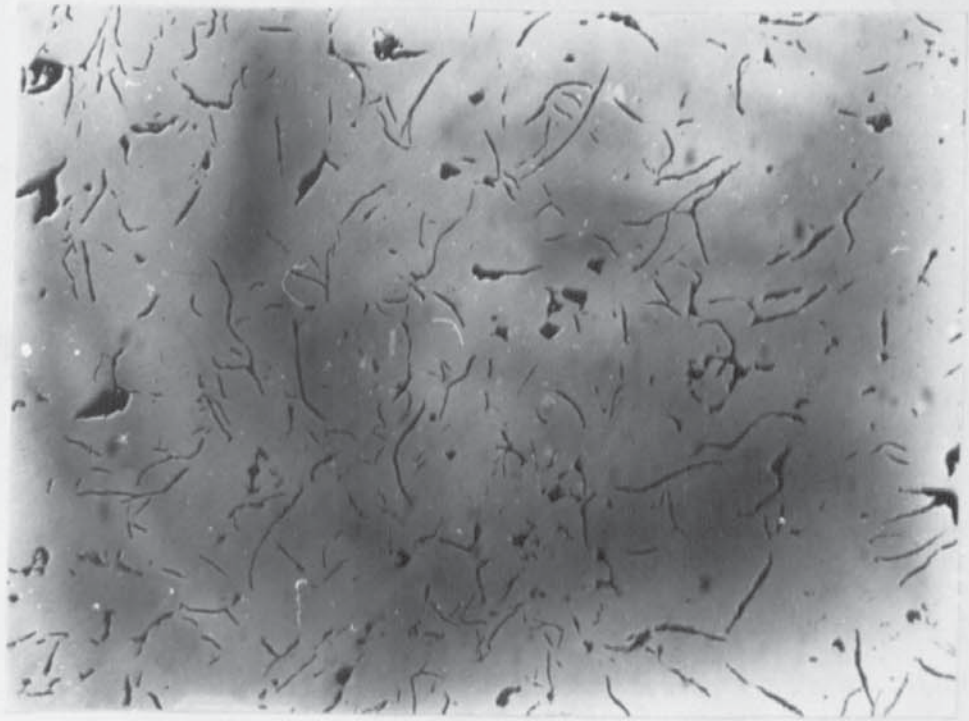

GRADE 17 CAST IRON. MAG. x100.

FIG. 5·2. CAST IRON MICROSTRUCTURE.

The composition of this material was found by chemical analysis to be,

Carbon	3.4%
Sulphur	0.15%
Phosphorus	0.09%
Manganese	0.61%
Silicon	1.1%

5.2.1 THE TEST SPECIMENS

Two test pieces were made to the drawing in Fig.5.3. These components had to perform two major functions,

1) To be analogous to an actual slideway system, operating under dry conditions .

2) To be capable of allowing the sliding surfaces to be studied using the S.E.M. Special mounting fixtures were made for the specimens, which are also illustrated in Fig. 5.3 .

The annular contacting surface of each piece was prepared in exactly the same manner as an actual slideway surface. They were fine turned and then ground using a C-30-HB-4.5 flared cup grinding wheel. The grinding specification was as follows,

1) Cup grinding wheel speed	3000 rpm
2) Feedrate	600mm/min
3) Roughing cut depth	0.1 mm
4) Finishing cut depth	0.05 mm
5) Second finish cut to spark out	

In order to establish a value of the newly cut surface finish, in terms of the conventional C.L.A. value, another cast iron specimen surface was prepared in the same manner. The measurements were made with the stylus moving at right-angles to the direction of the grinding marks or surface lay.

The results indicated that the surface roughness, across the lay had a measure of 0.7 μm. C.L.A. With this measurement it was hoped to

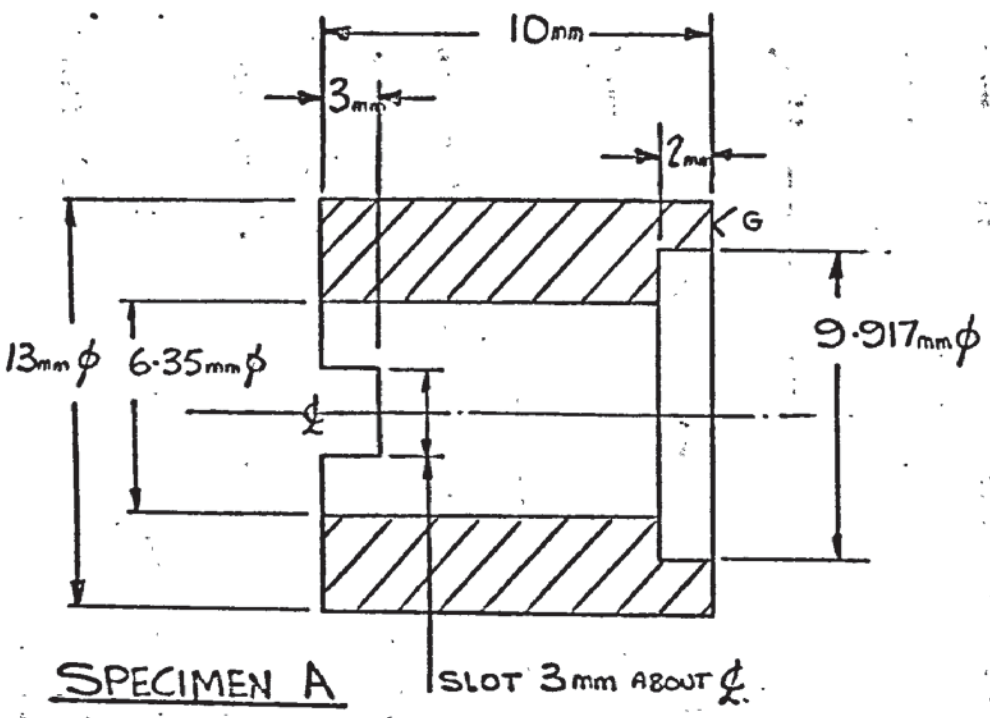

SPECIMEN A

GROUND AREA = 55·5mm²

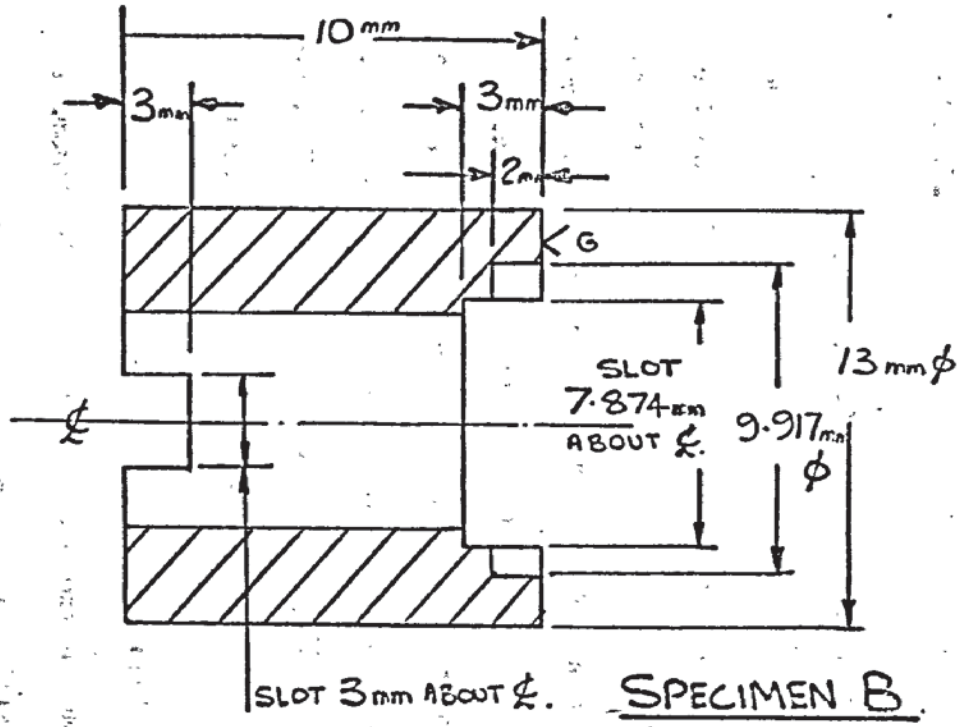

SPECIMEN B

GROUND AREA = 27·74mm²

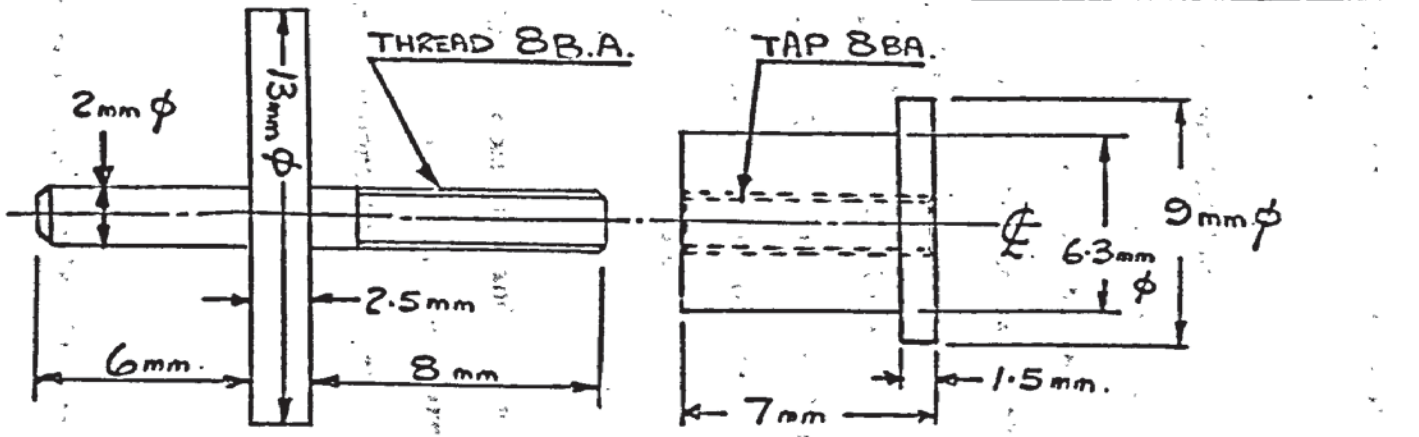

SPECIMEN HOLDER. – ALUMINIUM

FIG 5·3. SPECIMEN AND HOLDER DRAWING.

make some comparison when viewing the newly ground test surfaces under the S.E.M.

From Fig. 5.3 it can be seen that specimen 'A' has a complete ground annulus and this represented the surface of a machine slide. Specimen 'B' has two small part annuli, and represented the surface of a machine table. For convenience, the surface area of 'A' was twice the 'apparent' contact area of 'B'. The areas on 'B' were equally spaced about a mean diameter and the total was 27.74 mm^2. This allowed any one of these areas to completely pass over any particular point on surface 'A' in the same way that a machine table moves over a point on its guide-ways. To improve this model the radial width of the annuli on both specimens was made as small as possible.

The sliding tests took several weeks to complete and to reduce the amount of contamination and oxidation of the specimens, they were stored in small air-tight containers lined with proprietary rust-preventing paper.

5.2 ii THE TEST FIXTURE

The specimens were located and aligned in a simple fixture shown in Fig. 5.4.

Both specimens were placed on the location rod (4) with 'B' next to the driving dog (5). The rod passed through a support bearing (3) and specimen 'A' located in the fixed dog (2). A force between the two specimens was generated by a calibrated spring (6) adjusted by the spring location/nut assembly (7).

Specimen 'B' was rotated relative to 'A' by means of a driving handle (1). This operation was carried out manually.

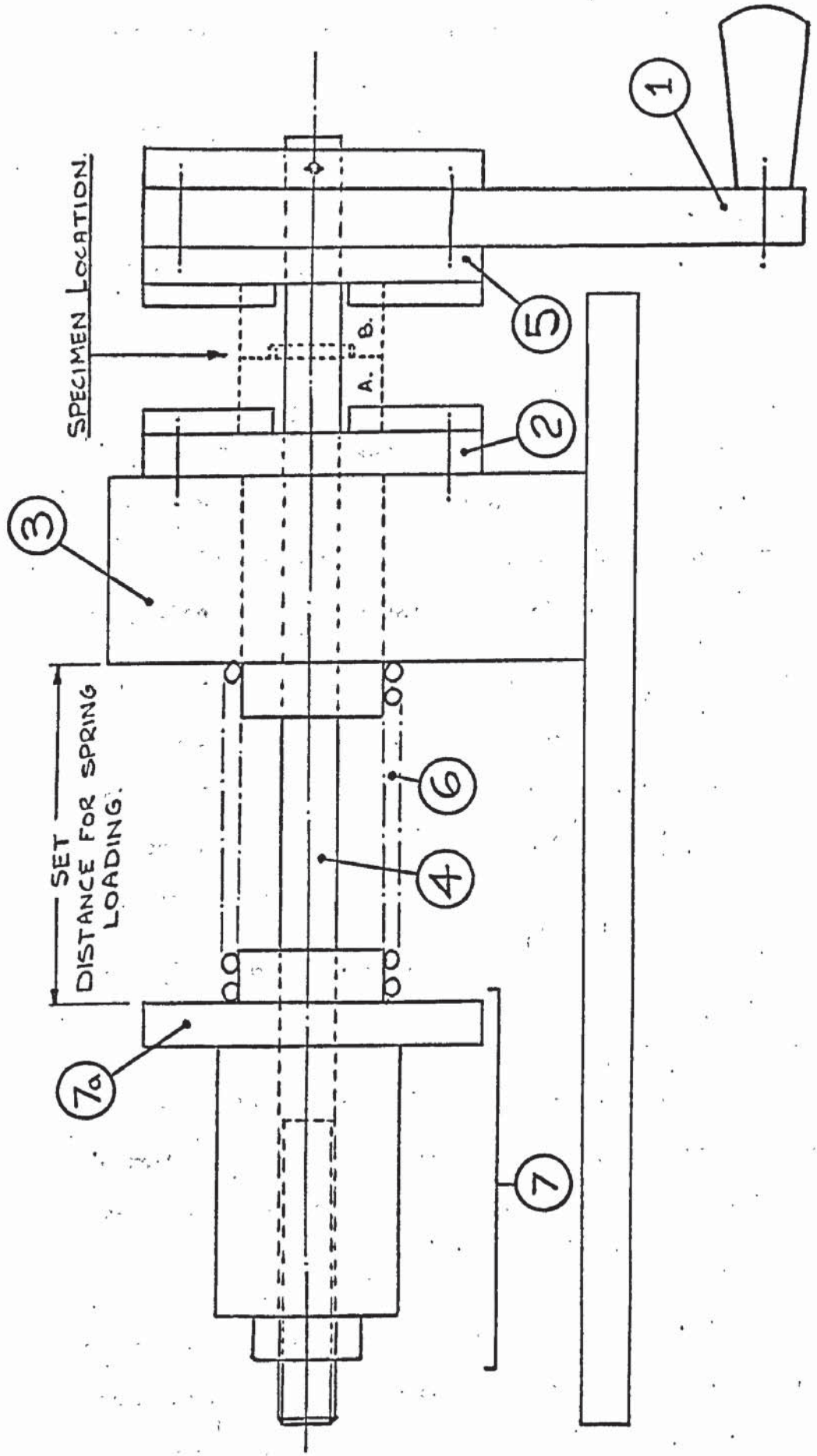

FIG. 5.4: TEST FIXTURE FOR SPECIMEN.

The information published by Bell et al (47) was used to select the apparent contact pressure for these tests. The range of table loads generally produced an apparent contact pressure between 60 kN/m^2 and 80 kN/m^2 and a pressure of 70 kN/m^2 was chosen.

The spring force (S_F) and hence the force between the contacting surfaces was calculated,

$$S_F = A_A . P_A$$

$$S_F = 1.9418N$$

The compressed length of the spring was measured using standard slip blocks, between the location collar (7a) and the support bearing (3). This simple technique was used since this measurement was made every time the fixture was assembled.

The angular position of the two sliding surfaces was the same at the start and finish of every test. Although this meant that the two locating dogs would be in a vertical position a discrepancy of 180 degrees may occur. This was overcome by scribing a fine line on the side of each specimen, during the initial assembly of the fixture.

5.2. iii EXPERIMENTAL PROCEDURE

The specimens were rotated relative to another by means of the driving handle. To simulate oscillatory motion the handle was turned one revolution clockwise then one revolution anti-clockwise. These two movements represented one oscillation.

As the radial width of the annulus was small, the mean diameter was used as a basis to calculate a sliding distance of 40 mm for every revolution. For convenience one complete turn was made in one second, so that the sliding speed would be 40 mm/s. This may be considered rather

high for machine tool slideways but is not impracticable.

There were 26 tests carried out and at the end of each one the specimens were weighed to establish their weight loss. They were viewed with the S.E.M. and the changes taking place in a particular location were noted. General changes in topography were also studied by scanning the entire surface of each piece.

Some details of these tests are listed in the table shown in Fig. 5.5 and the weight loss of each specimen plotted against sliding distance is illustrated in Fig. 5.6

Photographs were taken of the surface of each specimen at every test. The location of the test pieces in the S.E.M. was achieved by using specially made aluminium holders (see Fig. 5.3). To enable a specific area to be viewed the initial setting up of the S.E.M. entailed the positioning of the scribed lines on the side of each specimen. A technique was developed of viewing these lines, at a magnification of x100 and turning the specimen until they were aligned with a datum. This datum was drawn during the initial setting up, by tracing over the image of the scribed line on to a transparent plastic plate covering the C.R.O. screen. Masking plates were made for each specimen using the above magnification and also with a further magnification of x500.

The operation of the S.E.M. (Cambridge Stereoscan Mk.II) is detailed in Appendix 1 and it is sufficient to comment here that the initial setting of the specimens meant that the surfaces were inclined at an angle of 3^{o} with respect to the viewing position. This means the following photographs have an inclination such that the bottom edge is the highest line of the surface, and that it falls away up to the top edge.

The use of masking plates made the study of a specific area comparatively easy with exactly the same magnification settings. Selected

TEST NUMBER	NUMBER OF OSCILLATIONS	CUMULATIVE NUMBER OF OSCILLATIONS	APPROXIMATE CUMULATIVE DISTANCE MOVED - CENTIMETRES
0	0	0	0
1	1	1	8
2	1	2	16
3	2	4	32
4	2	6	48
5	4	10	80
6	4	14	112
7	8	22	176
8	8	30	240
9	16	46	368
10	16	64	512
11	32	96	768
12	32	126	1000
13	64	190	1500
14	64	254	2000
15	64	318	2500
16	64	382	3050
17	64	446	3600
18	128	574	4600
19	128	702	5600
20	128	830	6600
21	128	958	7700
22	128	1086	8700
23	128	1214	9700
24	128	1342	10,700
25	128	1470	11,800
26	256	1726	13,800

N.B. One oscillation consists of one anticlockwise revolution followed by one clockwise revolution. The distance moved in one revolution is approximately 40 mm.

FIG. 5·5. TABLE OF TEST DETAILS.

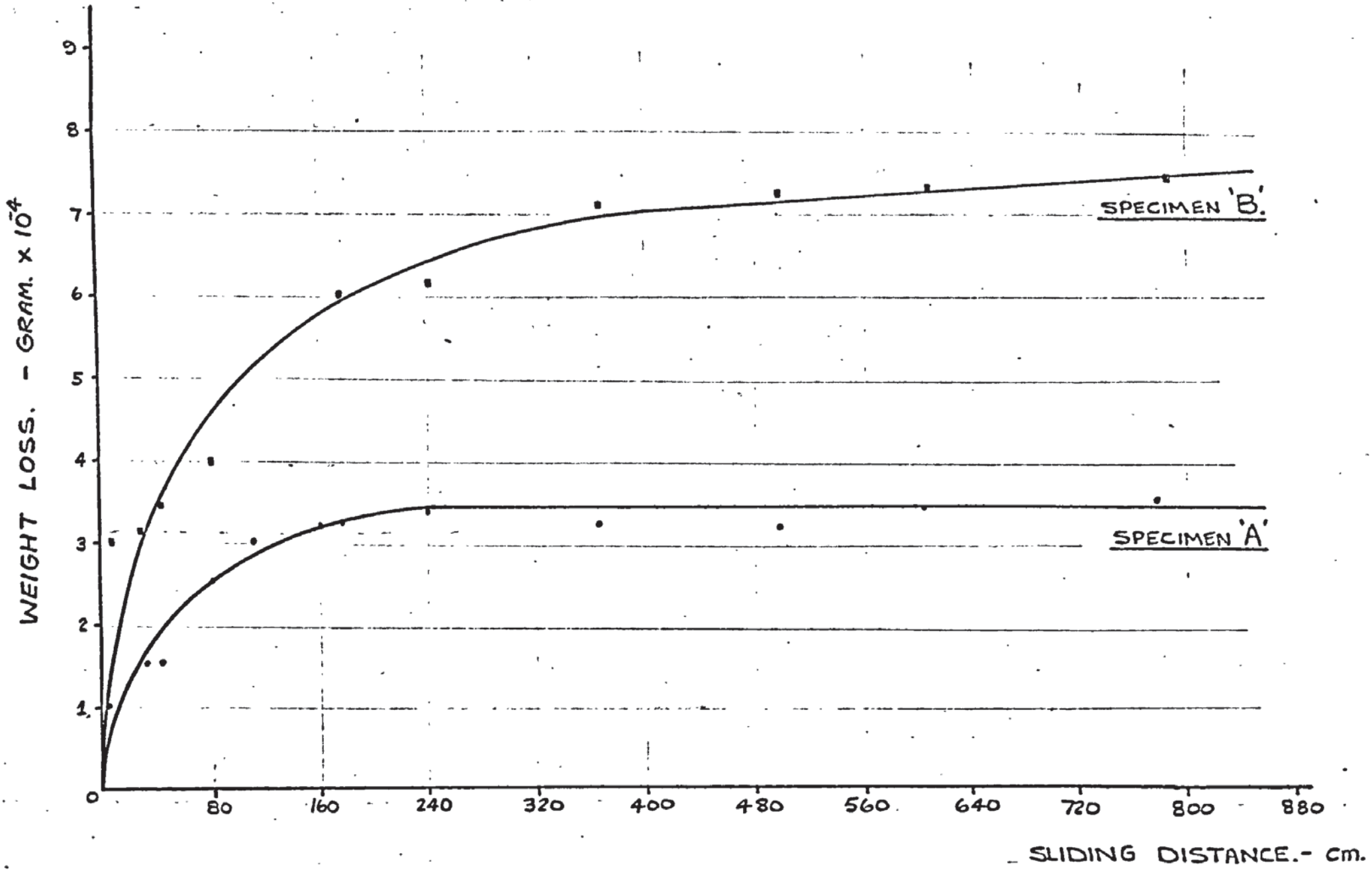

FIG. 5·6. SPECIMEN WEIGHT LOSS WITH SLIDING DISTANCE.

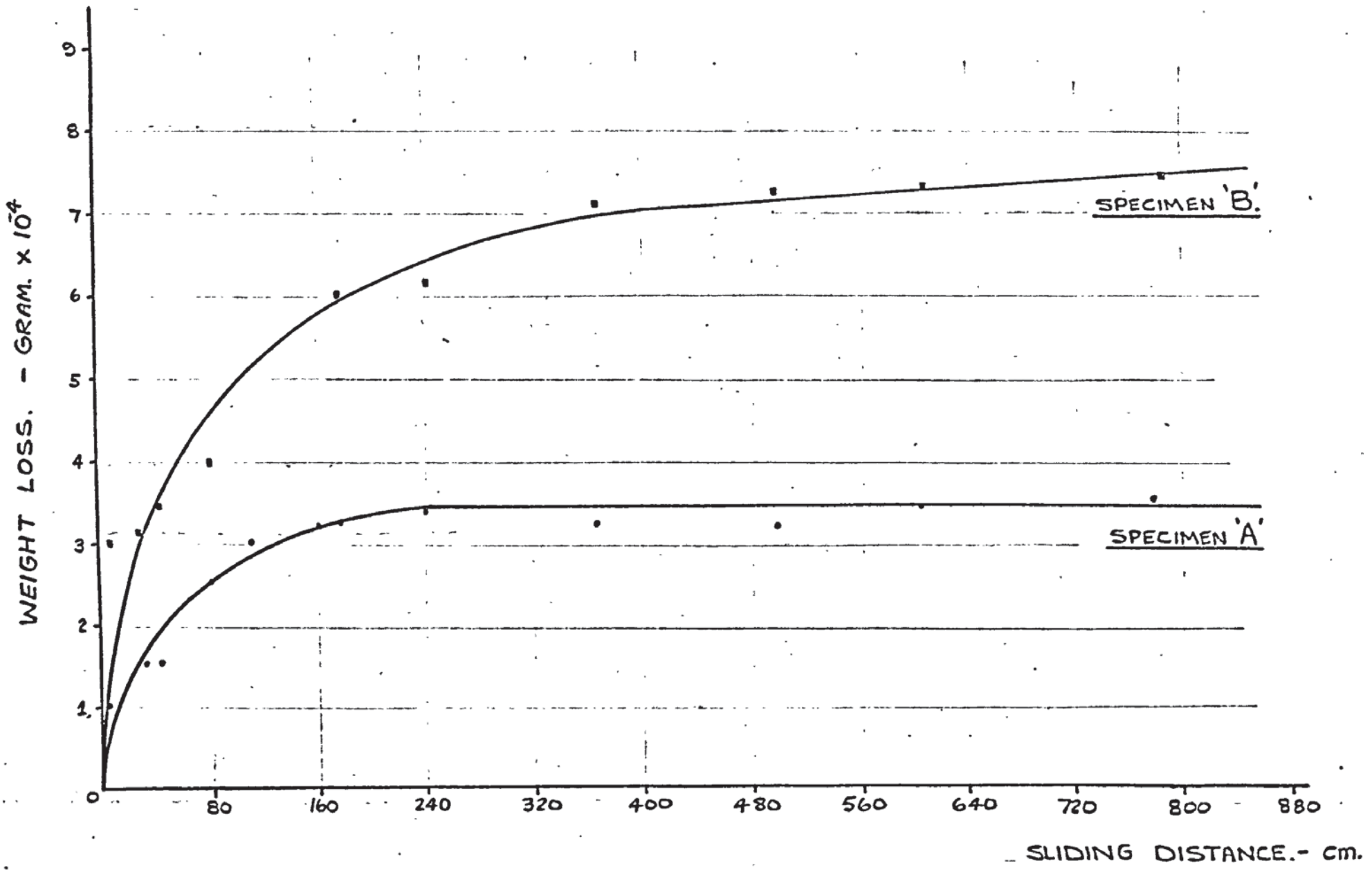

FIG. 5·6. SPECIMEN WEIGHT LOSS WITH SLIDING DISTANCE.

areas were close to the outer edge of the specimen surfaces and near to the scribed line.

Finally a study of the surface debris was undertaken using X-ray diffraction techniques developed by Quinn (40). It was hoped that this would indicate the temperature changes that had taken place at some points on the interface.

5.2.iv OBSERVATIONS ON POSSIBLE EXPERIMENTAL SHORTCOMINGS

It is felt that these tests would be improved if a long, serious study of surface topography changes were undertaken. The following observations are not intended to undermine this analysis as some useful knowledge and understanding has been gained using the simple equipment. Moreover, the basic concepts employed here could still be embodied into a specific study programme. These comments are listed below,

1) The sliding speed should be variable from 5 mm/s up to 40 mm/s and would be best achieved with a motorised drive and a mechanism capable of performing oscillatory motion.

2) The specimens are held in a horizontal position and loose debris falls away from the surfaces. The effect of all created debris on the surface topography is important and it is felt that the specimens should be mounted in a vertical position with specimen 'B' above 'A'.

3) Frictional losses have been reduced as far as possible in the fixture design although lubrication was not used. The effect of friction may slightly alter the loading between the specimens and any wear of the bearing surfaces may contaminate the specimens causing possible weight loss variations.

4) The cleanliness of the apparatus and the specimens is important and care must be taken in storing the test pieces. In these

experiments the continual handling of the specimens was reduced by placing them in their special holders.

5) The effect of environmental changes on the surfaces of the specimens may need to be considered, especially when repeated use of the S.E.M. is required.

6) In a prolonged study it may be beneficial to have many pairs of specimens, each pair being given a specific sliding distance and speed This would mean that a continual study of a particular surface would be hampered, although the pattern of surface changes may be more easily understood.

5.2.v EXPERIMENTAL RESULTS AND OBSERVATIONS

During the tests many photographs were taken, and only a selection are presented in this section. The first series of photographs (P.5 - 1 to P.5 - 12) are of the same small area on the test pieces. These areas are approximately 0.025 mm^2, and are shown in order of sliding distance.

The second series illustrates general surface conditions (P.5 - 13 to P.5 - 28) on each specimen and are intended to demonstrate the numerous activities which have occured. For consistency, they are also shown in order of sliding distance.

The tests are listed in the table of Fig. 5.5

SERIES 1) TOPOGRAPHICAL CHANGES OF PARTICULAR AREAS

Photographic details are as follows -

Scaling for specimens shown with photographs.
Time exposure based upon C.R.O. raster speed.
C.R.O. with low persistence phosphor screen.
Camera setting f8 - 35mm film.

The selected area on specimen 'A' has a small void in the new surface and is clearly seen in P.5 - 1. The lay of the grinding marks can be seen but it is not possible to establish a description of the

SPECIMEN A

SPECIMEN B.

P.5.-1. (0·0 mm T.O.) P.5.-2.

A.

B.

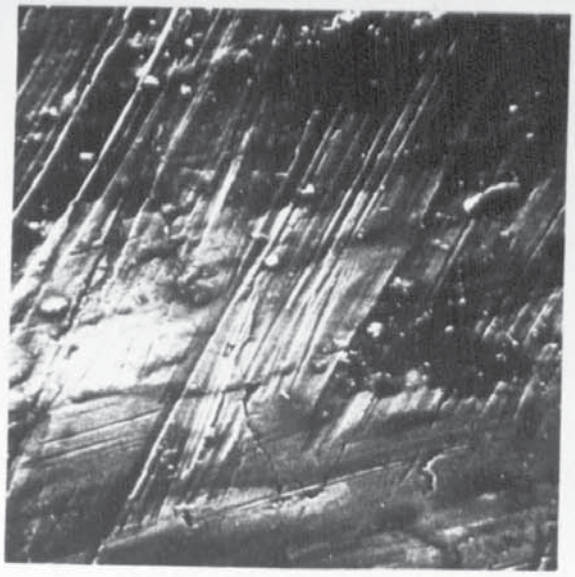

P.5.-3. (TEST 10) P.5.-4.

0·1 mm.

↔ DIRECTION OF SLIDING.

SPECIMEN A

P.5.-5 (TEST 13)

SPECIMEN B.

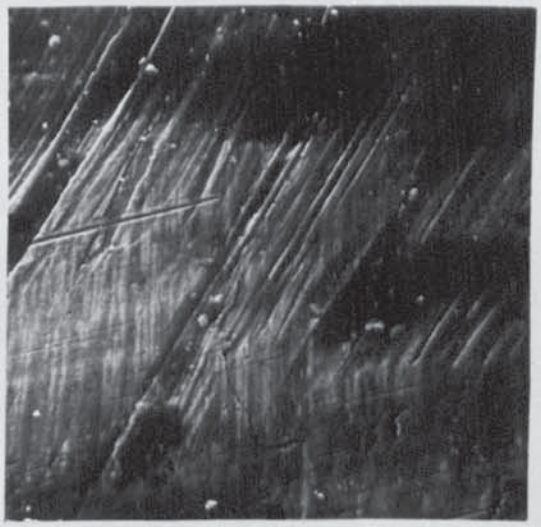

P.5.-6

A.

P.5.-7 (TEST 17)

B.

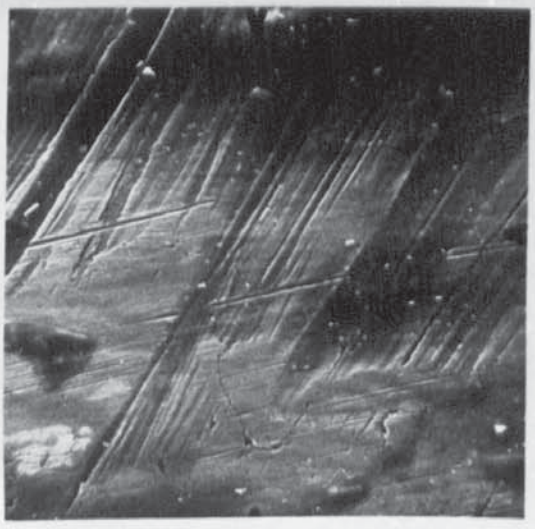

P.5.-8.

0·1 mm.

DIRECTION OF SLIDING.

SPECIMEN A.

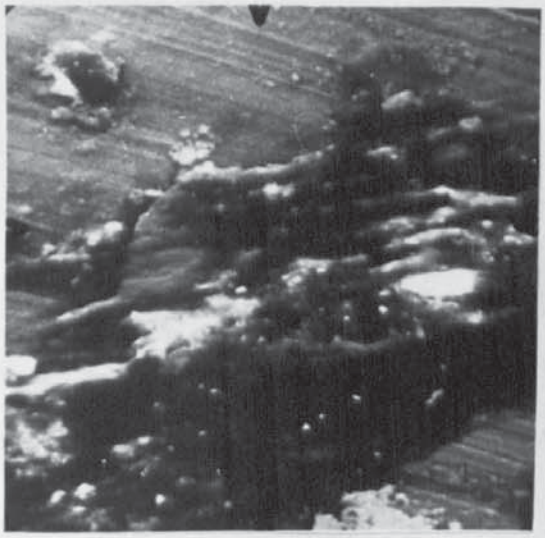

P.5.-9. (TEST 20) ⟷

SPECIMEN B.

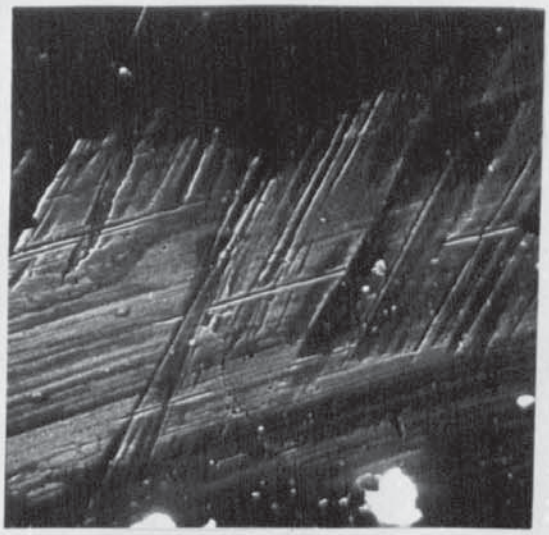

P.5.-10 ⟷

A.

P.5.-11. (TEST 25) ⟷

B.

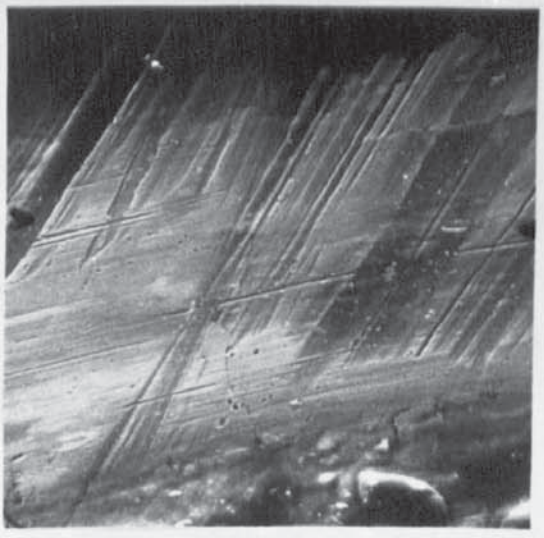

P.5.-12 ⟷

0·1mm.

⟷ DIRECTION OF SLIDING.

sizes of these grooves. Surface 'B' in P.5 - 2 does show the newly ground topography to advantage and an estimate has been made of groove dimensions.

Grinding groove width varies between 0.012 mm to 0.004 mm. and taking into account the lay of the surface and its general relative slope of 3° to the picture surface the groove depth is in the order of 0.05 times its width.

These two surfaces are not quite opposite each other in their fixture datum position, but the direction of the wear tracks in subsequent pictures of surface 'B' lie in approximately the same direction as the grinding marks on surface 'A'.

In both the above illustrations surface cracks can be seen and it is thought that they are related to the position of grain boundaries of the surface material. These areas are comparatively free from debris, which tends to be highlighted by small bright patches. Debris in the form of oxides usually has a higher brightness (due to its structure) than does any other cast iron particles.

As these tests progress then surface 'A' becomes contaminated with a layer of oxide which eventually completely covers the original void and most of the area. It can be seen through P.5 - 3, 5 and 7 that this formation has not completely adhered to the surface and the changing shape reveals parts of the original surface. This area has not been subjected to any degree of wear but it is likely that oxide debris has been created from the surface layer.

Surface 'B' does show extensive wear as the tests progress, especially over the lower half, which has become much smoother. The amount of surface debris shown in P.5 - 4, created after a relatively

short sliding distance, generally decreases in both size and quantity as tests proceed to the condition of P.5 - 12. The debris forms can be described as spherical, flat circular or round cigar shaped. These particles are moved into the grinding grooves and some remain undisturbed, which suggests that they are less than 0.0005 mm in height. It is estimated that the particle average diameter is in the range 0.0005 mm to 0.002 mm and in the early test stages the large particles are dominant.

The general change in surface lay is in the direction of motion and the longer wear grooves are estimated from P.5 - 10 to be 0.0015 mm wide. Their depth is difficult to ascertain but it would appear, from their intersection with the grinding lines, to be of the order of 0.0003 mm.

It can be seen that the edges of the grinding marks have been worn down, deformed into the grooves, and some edges have been broken away creating further debris.

The series of illustrations for area 'B' highlight the effect that the narrow individual grinding lines are superimposed on a larger surface waviness.

SERIES 2) GENERAL TOPOGRAPHICAL OBSERVATIONS

This set of illustrations is nearly all taken from surface 'B'. The various aspects have been grouped together for clarity and a note is made following each one.

P.5 - 13 to P.5 - 17

These photographs show the intersection of wear and grinding grooves.

The ridges of the grinding channel have been deformed and worn down. Fragments of these edges have broken away and others appear to be

SPECIMEN B.

P.5.-13.

SPECIMEN B.

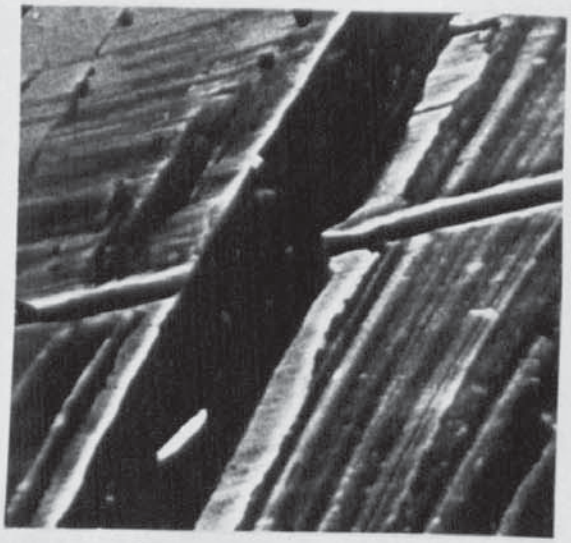

P.5.-14.

0·025 mm.

SPECIMEN B.

P.5.-15

0·050mm.

SPECIMEN B.

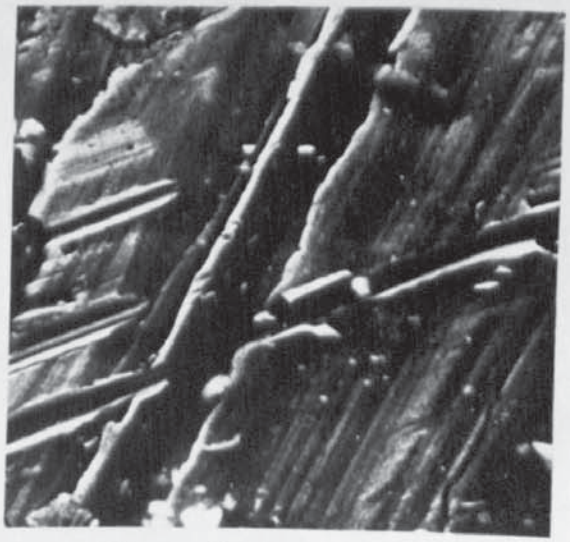

P.5.-16.

0·025mm.

SPECIMEN B.

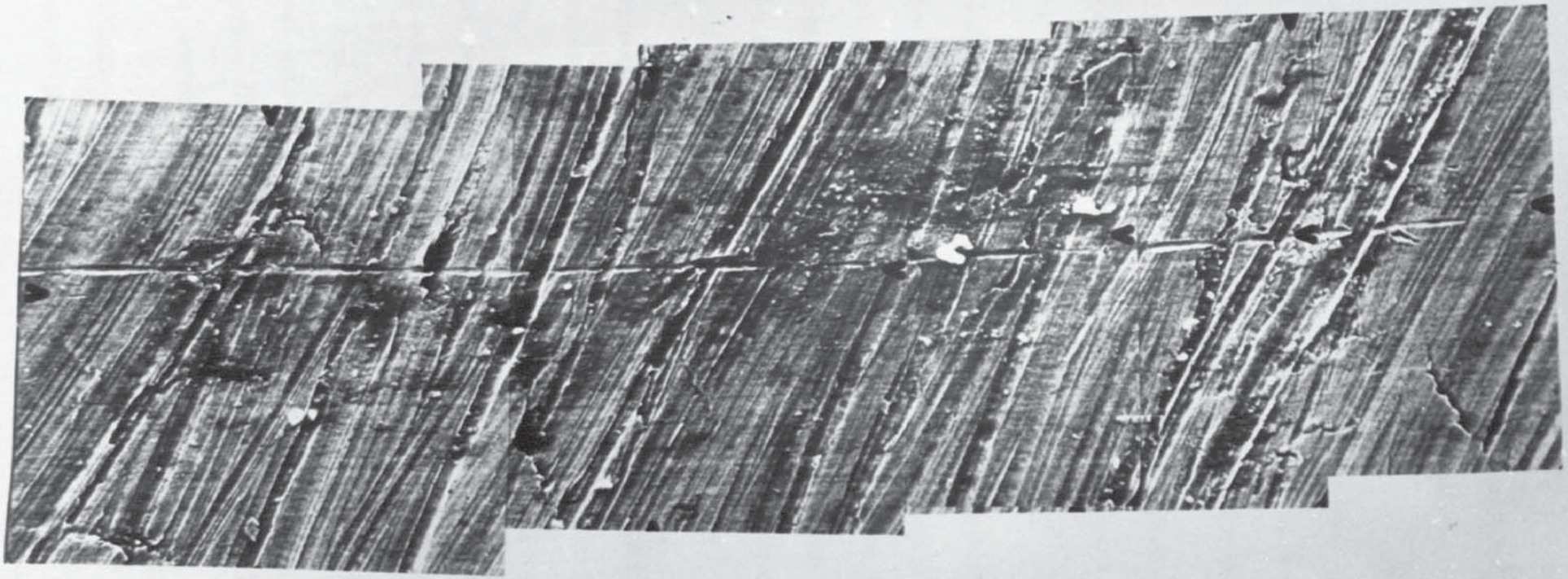

P.5.-17.

0·1 mm.

73.11.

in the process of doing so.

The wear grooves are seen to enter the grinding channel from the left in P.5 - 14 and P.5 - 16. Some of these tracks have a bottom in the form of two narrow grooves and it is thought that this is due to the oscillatory sliding motion. The edges are raised above the surrounding surface to form their own ridges. This would indicate some ploughing action by the debris or caused by a small protuberance on the mating surface.

Debris has fallen into the bottom of the grinding channel and some of these particles may have come from the wear track due to the cutting or ploughing action that was present.

The width of the grinding channels is approximately 0.008 mm and the width of the wear tracks 0.002 mm. Ridge to valley heights are difficult to estimate in both cases but their appearance would suggest rather steep sides and basically that the cross sectional profiles are circular. It is suggested that the width to depth ratio of the wear grooves is in the order of 4 : 1 and the grinding channel ratio 8 : 1.

The creation of cast iron debris occurs predominantly with the breakdown of grinding ridges which is accentuated at points of intersection with wear tracks. The general debris sizes in these pictures gives mean diameters in the range of 0.003 mm to 0.0005 mm. Their general appearance would appear to suggest a rather flake-like shape and some cigar shapes.

Apart from these tracks the general surface appears to be worn with the original grinding marks predominating. There is an appearance of a surface structure consisting of rather flat laminated plates, parts of which have been removed.

The illustration P.5 - 16 is an enlargement of P.5 - 15, and the surface has been subjected to a greater sliding distance. Some oxide debris

is present in both cases and it is suggested that the ball like nature of this is conducive to the generation of some wear tracks.

The composite picture of P.5 - 17 illustrates a long wear track, the very bright patches indicating oxide debris. The width of this track varies, being a maximum of 0.003 mm. These variations indicate the general waviness of this surface, which has given rise to changing ploughing conditions in making the track. By considering the points along this track of maximum width, a measure of this waviness can be obtained. The surface waviness appears to be repeated, on average, every 0.05 mm and has an amplitude in the order of 0.002 mm.

Again this larger area has several long cracks in the surface which are the broken edges of plates or grain boundaries. Several fissures can be seen which are likely to be the positions of graphite particles, some of which have been removed in the machining and sliding wear processes.

P.5 - 18 to P.5 - 21

The mechanism for the creation of debris will be complex and these illustrations indicate some of this generation which, it is felt, is associated with the material near to and on the surface.

P.5 - 18 and P.5 - 19 show an area from which a flake fragment has been removed. The general lay of the surrounding surface is in the direction of sliding motion. The bottom of the remaining crater appears to be quite flat and has steep sides. The depth of this hollow is estimated to be less than 0.005 mm and it is possible that this position was occupied by a graphite flake at some time. Such an area is a collector of surface debris and oxide can be seen lying on the bottom of the hollow. The rough appearance of the side wall, to the right, suggests that some adjoining metal was subsequently removed.

SPECIMEN A.

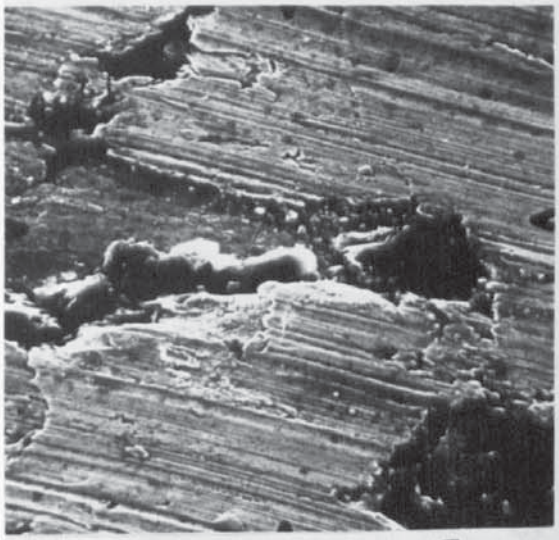

P.5.-18.

0·1 mm.

SPECIMEN A.

P.5.-19

0·05 mm.

SPECIMEN B.

P.5.-20.

SPECIMEN B.

P.5.-21.

0·025 mm.

P.5 - 20 and P.5 - 21 illustrate two possible alternatives of how the above hollow may have been formed. In P.5 - 20 part of the boundary edge of a flake has been completely turned over, again in the direction of motion. This turned-over portion has a diameter value of 0.005 mm and being extremely thin is likely to be removed and rolled up into a cigar shaped piece of debris. Surrounding the small fissure, above the flake, are very tiny black spots which may indicate small holes in a thin layer of surface oxide. The turned-over surface of the small flake is very bright and may indicate some oxidisation due to the heating of this area during deformation.

P.5 - 21 shows two thin flakes partially orientated in the direction of motion. Again the average diameter of these particles is 0.005 mm. It is possible that they have been removed from the surface in a position indicated by a dark hollow to their left. The general lay of this surface is due to the grinding marks but it is felt that these flakes have been torn from their original position by a protuberance on the mating surface. This has made a small groove in the grinding ridge immediately to the right of the flakes.

P.5 - 22 to P.5 - 25

The interaction between the surfaces to produce wear tracks and subsequent debris is illustrated in these photographs.

In P.5 - 22 the terminal point of a wear groove is shown. The direction of the track follows the sliding motion. Near the end of the track appears a thin layer of bent over material, similar in shape to the bow wave created by a boat. If we assume that the predominant track was created by a protuberance on the other surface, when moving from left to right, then in the return motion another much smaller track has been made. This commences at the small mound of material. This area was not viewed with greater magnification but it is suggested that the protuberance

SPECIMEN B.

P.5.-22. 0·05mm.

SPECIMEN B.

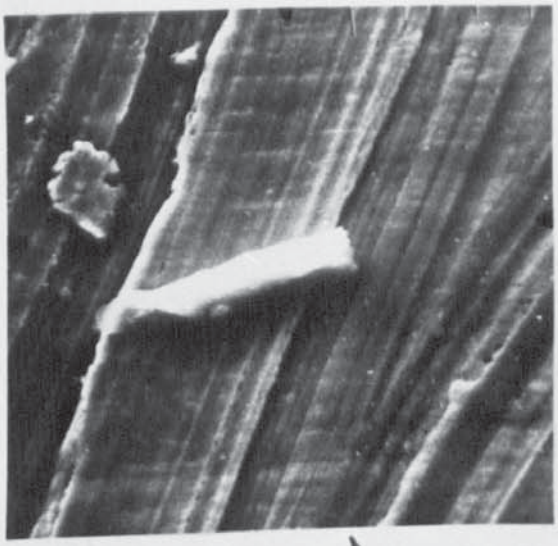

P.5.-23. 0·02mm.

SPECIMEN B.

P.5.-24. 0·025mm.

SPECIMEN B.

P.5.-25. 0·01mm.

was sheared at the mound position due to a rise in this surface. The remaining form then produced a short but larger groove. On the return of this ploughing element, some of the material in the prow formation, or even part of the sheared protuberance was picked up or perhaps rolled to produce the shallow secondary wear groove. The general surface area in P.5 - 22 indicates metal deformation of the grinding ridges which has tended to fill in the grinding channel.

P.5 - 24 is a similar example to the above but an opportunity was taken to magnify this area as indicated by P.5 - 25. The first wear track was made with the upper surface moving right to left. It can be argued that the material that has made this track has partially remained at the end, together with some surface material, which has apparently oxidised. Some attached material on the other surface has moved from left to right of this position taking a line of least resistance and created a small secondary track. In both these pictures the general surface lay is due to grinding but ridge deformation is in evidence.

P.5 - 23 indicates two different types of debris. One is a flat plate of cast iron material having a diameter value of 0.004 mm. The other dominant particle is rolled oxide debris approximately 0.015mm in length with a diameter of 0.0018 mm. It is suggested here that the debris shapes may be governed by the shape of the grinding grooves on each surface and the relative movements of these two surfaces, the general surface forms being used to deform and mould the debris into shape. This idea would conform with these observations, in that as the surfaces became generally smoother a deformation process would tend to create smaller debris sizes, especially if their material consisted of a thin oxide film or small cast iron flakes. Any such interaction and deformation would of course produce some surface grooving by the debris.

P.5 - 26 to P.5 - 28

The growth of surface oxide as part of the debris material is shown in these illustrations.

P.5 - 28 shows a general area of surface 'B' contaminated with oxide. The longitudinal shape of the large area indicates the direction of sliding motion. It can be seen that oxide possibly in the form of small particles has filled in one of the large grinding marks. There is some indication here that the oxide area may have been much larger but has been moved away by the process of wear during sliding. The general appearance of this area is one of smoothness due to the wearing down of the original ground surface.

P.5 - 26 and P.5 - 27 illustrate a deformed oxide film. P.5 - 26 was taken using high power on the electron beam and the oxide appears to be transparent and only the outline can be distinguished with clarity.

P.5 - 27 was taken with a reduced beam power (2.5 Kv) and indicates quite clearly the interior shape of the particle. The definition of the surrounding surface has now been lost. It should be noted that the viewing of oxide films is dependent upon the electron beam voltage. P.5 - 27 illustrates clearly that the oxide film is extremely thin. It is expected that this oxide would deform further to become cigar shaped.

A general picture of the area in which this oxide was found is not illustrated, but in an area 0.16mm^2 five such shapes, all very similar, were identified.

SPECIMEN B.

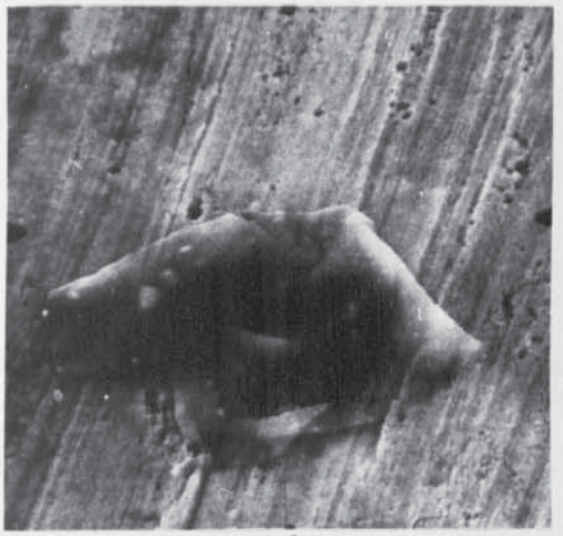

P.5-26. 0·025 mm

SPECIMEN B.

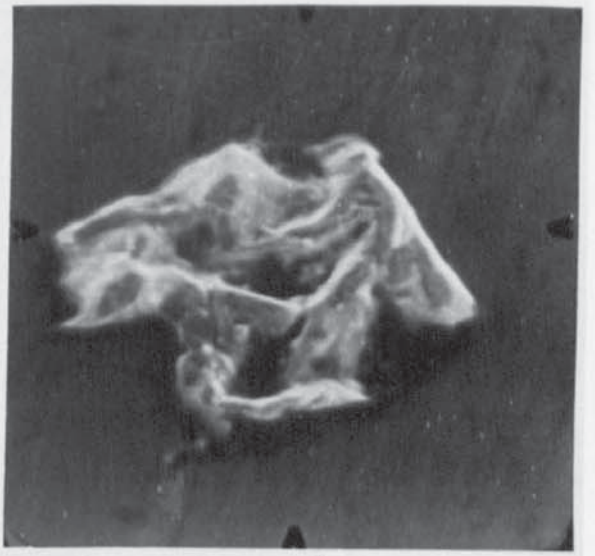

P.5.-27. 0·025 mm.

SPECIMEN B.

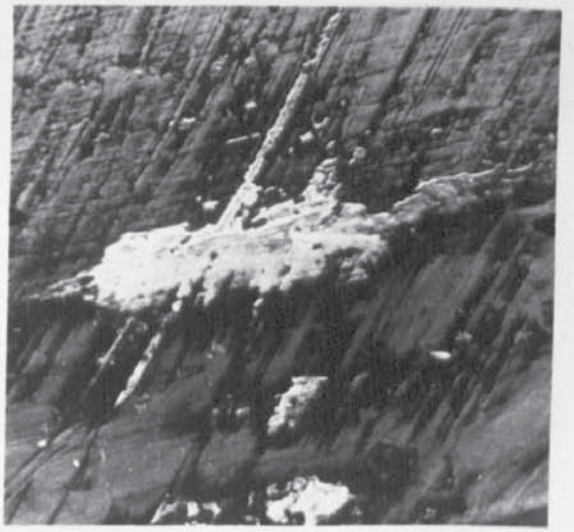

P.5.-28. 0·2 mm.

The test photographs illustrate that a complex system is in operation to change the surface topography.

Such a system will contain such factors as,

a) Original surface finish.
b) Surface preparation methods.
c) Metallurgical and crystalline structure of the surface material.
d) Atmospheric conditions.
e) Force applied between the surface.
f) Relative sliding speeds.
g) Degree of oxide formation.
h) The influence of surface debris.

In this particular experiment, which was meant to simulate dry slideway conditions, some general comments can be made.

1) The weight loss of 'B' (representing the machine table) is approximately twice the weight loss of 'A', (representing the machine slide). The loss rate is rapid in the early test stages and reaches an equilibrium condition, i.e. constant slope, when the sliding distance for 'A' is 2.4 m. and for 'B' 6.0 m. The equilibrium wear rate for 'B' is small and of the order of 0.5×10^{-5} gm/m. The wear rate for specimen 'A' is less than this figure and is calculated to be 0.2×10^{-5} gm/m.

These figures show some agreement with those found by Eyre (84) whose values are higher due to increased loads and sliding speeds (between $2 - 5 \times 10^{-5}$ gm/m).

2) The surface of 'B' had more wear tracks and was generally smoother than 'A'.

3) Surface 'A' had more oxide formations which continually changed in size.

4) X-ray diffraction of the oxide formations on both specimens indicated that they mainly consisted of Haematite (Fe_2O_3) with some Magnetite (Fe_3O_4). There was difficulty in distinguishing between these two using the A.S.T.M. index of crystalographic analysis. These

oxides are formed at temperatures in the range 250 - 350°C, and this indicates that the interface temperatures were low and of this order of magnitude. These findings are similar to those found by Eyre and Maynard (85)for dry cast iron equilibrium wear conditions.

5) The surface 'B' tends to be worn down by continual interaction with the ridges on surface 'A'. Both surfaces create debris, but it would appear that the bulk of this material stays on surface 'A'.

6) As parts of surface 'A' were exposed to the atmosphere during the tests, loose debris may have fallen off. There may also have been some oxidisation of this surface.

7) A general description of both surfaces can be attempted. In order to do so the presence of debris and oxide has been disregarded for basic simplicity.

The surfaces are covered with long shallow grooves whose width to depth ratio is the order of 20 : 1. These grooves are superimposed on another undulating series of wide troughs. An illustration of such a surface is shown in Fig. 5.7. The dimensions shown in this drawing are average values based upon test results.

The interaction of the surfaces and the generation of wear particles will depend to some extent upon the relative surface lay positions when contact is made. This will generally mean that the grooves on one surface lie across the grooves of the other at some arbitrary angle.

8) The size and shape of the debris particles will depend upon this basic surface shape and the relative directional lay of the contact faces.

In these tests the debris sizes are approximately half a magnitude smaller than the smaller grinding groove dimensions. The wear tracks are also smaller in width than these by a factor of 4 : 1. These observations are in agreement with those obtained by Endo, Fukuda and Takamiya (86).

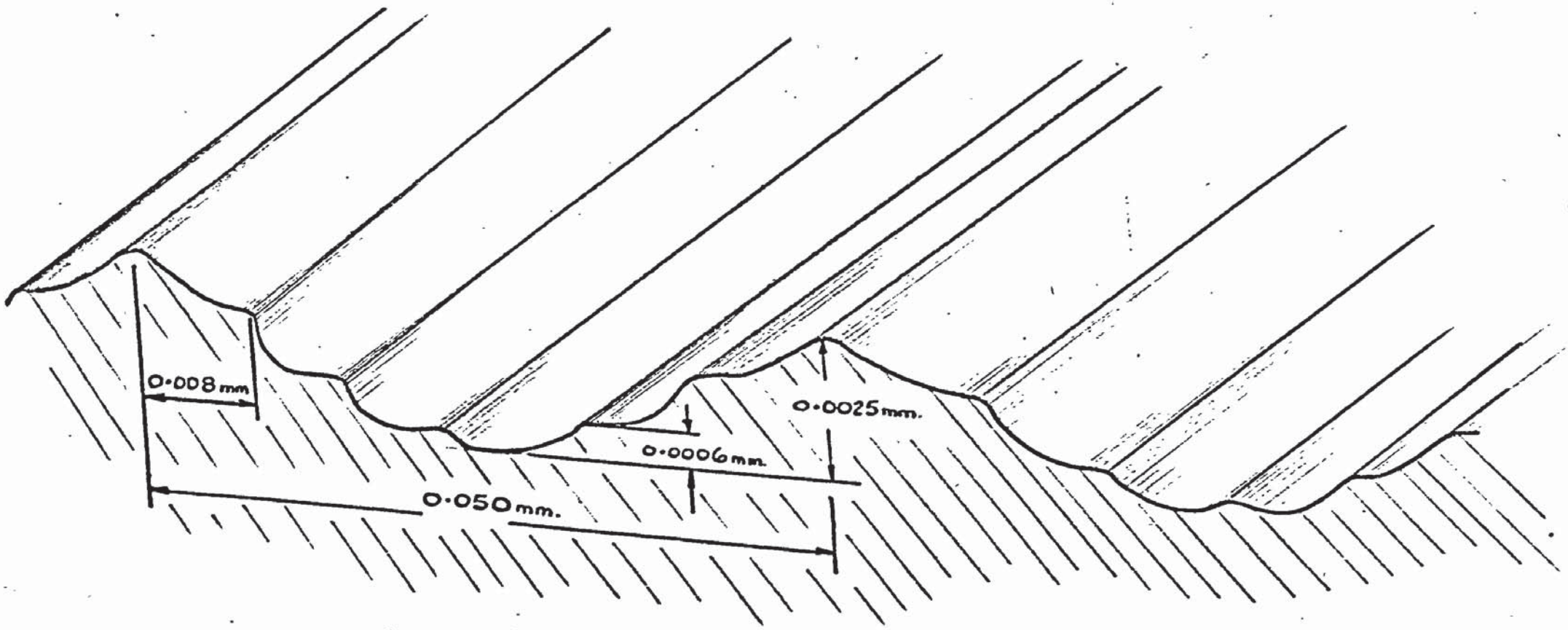

FIG 5·7. AN ILLUSTRATION OF SPECIMEN TOPOGRAPHY.

9) In all cases, it is estimated that any channel, groove or track will have width to depth ratios between 10 : 1 and 20 : 1.

10) The nature of the laminar characteristics of the cast iron surface will certainly give rise to the formation of debris. It would appear that surface wear due to deformation and mechanical erosion could be reduced if a smoother and harder oxide film were formed on the surfaces of the sliding pair.

In these tests it has been estimated that the detached oxide flakes had an average thickness of between 25 and 50 x 10^{-6} mm.

It is the initial formation of such an oxide film on the surface of specimen 'A' that has resulted in the wearing away and smoothing of surface 'B'.

11) Although extensive examination was made of surface 'B' it is difficult to estimate the degree of metallic contact at the end of the tests. This area is extremely small and a very approximate figure would be that only 0.3% of the surface area of 'B' has indications of metallic sliding contact.

The contact points appeared to be evenly distributed over the surface.

5.3 A STUDY OF TOPOGRAPHICAL CHANGES ON LUBRICATED SLIDEWAY SURFACES

To obtain further information regarding the surface changes likely to occur on working machine tool slideways, a further series of observations were made.

A replication technique was employed to give specimens of suitable size for viewing with the S.E.M.

Replicas were taken from the guideway surfaces of eighteen lathes, in a position midway along the length of each bed, this ensuring that these surfaces were representative of a regularly used portion.

The general slideway configuration on each machine was the same as that shown in Fig. 4.1, having two flat, plain guideways to support the moving table. All the slideways were made of grey cast iron and it was established that the guideways were in an unhardened condition. An estimation of contact pressure between the sliding surfaces was made, under non-cutting conditions, based upon table weight and apparent contact area. In all cases the pressure was between 50 - 80 kN/m^2. The original surface preparation of the slides was of a similar nature to that outlined in the previous section and in particular they were all finished by cup grinding. In all cases it was assumed that the table contact surfaces were peripheral ground in the direction of sliding motion.

The slideways were lubricated with various grades of mineral oil, using the principle of "wick feeding". None of the machines employed a system of automatic pressure lubrication. Therefore it was not possible to define accurately the degree or effectiveness of the slideway lubricants. Although most of the machines possessed slideway wipers, none of them had protective guideway covers.

The age of these lathes ranged from six months to eighteen years. It was impossible to calculate the sliding distance covered by each machine and therefore it was decided to arrange the surface profiles in terms of age coupled with a usage factor expressing the degree of work to which the slideway was subjected. These usage factors are as follows,

a) Usage Factor 1 (UF.1) - Light utilisation, such as a demonstration model or University machine used only for laboratory work (say average of one hour of work per day)

b) Usage Factor 2 (UF.2) - Medium utilisation, such as a toolroom machine or one committed to low batch production. (say average of three hours of work per day)

c) Usage Factor 3 (UF.3) High utilisation, having constant daily use for mass production, (say average of six hours work per day)

5.3 i SPECIMEN PREPARATION AND EXPERIMENTAL PROCEDURE

J. Grundy (87) at the School of Dental Surgery, Birmingham University, was extremely helpful in establishing the replication technique. This was a two stage method as follows,

1) A silicone elastomer was used to make a negative replica of the slideway surface. This was a two part compound known commercially as Verone Pink, the rubber based solution and catalyst being mixed in the ratio of 10 : 1. The setting time for this mix was normally five minutes.

A disadvantage of silicone elastomer is its high coefficient of thermal expansion. If the replica itself is to be examined in the S.E.M. it must be given a conductive coating of metal. This was found to crack and flake when subjected to environmental changes. The problem was overcome by making a positive model from the replica in a dimensionally stable material which had the added advantage of making subsequent interpretation of the surface easier.

2) The second stage model was made by pouring Araldite epoxy resin (CY212) over the replica laid in a small shallow glass dish. The covering above the specimen surface was approximately 5 mm.

The resin was left to harden for twenty four hours at room temperature. After setting, the elastomer replica was peeled off the araldite, leaving a good, positive copy. This block was cut to size and the replica mounted on a labelled aluminium stud suitable for the S.E.M. Prior to examination the models were metal-coated. For this process they were placed in a vacuum evaporating chamber and coated with gold/palladium about 300Å in thickness.

Electrical continuity between this coating and the stud was ensured by the application of Aquadag or Silver Dag.

To facilitate the production of the silicone elastomer specimens, mild steel washers 50 mm diameter by 3 mm thick were made.

A centre hole of 10 mm diameter, in these, formed the mould. To ensure correct orientation of the replicas two fine grooves were filed in the wall of the mould, 180° apart. This enabled the washer to be positioned on the slide with the two lines indicating the path of normal sliding motion.

A selected machine surface was cleaned to an area greater than that covered by the washer. This was done by wiping the surface with soft paper tissues and then spraying with acetone from a plastic bottle. The area was again wiped and sprayed, leaving the acetone to evaporate completely. It was hoped that this would remove all the lubricant which would have a deleterious effect on the surface replication. The effect of this cleaning of course was to remove most of the surface debris.

The metal washers were correctly placed on the slide and held in position temporarily by means of plasticine. A silicone elastomer compound was mixed thoroughly, in an attempt to remove all entrained air, and immediately poured into the mould. After filling was completed a small steel weight was placed over the mould with the intention of improving the surface replication.

When hardening was completed the washer was removed, complete with replica, and the specimen was labelled, trimmed to remove any flaking and carefully placed in a small, clean storage container.

For every machine examined three replicas were taken in the same general slide area, ensuring that a comprehensive picture of the topology was obtained and that any failure in reproduction would not seriously affect the study.

The positive araldite replicas were placed in the S.E.M. in an orientation based upon the mould lines, thus enabling the direction of sliding to be ascertained at low magnification. The general tilt of the

surface was greater than that obtained in the previous section, being of the order of 5°, and again sloping away from the plane of the photograph when moving from the bottom to the top.

5.3 ii EXPERIMENTAL RESULTS AND OBSERVATIONS

In order to assess the reproducibility of this two stage replication technique a new ground cast iron surface was produced. This was done using the same material and surface preparation procedure as outlined in section 5.2 i. A replica of this surface was made and compared with that of the actual machined specimen. Care was taken to ensure the same orientation and microscope magnification as far as possible.

The resulting photographs are shown in P.5 - 30 and P.5 - 31.

A qualitative assessment can be applied and the general matching features of the surfaces are such as to provide a good indication of reproducibility. The general lay and topography of the surface can easily be identified. The small lines labelled (A) on each illustration indicate a slight shift in viewing area.

The small sharply defined holes, usually exhibiting a bright halo, which appear in the surface of the replica are considered to be caused by entrained air in either of the compounds used.

The flake-like appearance of the actual cast iron surface does not entirely show itself in the reproduction, but considering the magnification of the area it is estimated that grinding marks of width 0.005mm can be reproduced using this technique. Small holes, cracks and the torn, jagged edges of grinding ridges are not so well defined. The small white dots which are apparent on the surface of the replica are probably due to contamination of the surface either before or after the plating process of the araldite specimen.

CAST IRON SURFACE.

P.5.-30

SURFACE REPLICA

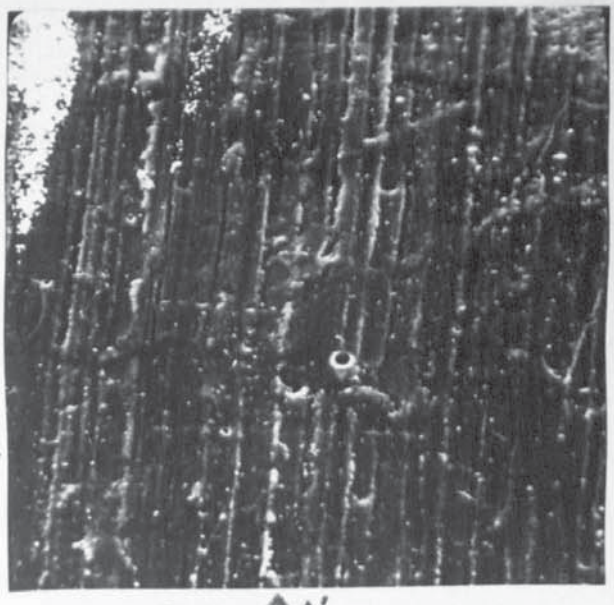

P.5.-31.

From the many photographs taken, a small selection (P.5 - 32 to P.5 - 42) are shown here, in order of machine age. They are taken from slides made of grade 17 cast iron, having the same surface preparation as that stated in section 5.2

P.5-32 to P.5 - 35

In P.5 - 32 the surface appears generally smooth, with the grinding marks dominant and having a width range between 0.02mm and 0.006mm. The enlargement shown in P.5 - 33 indicates the infilling of these grooves by the plastic flow of ridge material. The wear tracks on the surface have a width in the order of 0.0015 mm maximum.

It is considered that the topographical state of this surface is very similar to that of the test specimens, detailed in section 5.2, at the end of their sliding tests. Therefore an equilibrium wear condition has been achieved.

P.5 - 34 indicates a continuation of a smoothing action and the grinding marks appear to have reduced in depth. The width has decreased marginally on those remaining and the shallower grooves have been eliminated. The surface has been affected by the sliding action and many small wear ridges can be seen.

In P.5 - 35 an enlargement of the intersection of a large wear groove and a grinding hollow can be seen. The wear track indicates a double ridge caused by reciprocating motion and the width of such tracks appears to be larger, in the order of 0.004 mm.

Although surface contamination has affected the replication, the flow of surface material is in evidence, together with irregular shaped hollows indicative of the removal of small flakes of material, or the original position of graphite particles.

M/c. WARD 3.D. AGE 1 YR. USAGE FACTOR - 1

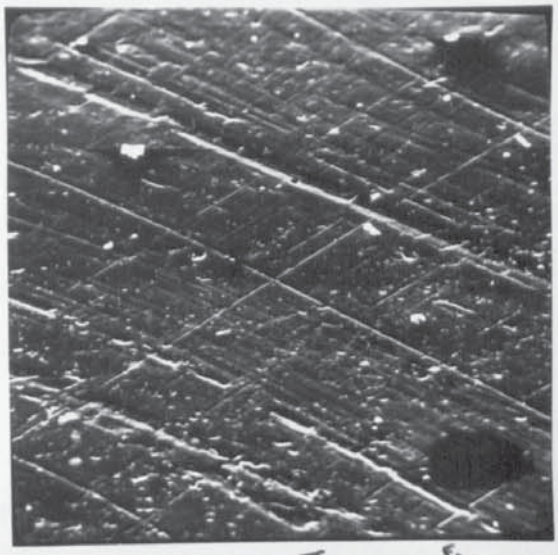

P.5-32. 0·5 mm.

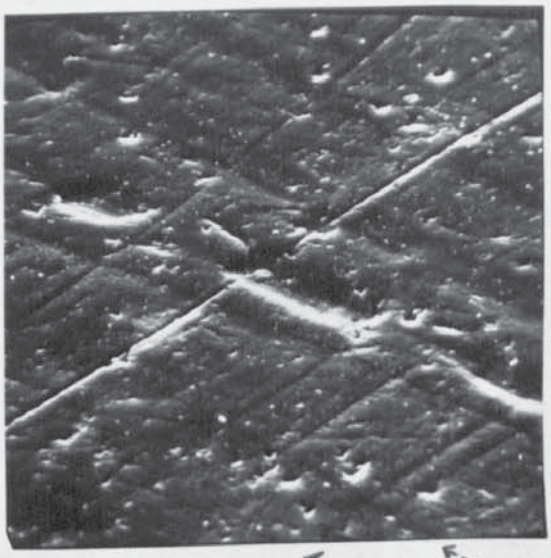

P.5.-33. 0·1 mm.

M/c. WARD 3.D. AGE 2 YRS. USAGE FACTOR - 2.

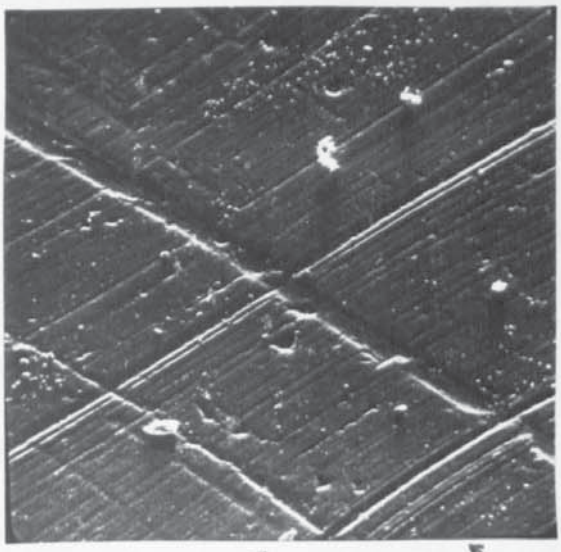

P.5-34. 0·25 mm.

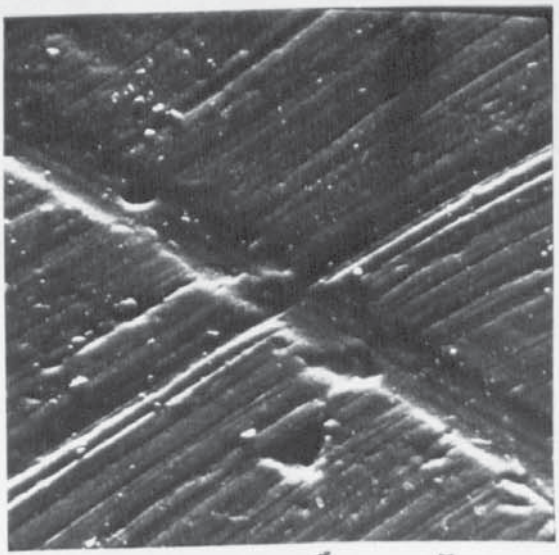

P.5.-35 0·1 mm.

↔ DIRECTION OF SLIDING.

↔ DIRECTION OF GRINDING.

P.5 - 36 to P.5 - 39

These photographs indicate very little change in the surface condition. The grinding marks have become shallow and have been reduced in size by the infilling of surface material. Surface hollows caused by the removal of small metal flakes appears to have increased.

Wear tracks are becoming dominant although this is not clear to see because of the viewing angle of these specimens. In general, the wear tracks have increased in width and the surface roughness shows the effect not only of the debris but also of the topography of the mating surface.

The relative sizes of grinding and wear tracks are nearly equal on the surface shown in P.5 - 38 and it is estimated that the maximum width of each is in the order of 0.008 mm.

P.5 - 40 to P.5 - 42

P.5 - 40 shows the surface of a machine slide subjected to high working conditions. The grinding grooves have been removed and the surface topography is represented by a series of wear ridges. An estimation of the width of these ridges gives values in the range of 0.002 mm to 0.004 mm and it is suspected that a general waviness of much greater peak to peak distance exists. General surface marks indicate the removal of small surface material particles.

Illustrations P.5 - 41 and P.5 - 42 are taken from the surface of the oldest machine slide examined. This machine has been subjected to extremely hard working conditions, and it is suspected, from an inspection of this machine, that the slideway lubrication was not satisfactory at that time. Due to its age the slideway configuration was slightly different from all the others mentioned here and in particular the slideway wipers were not present on the machine.

M/c. WARD 3.D. AGE 4 YRS. USAGE FACTOR-2

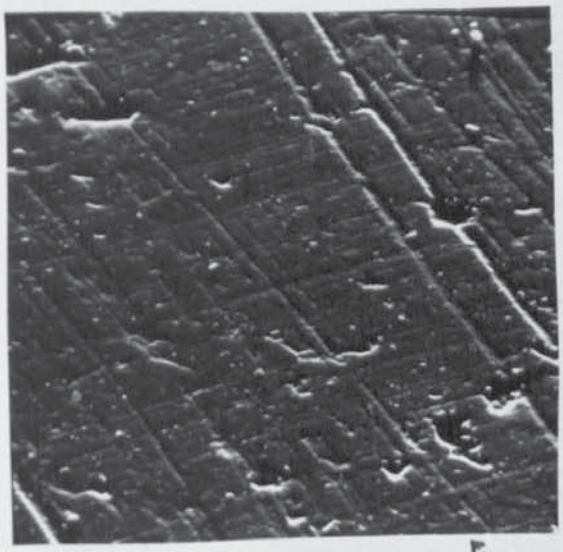

P.5-36.

0·25mm

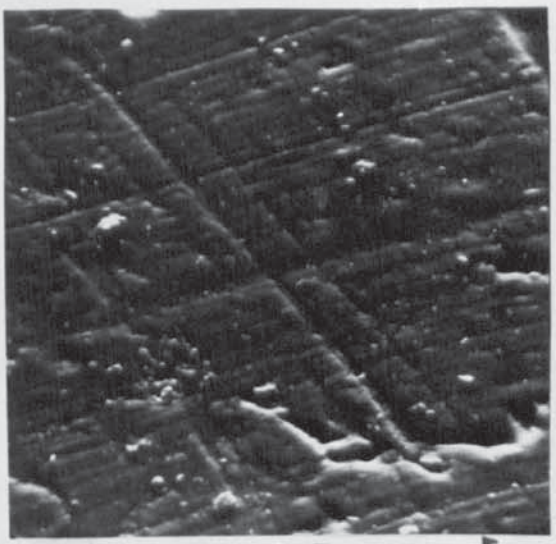

P.5.-37.

0·1mm.

M/c. WARD 3.D. AGE 6 YRS. USAGE FACTOR-2

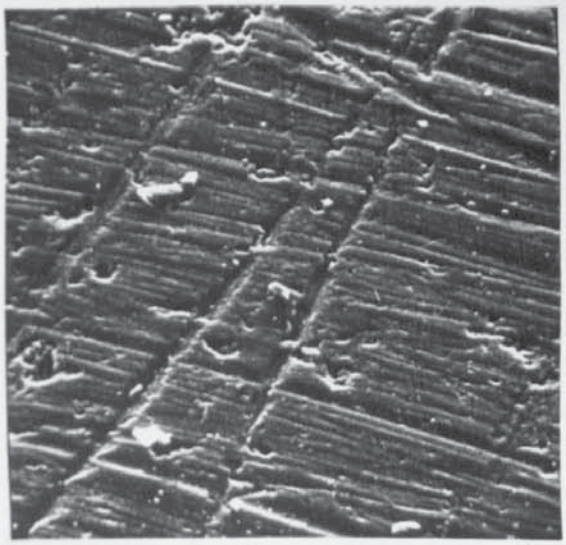

P.5.-38.

0·25mm.

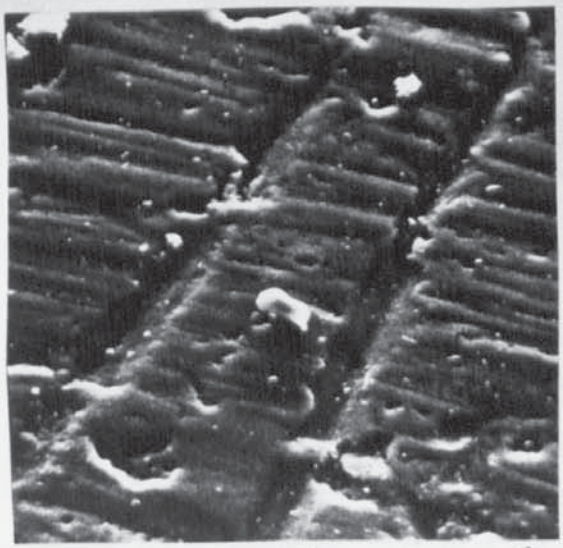

P.5.-39.

0·1mm.

The surface in P.5 - 41 is extremely rough, and this is due to the sliding action and possibly some localised corrosion. The wear track width ranges from 0.02 to 0.005 mm which is similar in size to the original grinding grooves.

An enlargement of such a groove is shown in P.5 - 42. The roughness of this channel indicates not only tearing of the surface due to some ploughing action but possible corrosion caused by the metal cutting fluid. This may have caused a softening of the surface material.

It is suggested by Grieve et al (81) that when the profile of a worn surface approaches a size equal to its original ground profile size, this is an indication of the completion of the useful life of the bearing surface.

Some general observations can be made as the result of these tests.

1) A boundary lubrication condition exists on machine tool slideways, and as a consequence asperity interaction produces the surface changes that take place.

2) The changes in surface topography occur over several years and depend upon,

   a) Degree of usage.
   b) Interface loading.
   c) The cast iron material.
   d) The lubricating oil and method of application.
   e) Particles fallen on the surface from the machining process and airborne pollutants.
   f) Fluids used in the cutting process.
   g) The degree of surface cleaning, especially by the use of any slideway wipers.

3) In all the cases investigated the width of wear tracks increased with time and regardless of material all appeared to have a size depending upon,

   a) Cast iron material of slide.
   b) Age and usage of machine.

This condition is especially true once the grinding marks have been completely removed.

4) The original surface lay due to grinding is gradually replaced by wear tracks and it is suggested that the rate at which this occurs depends upon several main factors,

   a) The original surface finish.
   b) The cast iron material.
   c) Interface loading.
   d) Machine age.
   e) Lubricants used.

5) The slide surface reaches an equilibrium condition with a fairly constant wear rate. The actual contact area, where wear tracks are likely to be made, will increase gradually with time, thus reducing local contact pressures. Suspension of debris in the lubricating oil will tend to maintain a constant wear condition.

6) The lubricant has the ability to capture and hold particles on the slide surface and, coupled with sliding load and contact area, tends to aid the equilibrium wear rate.

7) As sliding continues over the years, the slide surfaces appear to be smoother, having a more regular pattern of fine ridges, spreading over the surface. If this "smoothing" occurs more rapidly on the surface of the table slides, as suggested from the work in section 5.2, then the friction level at the interface is likely to reduce with time.

It is proposed that if some knowledge of the working conditions of a slideway are known and the cast iron material of the pair is established, then the age of a machine can be estimated by examining the surface topography.

The change in shape and size of both the grinding and wear tracks are plotted against machine age in Fig. 5.8 These curves are illustrative only, and show the changes in an aspect of surface topography that may take place on machine slideways. In drawing these curves it has been assumed that surface loading, lubrication and slideway material are constant factors. For higher grades of cast iron or for harder surfaces it is likely that the grinding tracks will take longer to be removed and that the final wear track size will be smaller.

These curves indicate an overall smoothing in surface roughness which would mean a reduction in measured C.L.A. value with machine age. Such a proposition is in general agreement with the observations of Endo et al (86).

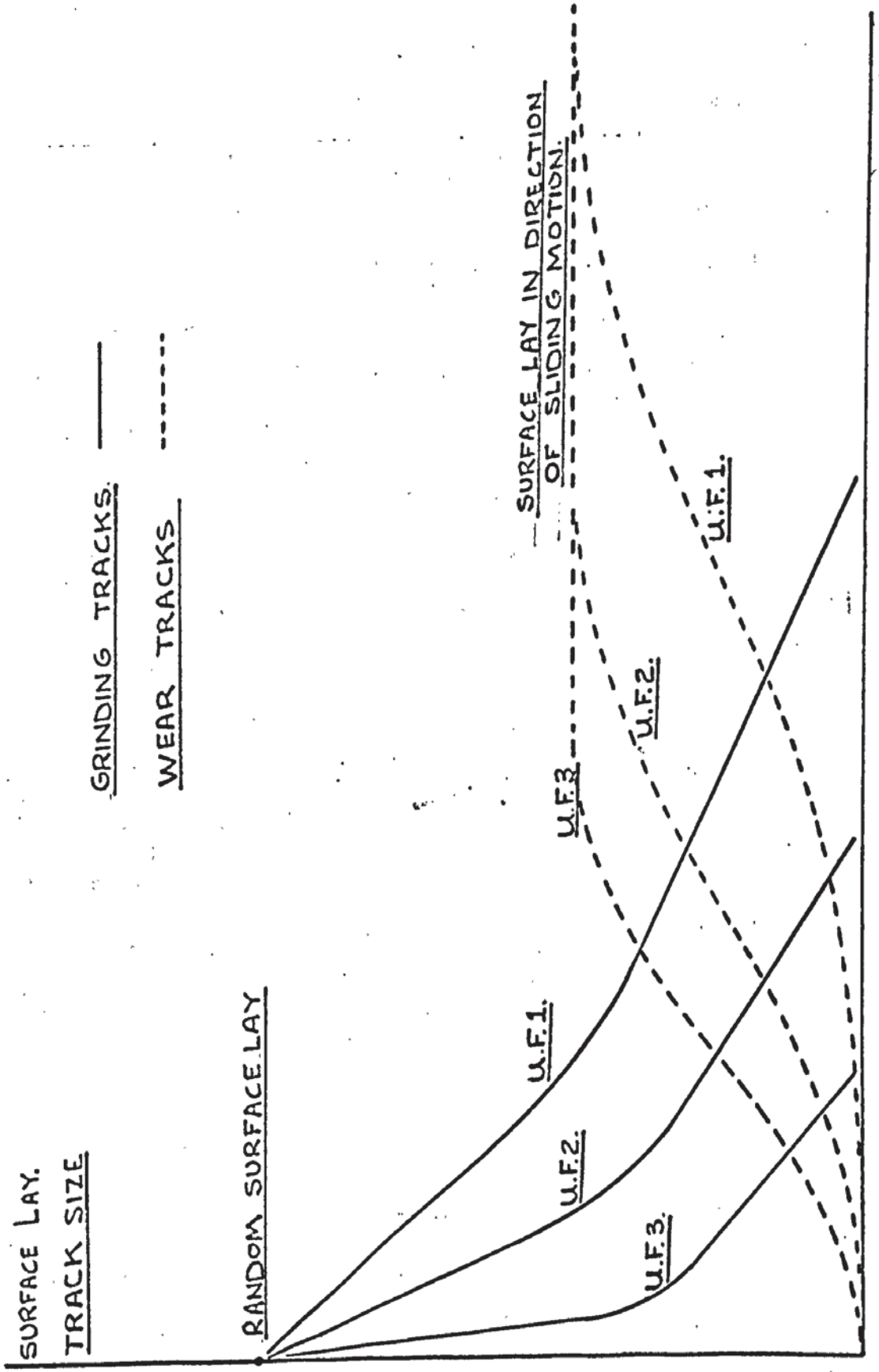

FIG. 5·8. TOPOGRAPHICAL SLIDEWAY CHANGES WITH AGE AND USAGE.

The friction levels of a slideway will be reduced with time and Fig. 5.9 illustrates such a change.

It is unusual that surface loading, lubrication and slideway material are considered to be constant parameters. At any point in the life of the machine the friction level will fall from a static value to some lower limit, before rising slowly again with sliding velocity. Although the velocity at which minimum friction level will occur is likely to reduce with age, the actual friction value and general profile shape thereafter will be largely dependent upon the characteristics of the lubricant.

Finally, the work of Finkin (88) is mentioned here as he reports similar observations. In essence, these are,

1) The finished roughness was found to approach a value independent of the initial condition, and determined by the dynamic equilibrium of the surface interface.

2) Equilibrium peak-to-peak roughness values were found to have a good correlation with the mean debris size when the slide pair was made of the same material.

3) The lubricant increases the length of time over which surface changes occur and equilibrium roughness is usually reduced. It may chemically react with surface material to produce this effect.

5.4 A MODEL FOR SURFACE DEFINITION

The two surface studies undertaken and described in this section have made the author aware of the many inter-related variables which go to make up a system capable of defining the changes in surface topography of cast iron slides.

It can be concluded from these tests that two system changes

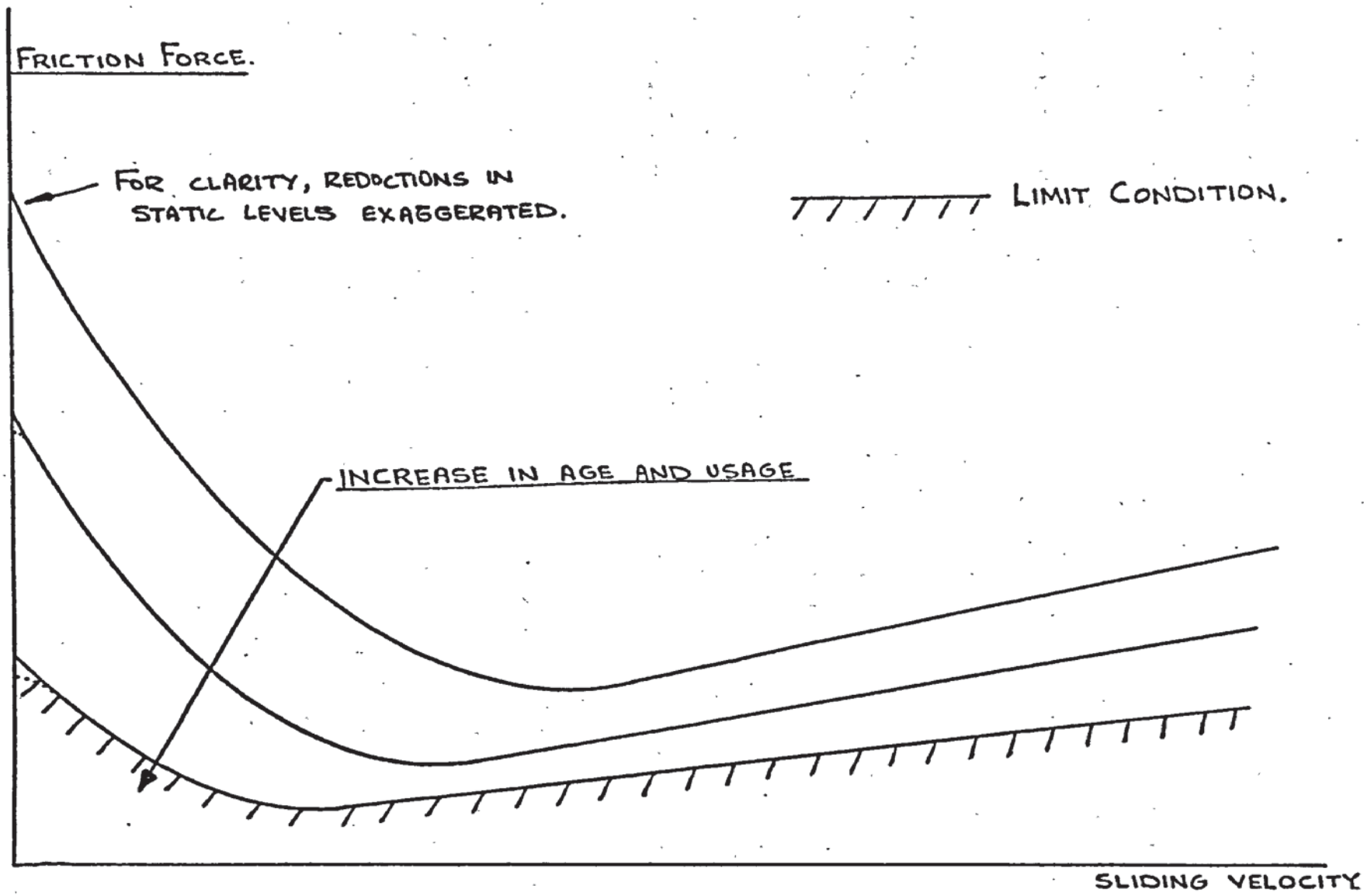

FIG. 5·9. SUGGESTED CHANGES IN FRICTION CHARACTERISTIC WITH AGE AND USAGE.

can be proposed which are related to the length of time of reciprocating motion. For a particular slideway configuration:-

1) The changes in surface topography in the initial stages are governed by the original surface roughness and the metallurgical properties of the cast iron.

2) In the long term the sliding surfaces have a topography governed by the debris size and more important, by the metallurgical properties of the cast iron.

The influence of surface lubricant is to lengthen the time over which the interface activities, such as rubbing, scoring, ploughing and rolling of formed wear tracks, takes place. These experimental investigations indicate that metallic contact has always been maintained by the surfaces either directly or through an intermediary such as debris. The degree of contact at any particular sliding speed will depend upon the ability of the lubricant to aid the separation of the metal surfaces.

It can be clearly seen from the investigation that a surface definition must be related to time or total sliding distance of the slideway system. To describe a ground surface as being covered in hemispheres or cones is quite impossible, regardless of the length of sliding time.

The surface topography of a model can be best described in terms of long wedge shaped asperities. The size of these and their lay relative to each other and the direction of sliding are important, and there will be changes with time.

It is therefore proposed that a two dimensional profile of a model surface can have the form as shown in Fig. 5.10. This initial profile has small wedge shaped grinding tracks superimposed on a larger wedge shaped waviness of the surface. This type of surface will occur, in the early stages of the slideway life. The wedges are assumed to be straight

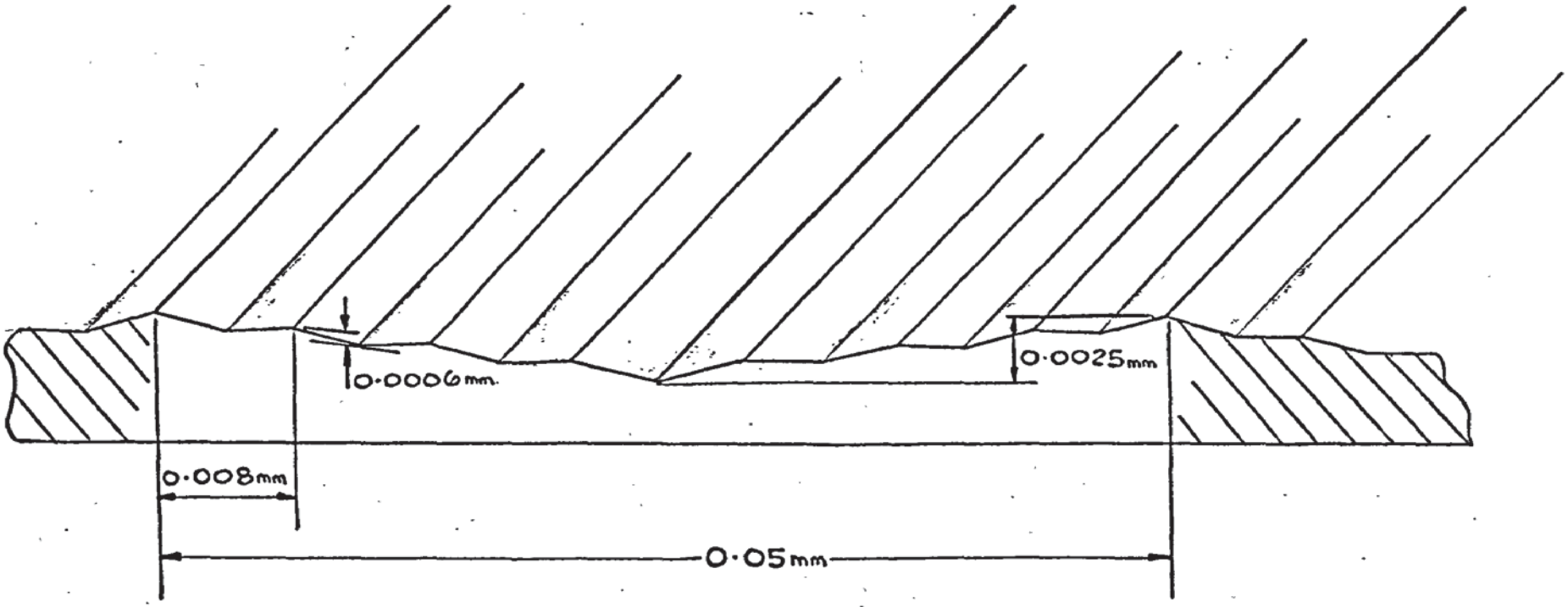

SCALE, 15cm = 0·05mm.

FIG. 5·10. MODEL SURFACE PROFILE.

and cover the entire contact surface. Their direction is such that the ridges cross each other when the two sliding surfaces are in contact.

The lay of the surfaces is considered to be arbitrary with respect to the direction of motion.

This description of a model surface is similar to that used by Tsukada et al (36) and Kawai et al (89) who were considering the elastic and plastic deformation of machined surfaces in contact and the resultant friction mechanism at such an interface.

The profile in Fig. 5 . 10 is an adaptation of the suggested surface shown in Fig. 5 . 7. It has been assumed that any wear tracks are small and can therefore be ignored in any analysis of joint behaviour. In order to obtain some basic mathematical descriptions of surface performance related to friction behaviour, especially over the very short periods of time occupied by oscillatory slideway motion, it is also assumed that,

1) Surface debris will not change the general friction behaviour.

2) Surface oxides are not present and that any metallurgical or mechanical properties of the model are related to those of the grey cast iron material.

3) "Cold welding", which may have caused the plucking of small flakes of material from the surface, does not occur.

4) The surface topography will not change enough to affect the analysis and this also means that the amount of short-time wear may be neglected.

In conclusion, dynamic friction characteristics of a slideway system will undoubtedly be affected by the surface topography. The differences in time scale required by these parameters to change condition are so vast that the surface state may be considered constant when

analysing dynamic friction phenomena. This observation leads to the proposition that the only other variable likely to affect a system response is the slideway lubricant.

In the next chapter lubricants are discussed in some detail and in chapter 7 information is drawn together in an attempt to analyse mathematically some aspects of the model slideway system.

CHAPTER 6

SLIDEWAY LUBRICATION

6.1 INTRODUCTION

It has been said, in the machine tool industry, that the best lubricant for a particular application will be the simplest and cheapest which will meet the requirements. In general the simplest and cheapest lubrication for machine mechanisms is a small quantity of plain mineral oil placed in the assembly. As A.R.Lansdown (90) points out, the quantity of lubricant will depend upon the required working life of the sliding surfaces, taking into account the problem of wear debris.

It has been the experience of the author that the selection of an oil for a particular machine requirement has been the responsibility of the chemical engineer and the oil manufacturing company. In most cases this dependence has proven satisfactory although companies such as Cincinnati (91) do produce their own oil specifications, especially for hydraulic systems and slideways.

Machine tool slideways are lubricated with mineral oils and the methods adopted for its application have developed over the years, from wick feeding to automatic pressure lubrication (5). The problem of oscillatory motion such as "stick-slip", has been overcome in many instances by replacing an oil with one of a higher viscosity, a remedy used in the past by engineers in many companies. With the advent of more sophisticated machines, controlled automatically, the oil companies have been able to market lubricants which combat this problem. These oils contain additive combinations which impart positive kinetic frictional properties which reduce friction and may eliminate "stick-slip" on the slideway. They also contain anti-wear and "tackiness" additives which

reduce wear and enable the lubricant to remain in position on the sliding surfaces, regardless of their orientation, due to improved adhesiveness.

The friction behaviour on slideways will depend to some extent upon the quantity and performance of the mineral oil in the "contact" area and therefore it is necessary to include any relevant information in order to complete a slideway model.

6.2 MINERAL OILS

Mineral oils are a mixture of hydrocarbons which can be separated in three groups.

1) Paraffinic - with significant amounts of waxy hydrocarbons but little or no ashphaltic matter. The naphthenes have long side chains and the oils have a 'wax' pour point.

2) Naphthenic - contain asphaltic matter in the least volatile fractions but little or no wax. Their naphthenes have short side chains and the oils have a 'viscosity' pour point.

3) Mixed base - are a combination of the two above and contain naphthenes having moderate to long side chains. They are considered to have a 'wax' pour point.

Lubricating oils are commonly classified by their change in kinematic viscosity with temperature and are given a kinematic viscosity index; K.V.I. This is divided into three basic groups for low (L.V.I.), medium, (M.V.I.) and high (H.V.I.) viscosities. In general most slideway oils have a medium viscosity index ranging from 35 to 95. Naphthenic oils have lower M.V.I.'s than do the paraffinics.

One of the most important parameters is the oil viscosity and T. I. Fowle (92) suggests that the range of dynamic viscosities for slideway

oils is between 0.01 - 0.1 Ns/m^2 at 60°C (this is 10-100 cP), and in general such oils exhibit Newtonian behaviour. This bulk viscosity is susceptible to temperature changes and it can be considered that a value is approximately halved for every increase in temperature of 10°C. (This point is also made by Bowden and Tabor (2)).

Although oil viscosity reduces with increased temperature it will increase with pressure. In general the viscosity will double for every 35 MN/m^2 increase in pressure. It can be considered that as general pressure fluctuations between slideway surfaces are likely to be relatively low, then subsequent changes in lubricating oil viscosity will be minimal.

When the lubricant is being used it will deteriorate with time depending upon environmental conditions. There are three main causes affecting its useful life (92),

a) Oxidation.
b) Thermal decomposition.
c) Contamination.

and in a machine tool situation, contamination is probably the most common. This can be classified as follows,

1) Gaseous - due to air and other substances such as ammonia.
2) Liquid - due to water and cutting oils.
3) Solid - due to wear particles, dust and ash.

Therefore it is essential to have some form of slideway protection and a reliable method of replenishing the lubricant in the system. Oil additives can be included to reduce contamination effects on the quality of the oil.

6.3 BOUNDARY LUBRICATION

The observations made in the previous chapter (see 5.3) indicate that the sliding surfaces are consistently in a condition known as

boundary lubrication. This has been defined by D. Godfrey (93) as a condition of lubrication in which the friction between two surfaces in relative motion is determined by the properties of the surfaces and by the surfactant properties of the lubricant.

It is considered that the friction regime existing under boundary lubrication is of a similar nature to that existing under dry conditions with some allowance being made for the effect of a thin lubricant film. D. Dowson (94) describes such a lubrication condition in terms of a ratio,

$$R = \frac{\text{Thickness of lubrication}}{\Sigma . \text{surface roughness (C.L.A.)}}$$

and under boundary lubrication $R \ll 1$ (say 0.001). This value can be compared with that for fluid film lubrication when R would be valued at 2 or more.

The thickness of oil films formed on metal surfaces will depend upon the lubricant and its additives.

The essential features of a desirable interaction between a bearing metal surface and a lubricant can be listed as follows (62)

1) The interaction should produce a layer thick enough to accommodate the majority of the asperities.

2) This layer should have a low shear strength, compared with the metal.

3) The interaction produced should adhere strongly.

These features are used in the concepts proposed by Bowden and Tabor (2), in which boundary lubricant films do not completely separate the surface but only reduce the area of metallic contact and therefore friction. Their work has shown that although surface interaction of the metals does provide a factor describing friction, this can be reduced with the assistance of a suitable lubricant film.

All plain mineral oils are capable of producing a thin film of close packed molecules on the surface of metals. A very interesting paper by Clayfield and Galvin (95) attempts to describe the nature of such films in terms of the relative surface energies. These can produce a film of several layers of oil molecules which can be very viscous or even considered 'solid'. In most cases basic mineral oil molecules can be physically adsorbed on the surface but as Godfrey (93) indicates, these molecules are nearly all non-polar and therefore their adhesion forces are weak. Their random orientation and low cohesion forces give rise to consequently low film strength. This strength can be improved by the addition of polar compounds to the bulk oil.

Physical adsorption is defined as the existence of a higher concentration of a component at the surface of a phase than is present in the main bulk of the phase. An important example of physical adsorption occurs in full fluid hydrodynamic lubrication where molecules of oil adhere to the metal, forming an immobile layer. The existence of this layer is a basic assumption in hydrodynamic lubrication theory, and no pressure would be developed if the first layer of molecules did not adhere and pull others into the bearing clearance. Physical adsorption is reversible, and when a surface is heated the energy of adsorption is reduced and metal to metal contact will be increased.

Another property of the film which affects boundary lubrication is the cohesion among the molecules comprising the film. The greater the cohesion the more difficult it is for an asperity to penetrate. A rise in temperature results in thermal motion which reduces cohesion and when the melting point of the film is reached asperities can readily penetrate the film. During sliding motion the adsorbed hydrocarbon molecules slide over each other, thereby providing a film of low shear strength and low friction. The stability of an oil film operating under boundary lubrication can be tested by measuring sliding friction at various temperatures and a sudden rise in friction is an

indication of the melting point of the surface film. (This is described by Bowden and Tabor (2)).

In a paper by L.V.Elin (26), lubricated surfaces sliding together under very high pressures still retain some film of oil provided that the temperature generated by friction is below the melting point of the film.

6.4 OIL ADDITIVES

The ability of a lubricant to perform well under boundary conditions is improved with the addition of polar additives. Plain mineral oils contain minute quantities (< 0.005%) but compounds are purposely added in small amounts (0.1% by weight) (95) which do not measureably change physical properties such as viscosity. These additives, often fatty acids, are sometimes called boundary lubricants.

The use of polar molecules increases the film strength and gives an oil the property commonly called "oiliness", a descriptive term proposed by Kingsbury (97). A polar molecule is one in which there exists a permanent unbalance of positive and negative charges so that a dipole moment exists. When they are physically adsorbed a mirror image of the charges is induced in the metal and the subsequent attraction helps bond the molecules to the surface. They tend to arrange themselves in a preferred manner and vertical orientation of the polar chain with close packing enhances cohesion among the molecules. This gives a greater film strength when compared to non-polar oil molecules. A typical arrangement of a monolayer of oil molecules both polar and non-polar on a metal surface is illustrated in Fig. 6.1

As Godfrey (93) indicates the kind and amount of polar molecules present create differences in the boundary lubrication performance of base oils. A lubricant containing such additives will produce a surface film which, if damaged, can be repaired in situ by further adsorption from the bulk oil. Clayfield et al

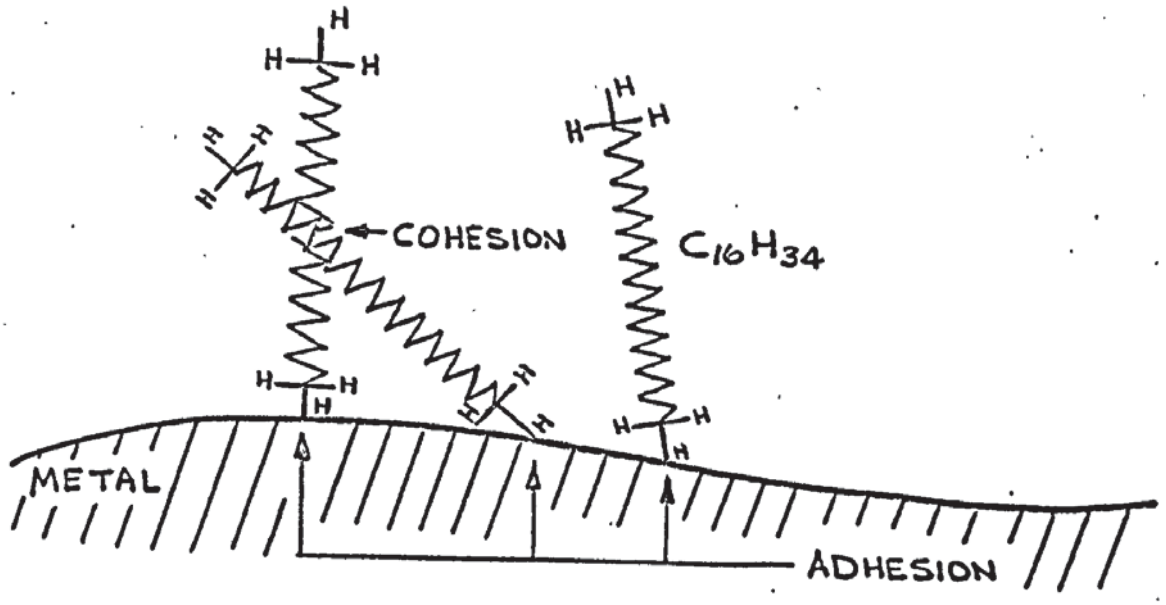

a) NON-POLAR OIL

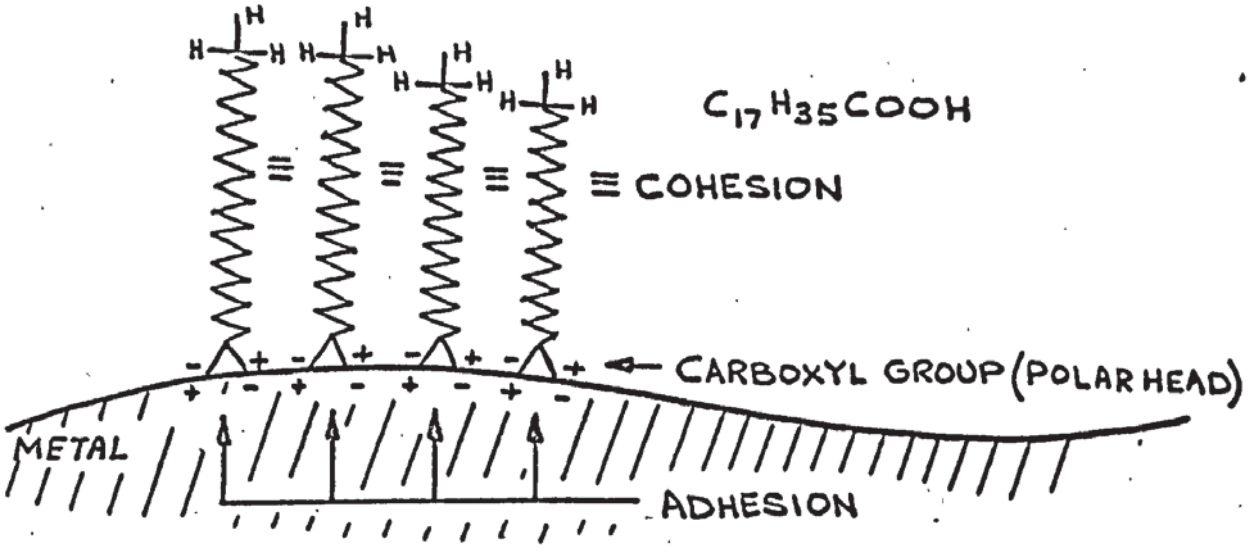

b) POLAR OIL

FIG. 6·1. MONOLAYER OF OIL MOLECULES ON METAL SURFACE.

(95) suggest that a monlayer of fatty acid is approximately 0.004 μm in thickness and Dowson (94) suggests a thickness of 0.002 μm. (0.001 μm = 10 Å)

The effect of a thin film of 'solid' lubricant on the metal surface gives rise to several observations:

1) The coefficient of static friction reduces with the length of the molecular chain due to a more effective separation of the metal surfaces (Tabor (2))

2) The longer the molecular chain, and consequently its molecular weight, the more effective will be the lubricant in reducing sliding friction. This can be considered to be the result of the increased durability of the film. (Dowson) (94), (Fuller) (97).

3) The melting point of physically adsorbed films varies from 20° C to approximately 70° C for paraffinic fatty acids such as stearic (C_{17} H_{35} COOH). (61). Thus temperature changes due to friction and dissipation of viscous energy will reduce the viscosity and the effectiveness of the surface films by changes in surface energies (95).

4) Tests carried out by Bowden and Tabor (2) suggest that the adhesion is independent of the thickness of the liquid film and for a contacting ball on a flat surface, they derive the adhesive force (A) as

$$A = 4.\pi R Y_o$$ where R is ball radius, Y_o is oil surface tension

5) Long chain acids such as stearic are used in engineering on less reactive metals such as cast iron. Fuller (97) suggests that only a comparatively small reduction in the static coefficient of friction is produced compared with a straight mineral oil for cast iron.

6) Although increased chain length reduces the coefficient of static friction, there is likely to be a lower limit for its value. The work by Tabor (2) suggests a lower limit of 0.07 for steel on steel, although Fuller (97) comments that this value could be lower.

7) The bulk viscosity of the lubricating oil is not a prime factor when considering boundary lubrication and friction levels (Dowson) (94)

The mathematical relationships for boundary lubrication are very much related to the work of Bowden and Tabor (2) and are briefly illustrated below:

Friction force (F) can be expressed as,

$$F = A_c\left[\alpha.S_m + (1-\alpha)\,S_o\right] \qquad 1-6$$

where A_c is contact area, S_m and S_o are the shear strength of the metal oil contact junctions respectively.

$$\mu = \frac{A_c}{W} \times \left[\alpha.S_m + (1-\alpha)S_o\right] \qquad 2-6$$

$$\text{or } \mu = \frac{1}{P_m} \times \left[\alpha.S_m + (1-\alpha)S_o\right] \qquad 3-6$$

This relationship has been modified by Tamir and Rightmire (5) to form,

$$\mu = \alpha.\mu_m + (1-\alpha).\mu_o \qquad 4-6$$

where $\mu_m = \frac{S_m}{P_m}$ and $\mu_o = \frac{S_o}{P_m}$

Their work suggests that for experimental values of μ and μ_m then in general $\alpha = 0.18$ and $\mu_o = 0.079$. Thus for negligible values of α the lowest friction coefficient would be 0.079, which is similar to that found by Tabor (2). This value can also be calculated from a similar equation to 4 - 6, derived by F.T. Barwell (5), who stated that if μ_m was unity, then

$$\mu = \alpha + (1-\alpha)\,\mu_o \qquad 5-6$$

and therefore in the limiting case for boundary lubrication, when α would be zero,

$$\mu = \mu_o \qquad 6-6$$

Tests carried out by Tamir et al (5) using large quantities of lubricant, showed that the coefficient of friction was larger than that using thin films. This resulted in S_o having higher values in bulk fluid lubrication. In order to explain this phenomenon, the hypothesis of an edge effect was proposed. This

edge effect results in higher friction, since in bulk lubrication the spaces around load-carrying areas are more likely to be filled with lubricant than is the case with thin film lubrication.

Finally, the relationship between wear under dry and boundary lubricated conditions has been expressed by Rabinowicz (98) using his energy concept as,

$$\frac{\text{Wear lubricated}}{\text{Wear dry}} = \left[\alpha + (1-\alpha).\left(\frac{We}{Wm}\right)\right] \qquad 7-6$$

where (We) is the energy of adhesion of fully lubricated areas and (Wm) the energy of adhesion of metallic junctions. (α - fraction of contact area over which breakdown of oil film has occurred)

6.5 LUBRICANT DATA USEFUL TO SLIDEWAY MODEL ANALYSIS

The effect of using mineral oils to lubricate slideways is usually to reduce friction and wear. The composition of the lubricant is important.

Although these friction and wear changes are of course measureable, the understanding of how they occur is not clear and one is left with only the concepts developed by Bowden and Tabor (2)

In assembling useful data that may become factors in a slideway model the mechanical engineer naturally looks for data which he can readily appreciate.

The chemistry of lubricants is highly specialised and it is suggested here that there may be a communications problem between the chemist and the engineer.

The work of Clayfield and Calvin (95) is considered to be a step forward and can be reconciled with the studies and lucid explanations propounded by Bowden and Tabor. The introduction of surface tensions does help to quantify the forces involved when an oil film adheres to the surface of a metal. The "mechanical" properties of a film are important and enable some relationships to be made with the properties of the metal surface. In particular, the support given to a

particular load depends upon the actual contact areas between the bearing metals and the metal-oil-metal interface. The resultant friction force under static and sliding conditions will depend upon the relative support given by these areas and the effort involved in possible shearing and deformation.

The following data will be used in any subsequent analysis and has been drawn from the works presented by authors mentioned in this chapter. In order to draw a comparison with experimental work carried out by Bell et al (46) (47) the same kinematic viscosity range, applicable to bulk mineral oils, has been used.

1) Mineral Oils

a) Dynamic viscosity range (η) - 0.019 to 0.59 Ns/m^2
at 30° C (19 cP to 590 cP)

b) Oil Density range (ρ) - 860 to 890 kg/m^3
at 25° C

c) Kinematic viscosity range (ν) - 0.22×10^{-4} to 1.12×10^{-4} m^2/s
at 30° C (22 cS to 112 cS)

$$\text{Kinematic viscosity} = \frac{\text{Dynamic viscosity}}{\text{Oil density}}$$

$$\nu = \frac{\eta}{\rho} \qquad 8 - 6$$

As an example $\eta = 0.019$ Ns/m^2 $\rho = 860$ kg/m^3

$$\therefore \nu = \frac{0.019}{860} = 0.22 \times 10^{-4} \text{ } m^2/s$$

ν = 0.22 Stokes (S) or 22 centiStokes (cS)

d) Isentropic secant bulk modulus (Bo) = 198 MN/m^2
At 35 MN/m^2 and 30° C
(This is an average value to cover all the oils)

e) Viscosity ratio for every pressure rise of 35 MN/m^2 = 2

f) Viscosity ratio for every temperature rise of 10° C = 0.5

(The viscosity ratio is the viscosity of oil at a new pressure or temperature divided by the viscosity at the original pressure or temperature)

g) Average surface tension (Yo) = 30×10^{-3} N/m (30 dynes/cm)
(against air at 20° C)

(Yo) decreases with increase in temperature and vanishes at the critical temperature. For many liquids then,

$$d\left(Yo.(M/\rho)^{\frac{2}{3}}\right)/dt = -2.12 \qquad 9 - 6$$

where M = molecular weight, ρ = density, t = temperature.

(This information is from Tables of Physical and Chemical Constants by W.C.Kaye and T.H.Laby (99)).

It is estimated that Yo will decrease by 0.4 to 0.9 dynes/cm for every 10 degree rise above 20° C ambient temperature.

2) Additives - Fatty Acids

a) Oleic acid $C_{18} H_{34} O_2$ (Ref. 99)

Melting point - 16° C

Density (ρ) - 898 kg/m^3

Surface tension - 32.2×10^{-3} N/m
(against Air)

b) Stearic acid $C_{18} H_{36} O_2$ (Ref. 99)

Melting point - 71.5° C

Boiling point (to decomposition) - 370° C

Density - 940 kg/m^3

c) Molecular length (Ref. 97)

1) Oleic acid $\simeq 11 \times 10^{-8}$ cm

2) Stearic acid $\simeq 24 \times 10^{-8}$ cm

The typical thickness of a boundary lubricating film composed of fatty acids is taken, from the work of Clayfield et al (95), to be in the order of 40×10^{-8} cm.

CHAPTER 7

AN ANALYSIS OF THE STATIC AND KINETIC BEHAVIOUR OF A MODEL SLIDEWAY JOINT.

"If according to tradition, friction forces are classified as mechanical forces, which, in general, are independent of velocity, it must be concluded that the friction forces occupy a peculiar position among mechanical forces, since their dependence on velocity has been determined experimentally. Hence, it follows that this dependence is not determined by the nature of friction forces but is of a secondary origin related to the conditions of the interaction between the surfaces".

A.S.Akhmatov.

7.1 INTRODUCTION

The data obtained in chapter 6 is to be used to define a surface model which will enable the friction between two such surfaces to be related to sliding velocity. In order to do this a step by step approach has been adopted and any theories derived will be tested for comparisons with other observed data.

Initially the surface model interaction should give comparable observations under static conditions. Many authors have written papers which include experimental work in this area, but using small models. Nevertheless, the author feels that such a starting point is unavoidable if a complete picture of the friction mechanism is to be understood, especially with such a large model as a machine tool slide.

The fact that one surface moves over the other does create further complications, for it is likely that certain elements in a model although "dormant" in the static condition will be activated by the motion and may play a dominant role in the dynamic condition. Therefore the slideway surface model should accommodate these elements as the development of its structure is accomplished.

It is important to view such a complex model as a system in its own right, and as such it will have inherent time dependent quantities. Their effect on the system will depend upon the rate of change of the inputs, e.g. load, displacement.

Finally a simplified equation relating sliding velocity to system friction will be derived in order to allow the slideway simulation to be set up on the analogue computer, using available components. It should be stated that the simplification will not entail the abandonment of system parameters or the concepts by which they were originally created.

7.2 THE STATIC CONDITIONS - LEADING TO A PROPOSED FRICTION MODEL

The model surface proposed in chapter 5 and illustrated in Fig 5 - 10 will be the starting condition for both contact areas. If a simplified structure of one larger ridge is taken then the contact area between two such ridges crossing at an arbitrary angle can be described in a simple mathematical expression. The relevant diagrams for such an analysis are shown in Fig. 7.1

The interaction of two wedges is shown in Fig 7.1b for a cross angle β of 90°. It is indicated that the total penetration or movement of one wedge relative to the other is a distance h, which is made up of equal deformations in each wedge of $h/2$.

By symmetry then,

$$h = b.\left[\frac{Z}{B}\right] \qquad 1 - 7$$

If the wedges cross at an angle β then the area can be calculated from the illustration in Fig. 7.2

The area will be,

$$\left(\frac{a + a}{2}\right) . c. = a.c. \qquad 2 - 7$$

now

$$d = \frac{b}{2 \sin \beta}$$

$$\sin \theta = \frac{b}{2a} = \frac{c}{2d}$$

Therefore

$$c = \frac{b.d.}{a}$$

and the area from eqn. 2.7 is

$$\text{area} = b.d. \qquad 3 - 7$$

substituting for d the contact area

$$Aa = \frac{b^2}{2.\sin\beta} \qquad 4 - 7$$

Substituting b for h then

$$Aa = \left[h.\frac{B}{Z}\right]^2 . \frac{1}{2.\sin\beta} \qquad 5 - 7$$

In order to relate this contact area and normal movement with ridge loading (W), the work of Timoshenko and Goodier (100) will be used. To do this the ridge profile has to be changed to that of a circular arc, as shown in Fig 7.3.

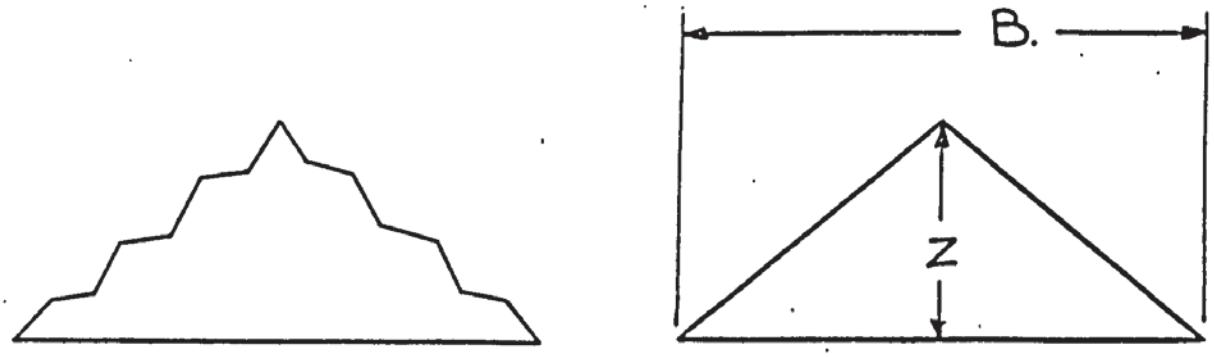

ORIGINAL WEDGE PROFILE. SIMPLIFIED PROFILE.

a) PROFILES.

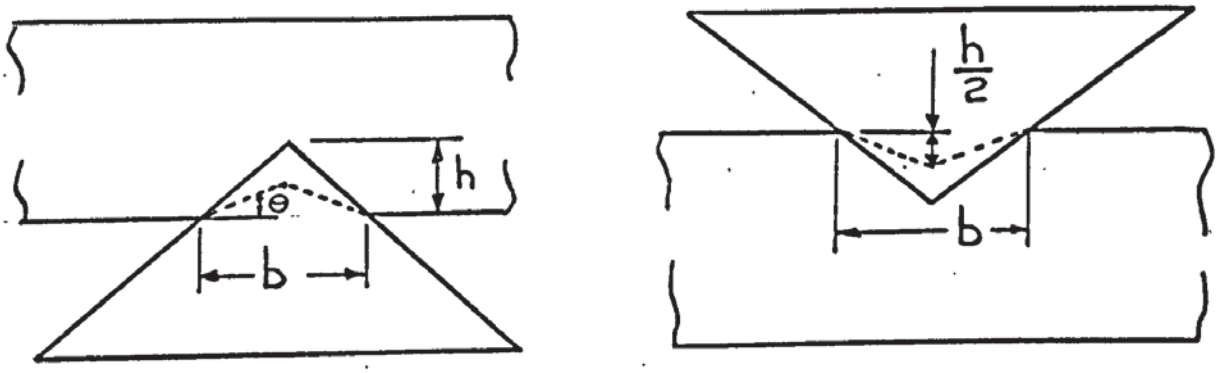

b) INTERACTION OF TWO WEDGES.

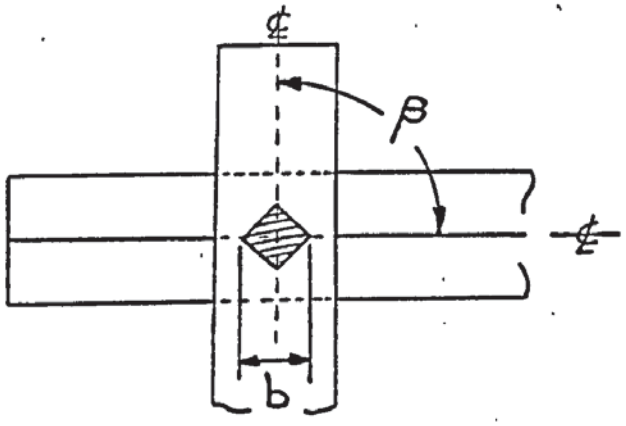

c) CONTACT AREA BETWEEN WEDGES CROSSING AT ANGLE β.

FIG. 7·1. INTERACTION OF SURFACE RIDGES.

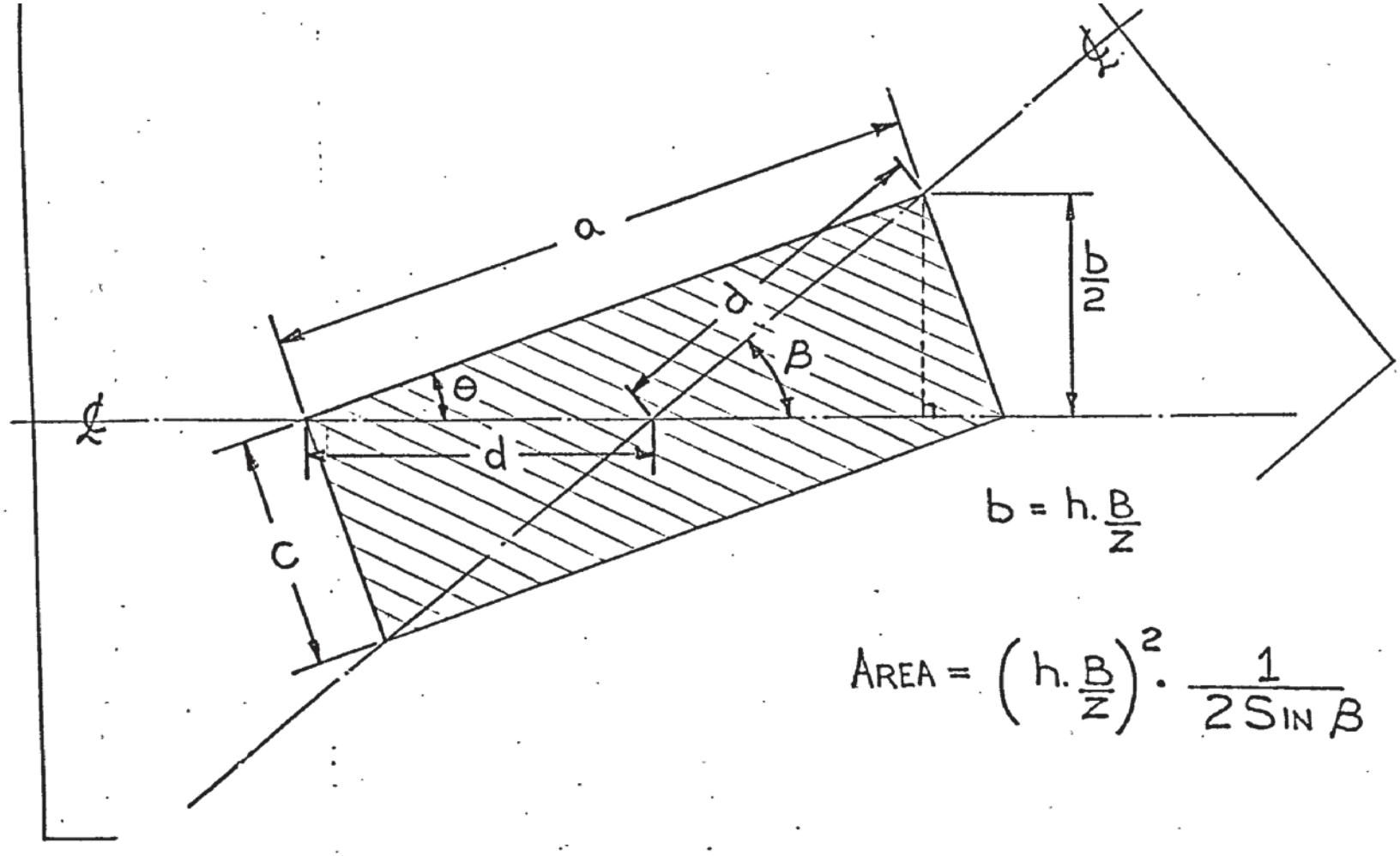

FIG. 7·2. CONTACT AREA BETWEEN TWO CROSSED RIDGES.

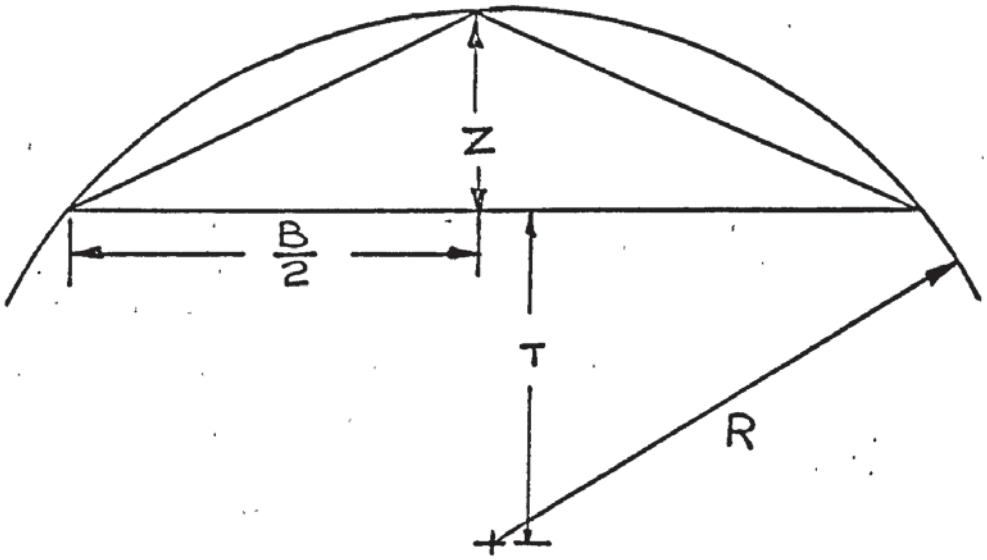

WHERE $T = r - R.$

$r = 2R - Z$

$$\text{RADIUS} = \frac{4Z^2 + B^2}{8Z.}$$

FIG. 7·3. RIDGE PROFILE CHANGED TO THAT OF CIRCULAR ARC.

The radius has been chosen such that the arc encompasses the simplified triangular profile. It could be argued, at this point, that such a shape would be a reasonable approximation to the original profile of Fig. 7 - 1(a)

The radius R can be expressed in terms of B and Z thus,

$$2R = Z + r \qquad - 6\text{-}7$$

$$Zr = \left[\frac{B}{2}\right]^2 \qquad - 7\text{-}7$$

$$r = \frac{B^2}{4Z} \qquad - 8\text{-}7$$

$$\therefore 2R = Z + \frac{B^2}{4Z}$$

$$R = \frac{4Z^2 + B^2}{8Z} \qquad - 9\text{-}7$$

The equations required in order to satisfy the analysis are taken from the work of Timoshenko et al (100)

The contact area will take the form of an ellipsoid whose major axis (a) and minor axis (b) are given by the following equations,

$$a = m\left[\frac{3}{4} \cdot \frac{W. \Delta}{(A + B)}\right]^{\frac{1}{3}} \qquad - 10\text{-}7$$

$$b = n\left[\frac{3}{4} \cdot \frac{W. \Delta}{(A + B)}\right]^{\frac{1}{3}} \qquad - 11\text{-}7$$

where $$\Delta = \frac{(1 - \nu_1^2)}{E_1} + \frac{(1 - \nu_2^2)}{E_2} \qquad - 12\text{-}7$$

$(A + B)$ is a factor depending upon the radii of the ridges in contact and for this model

$$(A + B) = \frac{1}{2}\cdot\left[\frac{1}{R_1} + \frac{1}{R_2}\right] \qquad - 13\text{-}7$$

m, n are constants depending on the ratio $\left(\frac{B-A}{A+B}\right)$

and $$(B - A) = \frac{1}{2}\cdot\left[\left(\frac{1}{R_1}\right)^2 + \left(\frac{1}{R_2}\right)^2 + 2\left(\frac{1}{R_1}\right)\cdot\left(\frac{1}{R_2}\right)\cdot \cos 2\beta\right]^{0.5} \qquad - 14\text{-}7$$

The angle β is that between the planes containing the curvatures $\left(\frac{1}{R_1}\right)$ and $\left(\frac{1}{R_2}\right)$ and is the same as the cross angle of the wedges.

Thus the constants m and n can be found from a table which is based upon the angular relationship $\cos^{-1}\left(\frac{B - A}{A + B}\right)$. (This tabulation has a minimum angular value of 30°).

In this analysis then the above equations may be simplified since,

$$\nu_1 = \nu_2,\ E_1 = E_2 \text{ and } R_1 = R_2$$

Thus $$\Delta = \frac{2(1-\nu^2)}{E} \qquad - 15 - 7$$

$$(A + B) = \frac{1}{R} \qquad - 16 - 7$$

If the angle β is 90° then (B–A) from eqn. 14 – 7 is zero and m and n are equal to unity since $\text{Cos}^{-1}\left\{\frac{B-A}{A-B}\right\}$ is equal to 90°.

From eqn. 10–7 and 11–7 then a and b will be equal,

$$a = b = 1\left[\frac{3}{4}.\frac{W}{E}.\frac{2(1-\nu^2)}{\left(\frac{1}{R}\right)}\right]^{\frac{1}{3}} \qquad - 17 - 7$$

substituting for R (eqn. 9–7)

$$a = b = \left[\frac{3}{4}.\frac{W}{E}.\ 2\ (1-\nu^2).\ \frac{(4Z^2 + B^2)}{8Z}\right]^{\frac{1}{3}} \qquad - 18 - 7$$

In general the contact area of the ellipsoid will be,

$$a_e = \pi.ab \qquad - 19 - 7$$

If the contact area for the wedge from eqn. 4 – 7 is equated to a_e above then

$$Aa = a_e \qquad - 20 - 7$$

and $$\left[h.\frac{B}{Z}\right]^2.\ \frac{1}{2\text{Sin}\,\beta} = \pi.ab \qquad - 21 - 7$$

$$\left[\frac{hB}{Z}\right]^2.\ \frac{1}{2\ \text{Sin}\,\beta} = \pi.(m \times n).\left[\frac{6}{32}.\frac{W}{E}.\ \frac{(1-\nu^2)\ (4Z^2 + B^2)}{Z}\right]^{\frac{2}{3}} \qquad - 22 - 7$$

Thus, for the single ridge interaction the contact area is proportional to the $(\text{load})^{\frac{2}{3}}$ and the penetration height (h) is proportional to $(\text{load})^{\frac{1}{3}}$. It should be noted that these relationships hold good for elastic contact deformation of the ridges and when lateral deformation of the profiles is negligible.

The relevant information for this model is as follows,

B = 50 μm = 0.050 mm.

Z = 2.5 μm = 0.0025 mm.

For grade 17 Cast Iron, $E = 1.32 \times 10^4$ kgf/mm^2

$\nu = 0.26$

From eqn. 9–7, $R = 126.25 \times 10^{-3}$ mm.

If $\beta = 90^\circ$ the contact area from eqn. 5 – 7 is

$$Aa = h^2.200 \qquad - 23 - 7$$

and from eqn. 18–7 then,

$$a = b = 2.37 \times 10^{-2}\ (W)^{\frac{1}{3}} \text{ mm.} \qquad - 24 - 7$$

The contact area given by eqn 19-7 is,

$$a_e = \pi.a.^2 = 0.001765\ (W)^{\frac{2}{3}}\ mm^2. \qquad - 25\text{-}7$$

Equating 23-7 and 25-7, $h^2.200 = 0.001765(W)^{\frac{2}{3}}$

Thus $h = 0.00297(W)^{\frac{1}{3}}$ mm. $\qquad - 26\text{-}7$

From Timoshenko's analysis using the Hertzian distribution of pressure over the area of contact, then the pressure at any co-ordinate x, y from the centre is given by,

$$p_o.\sqrt{1 - \frac{x^2}{a^2} - \frac{y^2}{b^2}} \qquad - 27\text{-}7$$

The maximum pressure p_o exists at the centre of the surface of contact whose boundary has the semi-axes a and b.

Since the total load W is equal to the volume of the semi-ellipsoid then,

$$W = \frac{2}{3}.\ \pi.\ a.b.p_o \qquad - 28\text{-}7$$

Thus $$p_o = \frac{3}{2}.\ \frac{W}{\pi\, ab} = \frac{3}{2}.\ \frac{W}{ae} \qquad - 29\text{-}7$$

Substitution for a_e from 25-7

$$p_o = 850\ (W)^{\frac{1}{3}}\ kgf/mm^2 \qquad - 30\text{-}7$$

The average pressure Pa over the contact area will be equal to,

$$Pa = \frac{W}{ae} = 567\ (W)^{\frac{1}{3}}\ kgf/mm^2 \qquad - 31\text{-}7$$

If the same calculations are repeated for a cross angle β of 30° then the following table in Fig. 7.4 summarises the results.

The effect of changing the cross angle is shown in Fig. 7.5 which plots the normal displacement of a single crossed ridge model against load. At a given load (W) changing β from 90° to 30° results in a comparatively small change in displacement (h). For this reason, in the further development and use of this surface model, most of the presentation is confined to the case when $\beta = 90°$. Obviously it can be applied for any value of cross angle within the range.

Indicated on the curves of Fig. 7.5 are the points where the average pressure across the contact area is equal to the 0.1% proof stress and in addition, from the work of Greenwood and Williamson (101) the points where plastic flow will occur. Their work suggests a maximum pressure for p_o which is approximately equal to 0.6 times the hardness of the material. For grade 17 cast iron this would be in the region of 132 kgf/mm^2 with a hardness of 220 kgf/mm^2.

CROSS ANGLE β	PENETRATION h mm.	MAX. PRESSURE P_o kgf/mm^2	AVE. PRESSURE. P_a. kgf/mm^2	a. mm.	b. mm.
90°	$0.00297(W)^{1/3}$	$850\,(W)^{1/3}$	$567\,(W)^{1/3}$	$0.0237(W)^{1/3}$	$0.0237(W)^{1/3}$
30°	$0.00244(W)^{1/3}$	$631\,(W)^{1/3}$	$420(W)^{1/3}$	$0.0647(W)^{1/3}$	$0.0117(W)^{1/3}$

FIG. 7·4. RIDGE EQUATIONS FOR LOAD AND CROSS ANGLE.

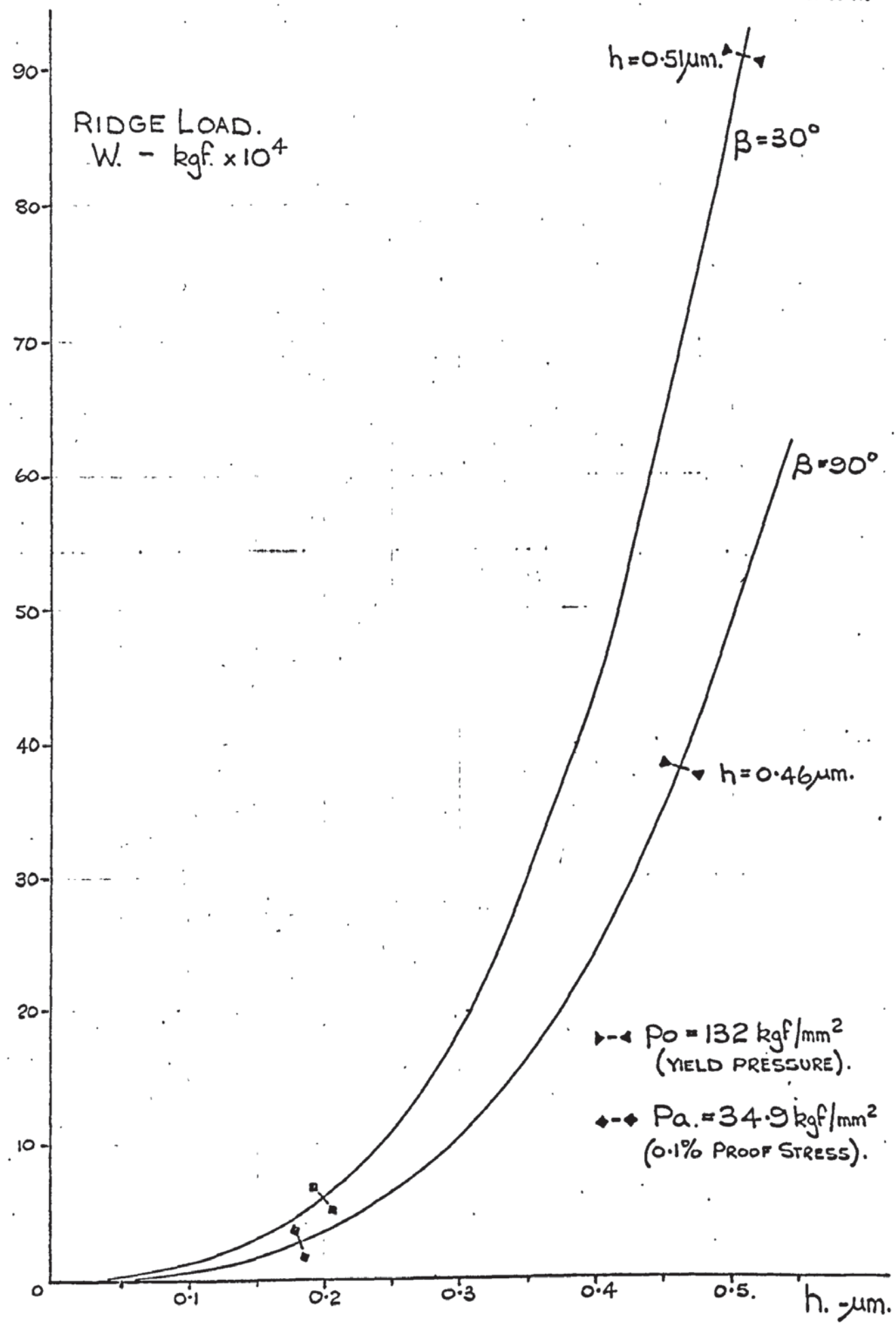

FIG. 7·5. RIDGE DISPLACEMENT FOR LOAD AND CROSS ANGLE.

From the work of several authors such as Greenwood et al (101) it can be generalised that the contact area between two surfaces is very nearly proportional to the load. It is also likely that the total load supported by all the areas will give a normal displacement greater than that suggested in Fig. 7.5 for the size of ridge configuration. These observations mean that there must be some distribution of these ridges such that a line joining their tops forms some sort of curve allowing increased interaction with increases in normal displacement.

In order to analyse this, the section through such a range of asperities is shown in Fig. 7.6 with β being equal to 90°. The resulting contact areas between two such ranges are also illustrated.

Fig. 7.6a shows a section through such a range where the horizontal ridge spacing is B, the base width of a single ridge. The fall-off in ridge top heights will be assumed to be linear, changing by h_T for every increment of B about the range centre line. Thus the range section is again triangular in shape.

In order to produce a mathematical relationship the value of h_T will be fixed at 0.03 μm, thus allowing only a small change in relative peak heights when moving over several of the ridges.

The contact areas are illustrated in 7.6 (b) and the number of points forming contact areas is governed by h_T and the total displacement. For a normal displacement h_d equal to $2h_T$ the centre ridges will be elastically deformed and contact will just be made with four other points formed by the centre ridge of each range and the two adjacent ridges. Thus one contact area has been established and four more are about to be formed.

If N_c is the number of contact areas formed, then

$$N_c = 1 + 2(n+1)n \qquad - 32\text{-}7$$

where

$$n = \left[\frac{h_d}{2h_T} - 1\right] \qquad - 33\text{-}7$$

Therefore when the normal displacement is equal to $4h_T$ the number of contact areas will be 5, with one ridge pair displaced by the total amount and 4 more pairs displaced by $2h_T$.

The movement on any ridge pair by an increment of $2h_T$ is equivalent to the normal displacement h of these ridges described in the earlier analysis. Equations 23-7 and 26-7 can be used to calculate the respective contact areas and load carrying capacity.

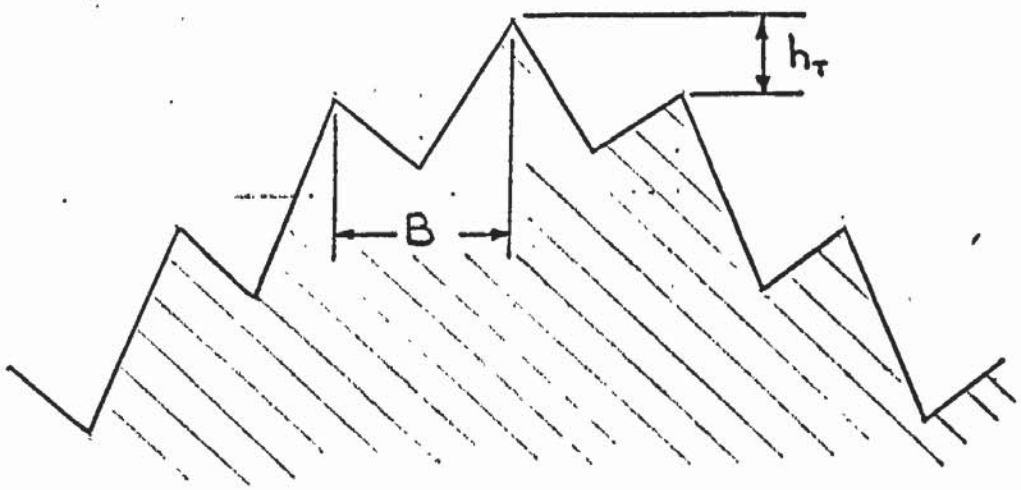

a) SECTION THROUGH A RANGE OF RIDGES (N.T.S)

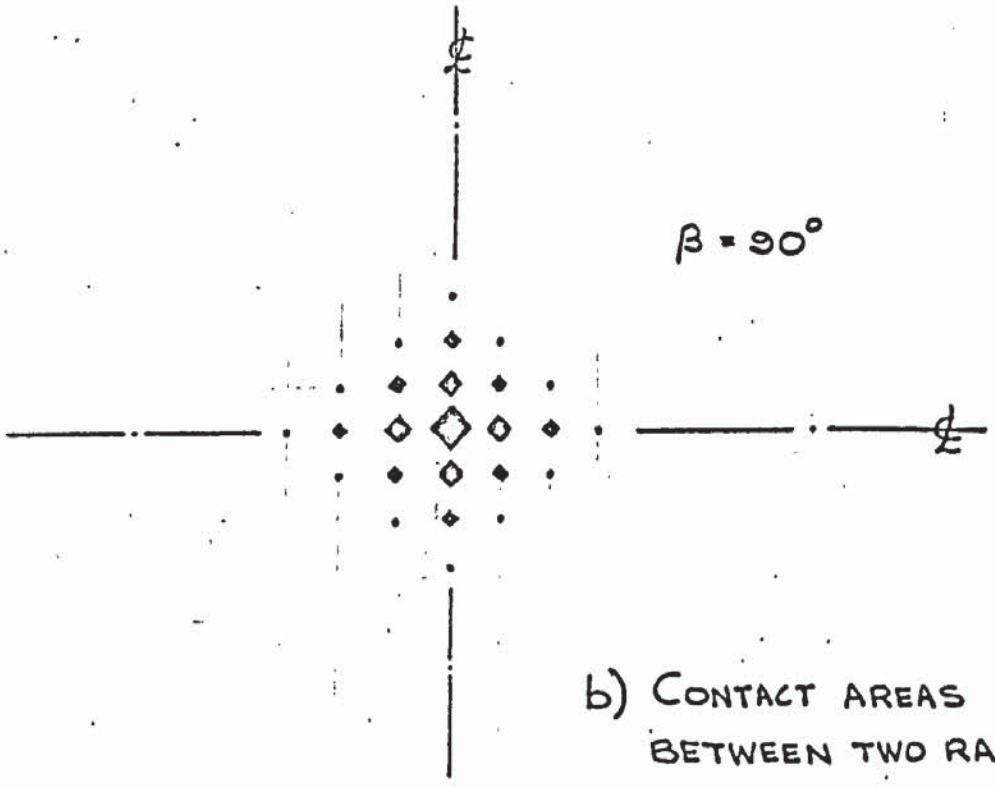

b) CONTACT AREAS BETWEEN TWO RANGES.

FIG. 7·6. PROFILE AND CONTACT AREAS FOR RANGE OF RIDGES.

As an example, if the displacement between two ranges was 4 h_T then the total contact area would be,

$$Ac = 1x(4h_T)^2 \times 200 + 4 \times (2h_T)^2 \times 200 - \mu m^2$$

and the total load

$$W_T = 1 \times \left(\frac{4\ h_T}{0.00297}\right)^3 + 4 \times \left(\frac{2h_T}{0.00297}\right)^3 - kgf$$

These equations take the form of a series and can be expressed in a general form, for $\beta = 90^\circ$, as follows,

$$Ac = 200.\left[(N.2h_T)^2 + \sum_{n=1}^{n=N} 4n(N2h_T - n2h_T)^2\right] - \mu m^2 \qquad 34 - 7$$

$$W_T = \left(\frac{1}{2.97}\right)^3.\left[(N2h_T)^3 + \sum_{n=1}^{n=N} 4n\,(N2h_T - n2h_T)^3\right] - kgf \qquad 35 - 7$$

where h_T is in μm

$N2h_T$ = hd, the total interface displacement

n = 1 in steps of one up to N

These equations are satisfactory so long as the deformation is elastic and modifications have to be made when the load on each contact gives a maximum pressure p_o of 132 kgf/mm^2. For $\beta = 90^\circ$ this will occur when a ridge pair displacement (h) is approximately 0.46 μm and for $\beta = 30^\circ$ when the displacement is 0.51 μm. Beyond this penetration level the load carried by a ridge pair is directly proportional to the area, maintaining the pressure p_o. Therefore,

$$W = 132 \times \frac{2}{3}.Ac \qquad 36 - 7$$

when $N2h_T$ and $(N2h_T - n2h_T)$ have values greater than these yield displacements.

Using equations 34 - 7 and 35 - 7 above, and equation 36 - 7 for higher loadings, the results have been calculated. These are illustrated in Fig. 7.7 for W_T and A_c, in Fig. 7.8 for h_d and W_T and in Fig. 7.9 for N_c and W_T.

The general mathematical relationships between these quantities are taken from these plots and listed below in Table T7.1

Table T.7.1

$\beta = 90^\circ$

$hd = 0.075\ Ac^{0.27}$	- μm
$Ac = 10460\ W_T^{0.82}$	- μm^2
$hd = 0.92\ W_T^{0.22}$	- μm
$Nc = 520\ W_T^{0.5}$	

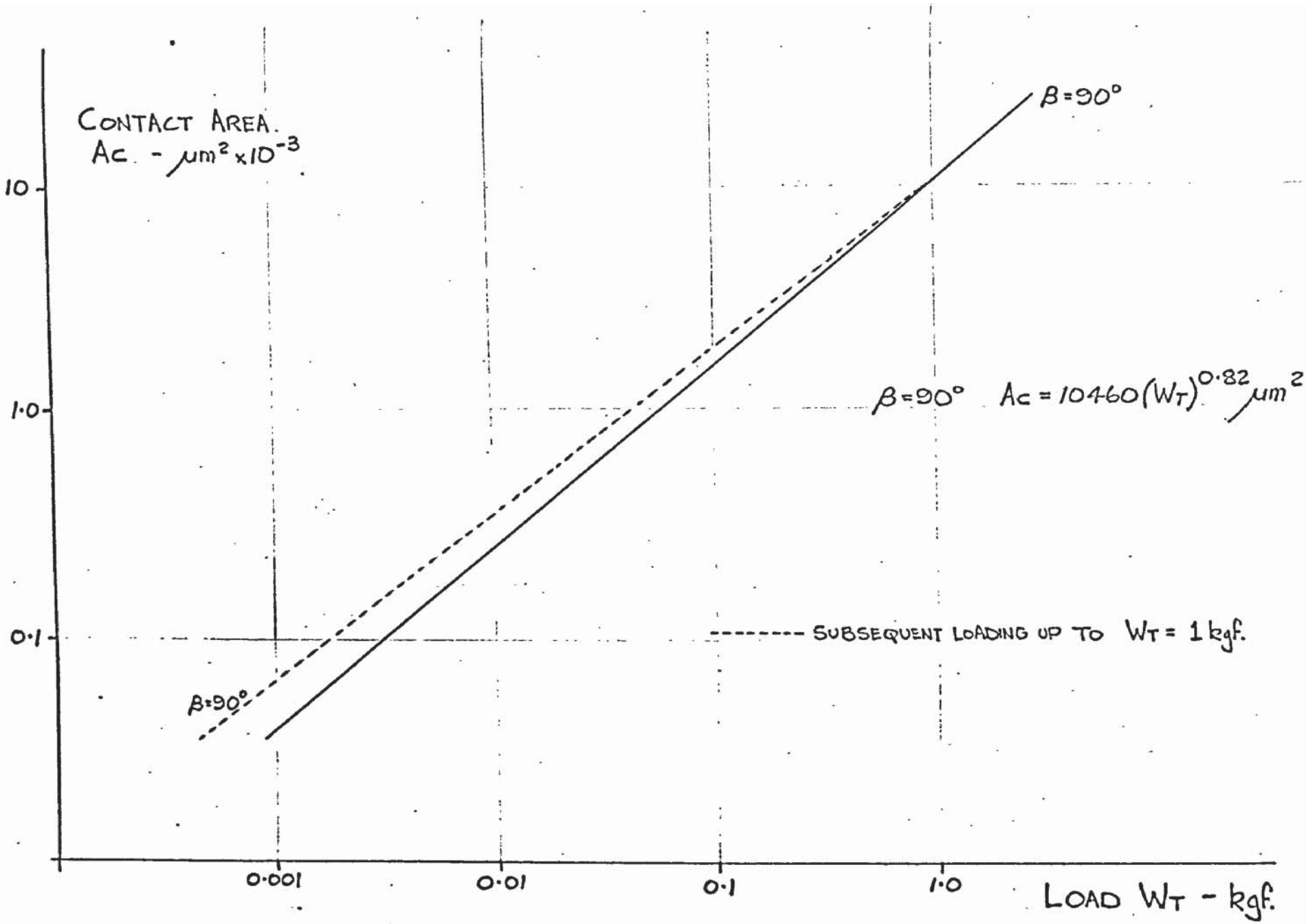

FIG. 7·7. CONTACT AREA AGAINST ASPERITY RANGE LOAD. (LOG. SCALES).

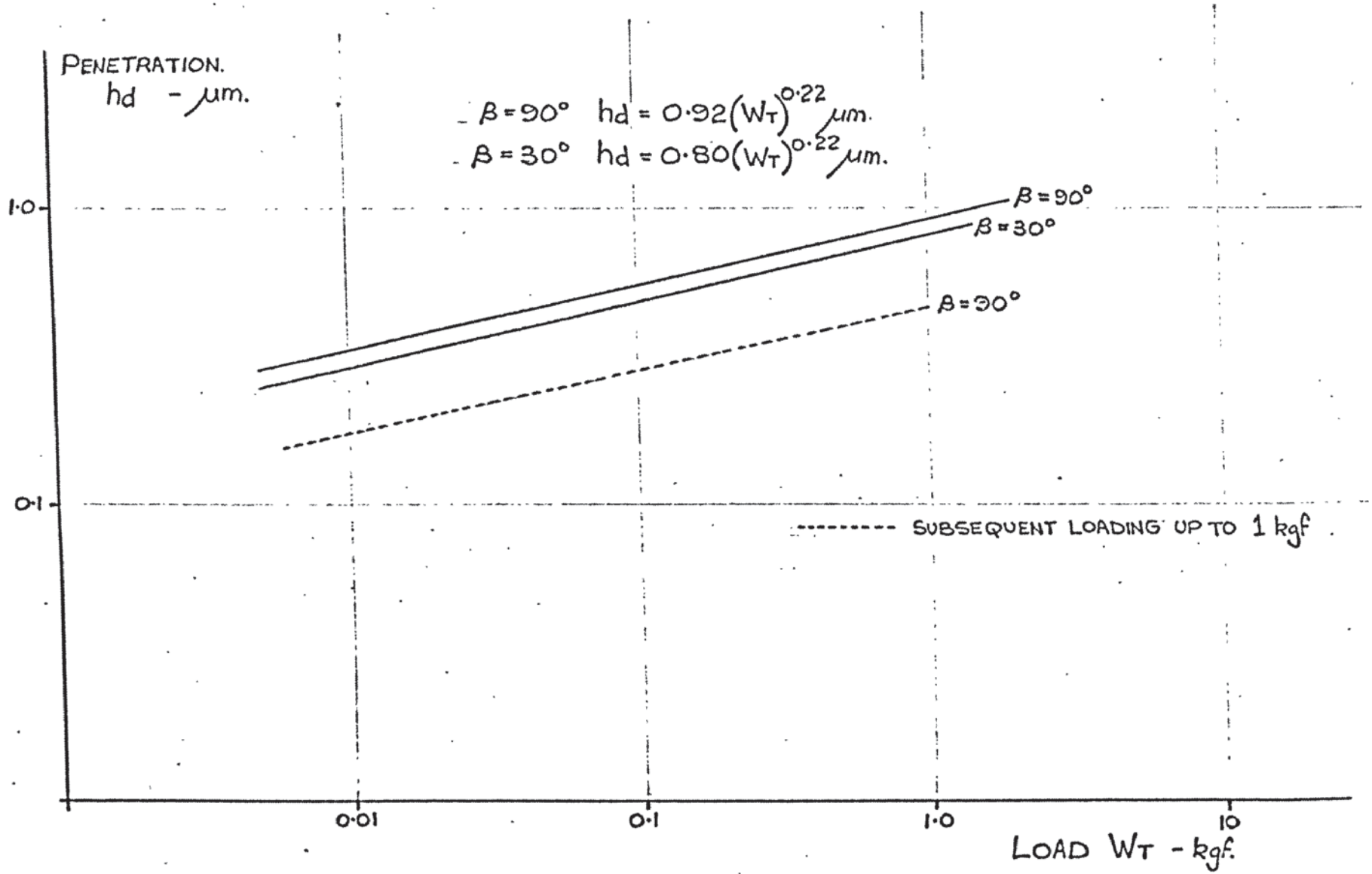

FIG. 7·8. PENETRATION AGAINST ASPERITY RANGE LOADING. (LOG. SCALES).

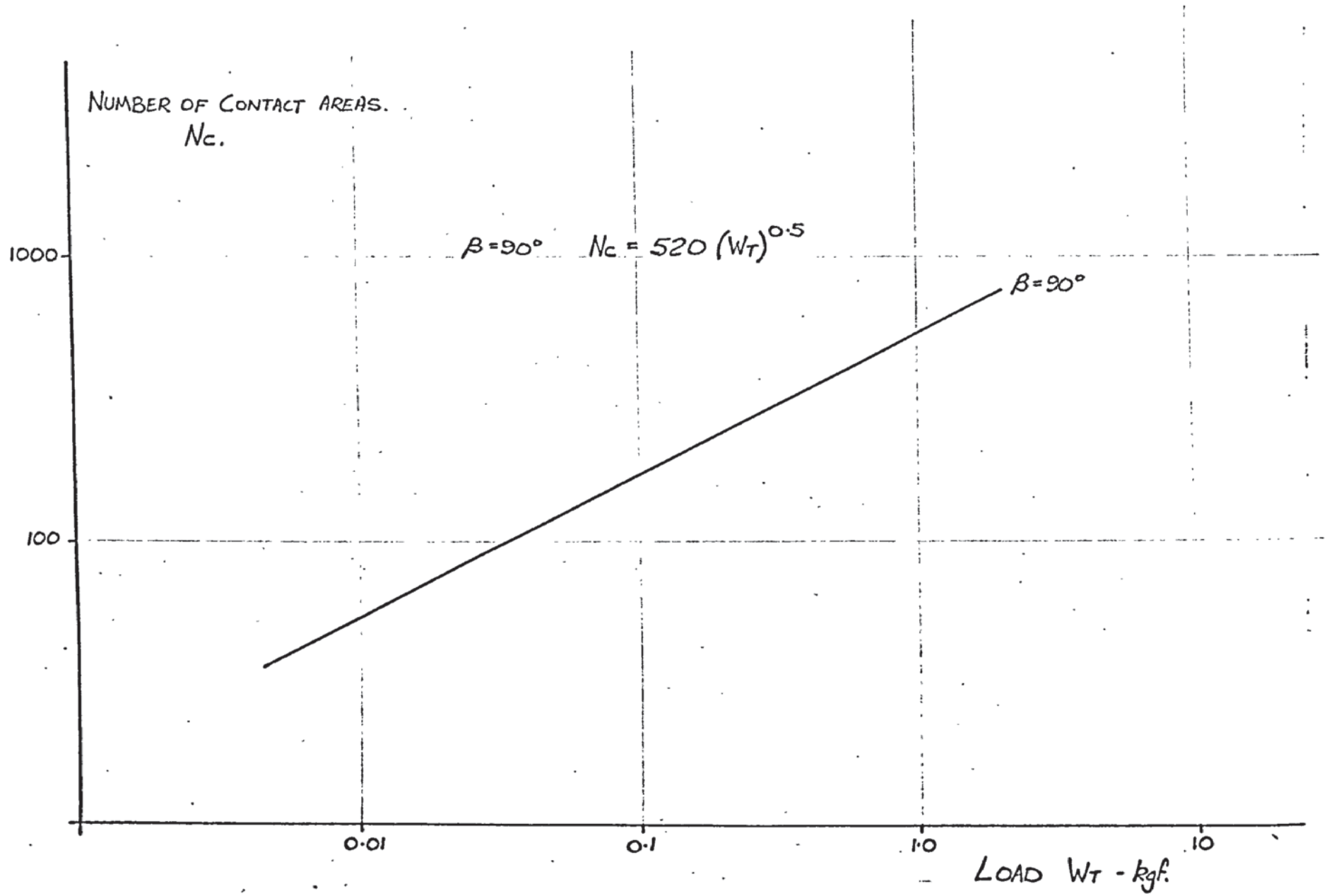

FIG. 7·9. NUMBER OF CONTACT AREAS FOR ASPERITY RANGE LOAD.

These results can be compared with those derivod by J.F.Archard (102) whose surface model is somewhat similar although adhering more closely to the basic analysis of Timoshenko. In his case of a large sphere of radius R_1 covered with smaller spheres of radius R_2 then the total area of contact was found to be

$$Ac = K_2 . W_T^{0.88} \qquad - 37\text{-}7$$

This is in close agreement with the formulae derived above where

$$Ac = KW_T^{0.82} \qquad - 38\text{-}7$$

In the same way Archard suggests that for his particular model then,

$$Nc \propto W_T^{0.66} \qquad - 39\text{-}7$$

whereas the above analysis gives,

$$Nc \propto W_T^{0.5} \qquad - 40\text{-}7$$

It is suggested that the model analysed here would give relationships for Ac, W_T and Nc very close to those stated by Archard if a smaller value of h_T had been selected.

A further plot of total deflection hd for increasing load W_T for the single asperity range is shown in Fig. 7.10 for the two values of β (90°,30°). Superimposed are the results of other authors'work when the load is expressed as that per cm^2. The results are clearly compatible if the load W_T , from this work, acts over the same unit area. It is possible that although cast iron ground materials were used, the ridges on the surfaces of their test pieces crossed at arbitrary angles giving a general relationship of

$$hd = 0.65W_T^{0.45} \qquad - 41\text{-}7$$

In a review by Back, Burdekin and Cowley (75) it is stated that the contact deformation is mainly elastic for these small unit area loads. This will be true after the initial increase in load as long as it does not exceed its original maximum for subsequent loading.

In a very interesting paper by Mikic (103), following the work of Greenwood and Williamson, an analysis shows that for an initial loading which gives some plastic deformation to the higher asperities, as the load is decreased the actual contact area relative to the same normal load increases. In particular the relationship between hd and W_T will alter.

If we consider Fig. 7.8 and the displacement (hd) for an initial loading W_T of 1 kgf on the asperity range, then a certain proportion of

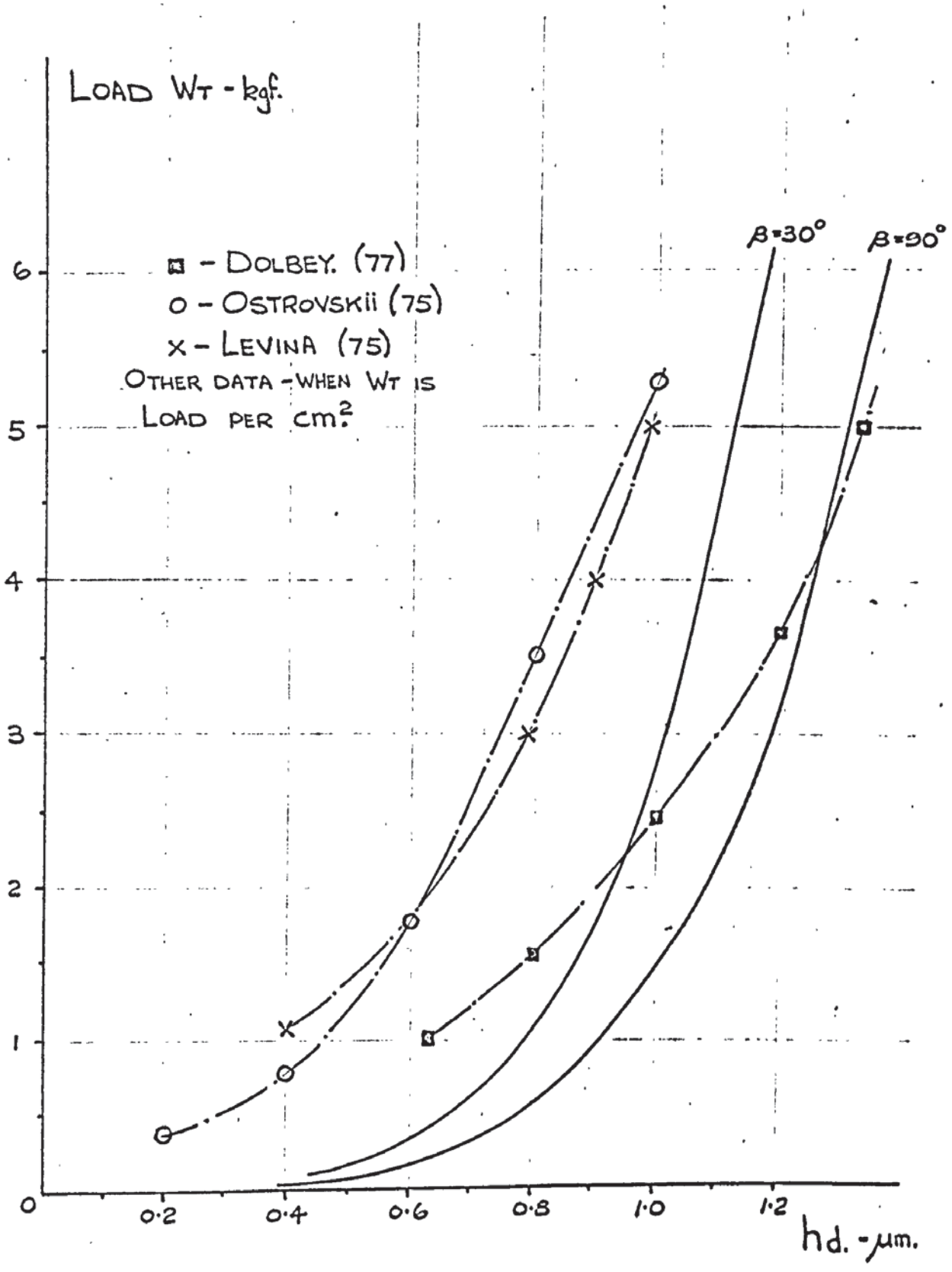

FIG. 7·10. PENETRATION FOR LOAD CHANGES.

the contact area will have been plastically deformed. The number of area points in question can be calculated.

If the load is reduced then these points may remain in contact even when the load is removed. As Mikic (103) points out the separation of the surface is due to the elastic deformation only and the contact area will be approaching the relationship,

$$Ac \propto W^{\frac{2}{3}}$$

This will mean an increase in contact area with reducing load due to some relaxation in the plastically deformed contacts. More importantly it will cause a datum shift in hd since the surfaces will not part to their original no load positions.

If we assume that for the model asperity range the number of points in contact at zero load are those points which have just avoided any plastic deformation and have retained their original shape, then these may be calculated from eqn. 32-7 and 33-7 as follows,

For $\beta = 90^{\circ}$ and initial load $W_T = 1$ kgf

hd = 0.92 μm (From fig. 7.8)

For the top ridge pair to start its plastic deformation hd will be 0.46 μm from,

$$h_d = 2.97 \frac{P_o}{850} - \mu m \qquad 42\text{-}7$$

The number of contacts possible at this point will be 85 since n = 6. Further movement takes place up to the loading of 1 kgf. This extra displacement is a further 0.46 μm, thus bringing all the 85 contact areas into the plastic deformation regime.

If hd is increased by $2h_T$ from 0.46 μm to 0.52 μm the number of contacts will be 113 since n = 7. Therefore there will only be 28 points available for contact for a new loading assuming those plastically deformed do not recover to give areas available at the same height.

For a new loading we start with 28 contacts instead of 1 as was the case originally. If these points deflect by $2.h_T$ then, from eqn. 35-7,

$$W_T = \left(\frac{1}{2.97}\right)^3 . \left[\quad (0.06)^3 \right] \times 28 = 0.000233 \text{ kgf.}$$

and if the deflection is $4.h_T$, $W_T = 0.00213$ kgf

The contact area for $2h_T$ from eqn. 34-7 is

$$Ac = 200 \left[0.06 \right]^2 \times 28 = 20.16 \ \mu m^2$$

The contact areas and loads were calculated up to the deflection required to establish the original load contact area. These points are plotted on Fig. 7.7 and Fig. 7.8 .

In Fig. 7.8 the curve appears to run parallel to the original but exhibits a datum offset,

$$hd = 0.53W_T^{0.22} \ \mu m. \qquad - 43 - 7$$

In Fig. 7.7 the contact area has increased for the same loading

$$Ac = 10500W_T^{0.74} \ \mu m^2. \qquad - 44 - 7$$

Thus it can be concluded that for two stationary surfaces in contact an increase in normal load for the first time will cause some plastic deformation of the asperities, the amount depending upon the surface topography. Initially the contact area is nearly proportional to load. When the load is reduced it has been shown that, due to only the elastic recovery of the asperities, the relationship approaches

$$Ac \propto W_T^{0.66}$$

This will be accompanied by a small datum offset which depends upon the amount of elastic recovery available in the plastically deformed asperities. This point is not pursued here as only a general appraisal of the static contact condition is required.

As stated earlier this analysis is substantiated by other work and if the data illustrated in Fig. 7.10 is used initially then a further description of the surface can be made.

It is reasonable to suggest that one asperity range occurs within every square centimetre of the total area. Thus the W_T values calculated can now be expressed as an average pressure Pw.
Thus,

$$hd = C.P_w^{\lambda} \ \mu m \qquad - 45 - 7$$

where C is 0.3 to 0.92, λ is approximately 0.22 and Pw is expressed in kgf/cm^2.

The shape of such a range of ridges can now be given some dimensions. The base width will be one centimetre, therefore the number of ridges will be,

$$\frac{10000}{B} = \frac{10000}{50} = 200.$$

The maximum height of the range will be

$$h_T \times \frac{200}{2} = 0.03 \times 100 = 3 \ \mu m.$$

This will mean that when two such surfaces are just in contact, under no load conditions the clearance between the lowest ridge crests will be 6 μm. The percentage area in contact will be given by

$$\frac{Ac}{A_A} = Pw^{0.82} \times 10^{-4} \ \% \qquad - 46\text{-}7$$

For Pw having a value of 1 kgf/cm^2 then the contact area is 0.01% of the apparent surface area (A_A).

Using data relevant to chaptor 4 for a slideway table having a weight of 454 kgf and a total apparent contact area of 697 cm^2 the average pressure will be 0.65 kgf/cm^2. The initial normal deflection will be of the order of 0.83 μm for $\beta = 90^\circ$, the total contact area will be approximately 0.0512 cm^2.

The static friction force can now be investigated using this surface model.

For convenience one asperity range pair is considered and all the asperity contacts are lumped together such that it is replaced by a single asperity pair whose contact area and load carrying capacity are the same as that for the original contacting range. The cross angle β for this new asperity ridge is taken to be 90° and thus the mathematical relationships will be those listed in table T.7.1. (page 109).

This asperity pair is illustrated in Fig.7.11 and the contact area is divided equally between the leading side and the trailing side of the ridge. A force F is applied to the bottom ridge which will cause it to move a distance x from its steady state position. This force will be a maximum when the leading edge of the ridge only is supporting the load W_T and this leading area is about to shear.

Thus $F = (A_{cL} \cos \theta).S_s + W_T.\tan \theta \qquad - 47\text{-}7$

where S_s is the shear strength.

In this situation it is suggested that the trailing edge does not support the load at all and that as A_{cL} must increase, a build-up of material takes place (Fig.7.11.b). This is taken from the top stationary wedge, thus forming a small prow of material. It is assumed that the plane of contact remains at an angle of θ to the horizontal plane.

With reference to the original asperity range it is noted that as some of the highest contact points have been plastically deformed the prow of material will be much greater on these areas, and thus likely to

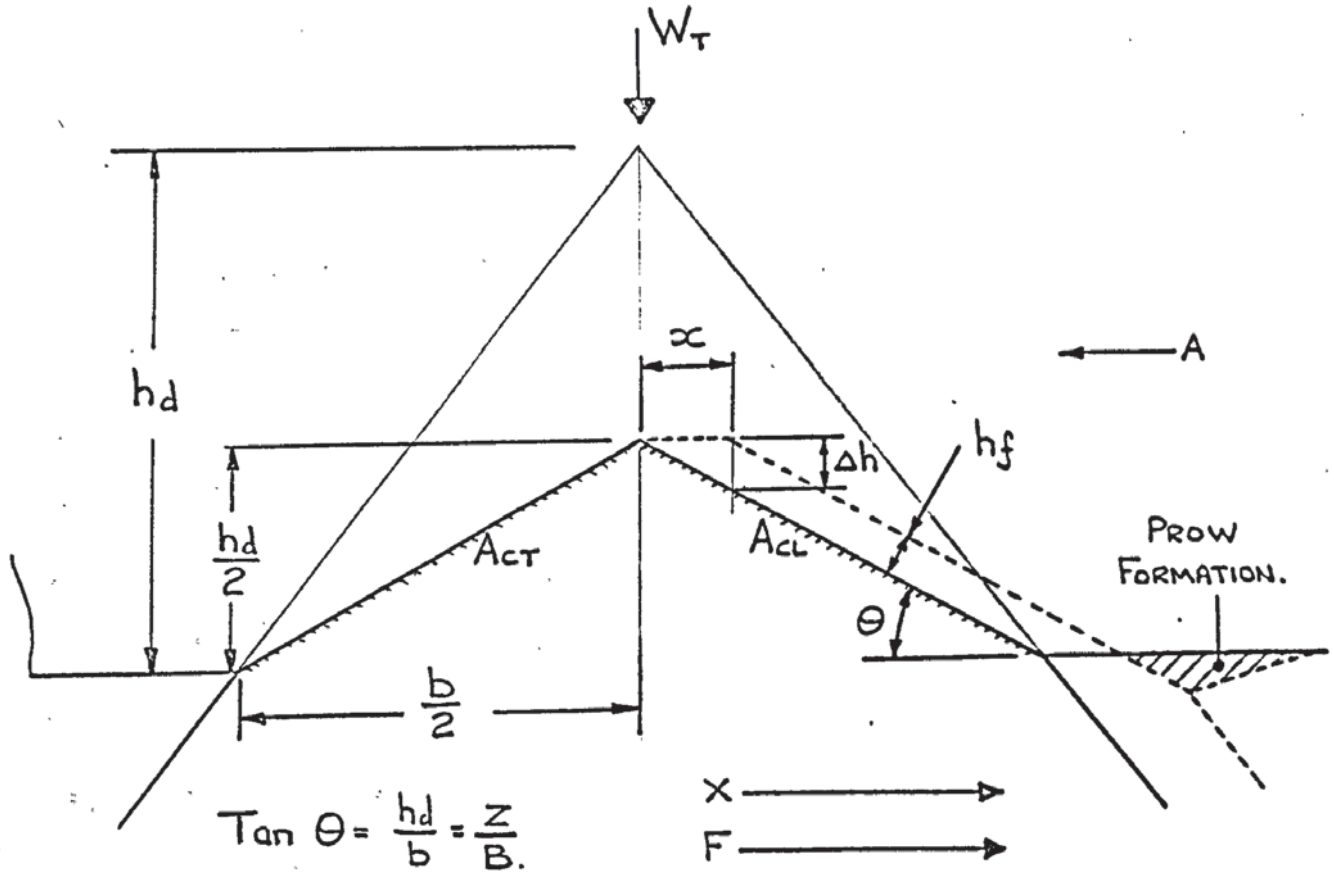

a) CONTACT AREA CONFIGURATION. ($\beta = 90°$).

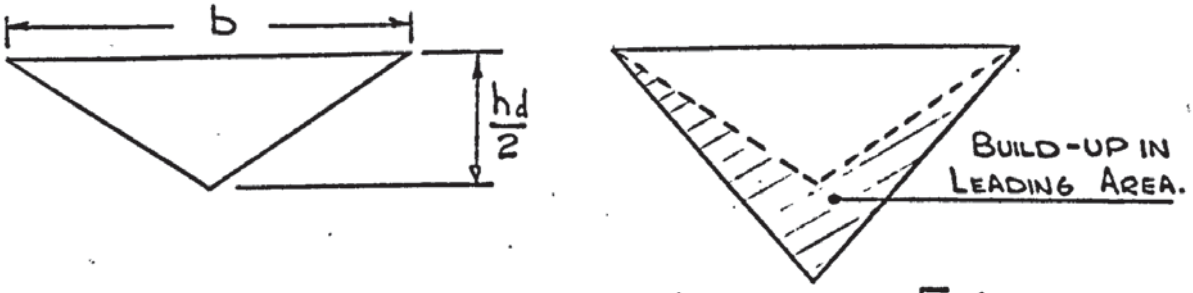

F AT ZERO. WITH FORCE F APPLIED.

b): CHANGES IN A_{CL} WITH FORCE (VIEW A. ABOVE).

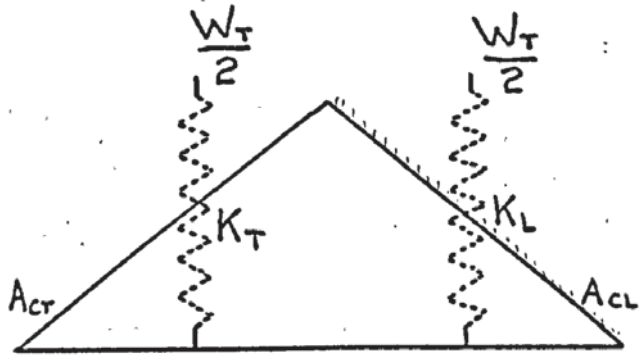

$$K_L + K_T = K_a = 4.94 \left(W_T\right)^{0.78} \text{ kgf/}\mu\text{m}.$$

c) REPRESENTATION OF CONTACT AREA STIFFNESS.

FIG. 7.11. INTERACTION BETWEEN NEW ASPERITY PAIR.

produce some metallic debris.

In order to find the displacement x, hf has to be calculated,

since $$x = \frac{hf}{Sin\theta} \qquad - 48\text{-}7$$

Now

$$h_d = 0.92\, W_T^{\,0.22} \quad -\mu m$$

and $$\frac{dW_T}{dh_d} = 4.94 W_T^{0.78} \text{ -kgf/}\mu m = Ka \qquad - 49\text{-}7$$

Thus Ka is the "stiffness" of the new asperity junction in the steady state position, and comprises two springs in parallel, one for A_{cL} and one for A_{cT} as shown in Fig. 7.11.c

Therefore the stiffness of both areas is the same

$$K_T = K_L = \frac{Ka}{2} = 2.47\, W_T^{\,0.78}$$

The increase in W_T on the leading area is $\frac{W_T}{2}$

i.e. $dW = \frac{W_T}{2}$ then

$$dh_d = \Delta h = \frac{2dW}{Ka} \quad -\mu m \qquad - 50\text{-}7$$

Thus $hf = \Delta h.\text{Cos}\,\theta = \frac{2dW\text{Cos}\theta}{Ka}$ $-\mu m$

hence $$x = \frac{2dW}{Tan\theta Ka} \quad -\mu m \qquad - 51\text{-}7$$

Therefore as x increases dW increases up to a maximum when dW is equal to $\left(\frac{W_T}{2}\right)$. Substituting eqn. 49-7 into eqn. 51-7 the maximum displacement will be,

$$x_m = \frac{0.2025}{Tan\theta} (W_T)^{0.22} \quad - \mu m \qquad - 52\text{-}7$$

In the same way,

(from Table T.7-1) $$h_d = 0.075(A_c)^{0.27} \text{ -}\mu m$$

$$\frac{dAc}{dh_d} = 51.44\, (A_c)^{0.73} = Kd \quad -\mu m \qquad - 53\text{-}7$$

Now $Ac = A_{cL} + A_{cT}$ and in the steady state $A_{cL} = A_{cT}$

$$\therefore A_{cL} = \frac{Ac}{2}$$

thus, $$\frac{dA_{cL}}{dh_d} = \frac{Kd}{2} = 25.72\, (Ac)^{0.73} \qquad - 54\text{-}7$$

Hence a change in hd by Δh will give a corresponding increment in area A_{cL} i.e. dA_{cL},

$$dA_{cL} = \Delta h.\frac{Kd}{2}$$

and the total area on the leading side of the asperity (when $\Delta h = hf_{max}$) will be,

$$Ac_L = \frac{Ac}{2} + hf_{max}.\frac{Kd}{2} = \frac{Ac}{2} + \alpha_m \sin\theta.\frac{Kd}{2} \qquad - 55\cdot7$$

Substituting eqns . 52 and 54-7

$$Ac_L = \frac{Ac}{2} + 0.2025(W_T)^{0.22}.\ \cos\theta\ 25.72\ (Ac)^{0.73}$$

from table T.7-1

$$Ac = 10460(W_T)^{0.82}\ -\mu m^2$$

and substituting this,

$$Ac_L = 5230(W_T)^{0.82} + 4476.6(W_T)^{0.82}$$

$$Ac_L = 9707(W_T)^{0.82}\ \mu m^2 \qquad - 56\text{-}7$$

Applying eqn. 47-7

$$F = (0.0097(W_T)^{0.82})\ Ss + W_T.\tan\theta \qquad - 57\text{-}7$$

From the B.C.I.R.A. (71) data on grade 17 cast iron the shear strength is 30.87 kgf/mm^2 and will be taken as the maximum value possible. As the load W_T is known,

$$F = 0.212 + W_T \tan\theta = Fs \qquad - 58\text{-}7$$

This is the maximum static friction force and the coefficient of static friction is,

$$\mu s = \frac{Fs}{W_T} \qquad - 59\text{-}7$$

$$\mu s = \frac{0.212}{0.65} + \tan\theta$$

$$\mu s = 0.325 + \tan\theta \qquad - 60\text{-}7$$

The work of Ernst and Merchant (5)

$$\mu s = \frac{Ss}{Pm} + \tan\theta \qquad - 61\text{-}7$$

and this gives,

$$\mu s = \frac{30.87}{132} + \tan\theta = 0.234 + \tan\theta \qquad - 62\text{-}7$$

The differences between eqn. 60-7 and 62-7 are due to the changes in contact area as the tangential force is applied.

From eqn. 57-7 it also follows that if the shear strength of the junction is zero then,

$$\mu s = \tan\theta = 0.050$$

which would be the lowest possible coefficient of friction due to the action of a good lubricant film. This value is in line with that suggested by Tamir and Rightmore (5).

The above analysis indicates how the area being sheared increases with the applied tangential force and the tendency to accommodate relative surface movement, (eqn.55-7). With zero applied force (hf=o) the shear force on the leading area alone $\left(\frac{Ac}{2}\right)$ can be used to give a hypothetical friction condition where,

$$F = \frac{Ac}{2} \cdot Ss + W_T . \text{Tan}\,\theta \qquad - 63\text{-}7$$

Obviously the static friction force is zero when the relative movement is zero and the load is shared equally between the leading and trailing areas. The above equation represents the initial value from which the static friction force builds up with accompanying deformation. It is possible to use this equation to evaluate a minimum coefficient of static friction (μso). For various values of dW up to a maximum of $\frac{W_T}{2}$, μ and x have been calculated for 4 values of asperity loading. These are plotted in Fig. 7-12 and two observations can be made.

1) The dry state coefficient rises with applied tangential force and is accompanied by a displacement in the direction of this force.

2) The value of μs which will occur varies with the asperity loading, and as the load increases μs reduces. This is an observation made by Gupta and Cook (34).

The minimum value of the coefficient of static friction μso and the maximum μsx are plotted against W_T on logarithmic scales in Fig. 7-13. These curves yield the following relationships,

$$\mu so = \frac{0.160}{W_T^{0.181}} \qquad - 64\text{-}7$$

$$\mu sx = \frac{0.35}{W_T^{0.165}} \qquad - 65\text{-}7$$

The maximum displacement x_m to give μsx is also plotted in Fig. 7-13 and gives the relationship,

Max. displacement $x_m = 4.00\, W_T^{0.22}$ -μm $\qquad - 66\text{-}7$

A closer analysis of eqn. 65-7 can be made in order to show the general relationship between μs and W.

Now $\mu so = \frac{F}{W_T} \doteq \frac{Ss}{W_T} \cdot \left(\frac{Ac}{2}\right)$ $\qquad - 67\text{-}7$

and $Ac = 0.01046\, W_T^{0.82}$ -mm^2 $\qquad - 68\text{-}7$

hence $\mu so = \frac{0.01046 W_T^{0.82} \times 30.87}{2W_T}$

$$\mu so = 0.160 \frac{W_T^{0.82}}{W_T} = 0.160/W_T^{0.18}$$

The change in the relationship between μs and W_T, with regard to eqns. 64-7 and 65-7 comes about from the change in contact area and the additio of the fixed value created by Tan θ.

To summarise the findings for W_T then the following observations can be made.

For asperity range loading - $W_T = 0.65$ kgf, $\beta = 90^\circ$

Using eqn. 60-7, $\mu s = \frac{F}{W_T} = 0.375$

From eqn. 52-7, $x_m = 3.6\ \mu$m. (similar values were obtained by Shchedrov (ref. 115))

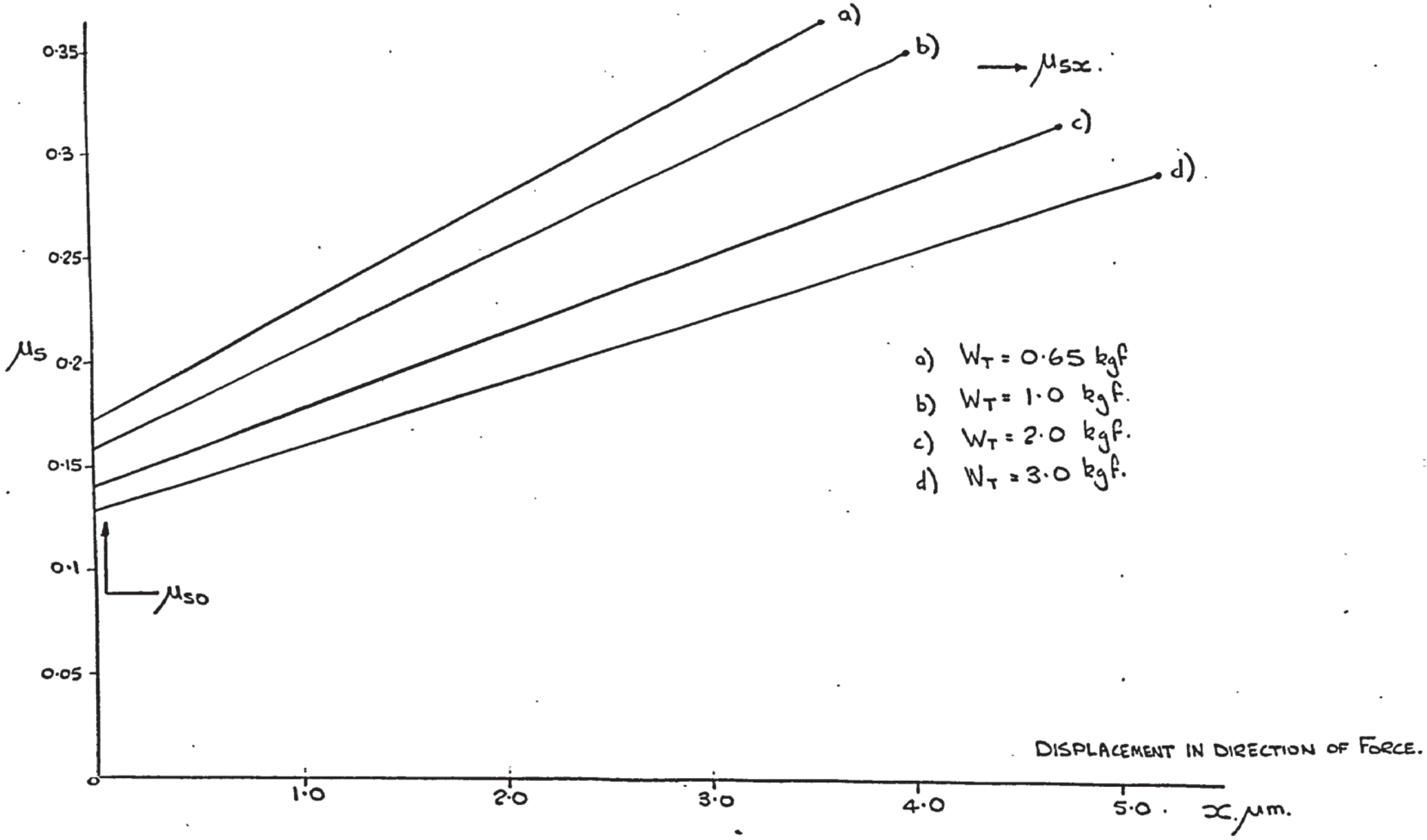

FIG. 7·12. CHANGE IN STATIC FRICTION COEFFICIENT WITH DISPLACEMENT.

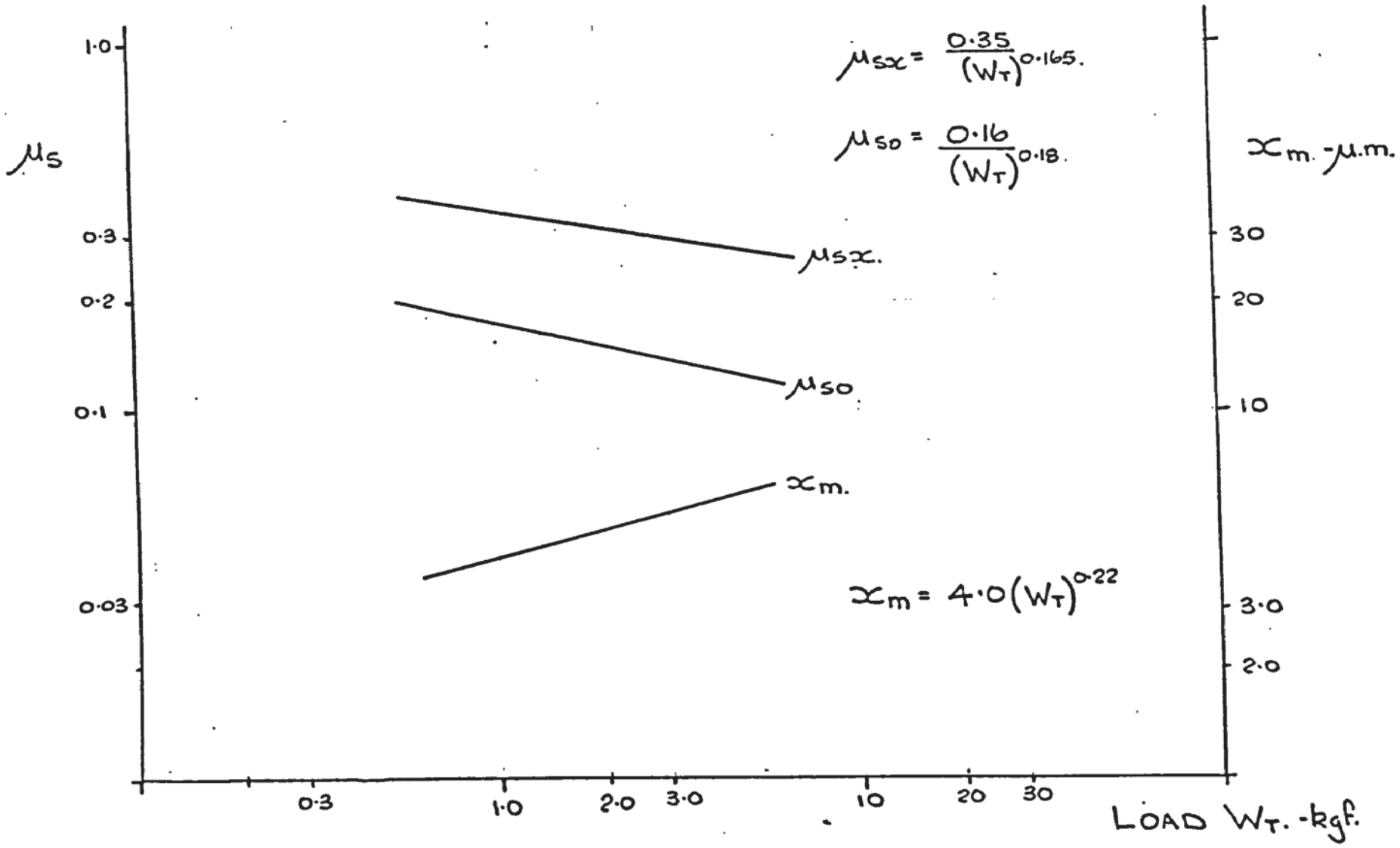

FIG. 7·13. RELATIONSHIP BETWEEN FRICTION, DISPLACEMENT AND ASPERITY LOAD.

Amontons Law is not obeyed in this analysis since μ is a function of W_T, thus μ will vary with the load. It is interesting to observe that this relationship is created by the shape of the asperity junction. If the angle θ was very close to zero and the whole surface in contact was extremely smooth then it can be suggested that the coefficient of friction would become independent of the applied load.

i.e. $\mu sx = \mu so = \frac{K}{W_T^{0.0}}$ - 69-7

since $Ac \propto W_T$.

In conclusion, the selection of shear strength value is important and if we make Ss equal to $\frac{Pm}{\sqrt{3}}$ from Tabor (2), i.e. Ss = 76.2 kgf/mm^2,

eqn. 65-7 would become,

$$\mu sx = \frac{0.79}{W_T^{0.165}} \quad - 70\text{-}7$$

Using the model data then, the value of μsx for dry cast iron would be 0.85.

7.2.i. EFFECT OF LUBRICANT ON STATIC FRICTION

The effect of a lubrication film will now be analysed.

When an oil film is present on the contacting surfaces their approach will squeeze out the film. As the higher asperities are deformed it may be possible for a very thin film to remain between these highly pressurised surfaces. Eventually this film will rupture and therefore a contact area will have some metallic interface and the remainder will be separated by an oil film.

The rupturing of such a lubricant film is not clearly understood although mechanical analogies of the behaviour of hydrocarbon chains have been attempted as outlined by A.S.Akhmatov (104). Their molecular elasticities are not linear and therefore difficult to use.

From the work carried out by Akhmatov the following observations are made,

1) The smaller the oil film the greater is its "yield pressure".
2) The "shear stress" of the oil film area reduces with reductions in area loading.
3) Non-polar oils have smaller "yield pressures" than those containing polar additives.
4) The "yield pressures" depend upon the chain length of the hydrocarbon molecules and therefore on oil density and bulk viscosity, especially for non-polar oils since their adhesion on to the surface is very weak.

5) Polar additives adhere strongly to metal surfaces, therefore their "yield pressures" can be high, governed by their chain length and amount present in the bulk oil material.
6) In general "yield pressures" are influenced also by the orientation of the molecules on the metal surface. Non-polar molecules are usually lying flat along the surface, whereas polar additives stand normal to the surface.
7) The "shear stress" for non-polar oils is of the same order as that for polar additives.

Thus it may be said that for a particular mineral oil the pressure required to rupture a fluid film will be small and the force required to shear the film will also be small. If polar hydrocarbons are added the thin film strength is much increased and higher pressures are required to rupture the film, although the shear force remains small. Therefore polar additives will reduce the static friction coefficient to a value below that of a plain mineral oil.

The following analysis is based upon the above comments.

If P_{OL} is the "yield pressure" of a lubricant film, then using data from Akhmatov,

$$P_{OL} = Ko.e^{-10.ho} + 0.06 \text{ -kgf/mm}^2 \qquad - 71\text{-}7$$

where Ko is a function of molecular chain length, strength of adhesion to the metal surface, density and bulk viscosity.

ho is the oil film thickness. (μm)

When ho = 0

then $P_{OL} = Ko + 0.06$ - kgf/mm^2

which will be the pressure required to rupture the oil film.

When ho = ∞

then $P_{OL} = 0.06$ kgf/mm^2

which is the minimum pressure an oil film will support per unit area, and as ho reduces P_{OL} will increase to some maximum value.

Also if S_{OL} is the shear strength of the oil film,

$$S_{OL} = e^{ko.Pa} - 1. \qquad - 72\text{-}7$$

where Pa is the average pressure over the contact area; ko is a function of chain length, density and intermolecular bonding.

In eqn. 55-7 it can be seen that the contact area of the leading face of the asperity (A_{CL}) after a tangential movement of x_m has taken place is given by,

$$A_{CL} = \left(\frac{Ac}{2} + x_m . \text{Sin}\,\theta . \frac{Kd}{2}\right) \qquad - 73\text{-}7$$

The average pressure over this area (Pa) is given by,

$$Pa = \frac{W_T}{Ac_L} \qquad - 74\text{-}7$$

Using Hertzian pressure distribution over the area Ac_L

and if $Ac_L = \pi r_a^2$ - 75-7

the pressure at any radius r_t can be calculated from

$$P = Pm \cdot \sqrt{1 - \left(\frac{rt}{ra}\right)^2} \qquad - 76\text{-}7$$

where Pm is the yield pressure of the metal surface.

If P is equal to Po_L of eqn. 71-7 when ho is zero then r_t can be found, and for values of radius greater than r_t it is assumed that an oil film will be present.

Thus

$$r_t = r_a \cdot \sqrt{1 - \left(\frac{Po_L}{Pm}\right)^2} \qquad - 77\text{-}7$$

$$r_t = r_a \cdot \sqrt{1 - \left(\frac{Ko + 0.06}{Pm}\right)^2} \qquad - 78\text{-}7$$

The metallic contact area will be,

$$Am = \pi . r_t^2 \qquad - 79\text{-}7$$

The oil film area will be,

$$Ao = \pi . (r_a^2 - r_t^2) \qquad - 80\text{-}7$$

Using eqn. 75-7 and 78-7 then eqn. 79-7 becomes

$$Am = Ac_L . \left[1 - \left(\frac{Ko + 0.06}{Pm}\right)^2 \right] \qquad - 81\text{-}7$$

$$Ao = Ac_L . \left[\left(\frac{Ko + 0.06}{Pm}\right)^2 \right] \qquad - 82\text{-}7$$

The tangential force F required to shear the contact area will be given by a modified form of eqn. 57-7,

$$F = AmSs + AoSo_L + W_T . \tan\theta . \qquad - 83\text{-}7$$

$$F = Ac_L . \left[1 - \left(\frac{Ko+0.06}{Pm}\right)^2 \right] . Ss + Ac_L . \left[\left(\frac{Ko+0.06}{Pm}\right)^2 \right] . So_L + W_T . \tan\theta \qquad - 84\text{-}7$$

The static coefficient μs will be equal to the ratio F/W_T.

For the model under consideration $W_T = 0{\cdot}65\,kgf$, $Ac_L = 0{\cdot}00683\,mm^2$, $Pm = 132\,kgf/mm^2$, $Ss = 30{\cdot}87\,kgf/mm^2$, $Pa = 95{\cdot}2\,kgf/mm^2$ and from Akhmatov let $ko = 0{\cdot}014$, whence $So_L = 2{\cdot}9\,kgf/mm^2$.

Then,

$$\mu s = \frac{0.00683}{0.65} . \left[\left(1 - \left(\frac{Ko+0.06}{132}\right)^2\right) . 30.87 + \left(\frac{Ko+0.06}{132}\right)^2 . 2.9 \right] + 0.05 \qquad - 85\text{-}7$$

A plot of μs against Ko is made in Fig. 7-14, when Ko = 0

$$\mu s = 0.373$$

when Ko = 131.94 $\triangleq$ Pm

$$\mu s = 0.0807$$

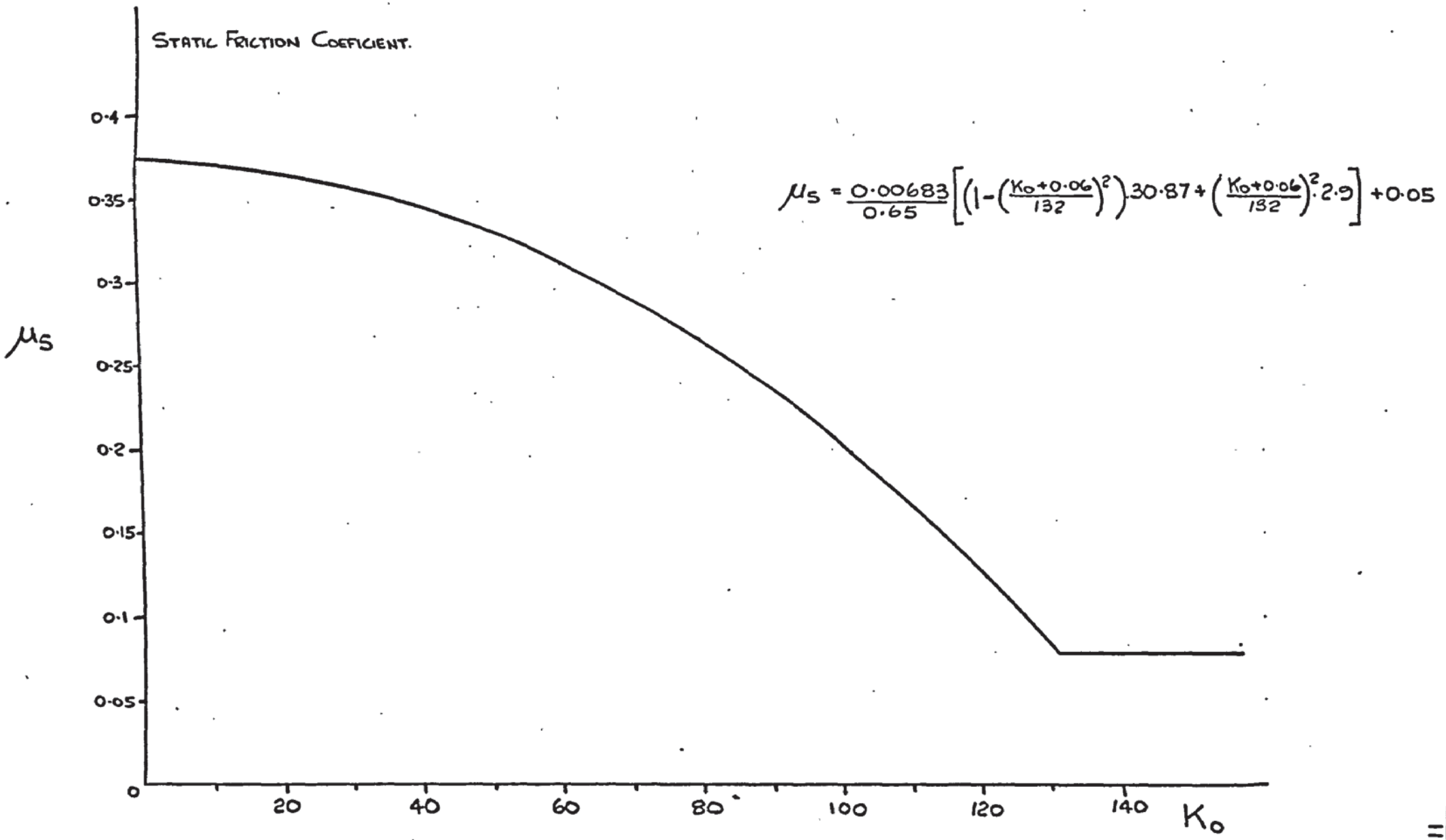

FIG. 7·14. CHANGES IN STATIC FRICTION COEFFICIENT WITH OIL PARAMETER K_o.

Thus as Ko increases μs decreases until a minimum value is reached when Ko is numerically the same as the metal yield pressure. This value 0.0807 is compatible with that obtained by tests carried out by Tabor (2). If Ko is greater than Pm then μs will remain at its lowest value. It is interesting to note that the coefficient Ko is dependent upon several parameters and it is suggested that Ko can have the same value when,

1) The lubricating oil has a high bulk viscosity due to long chain length, but containing no polar molecules.
2) The lubricating oil has a low bulk viscosity but does contain polar additives.

Tests carried out by Tabor, following the earlier work of Hardy (2), indicate that the static coefficient of friction falls with increasing molecular weight of the lubricant. Taking an example from this work, the molecular weight of a straight-chain paraffin is approximately twice that of a saturated fatty acid and both have the same μs value. In the above analysis μs will depend upon Ko, therefore it is suggested the following expression may be possible,

$$Ko \propto f(\text{Chain Length}) + f(\text{Surface adhesion and orientation}) \quad - 86\text{-}7$$

or in more general terms,

$$Ko \propto f(\text{lub.viscosity}) + f(\text{Polar additive performance}) \quad - 87\text{-}7$$

As lubricant viscosity is proportional to $(\text{molecular weight})^{\frac{1}{2}}$ (99) then a straight mineral oil will need to have a very high viscosity in order to substantially reduce μs. In practice the bulk viscosity of slideway lubricants is fairly low for several reasons. It is well known that, in the past, slideway "stick-slip" has been reduced by applying "thicker" lubricants. This of course has the effect of reducing μs which is related to the stick-slip phenomenon.

To reduce μs substantially using an oil with a useful bulk viscosity polar additives must be included. In this situation it is not the bulk lubricant properties that affect μs so much as the properties and performance of the polar molecules.

In conclusion, it can be stated that the coefficient of static friction between two metal surfaces depends upon many parameters. To illustrate this point, the friction force F is expressed below using Eqn. 73-7 and 84-7,

$$F = \left[\frac{0.01046(W_T)^{0.82}}{2} + \frac{W_T}{2}\frac{Kd}{Ka}\right]\left[\left(1 - \left(\frac{Ko+0.06}{Pm}\right)^2\right)Ss + \left(\frac{Ko+0.06}{Pm}\right)^2 . So\right] + W_T . \tan\theta . \quad - \quad 88-7$$

As Kd and Ka are functions of W_T then,

$$F = \left[0.009707(W_T)^{0.82}\right]\left[\left(1-\left(\frac{Ko+0.60}{Pm}\right)^2\right),Ss + \left(\frac{Ko+0.06}{Pm}\right)^2 . So\right] + W_T.\tan\theta . \quad - \quad 89-7$$

This eqn. has the form

$$F = [A][B] + C$$

[A] is a function of mechanical and metallurgical parameters relating to the surface topography and ridge shape.

[B] is a function of the yield strength of metal and lubricant, and their shear strengths

C is a function of base angle of wedge asperity profile

[A] and [B] are both functions of metal hardness, which has been related to the yield stress. For the same surface topography, with an increase in hardness, it can be said that [A] will reduce and [B] will increase, so that the effect of hardness on μs is likely to be small. It is suggested from the work of Hardy (2) that μs will increase slightly with hardness since [B] will change at a greater rate than [A].

As F is a function of W_T then μs will still be a function of the reciprocal of W_T (eqn.65-7). With a reduction in load the coefficient of static friction will increase, even when the surface is lubricated, as reported by such researchers as Akhmatov (104).

7.3 THE KINETIC CONDITIONS

It has been shown by many authors that, as the sliding velocity between most contacting metal surfaces increases the friction force will decrease to some minimum value at a particular velocity (Vm). This force may rise again at higher velocities depending upon the surface conditions.

If we consider temperature changes at the interface to be negligible the deformation processes that take place can be considered, from Akhmatov (104) to be "quasi-isothermal". In such a process, a rise in sliding velocity increases the resistance to plastic deformation of the asperities. This is brought about by increases in the yield stress, elastic modulus and elastic limit and will lead to the descending friction-velocity characteristic.

It is suggested that this process occurs at the interface of dry and lubricated cast iron surfaces, but in the latter case the effect of the metallurgical changes is masked by those of the lubricant. Initially it is worth considering the changes in the friction coefficient between dry sliding surfaces.

7.3.i. DRY CAST IRON SURFACES

If we look at eqn. 57-7 then the friction force is dependent upon the contact area only if the shear strength Ss and the asperity contact angle θ remain constant. These assumptions have been made in the following analysis.

From eqn. 22-7 it can be seen that the elasticity modulus (E) is the only material parameter that affects the asperity contact area, in basic form

$$Ac = K\left(\frac{W_T}{E}\right)^n \qquad - 90\text{-}7$$

and if E increases then the contact area will reduce.
For this model analysis (when $\beta = 90^\circ$) the leading contact area (from eqn. 56-7), replacing W_T with Pw is

$$Ac_L = 9707.(Pw)^{0.82} \quad - \mu m^2$$

and has been established for a particular value of E.
If Eo is the material elasticity modulus at zero sliding velocity and Ev is the increased modulus brought about by some sliding velocity, then the leading contact area during sliding can be expressed as,

$$Ac_{LV} = 9707.\left(\frac{Pw}{Ev/Eo}\right)^{0.82} \quad - \mu m^2 \qquad - 91\text{-}7$$

$$Ac_{LV} = 9707\left(\frac{Pw}{\alpha}\right)^{0.82} \quad - \mu m^2 \qquad - 92\text{-}7$$

where α is the ratio of the "dynamic" to "static" modulus.

$$\alpha = \frac{Ev}{Eo} \qquad - 93\text{-}7$$

In this particular analysis, as the velocities are small (typically 0 - 10 mm/s for machine tool slideways), the value of α will increase with such sliding speeds. As the contact area reduces so will the penetration level h_d.

Now, at rest (from table T.7-1, $\beta = 90^\circ$)

$$h_d = 0.92\ (Pw)^{0.22} - \mu m \qquad - 94\text{-}7$$

and therefore at some sliding velocity the level will be,

$$h_{dv} = 0.92\left(\frac{Pw}{\alpha}\right)^{0.22} \quad -\mu m \qquad - 95\text{-}7$$

The relationship between h_d and A_{CL} remains independent of α and in general terms,

$$h_d = 0.077.(A_{CL})^{0.27} \quad -\mu m \qquad - 96\text{-}7$$

Transposing eqn. (94-7) then,

$$Pw = 1.46\,(h_d)^{4.55} \text{ -kgf/cm}^2 \qquad - 97\text{-}7$$

From this a normal surface "stiffness" per cm^2 can be formed

$$K_E = \frac{Pw}{h_d} = 1.46\,(h_d)^{3.55} \times 10^4 \text{-kgf/cm} \qquad - 98\text{-}7$$

Let C_E be the normal "damping" coefficient of the contacting surface asperities, per cm^2. This has been created from the following equation,

$$C_E = \frac{U_A.A_{CL}}{h_d} \quad -\text{kgf.s./cm} \qquad - 99\text{-}7$$

where U_A is a "dynamic viscosity" coefficient ($kgf.s/cm^2$) related to the surface asperities.

Transposing eqn. 96-7 the leading asperity contact area is,

$$A_{CL} = 1.32\,(h_d)^{3.7} \times 10^{-4} \quad -cm^2 \qquad - 100\text{-}7$$

and eqn. 99-7 becomes,

$$C_E = U_A \times 1.32\,(h_d)^{2.7} \text{ -kgf.s/cm} \qquad - 101\text{-}7$$

If we consider the normal interaction of the sliding surfaces in terms of a spring/dashpot represented by the Voigt model (105) in Fig. 7-15 then a simple linear expression can be written for the equilibrium condition,

$$Pw = K_E . h_d + C_E . \dot{h}_d \quad - \text{kgf.} \qquad - 102\text{-}7$$

where Pw is the load supported by this Voigt model per unit area (cm^2). Substituting eqns. 98 and 101-7 then Pw becomes,

$$Pw = \left[1.46\,(h_d)^{3.55} \times 10^4\right] . h_d + \left[U_A . 1.32 (h_d)^{2.7}\right] . \dot{h}_d \qquad - 103\text{-}7$$

This is a non-linear form of eqn. 102-7 and several general observations can be made.

1) Pw is the load per unit area and in this model will remain constant as it is only associated with the table weight and the apparent contact area between table and slides.

2) $\dot{h}_d$ is an equivalent normal velocity related to the tangential sliding velocity V through the shape of the individual asperities in contact, especially their interacting wedge angle. Therefore,

$$\dot{h}_d = \left(\frac{2Z}{B}\right).V \qquad - 104\text{-}7$$

and as $\frac{Z}{B}$ has been shown to be equal to Tan Θ on Fig 7.11a ,

$$\dot{h}_d = 2 \text{ Tan } \Theta . V \qquad - 105\text{-}7$$

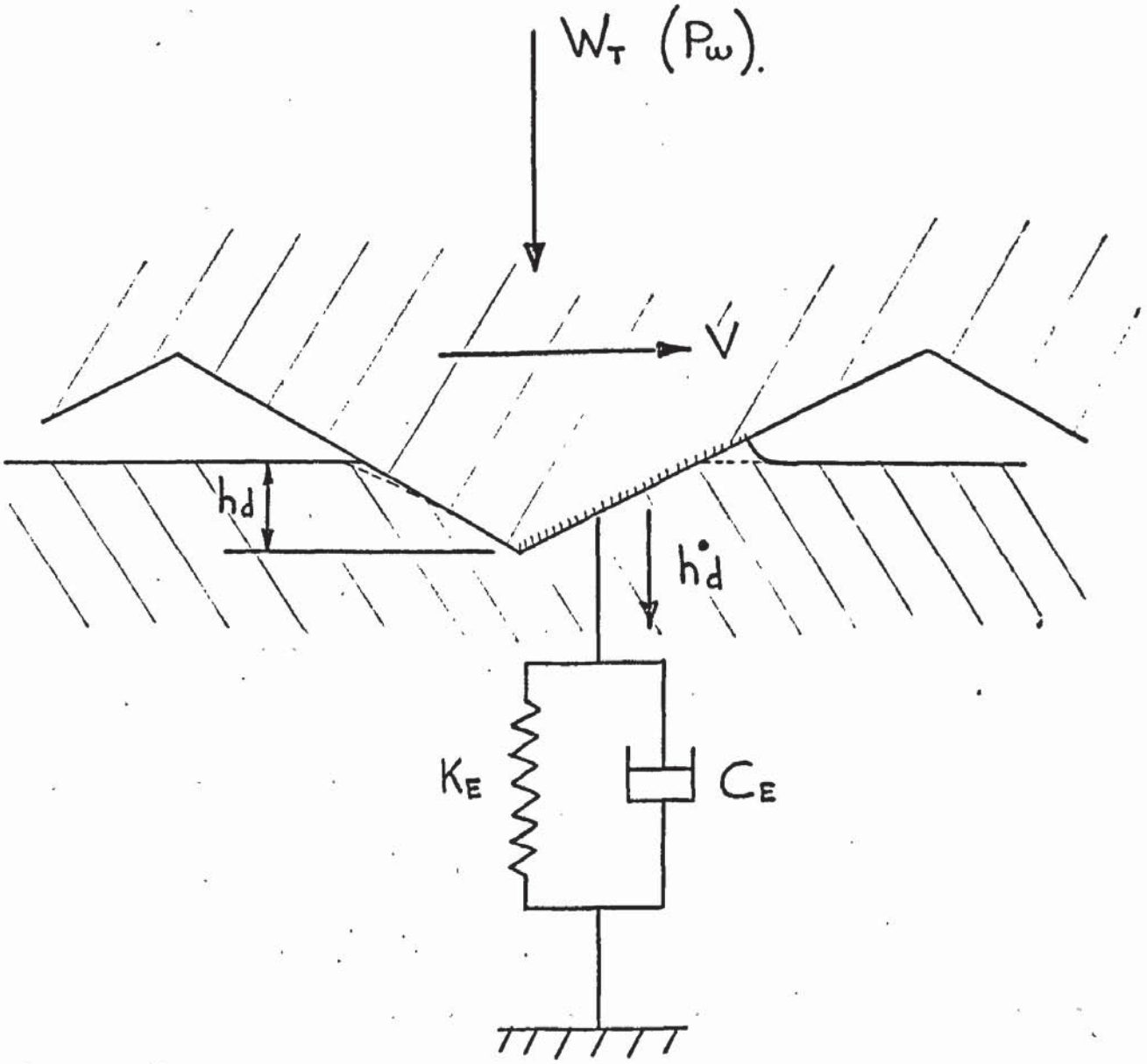

FIG. 7·15. ASPERITY INTERACTION IN TERMS OF A SIMPLE VOIGT MODEL.

Substituting this identity into eqn. 103-7 we obtain,

$$Pw = \left[1.46(hd)^{3.55} \times 10^4\right].hd + \left[U_A \cdot 1.32(hd)^{2.7}\right].2Tan\Theta.V \quad - 106.7$$

3) As it is assumed that hd will decrease with increasing sliding velocity it follows that,

a) K_E will reduce and,

b) C_E will also decrease in value.

4) Had the equation been linear, an associated time constant could have been formed, being the ratio of the coefficients of $\dot{hd}$ and hd. This would have happened if the actual contact area had been proportional to apparent surface pressure (Pw). The Voigt model would then have linear coefficients and the normal time constant would have the form

$$T_L = \frac{C_E}{K_E} \quad - s \quad - 107-7$$

As the equation is non-linear, a useful time constant analogy cannot be made.

If we consider eqn. 97 and 98-7, as $\dot{hd}$ reduces so does $\dot{K}_E$ and so must the "effective" Pw. The rate at which Pw reduces must be greater than that of hd. For some velocity V let hd reduce to hdv and eqn. 97-7 becomes,

$$\text{"effective" } Pw = 1.46\,(hdv)^{4.55} \quad - 108-7$$

By considering the α term described earlier in this section (eqn.93-7) the above relationship can be rewritten as,

$$\frac{Pw}{\alpha} = 1.46\,(hdv)^{4.55} \quad - 109-7$$

Therefore α has the effect of attenuating the value of Pw as one surface slides over the other.

For a value hdv, eqn. 98-7 can be expressed as,

$$K_{EV} = 1.46\,(hdv)^{3.55} \times 10^4 \quad - 110-7$$

If eqn. 97-7 is divided by eqn. 109-7 then,

$$\alpha = \left(\frac{hd}{hdv}\right)^{4.55} \quad - 111-7$$

and by dividing eqn. 110-7 by eqn. 98-7 then,

$$\frac{K_{EV}}{K_E} = \left(\frac{hdv}{hd}\right)^{3.55} \quad - 112-7$$

Substituting eqn. 112-7 into eqn. 111-7 a relationship between the model normal "stiffness" ratio and α can be established thus,

$$\propto = \left(\frac{K_E}{K_{EV}}\right)^{1.28} \qquad - 113\text{-}7$$

From a dry friction point of view, it has been shown by several researchers (e.g. Dolbey (77)) that as the velocity increases the coefficient of friction falls to some constant level. The speed required to reach this condition is quite small, typically 0.5 - 1.5 cm/s for machine tool slideways. This means that at some velocity (V_{CL}) the friction force will just reach the lower level and the above model analysis indicates that this is the consequence of a reduction in the contact area. Therefore at velocity (V_{CL}) the surface penetration has also reached a new reduced value of hdv which may be considered as being constant for small increases in velocity above this value.

In order to obtain some numerical data for a friction-velocity curve to be constructed, some model assumptions have to be made. Following the ideas postulated by Akhamatov (104), let the yield stress at the interface increase with sliding speed from 132 kgf/mm^2 to a maximum of 220 kgf/mm^2, this is numerically the same as the Brinell hardness number for grade 17 cast iron. It is also assumed that this stress is operating over the entire leading edge area at velocity (V_{CL}), thus the contact area will be,

$$A_{CLV} = \frac{P_W}{220} \ -mm^2 \qquad - 114\text{-}7$$

As the load per unit area is 0.65 kgf then at V_{CL}

$$A_{CLV} = \frac{0.65}{220} \times 10^6 = 2950 \ \mu m^2$$

Using eqn. 96-7 then,

$$hdv = 0.663 \ \mu m$$

This value of surface penetration is that reached at velocity V_{CL} and the corresponding friction force will be (eqn. 57-7)

$$F_V = (A_{CLV}) . S_S + W_T . \tan \Theta \qquad - 115\text{-}7$$

and as

$$\mu_K = \frac{F_V}{W_T} \qquad - 116\text{-}7$$

at velocity V_{CL} , μ_K will have the value of 0.185. (The static coeffieient for this model is $\mu_S = 0.373$).

Substituting the value for hdv, from above, into eqn. 106-7,

$$P_W = 0.227 + 0.874 \ U_A . \tan \Theta . V$$

It is clear from this equation that to maintain Pw, at velocities above V_{CL}, then the value of $U_A.\tan\Theta.V$ must become a constant. As we are only interested in the falling friction characteristic, then the relationship between V and U_A is of little consequence once the steady value of μ_K is reached. Nevertheless it is suggested that either,

a) The value of U_A alone, reduces with increased velocity,

or

b) Both U_A and Tan Θ reduce due to some complex process of asperity deformation. It is likely that, at high sliding speeds, the thermal effects (e.g. softening of surface material) will change the model parameters in such a way as to give rise to an increase in the friction coefficient.

The author is of the opinion that the use of a coefficient such as α (mentioned previously, eqn. 93-7), would be most useful in any further work since the non-linear equations can then be used to good effect. It is interesting to note that as α increases the effective material modulus increases, but the expression in eqn. 113-7 indicates that the model normal "stiffness" K_{EV} will reduce.

The magnitude of α can be established using eqn. 111-7 since,

at zero velocity hd = 0.84 μm and α = 1,

at velocity V_{CL} hdv = 0.663 μm and α will be 2.9

As α changes between two values as the velocity increases from zero to V_{CL} then the expression for α can be written in the form of a first order transfer function thus,

$$\alpha = \frac{(1 + 2.9\ Ts)}{(1 + Ts)} \qquad - 117\text{-}7$$

This equation is based upon the work of D.F.Moore (106) who analysed the behaviour of viscoelastic materials using linear spring/dashpot models.

Equation 117-7 is expressed in terms of the Laplace operator, the coefficient T is the equation time constant and in the terminology of the sliding surface model becomes,

$$T = \frac{Um}{(\alpha - 1).Eo} \quad - \text{seconds} \qquad - 118\text{-}7$$

The term Um describes the "dynamic viscosity" of the bulk cast iron material. It has proved difficult to establish a value for this coefficient. As J.Gilman (107) points out, its magnitude could be wide-ranging and will depend upon such factors as intermolecular bonding, types

of molecular structure present in the material, temperature and the rate of the atomic dislocations.

The denominator of eqn. 118-7 expresses the increase in the material modulus above its original value and the magnitude of E_v is expressed as,

$$Ev = (\alpha - 1).E_o + E_o = \alpha.E_o$$

which corresponds to the relationship shown in eqn. 93-7

If the Laplace term "s" in eqn. 117-7 is replaced by the complex notation $j\omega$ the subsequent rationalised equation will be,

$$\alpha = \left[\left| \frac{1 + 2.9.(T\omega)^2}{1 + (T\omega)^2} + j. \frac{1.9.T\omega}{1 + (T\omega)^2} \right|\right] \quad - 119\text{-}7$$

In control theory analysis ω is a frequency applied to the system. Although, in this model, ω is not a sinusoidal variation and a frequency of deformation is not strictly true, since the asperities may experience deformation only once in the sliding operation, it is convenient to use such a concept in order to solve the equation.

The value of ω is related to the sliding velocity such that,

$$\omega = \frac{V}{L} \quad - 120\text{-}7$$

where L is a characteristic length, lying in the direction of motion and related to the leading edge contact area A_{cL}

This area is the sum of all the asperities in a single crossed range which are in contact. These individual areas will be similar in shape when viewed normal to the surface, and it is assumed that their combined area can be expressed as having the same shape. The required length characteristic can be taken as,

$$L = (A_{cL})^{0.5} \quad - 121\text{-}7$$

It is clear that as V increases the contact area will reduce, due to changes in hd and so will the value of L.

A plot of α against ω is shown in Fig 7.16 when Um is assumed to have a constant value of 8×10^{10} Poise or 800 kgf.s/mm^2.

The time constant will be from eqn. 118-7

$$T = \frac{800}{1.9 \times 1.32 \times 10^4} = 0.0318 \text{ seconds}$$

and from eqn. 117-7

$$\alpha = \frac{(1 + 2.9(0.0318)s)}{(1 + (0.0318)s)}$$

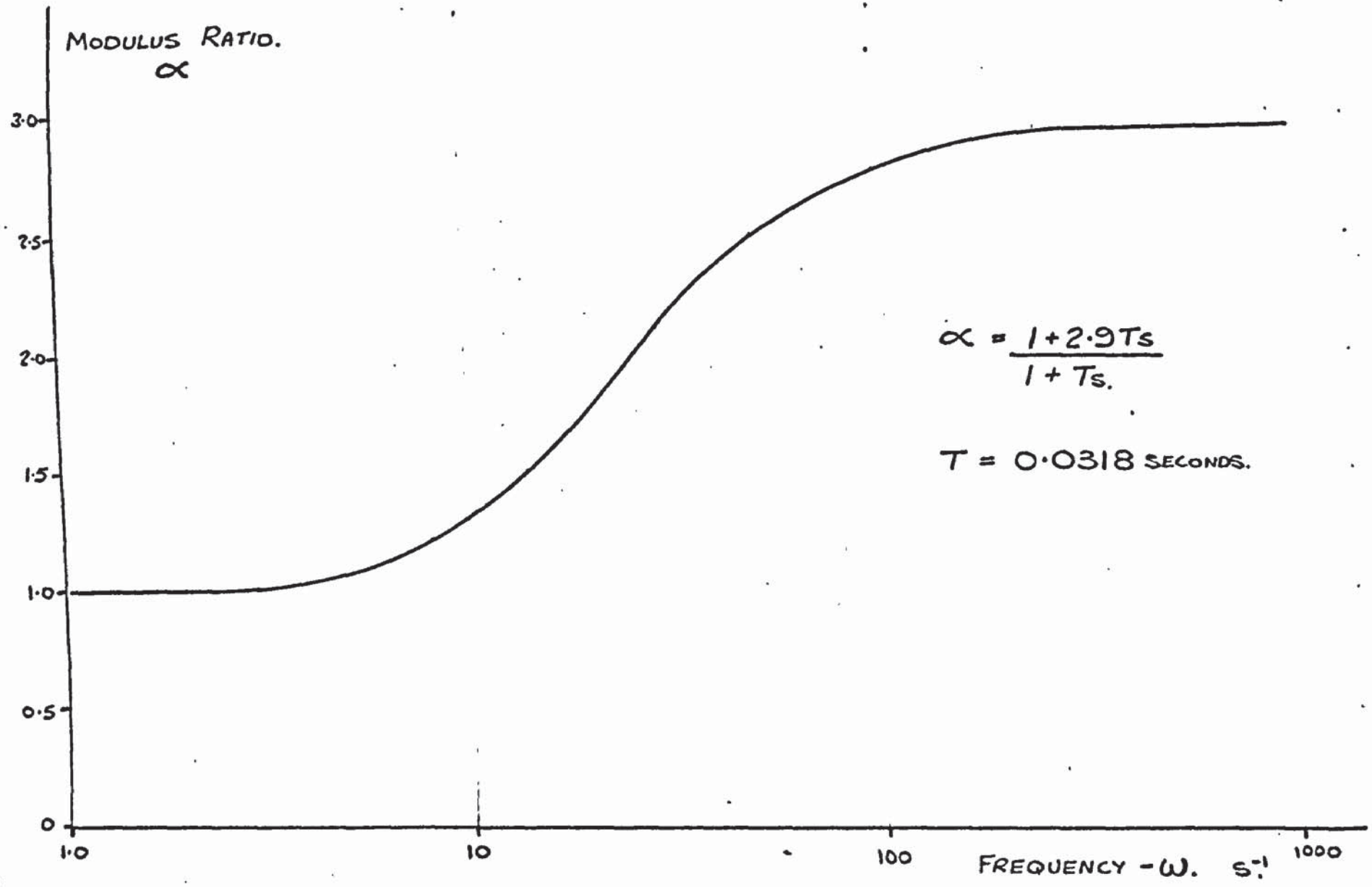

FIG. 7·16. CHANGE IN MODULUS RATIO WITH FREQUENCY.

With these values of α the contact area A_{CLV} is plotted against ω in Fig.7.17 using eqn. 92-7.

The values of sliding velocity were calculated using eqn. 120-7 and 121-7 thus,

$$V = \omega(A_{CLV})^{0.5} \quad -mm/s \qquad - 122\text{-}7$$

and Fig. 7.18 illustrates the relationship between ω and V. Fig. 7.19 indicates the changes in μ_k and h_{dv} with respect to sliding velocity V. Fig. 7.20 illustrates the changes in K_E and the magnitude of table rise (h_s) or surface separation where,

$$h_s = h_d - h_{dv} \qquad - 123\text{-}7$$

Using these results, eqn. 102-7 has been used to calculate the values of C_E for changing velocity and these are plotted against V in Fig.7.21 together with the values of U_A found from eqn. 101-7.

To obtain some correlation between K_E, C_E and α for changes in "frequency" ω, eqn. 119-7 is broken down into its real and imaginary parts.

In Fig. 7.22 K_E is plotted together with the inverse of the real part of the equation, i.e.

$$\alpha' = \frac{1 + (T\omega)^2}{1 + 2.9\ (T\omega)^2}$$

In Fig. 7.23 C_E is plotted together with the imaginary part of eqn.119-7, i.e.

$$\alpha'' = \frac{1.9\ T\omega}{1 + (T\omega)^2}$$

It can be seen that apart from scaling changes, the variation of K_E with frequency is a similar shape to the term α'. The non-linear equation for K_E has caused the divergence of the two curves at low frequencies.

The curves of C_E and α'' are also very similar in shape. The maximum value of α'' occurs when the frequency ω is equal to the value $T^{-1.0}$ but the maximum value of C_E occurs at approximately $T^{-0.78}$. It is suggested that the value of the time constant index arises from the non-linear relationship between the actual contact area and the associated load per unit area.

It would appear that the transfer function for α (eqn. 117-7) can be rationalised in its complex form to produce a real part $(\frac{1}{\alpha'})$ and an imaginary part (α'') identifiable with this surface model parameters, K_E and C_E.

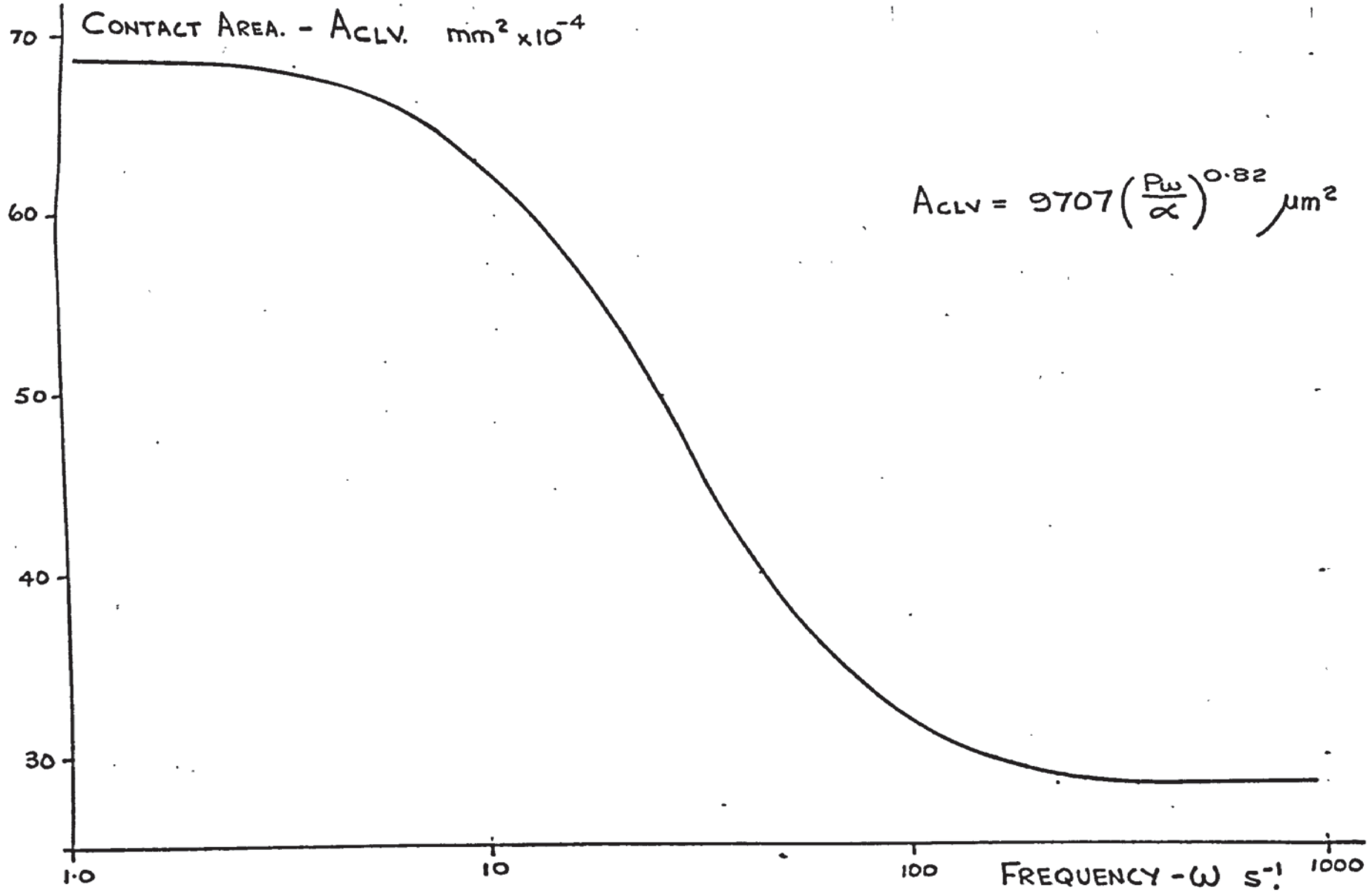

FIG. 7·17. CHANGES IN CONTACT AREA WITH FREQUENCY.

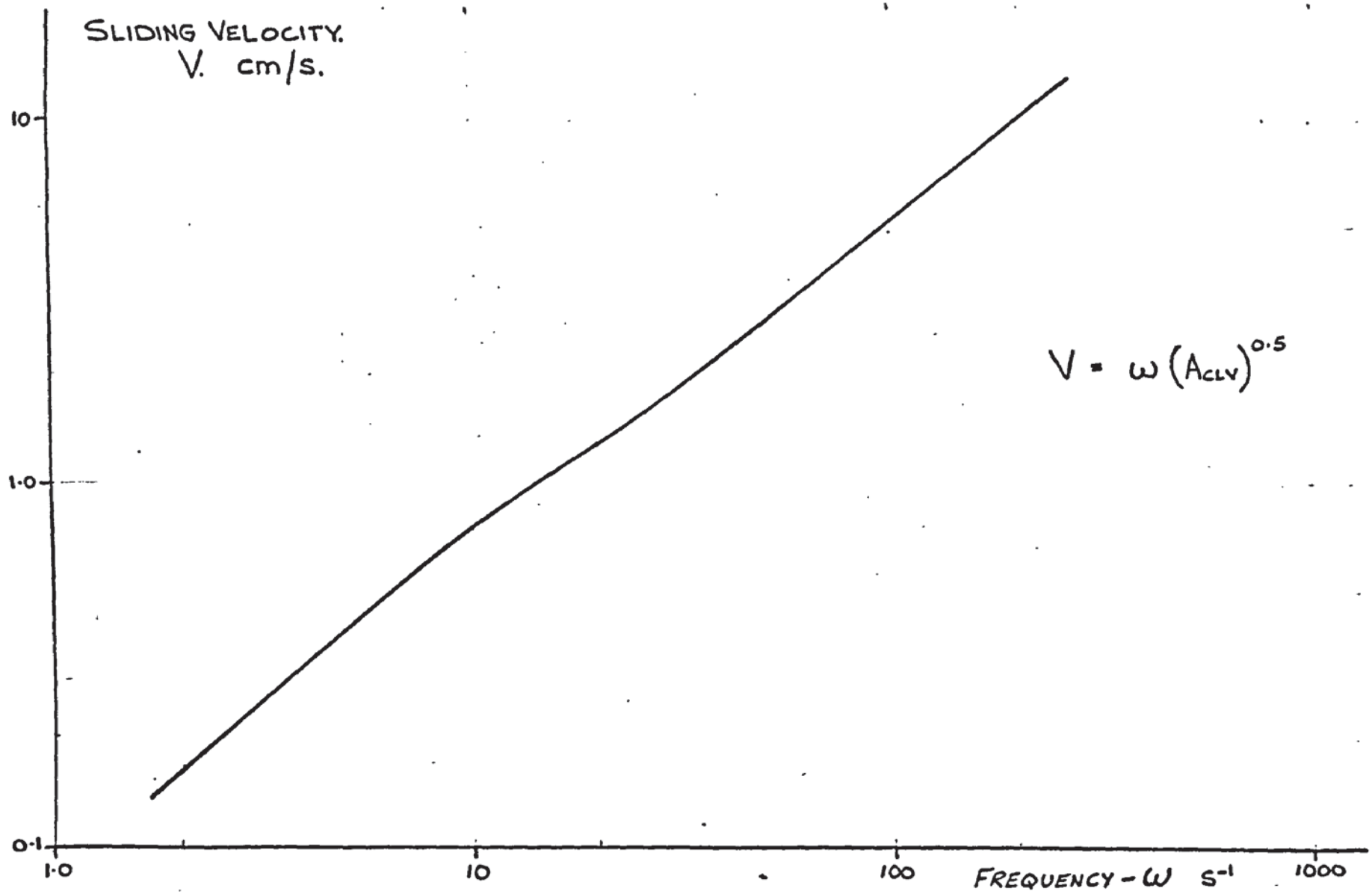

FIG. 7·18. RELATIONSHIP BETWEEN SLIDING VELOCITY AND FREQUENCY.

11'82T

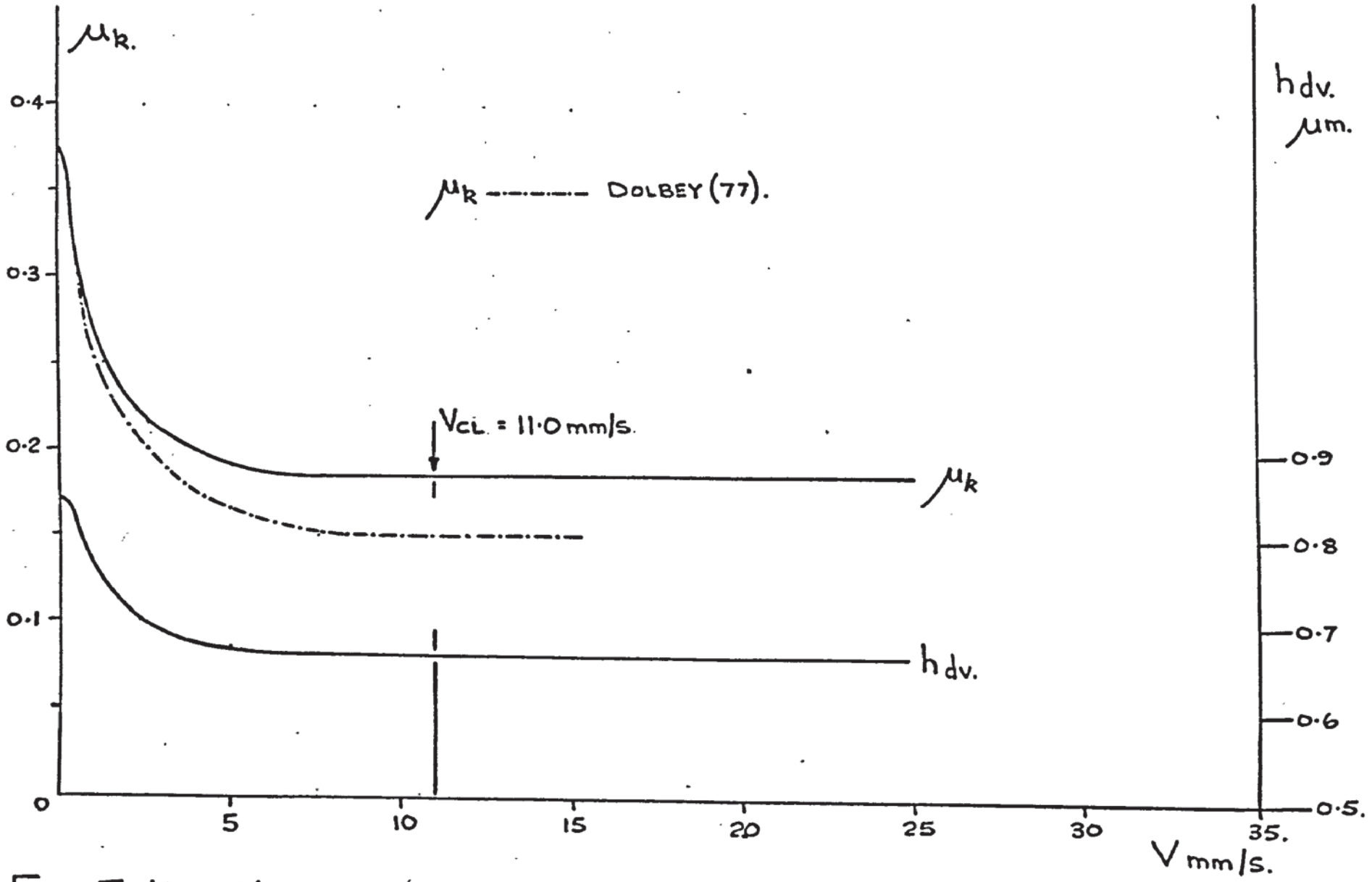

FIG. 7·19. KINETIC FRICTION COEFFICIENT AND PENETRATION LEVEL. - DRY SLIDING CONDITION.

128.III.

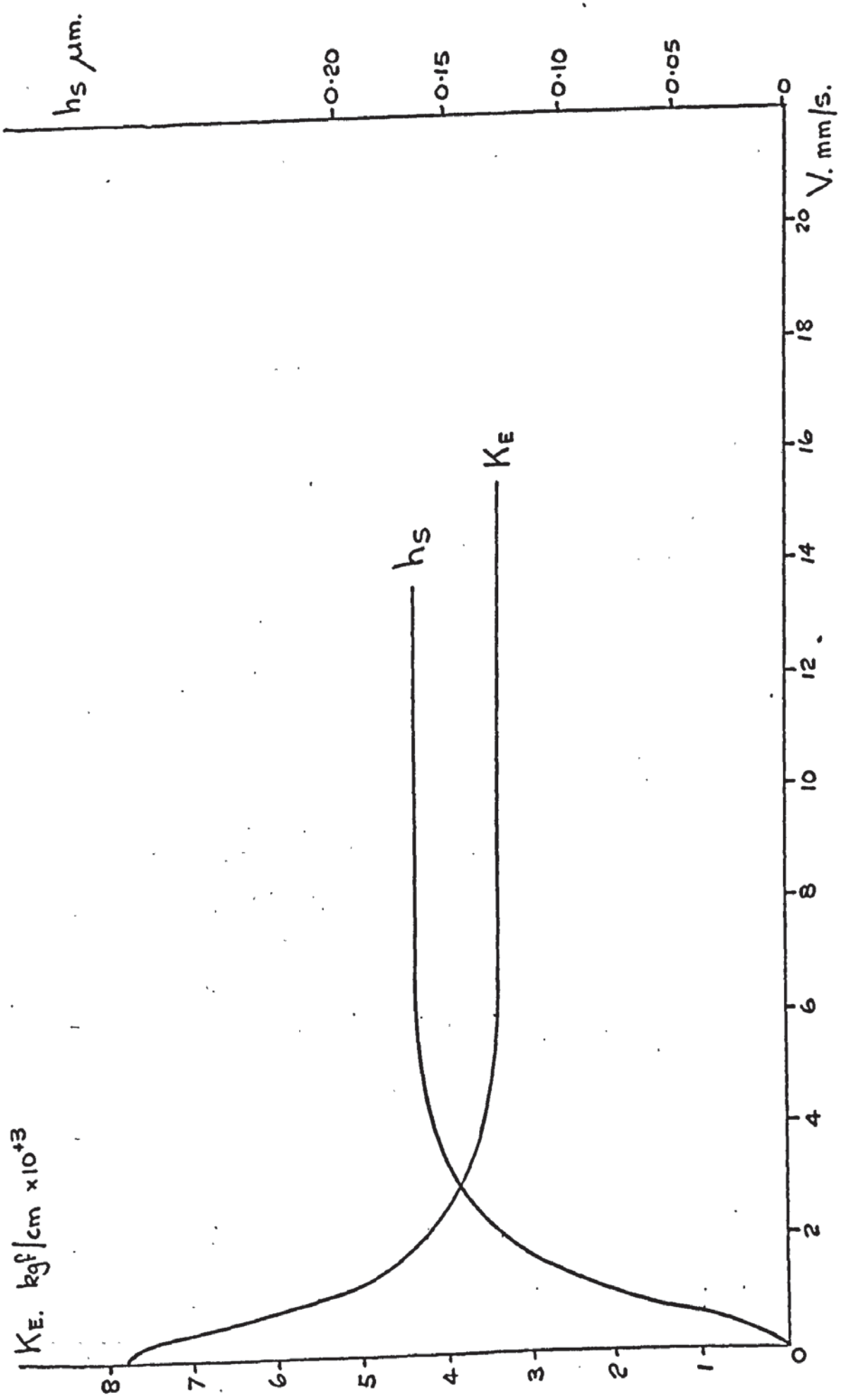

FIG. 7.20. SURFACE SEPARATION AND K_E FOR CHANGES IN SLIDING VELOCITY. - DRY CONDITION.

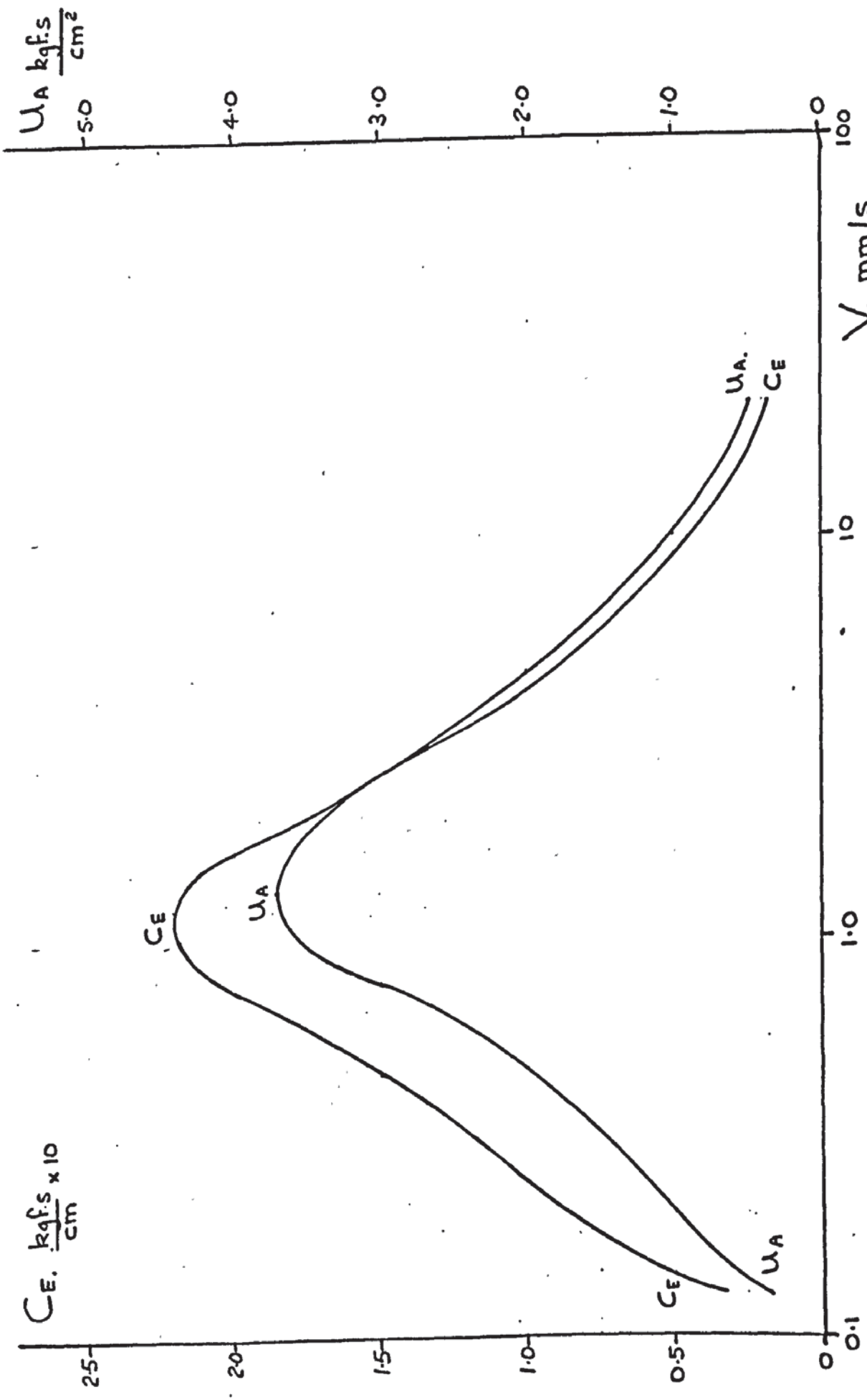

FIG. 7.21. VARIATIONS IN C_E AND U_A FOR CHANGES IN VELOCITY.

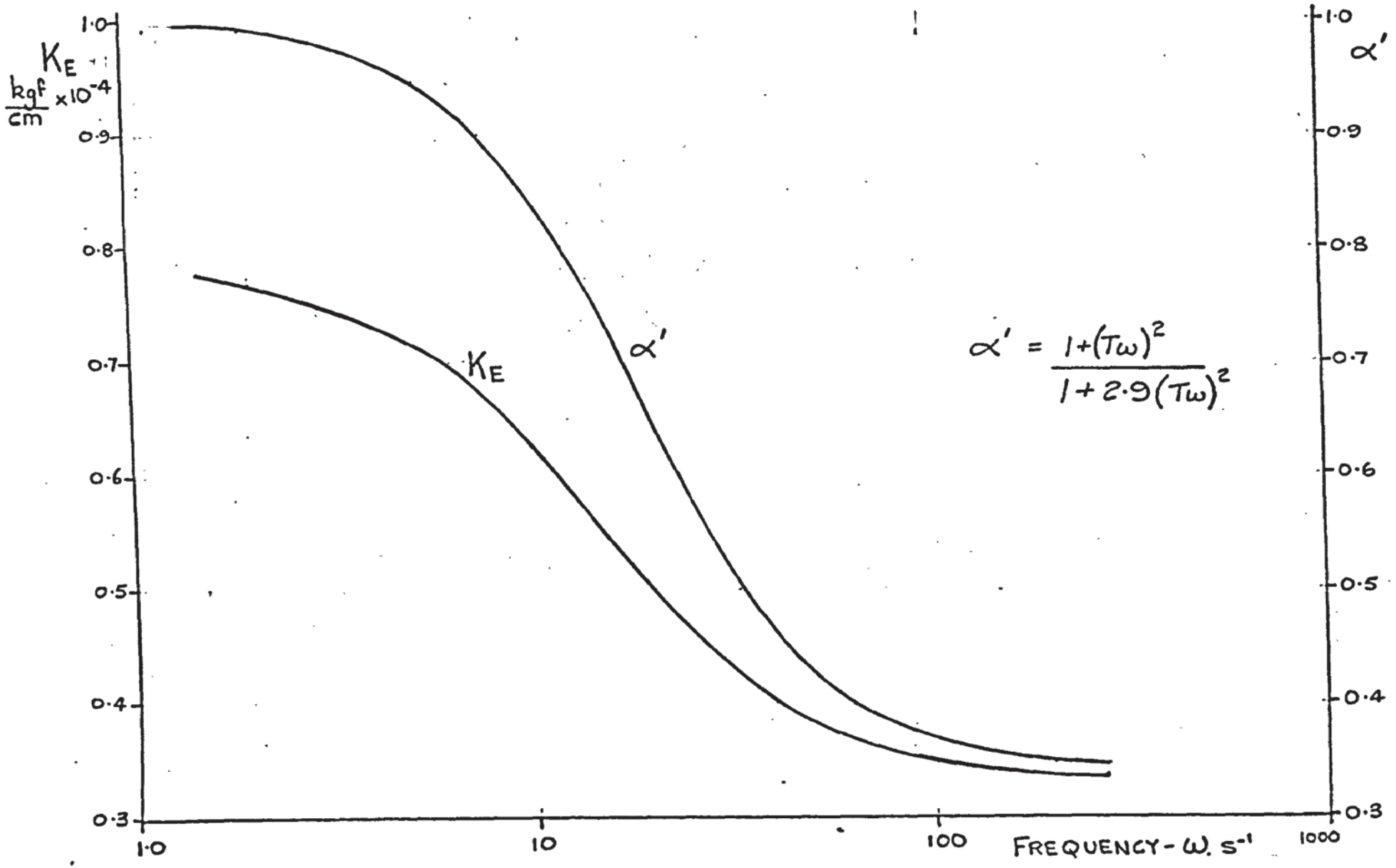

FIG. 7·22. CHANGES IN K_E AND α' WITH FREQUENCY.

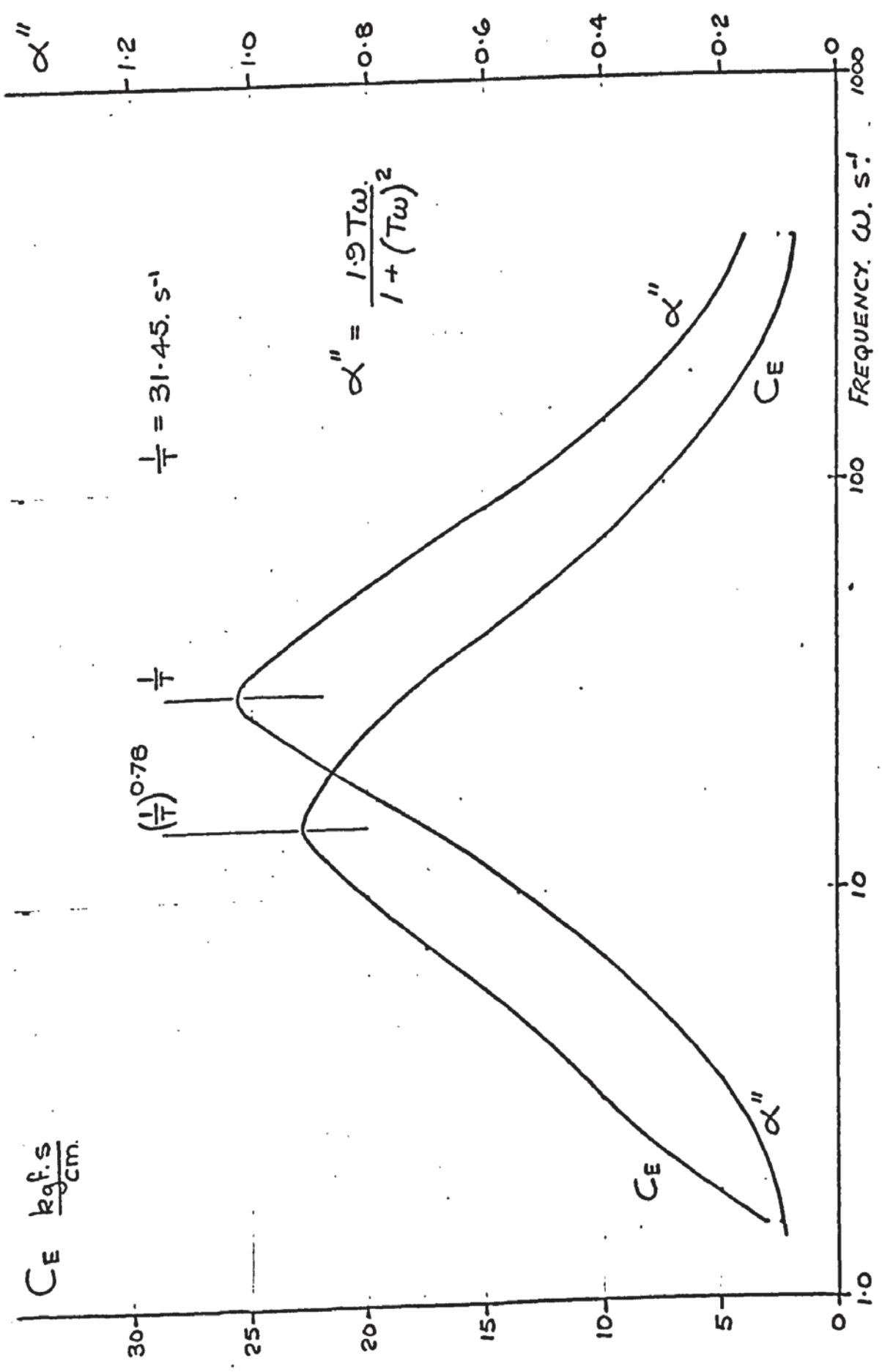

FIG. 7.23. CHANGES IN C_E AND α'' WITH FREQUENCY.

In Moore's (106) analysis the treatment is purely linear but his simple model approach does describe the likely changes in system parameters. It is felt that a more detailed discussion on his method is not required here although the concept may provide an avenue for further study. One initial modification for closer comparison could be to divide the terms of eqn. 102.7 by the actual contact area A_{CLV} in order to obtain a pressure equation instead of the force equation used here. This would tend to linearise the equation and may make his techniques more applicable.

The use of the α term in illustrating the change in contact area with sliding speed does give results similar to those obtained experimentally. The value of h_{dv} reduces as sliding speed increases as shown in Fig.7.19 and it is estimated that the value of V_{CL} would be approximately 11.0 mm/s. The calculated coefficient of friction is also illustrated and has the same characteristic shape as that obtained experimentally by researchers such as Dolbey (77), his results are also shown. A theoretical curve can be drawn to fit his experimental results and, using the model surface parameters as detailed here, this would mean changing the value of T and the maximum contact surface pressure to give a larger value of α (if μ_k were 0.15 at V_{CL} , α would be 4).

The normal stiffness per unit area, and the amount of surface separation are shown in Fig. 7.20 plotted against sliding velocity. The surface separation curve has the same shape as that found experimentally by Dolbey (77), but his curve seems to indicate that separation continues well after the lower value of μ_k has been reached. Dolbey also calculates a dynamic stiffness of his slideway. This necessitates the use of a large vibrator mounted on the sliding table and his stiffness was evaluated as the ratio of force amplitude to displacement amplitude. The resulting curve of his values plotted against sliding velocity is similar in shape to that of K_E plotted in Fig. 7.20. It is suggested that the form of his tests is illustrated by modifying equation 102-7 thus,

$$P_W + P_V \mathrm{Sin}.\omega_V t. = K_E.h_d + C_E.\dot{h}_d \qquad - \ 124\text{-}7$$

where Pv is the amplitude of vibrator force and ω_V is the frequency of Pv.

The above analysis of kinetic friction indicates that the relationship between μ and sliding velocity is complex under dry surface conditions. Fig. 7.24 is a plot of μ_k against $\frac{1}{\alpha}$ which results in the following relationship,

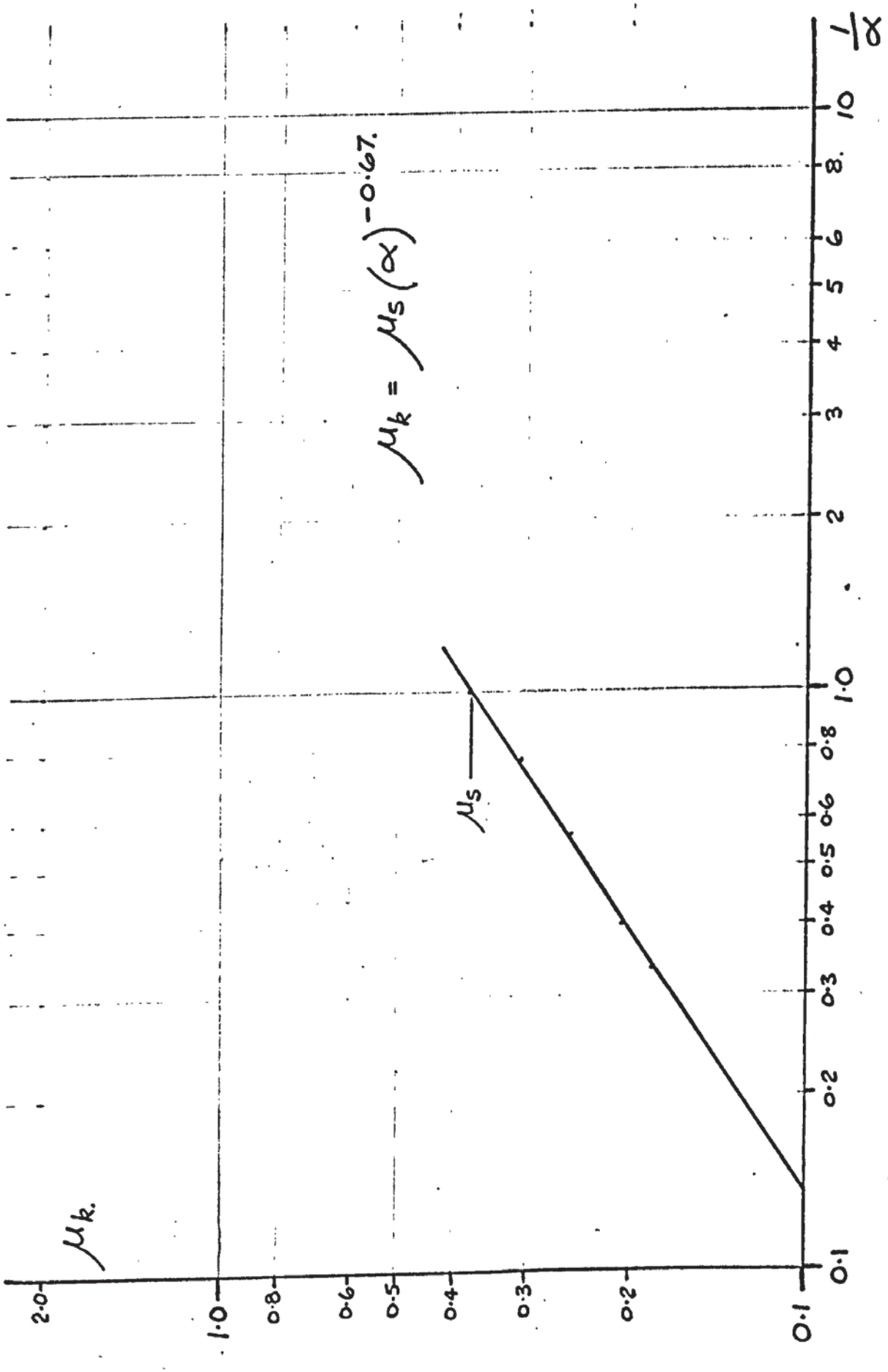

FIG. 7·24. RELATIONSHIP BETWEEN μ_k AND $1/\alpha$.

$$\mu_k = \mu_s \cdot \left[\alpha \right]^{-0.67} \quad - 125\text{-}7$$

substituting eqn. 119-7

$$\mu_k = \mu_s \cdot \left[\left| \frac{1 + 2.9\,(T\omega)^2}{1 + (T\omega)^2} + j \cdot \frac{1.9\,T\omega}{1 + (T\omega)^2} \right| \right]^{-0.67} \quad - 126\text{-}7$$

and combining eqn. 92-7, 120-7 and 121-7, then the corresponding velocity is

$$V = \omega \cdot \left[P_w / \alpha \right]^{0.4} \times 0.00985 \text{ .-cm/s} \quad - 127\text{-}7$$

If eqn. 126 and 127-7 are restated in terms of Pw and, if the maximum pressure across the contact area is denoted by P_x then, at velocity Vcl

$$A_{CLV} = \frac{Pw}{Px} \text{ - mm}^2 \quad - 128\text{-}7$$

and using equations 96-7 and 111-7,

$$\alpha = \frac{0.00335\,(P_x)^{1.23}}{(Pw)^{0.22}} \quad - 129\text{-}7$$

Substituting this α quantity into 126-7 together with eqn. 65-7 (μ_s) then,

$$\mu_k = \left[\frac{0.35}{(Pw)^{0.165}} \right] \cdot \left[\left| \frac{1 + (T\omega)^2}{1 + (T\omega)^2} + j \cdot \frac{(\alpha - 1)T\omega}{1 + (T\omega)^2} \right| \right]^{-0.67} \quad - 130\text{-}7$$

If the maximum value of α is still unity at Vcl then from equation 129-7 there will be a maximum for Pw thus,

$$Pw(max) = \left[0.00335 (Px)^{1.23} \right]^{4.55} \text{ kgf.} \quad - 131\text{-}7$$

If Px is 220 kgf/mm^2 then Pw(max) is approximately 70 kgf which would act on every cm^2 of apparent area. Although this value is unacceptably large, the fact that α will then remain at unity means that the coefficient of friction will remain constant, i.e. $\mu_s = \mu_k$ and in this case the value will be approximately 0.17.

In order to fix a value for Vcl , the following equation is suggested, from eqn. 127-7,

$$V_{CL} = \frac{8}{T} \left[\frac{Pw}{\alpha} \right]^{0.4} \times 0.00985 \quad - 132\text{-}7$$

where $\frac{8}{T}$ is the frequency ω which is 3 octaves above the highest corner frequency $\left(\frac{1}{T}\right)$ in the transfer function for α (eqn. 117-7).

It is not particularly clear from eqn. 130 and 132-7 how μ_k will change with sliding velocity for various values of Pw. In Fig.7.25 four such curves are sketched for reasonable values of Pw, using the model data. At velocity Vcl eqn. 130-7 can be rewritten with the substitution of eqn. 129-7, as

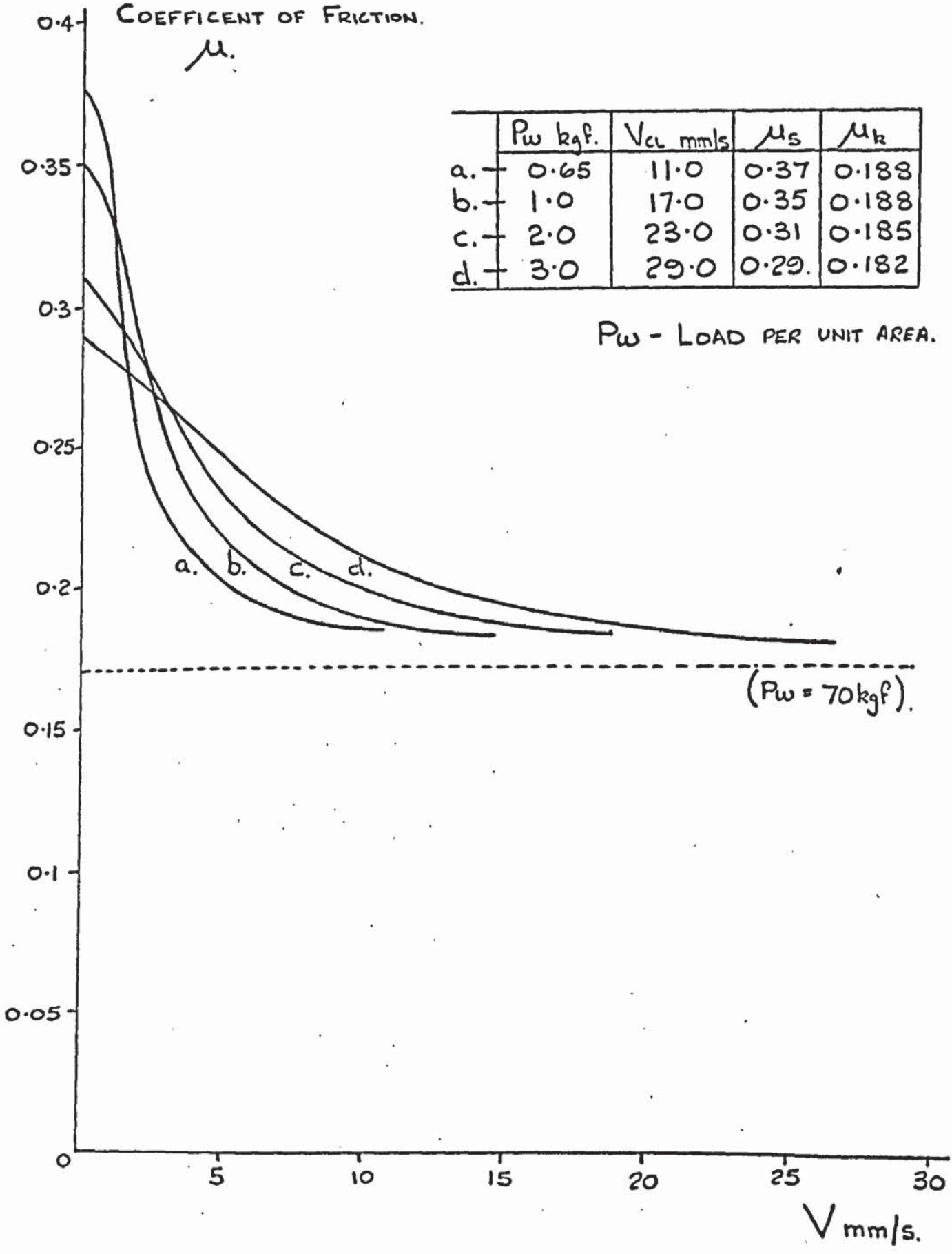

	P_w kgf.	V_{cl} mm/s	μ_s	μ_k
a.	0·65	11·0	0·37	0·188
b.	1·0	17·0	0·35	0·188
c.	2·0	23·0	0·31	0·185
d.	3·0	29·0	0·29.	0·182

P_w - LOAD PER UNIT AREA.

FIG. 7·25. MODEL FRICTION CHARACTERISTICS.
FOR VARIOUS LOADS. - DRY CONDITIONS.

$$\mu_k = \left[\frac{0.35}{(Pw)^{0.165}}\right]\left[\frac{0.00335(Px)^{1.23}}{(Pw)^{0.22}}\right]^{0.67} \quad - 133\text{-}7$$

$$\text{thus } \mu_k = \frac{(\text{Constant})}{(Pw)^{0.018}} \quad - 134\text{-}7$$

Therefore at V_{CL} the value of μ_k varies by only a very small amount, but does reduce as Pw is increased. This equation can be compared with that for μ_s (eqn.67-7) where this value varies as $(Pw)^{-0.165}$. This indicates that, for this model, the static coefficient may change substantially with Pw but the minimum value for μ_k will be practically the same in all cases.

Finally, it is unfortunate that a surface time constant cannot be specified as a fixed value for the surface model expressed by eqn.107-7. As K_E and C_E vary with velocity the calculations of a 'relative' time constant indicate that they will range from 0.00039s to 0.0044s. Therefore under dry conditions there will be a small lag between a rapid change in velocity and the corresponding change in friction.

The fact that there will be a lag means that for continually changing velocities, the corresponding 'dynamic' friction values will not be equal to their steady state values as calculated from eqns. 126 and 127-7. This observation is borne out by the experimental work of Bell et al(46) during stick-slip conditions on a slideway system.

7.3.ii. LUBRICATED CAST IRON SURFACES.

When a lubricant is applied to the contacting surfaces the friction force reduces in both the static and kinetic conditions. In machine tool applications it is usual to find a minimum friction value is obtained at some low sliding velocity, followed by a slow rise with further increases in speed.

In section (7.2 ii) of this chapter it was suggested how the lubricant brought about changes in the static friction. When the surfaces are moving relative to each other the fluid lubricant may give rise to an increased lifting action, eventually causing complete "solid" separation. To achieve this the lubricant film must be capable of supporting the load by remaining between the two surfaces.

It is worth noting at this point, some observations made by previous researchers.

1) The orientation of the molecules must favour an increase in the boundary viscosity during flow around the surface micro profiles - Akhmatov (104)

2) The parameters affecting friction at low velocities include, (108)
   a) Physical nature and properties of the surfaces.
   b) Structure and physicochemical properties of the lubricant molecules.
   c) Nature of the adsorptional adaptations of the lubricant molecules.
   d) Interface pressures.
   e) Effective thickness of lubricant film.
   f) Sliding velocity.

3) The surface roughness affects the friction of a lubricated sliding pair. The surface topography may increase or decrease the frictional properties compared with a bearing having smooth surfaces - Christensen(108)

4) In boundary friction conditions the bulk viscosity of the lubricant is not so important. Its molecular structure and properties are the prime factors influencing this complex process. Akhmatov (104)

Both these researchers realise the interactive effect of both the surface topography and the nature of the lubricant film.

It is easier to visualise the friction force as being composed of two separate quantities,

$$F = \left[\text{Solid friction due to metallic contact}\right] + \left[\begin{array}{l}\text{lubricant friction}\\ \text{due to fluid shear}\end{array}\right]$$

- 135-7

The solid friction is influenced by the degree of support given by the lubricant and, as importantly, the lubricant friction may be affected by the surface asperities causing redistribution of the lubricant over the profile giving rise to accumulations of any polar additives in surface hollows.

In order to arrive at some relationship between friction and velocity the following analysis has been attempted in the context of the above equation. Due to a lack of information regarding lubricant physicochemical behaviour during conditions of metallic contact the linear laws developed by Reynolds (97) have been used with several modifications, in particular his equation governing the pressure generated by a lubricant between two solid surfaces,

$$P_L = \frac{6.\mathcal{L}.V.\ell.Kp}{[H]^2} \qquad - 136\text{-}7$$

This is the hydrodynamic equation for two smooth surfaces. The constant Kp is dependent upon the geometry of the wedge formed between the surfaces. Because of the nature of the model surface topography a film thickness $[H]$ is difficult to visualise.

If we consider two pairs of asperity ridges crossing at right angles and just in contact as shown in Fig. 7.26, then the equivalent free space between two ridges in Fig. 7.26(a) will be

$$\text{area} = \frac{(\ell - B) \times (100\ h_T)}{2} + \frac{(2\ell - B)}{2} \times \left(\frac{Z}{2}\right) \qquad - 137\text{-}7$$

$$\text{area} = 27440\ \mu m^2$$

The effective "constant" height over length ℓ between ridges will be,

$$h_e = \frac{\text{area}}{\ell} = 2.74\ \mu m. \qquad - 138\text{-}7$$

This same height can be calculated for Fig. 7.26b whose area is at right angles to the other, thus the total equivalent height in an area $\ell \times \ell$ will be

$$2.h_e = 5.48\ \mu m. \qquad - 139\text{-}7$$

If the penetration level is h_d at rest then the minimum equivalent height will be

$$Ho = 2he - hd = 4.64\ \mu m \qquad - 140\text{-}7$$

In the hydrodynamic conditions applicable to eqn. 136-7 the "wedge" profile shown in Fig. 7.27 is assumed.

The quantity H_1 is made up of H plus an additional height gained over length ℓ, which in this asperity configuration will be $100.h_T$ $(3\mu m)$.

It is suggested that when asperity ridges cross at 90° the maximum lifting conditions will prevail and as this angle reduces H_1 will also reduce. Let m relate H to H_1 such that

$$m = \frac{H_1}{H} - 1 = \frac{(H + 3)}{H} - 1 \qquad - 141\text{-}7$$

The coefficient Kp is related to H through parameter m, a hydrodynamic variable. From Fuller (97),

$$Kp = \left[\frac{1}{m^2}.\log_e (1 + m) - \frac{2}{m(2 + m)}\right] \qquad - 142\text{-}7$$

It has been assumed that when the asperities have just lost contact the pressure generated by the oil will be equal to the load per unit area(Pw).

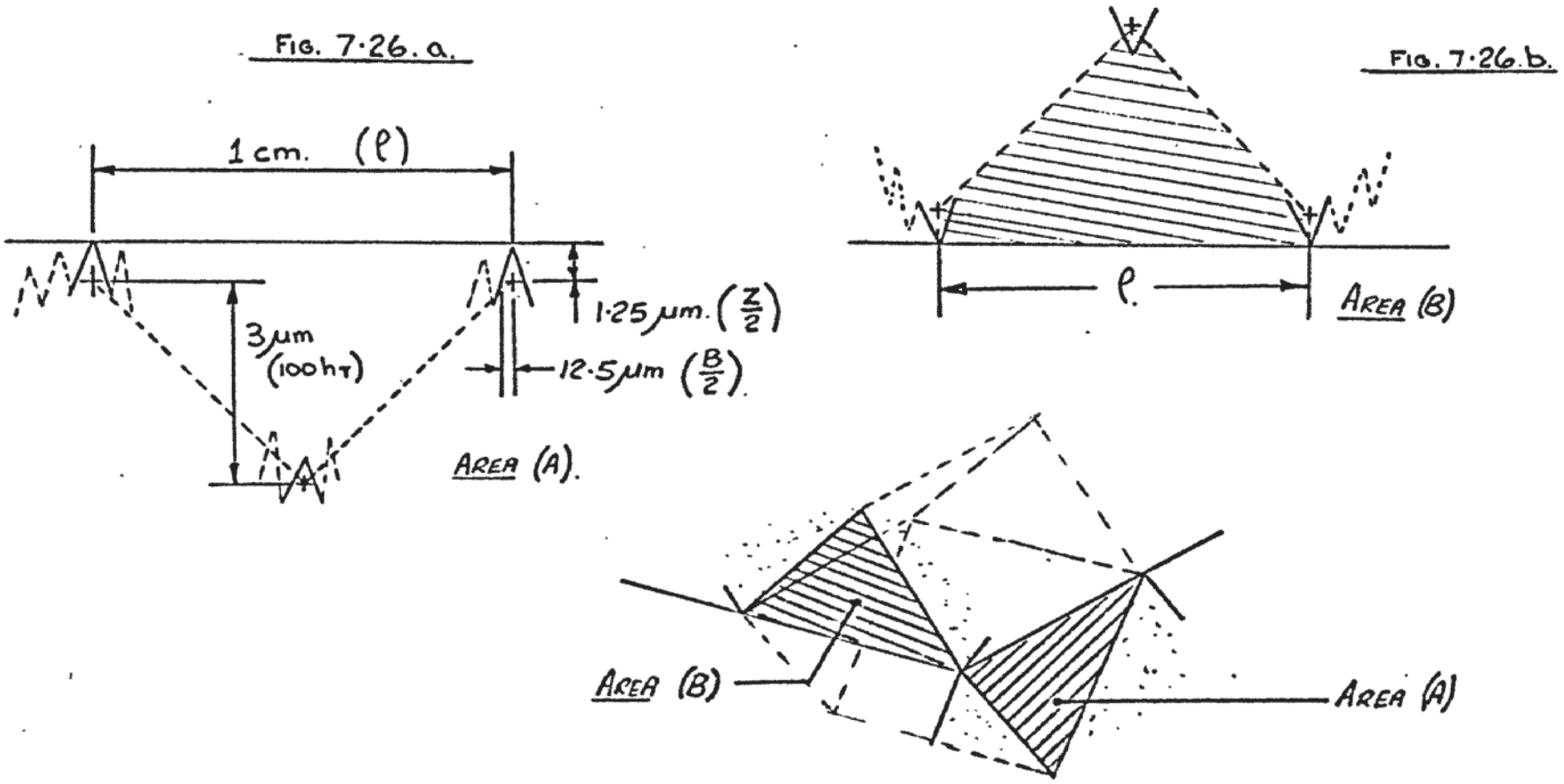

Fig. 7·26. Two Ridge Pairs, just in contact - showing free space available.

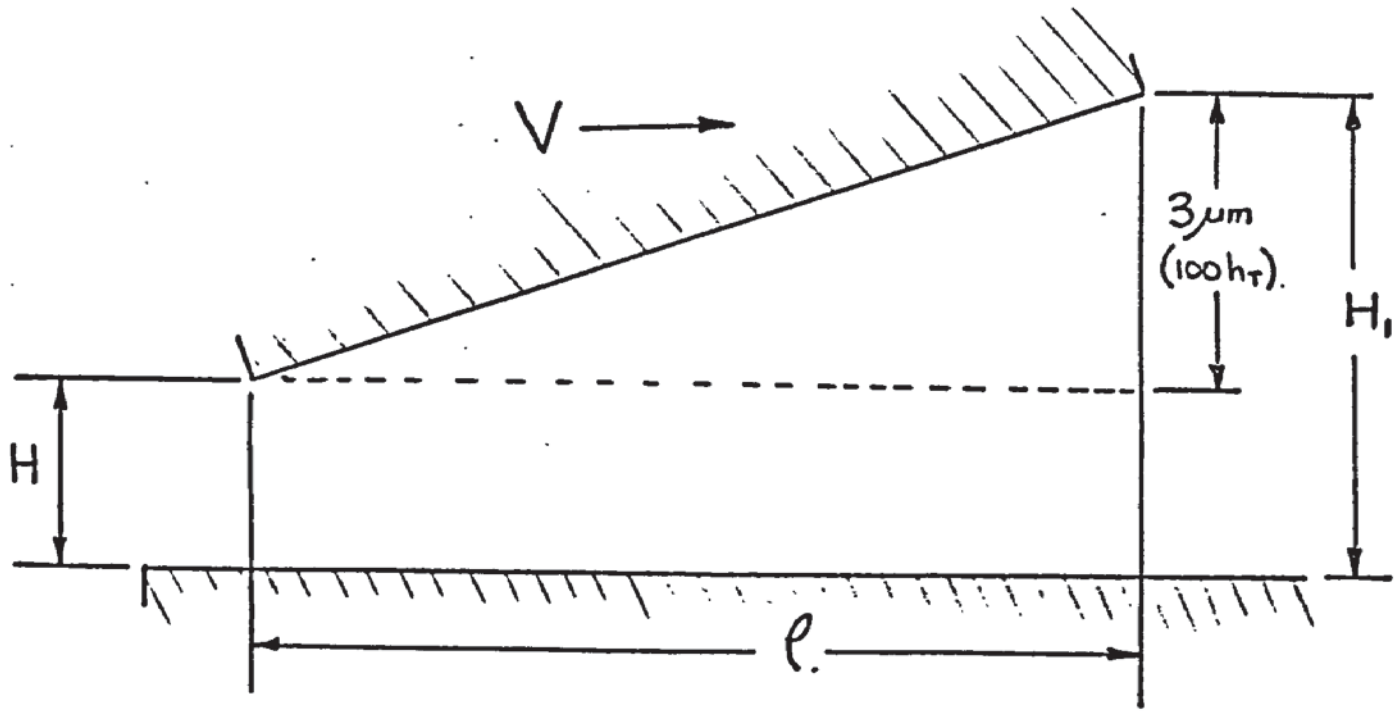

FIG. 7·27. A HYDRODYNAMIC WEDGE PROFILE - FOR MODEL SURFACE.

Using eqn. 136-7 in this condition,

$$Pw = \frac{6.\zeta.Vc_L.\ell.Kp}{\left[H\right]^2} \qquad - \quad 143\text{-}7$$

where $H = Ho + hd$

Using data presented by Dolbey as being reasonable for this model surface, then for his two oils, both with and without polar additives, the following average values apply,

Oil (1) ζ = 0.74 Poise
Vc_L = 5 cm/s

Oil (2) ζ = 5.9 Poise
Vc_L = 2.2 cm/s

Pw is 0.65 kgf/cm^2 and the value of Kp for both oils was calculated. However, it was found that these were not the same values as those calculated using the appropriate value of (m) (eqn. 142-7).

The value of ℓ in eqn. 143-7 was 1 cm, the distance between ridge asperities and it was decided to replace the term Kp by Ks, i.e.

$$Ks = \ell.Kp \qquad - \quad 144\text{-}7$$

and in this case it would have the same value as Kp. It was considered that the quantity ℓ represents a unit surface distance and that for every displacement ℓ along the surface, in the direction of sliding, the contact profile would be repeated.

Equation 143-7 is rewritten as,

$$Pw = \frac{6.\zeta.Vc_L.Ks}{\left[H\right]^2} \qquad - \quad 145\text{-}7$$

and because this equation was not satisfied a correction factor (Cv) was introduced thus,

$$Pw = \frac{6.\zeta.Vc_L.Ks}{\left[H\right]^2.Cv} \qquad - \quad 146\text{-}7$$

To establish an equation for Cv another value of H was required with its corresponding value of velocity. Again using Dolbey's (77) results, this time selecting a velocity (10 cm/s) well into the apparent hydrodynamic region, Ks could be calculated from Eqn. 146-7 and using eqn. 142-7 also.

It was decided to adopt a linear relationship between Cv and velocity V and the following relationship was established.

For Oil (1) $Cv = 1.6 + 0.14V$ - 147-7

For Oil (2) $Cv = 7.4 + 0.64V$ - 148-7

In order to ease calculations two further relationships were established. These were,

i) a relationship between $\left(\frac{V}{Cv}\right)$ and V

ii) a relationship between Ks and H

Using eqn. 147 and 148-7 the following eqns. were found relating $\left(\frac{V}{Cv}\right)$ to V

For Oil (1) $\left(\frac{V}{Cv}\right) = 0.79(V)^{0.624}$ - 149-7

For Oil (2) $\left(\frac{V}{Cv}\right) = 0.145(V)^{0.7}$ - 150-7

It should be noted that this relationship was very good for the range between the two velocities selected for each oil, but it will be used in the analysis for sliding velocities from zero to 10 cm/s. The relationship between Ks and H is shown in Fig. 7.28 giving the following equation,

$$Ks = \frac{0.05}{(H)^{0.478}} \qquad (H \text{ in } \mu m) \qquad - 151\text{-}7$$

Thus if we start with the general equation for P_L (eqn.136-7) this becomes,

$$P_L = \frac{6.\eta.V.Ks}{(H)^2 Cv.} \times 100 \qquad - 152\text{-}7$$

where η is in Poise and H is in μm.

Eqns. 149, 150 and 151-7 can be substituted giving the final relationships for both oils,

Oil (1) $\eta = 0.74P$ $\quad P_L = \frac{23.89.\eta.V^{0.624}}{(H)^{2.478}}$ - 153-7

Oil (2) $\eta = 5.9P$ $\quad P_L = \frac{4.38.\eta.V^{0.7}}{(H)^{2.478}}$ - 154-7

In this way the pressure developed by the lubricant between the model surfaces is expressed in terms of only two variables for each oil, V and H.

During these calculations it was decided to leave the lubricant viscosity as an independent parameter and not relate it to other variables. Substituting Ks alone into eqn. 152-7 then,

$$P_L = \frac{30.\eta.V.}{(H)^{2.478} Cv} \qquad - 155\text{-}7$$

This equation remains sensibly the hydrodynamic equation but eqns. 153 and 154-7 both show how Cv has made significant changes. It is likely that Cv is not only a function of viscosity but also of the physicochemical properties of the lubricant molecules.

As one surface slides over the other some of the load is taken by the oil film and the remainder by the contacting asperities. If we consider eqn. 102-7 in conjunction with eqns. 153 or 154-7 then the distribution of load per unit area is expressed completely. Hence,

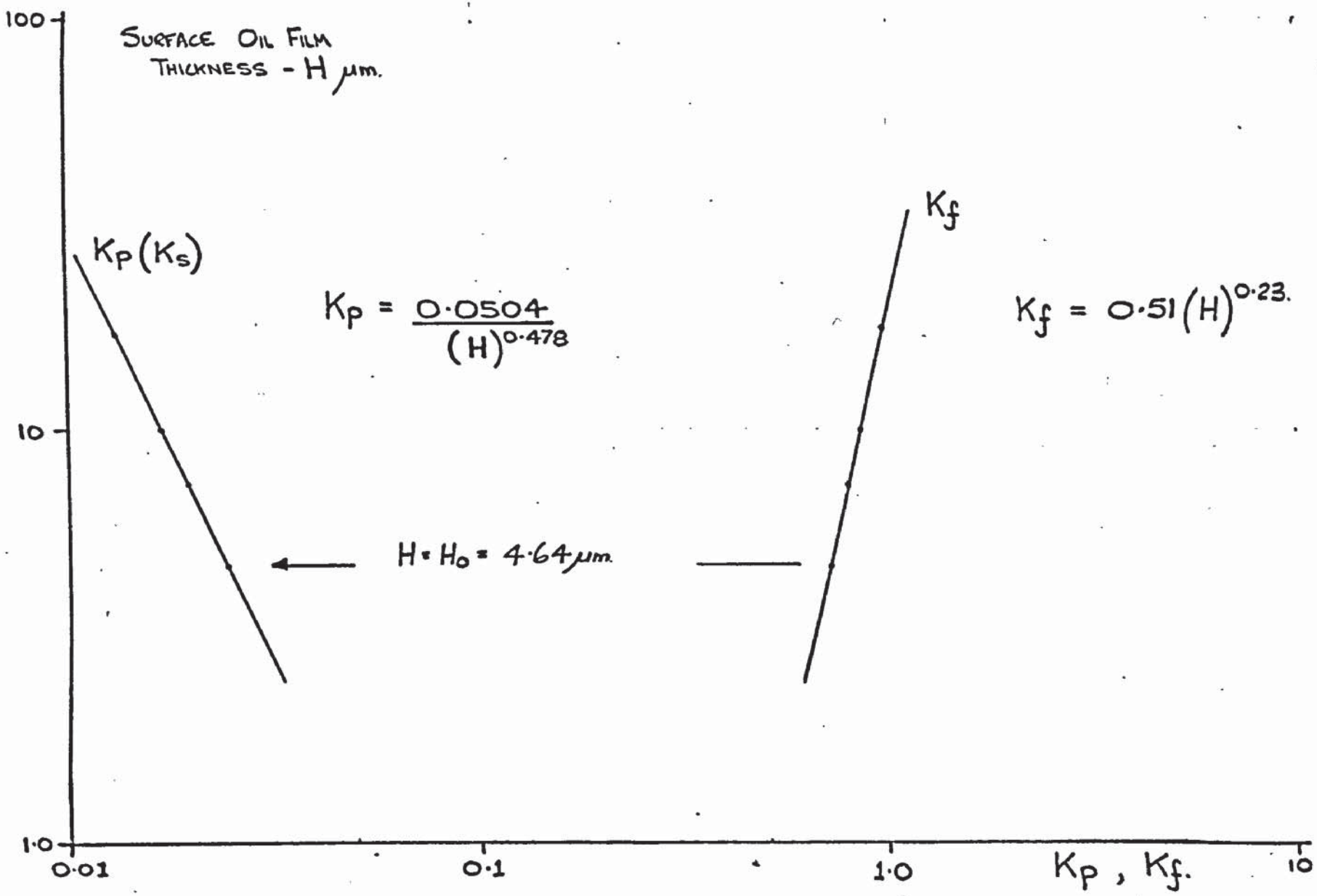

Fig. 7·28. Relationship between Coefficients Kp and Kf and Film Thickness H.

$$Pw = K_E.hd + C_E.\dot{hd} + P_L \qquad - 156\text{-}7$$

It has been pointed out in the previous section that C_E was difficult to establish and as this quantity ($C_E.\dot{hd}$) will be small in comparison with P_L above quite low velocities it has been excluded in order to facilitate calculations.

Using the expression for $K_E.hd$ from eqn. 103-7 then for Oil (1)

$$Pw = 1.46\,(hdv)^{4.55} + \frac{23.89.\zeta.V^{0.624}}{(H)^{2.478}} \qquad - 157\text{-}7$$

where hdv is the metallic surface penetration at some velocity. If hs is the amount of surface separation from the rest condition at some velocity V

$$hdv = hd - hs \quad \mu m \qquad - 158\text{-}7$$

and,

$$H = Ho + hs \quad \mu m \qquad -159\text{-}7$$

It is obvious that when $hs \geqslant hd$ then the term ($K_E.hd$) will be zero. Substituting 158 and 159-7 with eqn. 157-7

$$Pw = 1.46(hd - hs)^{4.55} + \frac{23.89.\zeta.V^{0.624}}{(Ho + hs)^{2.478}} \qquad - 160\text{-}7$$

A similar equation to that above exists for Oil (2).

Equation 160-7 has two unknowns hs and V and for values of hs up to hd the corresponding velocities were calculated. After this point values of V were used to determine hs.

Fig. 7.29 illustrates the values of hs for changing velocity using the equations for both oils. Had it been possible to include the C_E term (eqn.155-7) the curves would have been modified at low velocities. The likely changes are shown by the two dotted curves.

Also shown in Fig. 7.29 are the experimental results obtained by Dolbey and Burdekin (77) using the same two oils. These show some agreement over the velocity range.

The relationship between hs and sliding velocity can only be obtained through an equation such as that of 160-7 or the curves derived from it. There is no possibility of a simple mathematical expression.

In order to obtain the 'solid' friction value the contact area A_{CLV} must be calculated using eqn. 92-7 where the term α is obtained from eqn.111-7

$$A_{CLV} = 0.009705\left(\frac{Pw}{\alpha}\right)^{0.82}$$

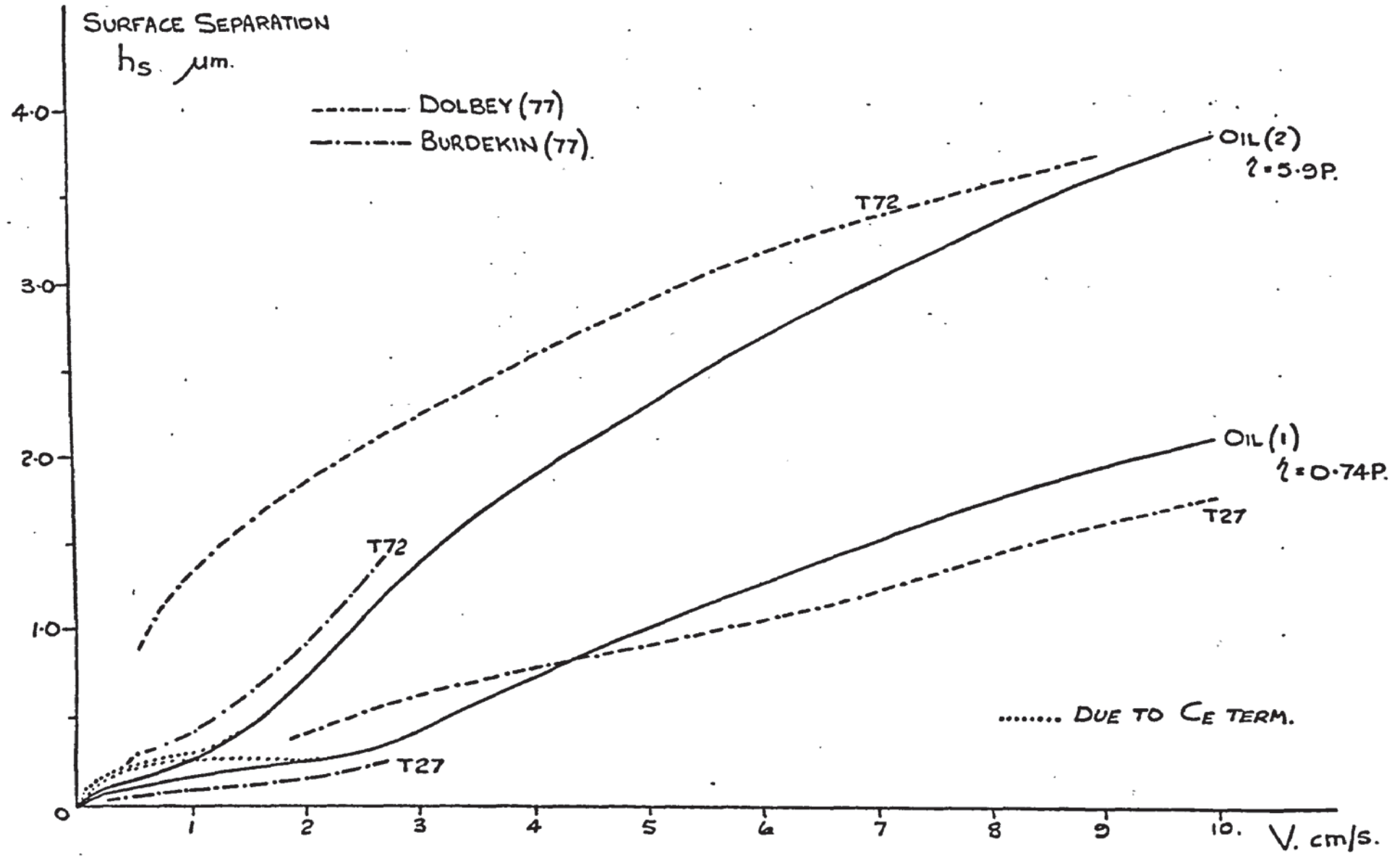

FIG. 7·29. SURFACE SEPARATION VERSUS SLIDING VELOCITY. - LUBRICATED CONDITIONS.

where $\alpha = \left(\frac{hd}{hdv}\right)^{4.55}$ and using eqn. 158-7

$$\alpha = \left(\frac{hd}{hd - hs}\right)^{4.55} \qquad - 161\text{-}7$$

The term α can alternatively be described using a general form of eqn. 160-7, thus,

$$\alpha = \left(\frac{Pw}{Pw - P_L}\right) \qquad - 162\text{-}7$$

The value of α will now range between unity and infinity as P_L increases to Pw.

The friction force can be calculated from eqn. 84-7 in which W_T is replaced by Pw/α

$$F = 0.009705.\left(\frac{Pw}{\alpha}\right)^{0.82}.\left[K_{LP}\right] + \frac{Pw}{\alpha}.\text{Tan }\theta \qquad - 163\text{-}7$$

where

$$K_{LP} = \left[1 - \left(\frac{Ko + 0.06}{Pm}\right)^2\right]Ss + \left[\frac{Ko + 0.06}{Pm}\right]S_{OL} \qquad - 164\text{-}7$$

A value of Ko has to be selected and is based upon the μs value. In this case the results obtained by Dolbey are used and μs values are estimated for polar and non-polar oils, the value of bulk viscosity having very little effect.

1) For Polar Oils $\mu s = 0.13$
   and using Fig. 7.14 $Ko = 120$
2) For Non-Polar Oils $\mu s = 0.288$
   $Ko = 70$

Using other data from section (7.2.ii) then,

K_{LP} (Polar) = 7.87

K_{LP} (Non-Polar) = 22.8

Therefore for each oil we have two curves of F against velocity. (One polar and the other non-polar). As an example

For Oil (1) (Polar) $\eta = 0.74$Poise.

$$F = 0.009705.\left(\frac{Pw}{\alpha}\right)^{0.82}.\left[7.87\right] + \frac{Pw}{\alpha}.\text{Tan }\theta \qquad - 165\text{-}7$$

The previously calculated values of V and hs are used in these equations and then μk is found by dividing F by Pw. The resulting four curves are drawn in Fig.7.30 using linear scales. If we let V_{CL} be the velocity when the solid friction is just zero, i.e. when solid contact has just ceased, a plot can be made of μk against $(V_{CL} - V)$ where V has values from zero

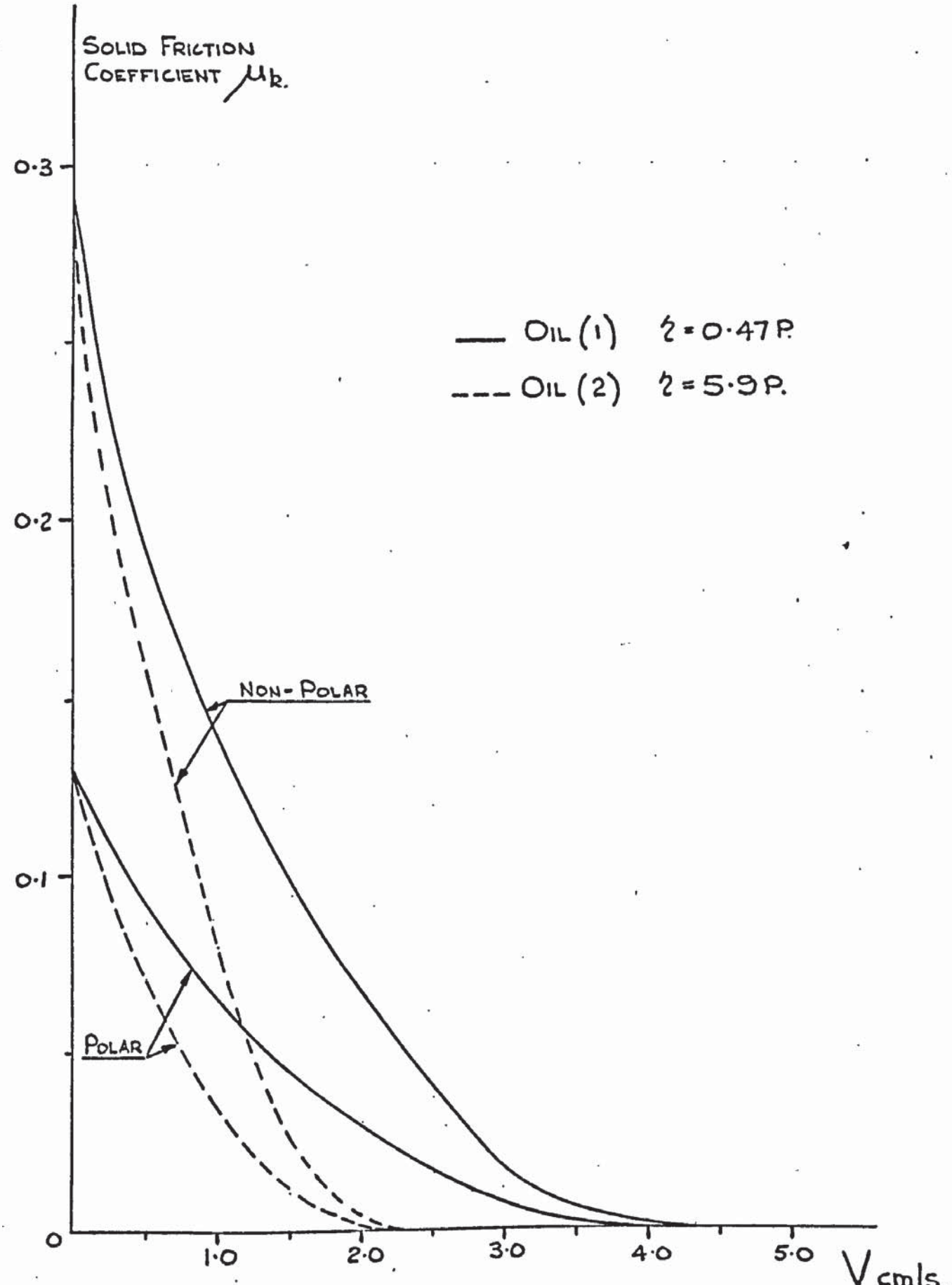

FIG. 7·30. SOLID FRICTION CHARACTERISTICS.

up to V_{cL}. The value of V_{cL} can be calculated from eqns. 153-7 and 154-7. ($P_L = Pw$).

For Oil (1) $$V_{cL} = \left[\frac{Pw\,(Ho + hd)^{2.478}}{23.89.\eta}\right]^{1.6} \text{ - cm/s.} \quad - 166\text{-}7$$

For Oil (2) $$V_{cL} = \left[\frac{Pw\,(Ho + hd)^{2.478}}{4.38.\eta}\right]^{1.43} \text{ - cm/s.} \quad - 167\text{-}7$$

Fig. 7.31 illustrates the four conditions and a general relationship does emerge.

$$(\text{Solid}) - \mu k = N.(V_{cL} - V)^{2.18} \quad - 168\text{-}7$$

Term N can be calculated when V is zero,

$$N = \frac{\mu s}{(V_{cL})^{2.18}} \quad - 169\text{-}7$$

Therefore eqn. 168-7 can be rewritten as

$$(\text{Solid}) - \mu k = \frac{\mu s}{(V_{cL})^{2.18}} . (V_{cL} - V)^{2.18} \quad - 170\text{-}7$$

Thus the solid kinetic coefficient of friction can be established and it is suggested from eqn. 166 and 167-7 that the terminal velocity V_{cL} will reduce as the bulk oil viscosity increases and when the surface topography is "smoother", reducing the term (Ho + hd).

The friction attributed solely to the lubricant has now to be established and again the hydrodynamic equation is used. From Fuller (97)

$$F = \frac{2.A_A.V}{(H)} \times Kf \quad - 171\text{-}7$$

The 'load' taken by the oil is equal to P_L therefore the above eqn. can be rewritten as, ($A_A = \ell^2 = 1 cm^2$)

$$\frac{F}{P_L} = \mu o = \frac{2.V.Kf}{P_L.(H) \times 100} \quad - 172\text{-}7$$

(η in Poise, H in μm)

If eqns. 153 and 154-7 are substituted then,

For Oil (1) $$\mu o = \frac{Kf.(H)^{1.478}\,V.^{0.376}}{2389} \quad - 173\text{-}7$$

For Oil (2) $$\mu o = \frac{Kf.(H)^{1.478}\,V.^{0.30}}{438.5} \quad - 174\text{-}7$$

Again to ease calculations a relationship between Kf and H has been established through the equation,

$$Kf = \left[\frac{6}{2 + m} - \frac{2}{m} . \log_e (1 + m)\right] \quad - 175\text{-}7$$

This is taken from Fuller (97) and (m) has been defined in eqn. 141-7.

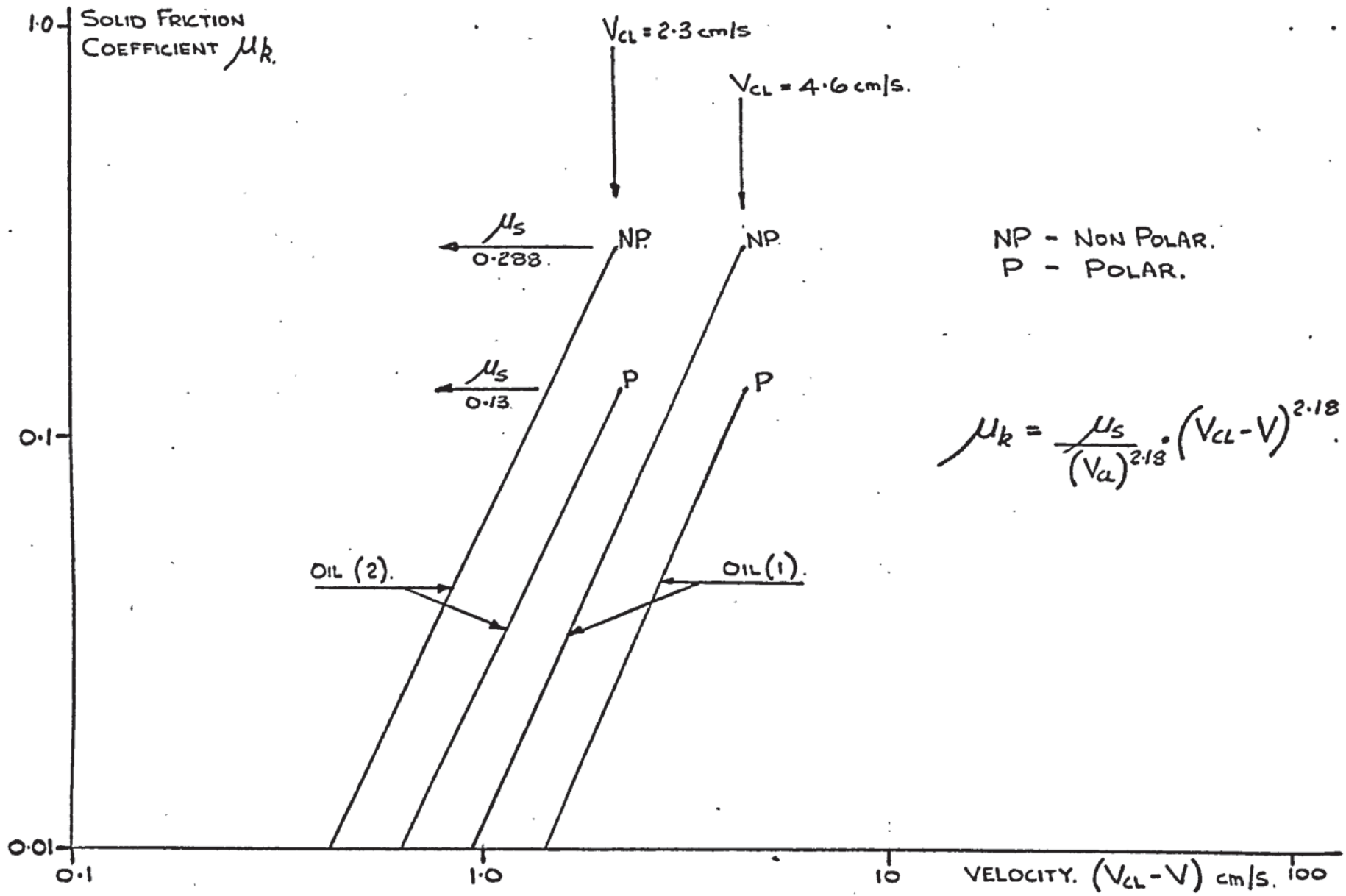

Fig. 7·31. Friction Coefficient versus $(V_{CL}-V)$. - Lubricated condition.

A plot of Kf against H is included in Fig. 7.28 and a related equation gives

$$Kf = 0.51\,(H)^{0.23} \qquad - 176\text{-}7$$

Substituting this expression in 173 and 174-7,

For Oil (1) $$\mu o = \frac{(H)^{1.71}\ V^{0.376}}{4684} \qquad - 177\text{-}7$$

For Oil (2) $$\mu o = \frac{(H)^{1.71}\ V^{0.30}}{859.8} \qquad - 178\text{-}7$$

where H = (Ho + hs)

Having already established values of hs and V, μo can be calculated. Fig. 7.32 illustrates the changes in μo with V. These curves show a steep rise in μo at low velocities and give a nearly linear relationship thereafter. It is interesting to note that if a straight line is drawn through the latter part of the curves, when V is zero the coefficient of friction still has some small value which increases with the higher viscosity oil. This will mean that a complete friction/velocity curve will have some form of linear rise in friction as the sliding speed increases above the minimum condition. Dolbey's (77) results and those of other researchers (46) indicate that if this linear portion of the curve is projected back to zero velocity it does result in a standing friction value. This affect then is attributable to the lubricant friction characteristic which in turn is influenced by the surface topographical conditions.

It could be argued that with even larger amounts of apparent surface separation the table attitude could still give rise to small amounts of solid friction, and this could account for the friction offset at zero velocity. In this case an analysis would be very difficult.

The complete friction/velocity curves for the two oils, with and without polar additives, are illustrated in Fig. 7.33 and μ_T is the total friction coefficient given by

$$\mu_T = \mu k + \mu o \qquad - 179\text{-}7$$

As an example of the complete expression in parameter terms,

For Oil (1) Polar, (using eqn. 165-7 and 177-7)

$$\mu_T = \frac{0.009705}{Pw}\cdot\left(\frac{Pw}{\alpha}\right)^{0.82}\cdot\left[7.87\right] + \frac{\tan\theta}{\alpha} + \frac{(Ho+hs)^{1.17}V^{0.376}}{4684} \qquad - 180\text{-}7$$

where α is given by eqn. 161-7.

This complete result hinges on the relationship between hs and V established from eqn. 160-7.

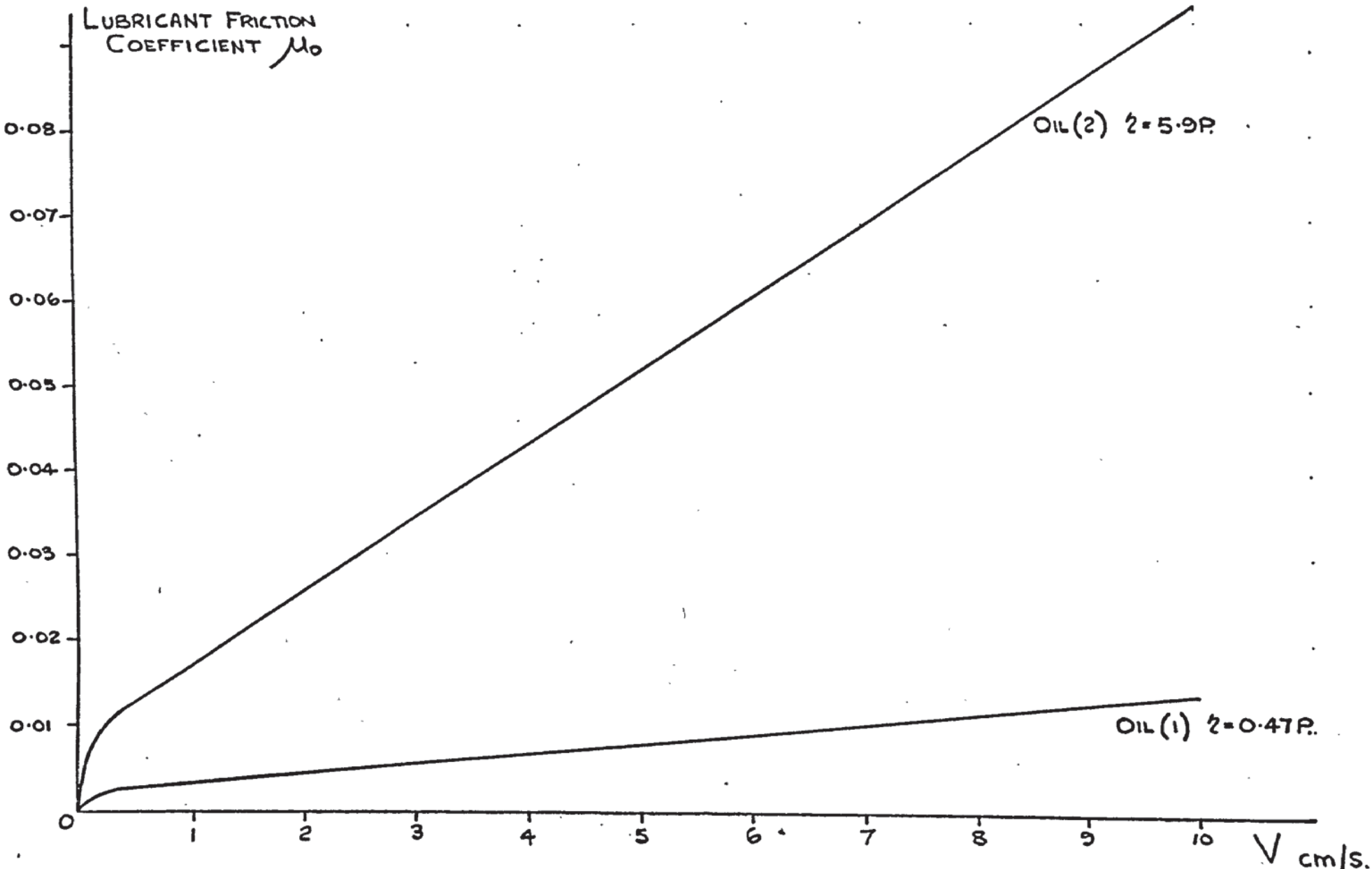

FIG 7·32. LUBRICANT FRICTION CHARACTERISTICS.

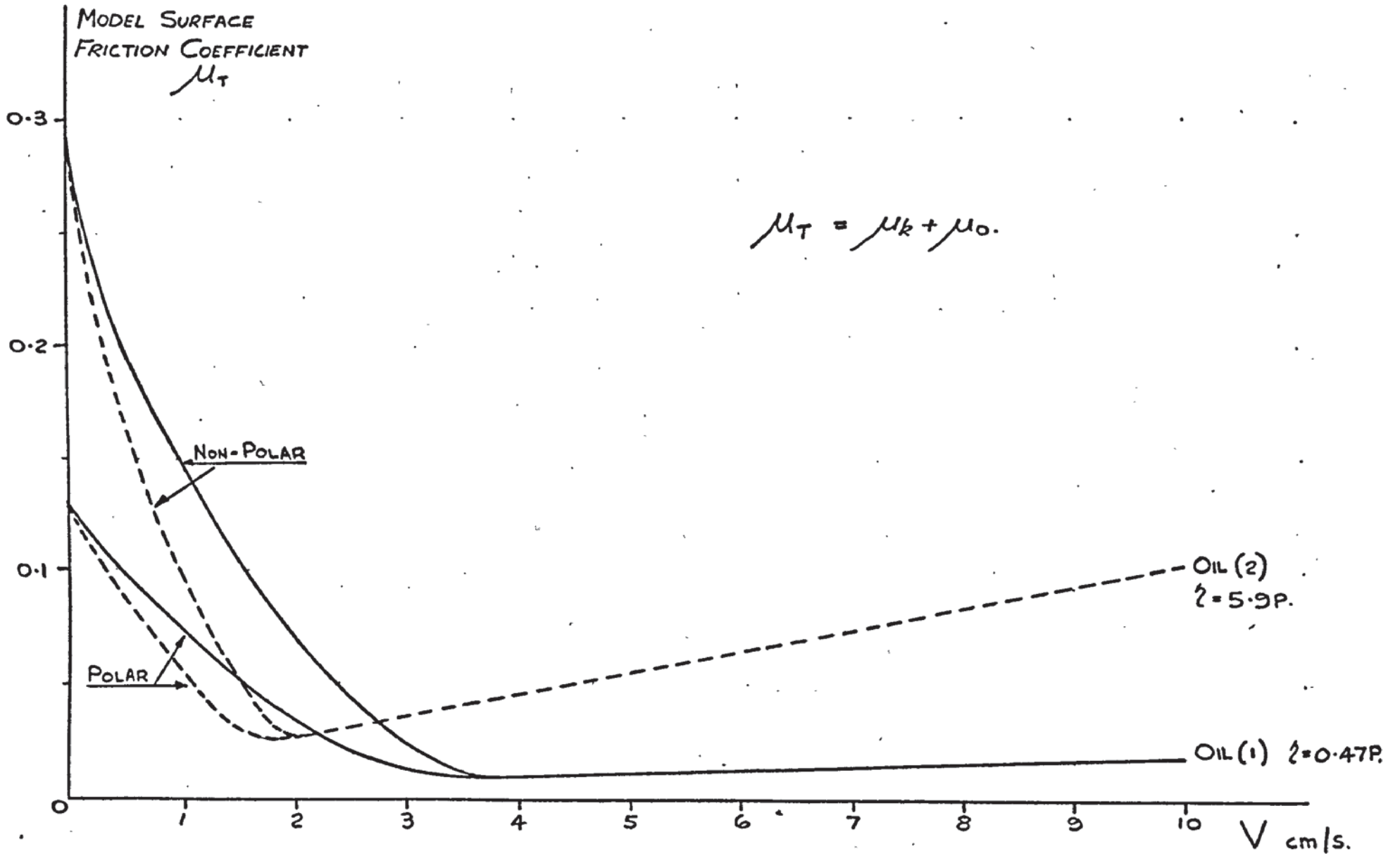

FIG. 7·33. COMPLETE MODEL FRICTION CHARACTERISTICS - LUBRICATED CONDITION.

To end this section some general comments can be made concerning the analysis of the model surface and its relationship to machine tool slideways.

1) The initial fall in the friction characteristic at low sliding velocities can be attributed to three main factors,

a) The degree of metallic contact.

b) The support given to the load by the oil.

c) The molecular strength of the surface layers of the oil film.

2) The amount of table rise is small even at higher velocities so that the rising "linear" portion of the friction characteristic is still influenced by surface topography as well as bulk lubricant viscosity.

3) The lifting action is due mainly to the surface topography enabling the interface oil pressure to be generated.

4) The amount of oil between the slides at velocity Vcl would be (Ho + hd) multiplied by the total area. In this case for a slide area of 696 cm^2 the volume is 0.382 cm^3. This quantity is extremely small but is most effective in reducing friction especially at very low speeds and when polar additives are present.

Finally it was shown in the dry surface condition that some form of surface time constant would be present causing a lag between changes in friction force and velocity. In the lubricated condition the author feels that although such a time constant must exist, especially during the falling friction characteristic, the contribution made by the oil is still in question. Several authors (77) (54) have attempted to apply squeeze film techniques under static conditions to obtain a damping term and so calculate a time constant. Without the inclusion of the effects of surface topography and sliding conditions there must be some doubt as to the validity of this technique. Further comment on this matter will be made following the next chapter which deals with the analogue simulation.

7.4 FRICTION EQUATIONS USED FOR SIMULATION PURPOSES.

The friction characteristic has been broken down into two parts,

1) A non-linear portion attributed to the 'solid' friction.

2) A linear part due to viscous conditions.

The solid friction force can be established from eqn. 168-7, but in order to use the available functions on the analogue computer this equation has had to be modified by taking the index as 2.0 instead of 2.18.

$$F\ (Solid) = N\ (V_{CL} - V)^2 \times Load \qquad - 181\text{-}7$$

$$\text{or} \quad F\ (Solid) = \frac{\mu s}{(V_{CL})^2} \cdot (V_{CL} - V)^2 \times W \qquad - 182\text{-}7$$

The viscous friction term has been considered to be completely linear whi is not apparently possible by modifying an equation such as 178-7. The standard form of linear equation has been adopted,

$$F\ (Viscous) = f \times V. \qquad - 183\text{-}7$$

The total friction force will be,

$$F = F(Solid) + F\ (Viscous)$$

$$F = \frac{\mu s}{(V_{CL})^2} \cdot (V_{CL} - V)^2 \times W + f.V \qquad - 184\text{-}7$$

This equation can be compared with eqn. 6.4 which is repeated here for completeness,

$$F = N\ (V_{CL} - \dot{X}o)^2 + f\dot{X}o$$

A time dependent arrangement has been introduced into latter simulation circuits affecting only F(Solid)

$$F(Solid) = N\ (V_{CL} - \dot{X}o)^2 \times \left[\frac{1}{1 + Ts}\right] \qquad - 185\text{-}7$$

The bracketed term describes a first order lag system in terms of the Laplace operator.

CHAPTER 8

AN ANALOGUE COMPUTER SIMULATION OF NON-LINEAR FRICTION BEHAVIOUR ON A MACHINE TOOL SLIDEWAY

8 : 1 INTRODUCTION

The simulation of the slideway system was carried out on the Solartron 1451 (110) which is illustrated with other preipheral equipment in Fig. (8.1).

A detailed description of the analogue computer is not required here, but a list of main elements is given below.

1) 16 summing amplifiers - gains of x 1 and x 10
2) 8 integrating amplifiers - gains of x 1, x 10, x 100 and x 1000
3) 12 fixed potentiometers
4) 6free potentiometers
5) 4 Diode pairs
6) 2 quarter squares multipliers
7) digital voltmeter

The machine operating voltages are $\pm$ 100 V d.c.

Many books have been written about the operation and use of the analogue computer and the author has found the works of Charlesworth and Fletcher (111) and Jackson (112) most helpful.

This chapter has been broken down into sections in order to fully illustrate the details of the simulation and the results that have been produced over the several years of use and subsequent modification.

Some general observations regarding this work can be made.

1) The accuracy of the results is of the order of $\pm$ 2% for the size of these simulation circuits. This will depend mainly upon the setting of potentiometers.

2) Although the simulated system frequencies varied they were well within the bandwidth of the amplifiers, for all input gains.

3) The machine is about twelve years old and has valve type amplifiers with mechanical chopper stabilisation. This has caused some minor problems, one being the appearance of high frequency parasitic oscillations superimposed on the output voltages.

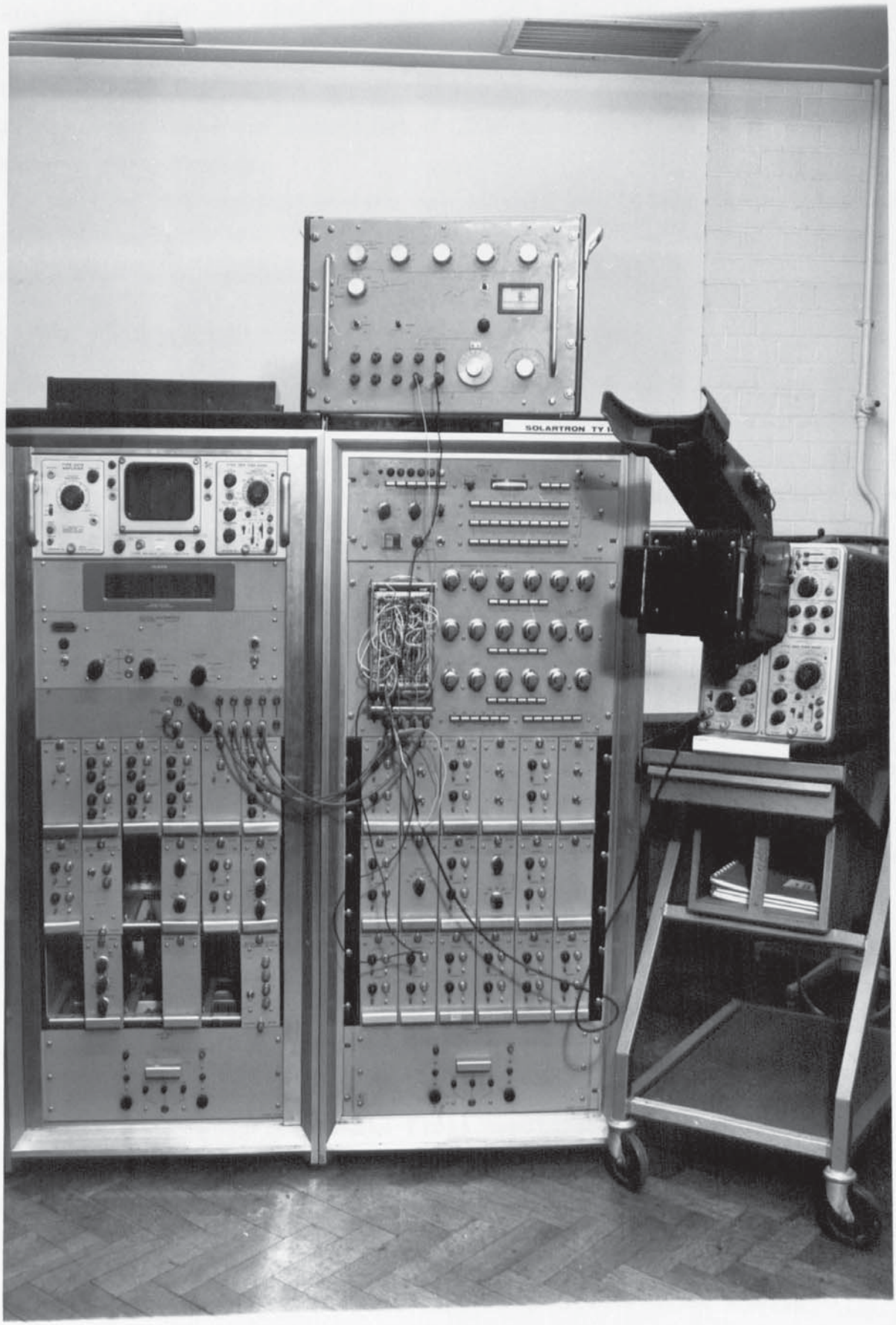

FIG. 8·1. SIMULATION EQUIPMENT.

4) The computer was thoroughly checked for electrical faults before any simulation work was attempted, and included recalibration of the amplifiers.

5) All recordings were made on the same storage oscilloscope, the Tektronix Type 564 and where necessary photographed with the attached polaroid camera (Polaroid series 125). The calibration of this equipment was checked periodically.

6) Most of the simulation work was carried out before the mathematical analysis in chapter 7 was developed. Some parameter values had to be estimated from data recorded by other researchers (76)

8 : 2 THE SIMULATION CIRCUIT - EARLY DEVELOPMENT WORK

The analogue computer is used to simulate physical systems and a scaled voltage quantity is used to represent all the physical variables. Usually the system is described by a differential equation and care must be taken in selecting the amplitude scaling factors and the time scaling factor.

The amplitude scaling factor ensures that any voltage representing a physical variable does not exceed the linear range of the amplifiers (in this case ± 100 V d.c.). There are several ways of deriving these factors but those most often used by the author are the Equal Coefficient Rule (112) and the Computer Block Gain technique (113). In this simulation the latter technique has been used. Although it can be quite complex to operate it does have the advantage of allowing each individual system element to remain as a discrete unit in the computer diagram.

The time scaling factor is not necessary for this work, but would have to be used in other simulations under the following conditions.

1) The recorder frequency is lower than the frequency of signal to be recorded.

2) The simulation frequencies are calculated to be above the bandwidth of the amplifiers.

3) Extremely slow processes are to be computed.

In the author's experience the first condition has proved to be the most common and the time scaling factor is usually worked out with the following formula.

$$\text{TIME SCALING FACTOR} = \frac{\text{PLOTTER FREQUENCY}}{\text{MAXIMUM SYSTEM FREQUENCY}} \qquad - \ 1\text{-}8$$

The maximum system frequency is that which occurs under stable conditions. The plotter frequency can be expressed as,

$$\text{PLOTTER FREQUENCY} = \frac{\text{PLOTTER SLEWING RATE x INPUT GAIN}}{\text{2 x INPUT VOLTAGE AMPLITUDE}} \qquad - 2\text{-}8$$

To illustrate the amplitude scaling required the linear part of the slideway system is analysed and the computer simulation diagram produced. Consider the diagram shown in Fig. (8.2) which represents the slideway system. The differential equation is,

$$M\ddot{x}o + f\dot{x}o + Kxo = Kx_i \qquad - 3\text{-}8$$

This equation can be represented by the block diagram of Fig. (8.3).

Knowing the values of the system coefficients M, f and K, the value of the input x_i must be chosen.

In the steady state or rest condition xo and x_i are zero and the magnitude of input is taken about this point.

Setting x_i maximum at 2.54 mm the input scaling factor will be 0.0254 mm/Volt. This scaling factor applies to xo and to the output of summing junction (A) which is also a positional quantity.

The summing junction (A) of Fig. (8.3) represents a device whose output will be the difference between x_i and x_o and must be a summing amplifier. The gain is calculated from the following formula,

$$\text{Computer gain for (A)} = \frac{\text{input scale factor}}{\text{output scale factor}} \text{ x block gain} \qquad - 4\text{-}8$$

$$\text{Computer gain for (A)} = \frac{0.0254}{0.0254} \times 1 = 1$$

With K the stiffness coefficient equal to 17.86 MN/m, the maximum input force will be,

$$\text{Max. Input Force} = K(x_i - x_o) = K.x_i \qquad - 5\text{-}8$$

$$= 17.86 \times 2.54 \times 10^{-3} \quad \text{MN}$$

$$= 45.36 \text{ KN}$$

An appropriate force scaling factor will be 453.6 N/V so that the computer gain for block K will be,

$$\text{C.G. (K)} = \frac{0.0254}{453.6} \times 10^{-3} \times K \qquad - 6\text{-}8$$

$$\text{C.G. (K)} = \frac{0.0254}{453.6} \times 10^{-3} \times 17.86 \times 10^{6}$$

$$\text{C.G. (K)} = 1.0$$

At summing junction (B) inputs and output are all forces, therefore the computer gain is unity. It is necessary to select a maximum acceleration and an acceptable value would be 254 m/s^2, and with the mass M equal to 454 kg, the acceleration scaling factor will be 2.54 m s^{-2}/V and the

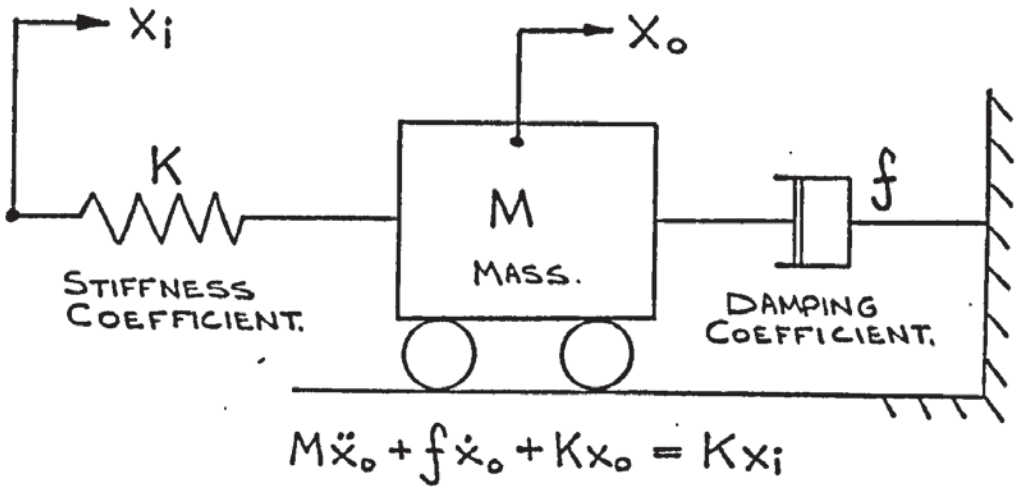

FIG. 8·2. LINEAR SLIDEWAY SYSTEM.

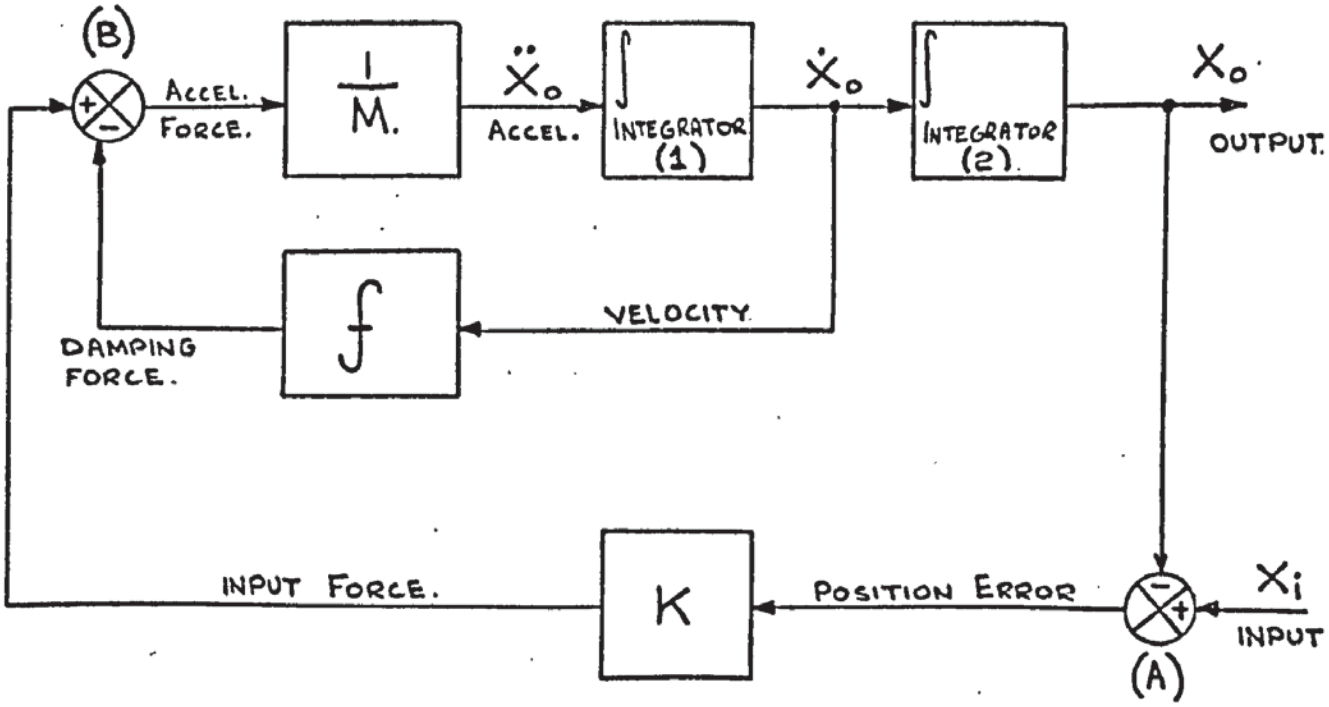

FIG. 8·3. BLOCK DIAGRAM OF LINEAR SYSTEM.

computer gain can be calculated as

$$C.G.\left(\frac{1}{M}\right) = \frac{453.6}{2.54} \times \frac{1}{454} = 0.39 \qquad - 7\text{-}8$$

Again the maximum velocity is given a value 0.254 m/s so that the scaling factor will be 0.00254 m s^{-1}/V giving a computer gain for integrator (1) as,

$$C.G.Int\ (1) = \frac{2.54}{0.00254} \times 1 = 1000 \qquad - 8\text{-}8$$

The gain of integrator (2) can now be calculated as the position scaling factor is known, thus

$$C.G.Int\ (2) = \frac{0.00254 \times 1000}{0.0254} \times 1 = 100 \qquad - 9\text{-}8$$

The linear damping coefficient (f) has a value of 17.86 KN s/m. and,

$$C.G.\ (f) = \frac{0.00254}{453.6} \times 17.86 \times 10^{3} = 0.1 \qquad - 10\text{-}8$$

The computer diagram suitable for patching on the analogue computer can now be drawn and this is shown in Fig. (8.4). All the amplifiers and fixed potentiometers are addressed. It should be noted that the computer gain for K was 1.0 but this has been shared between amplifier A5, having a gain of x 10 and potentiometer PC6 having a value of 0.1. This means that for changes in K the potentiometer setting can be modified, e.g. K = 45MN/m then PC6 = 0.252, $\left(\frac{45}{17.86} \times 0.1\right)$

Potentiometer PA3 is set in relation to the reciprocal value of M therefore if M = 810 kg then PA3 = 0.218, $\left(\frac{4.54}{810} \times 0.39\right)$

It can be seen that the computer diagram in Fig. 8.4 shows a marked similarity to the block diagram of Fig (8.3) which describes the system differential equation.

Two main parameters required from eqn. 3.8 are the undamped natural frequency ωn and the damping ratio ζ. These can be found by the following relationships (20)

$$\omega n = \left(\frac{K}{M}\right)^{0.5} \qquad - 11\text{-}8$$

and

$$\zeta = \frac{f}{2(M.K.)^{0.5}} \qquad - 12\text{-}8$$

Using the values given above,

$$\omega n = 198.34 \text{ rad/s}$$
$$= 31.57 \text{ Hz}$$
$$\zeta = 0.1$$

The diagram of Fig. (8.4) represents the heart of the simulation circuit. We now have to modify this with respect to non-linear friction.

$$M\ddot{x}_o + f\dot{x}_o + Kx_o = Kx_i$$

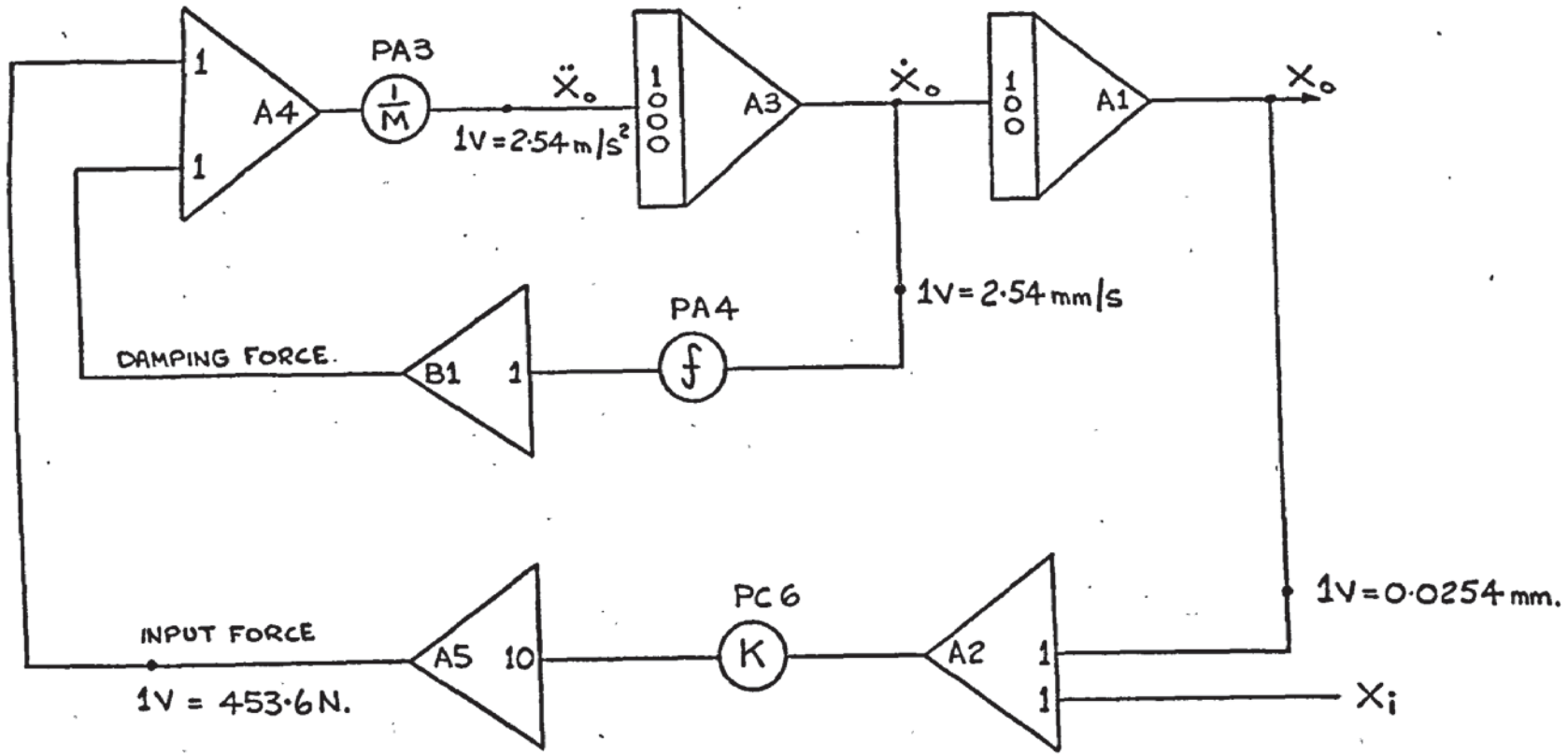

PA3. - $\left(\frac{1}{M}\right)$ = 0·39 FOR M = 454 kg.

PA 4. - (f) = 0·1 FOR f = 17·86 kN.s/m.

PC 6 - (K) = 0·1 FOR K = 17·86 MN/m.

FIG. 8·4. COMPUTER SIMULATION DIAGRAM FOR LINEAR SYSTEM.

If the system has a static friction value Fs, the friction/velocity diagram will be as shown in Fig. 8.5 (a) and a system characteristic equation will be of the form, (25)

$$M\ddot{x}_o + f\dot{x}_o + \frac{\dot{x}_o}{|\dot{x}_o|}.\,Fs + Kx_o = Kx_i \qquad - 13\text{-}8$$

This eqn. is non-linear (25) but can be analysed for particular conditions using either the describing function technique (109) or the phase-plane method, (109).

To modify the original simulation diagram an arrangement has to be made for accommodating the static friction term. If eqn. 13-8 is rewritten in terms of the input force then for $x_o = \dot{x}_o = 0$,

$$Fs = K(x_i - x_o) \qquad - 14\text{-}8$$

If the system is in a rest condition ($x_i = o$) it is suggested by eqn.14-8 that an equality will only be achieved when x_o has some negative value. This would mean that the force Fs would move the mass M backwards. Obviously a friction force does not do this, but some early simulations, (53), do in fact operate this way.

What is inferred in eqn. 14-8 is that in order to move the mass M and overcome the viscous friction f the system input force must be greater than $\pm Fs$. Therefore,

$$M\ddot{x}_o + f\dot{x}_o = \text{Useful input force} \qquad - 15\text{-}8$$

where the useful input force is given by,

$$\text{Useful input force} = K(x_i - x_o) - Fs \qquad - 16\text{-}8$$

and is zero when $K.(x_i - x_o) < Fs$

A plot of input force against useful input force is illustrated in Fig. 8.5 (b).

In order to achieve this characteristic a dead zone circuit is introduced between amplifiers A5 and A4 of Fig. (8.4). This circuit is illustrated in Fig. 8.5 (c) and is made up of two free potentiometers PB1 and PB2 and one diode pair. D1-D2.

The operation of this network is described briefly as follows,

1) The voltages $\pm V_B$ are constant (in this case $\pm$ 50V)

2) When V_1 is positive diode D2 will conduct only when the voltage on the wiper arm of PB2 is just positive. This depends upon the value of V_B and the position of the wiper arm on the resistive track. If the arm was at the centre of the track length, then D2 would conduct when + V_1 was just

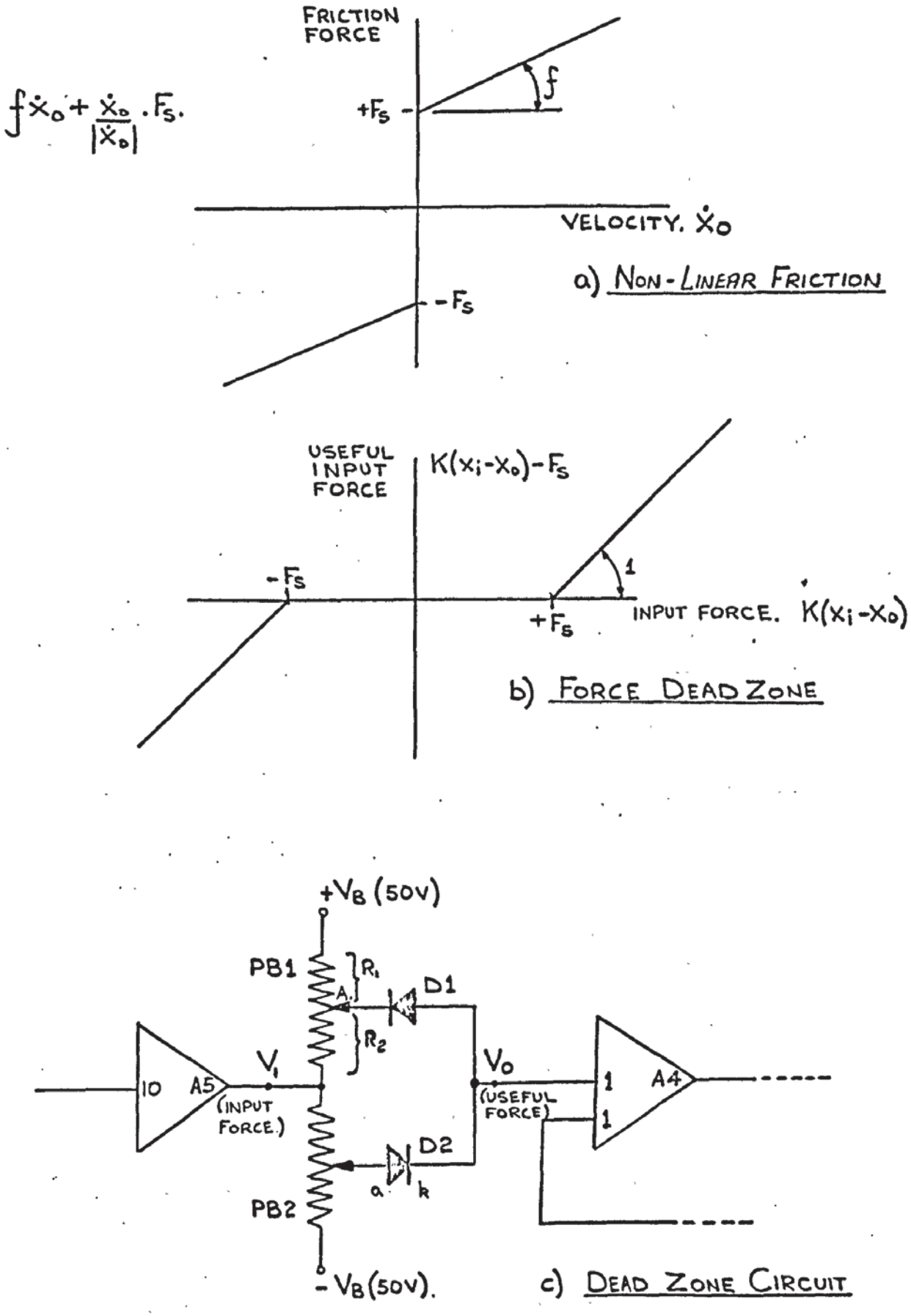

FIG. 8·5. A FRICTION NON-LINEARITY.

greater than $-V_B$ in magnitude. In this situation then,

$Vo \doteqdot V_1 - V_B$ when $V_1 > V_B$

$Vo = 0$ when $V_1 < V_B$

3) Similarly when V_1 is negative diode D1 will conduct when the voltage on the wiper arm of PB1 is just negative. The diodes require a small positive potential between the anode (a) and the cathode (k). Therefore it is much easier to set this circuit on the computer in the following way, using the Problem Check (111) computer mode.

Let V_F be the scaled voltage for F_s and V_1 the scaled input force with a voltage level between 3V and 6V greater than V_F.

1) V_1 is checked at the output of A5 (see Fig.815(c)) with the D.V.M. and the polarity is set positive.

2) Vo is checked at the output of A4, which has unity gain. This voltage will be negative due to a sign change through the amplifier.

3) PB2 is adjusted until the output Vo is equal in magnitude to $V_1 - V_F$

4) The polarity of V_1 is changed and the level of Vo again checked whilst adjusting PB1.

Care must be taken with the amplitude scaling in order to reduce the effect of the diode threshold. Generally V_F needs to be at least five times greater than the diode breakdown voltage, i.e. $V_F > 1.3V$. It is obvious that the smallest dead zone voltage will be approx. 0.26V when the wiper arms are at the bottom of their tracks, or when V_B is zero.

During the bulk of this simulation work the zero velocity friction force was 771N, for a selected μ_s value of 0.17. The force scaling factor was 453.6 N/V so that V_F would have been 1.7 volts. This was too low for the dead zone voltage and therefore some of the scaling factors were changed as follows,

i) Force scaling factor - 45.36 N/V

ii) Acceleration scaling factor - 0.254 m s^{-2} /V

iii) Velocity scaling factor - 0.254 mm s^{-1} /V

Only the gain of integrator A1 had to be changed from x 100 to x 10. The dead zone voltage V_F representing the friction force Fs was now,

$$V_F = \frac{771}{45.36} = 17V$$

It was not obvious immediately that the dead zone circuit itself had an attenuating effect when the circuit was conducting and this modified the value of the system stiffness K.

Consider the circuit in Fig. 8.5 (c). To set the dead zone of $\pm$ 17V the input voltage was $\pm$ 20V and the potentiometers were adjusted to give an output of $\pm$ 3 volts.

Taking one half of this circuit, when V_1 is - 20V the voltage at point A on PB1 will be - 3V and so will the value of Vo. (The input resistance of A4 was much greater than the effective potentiometer resistance and therefore the wiper arm loading was neglected).

The total voltage drop across the potentiometer resistance was $(V_B + V_1)$ and the voltage across the section of the wiper arm from the input to point A was $(V_1 - V_o)$, thus the resistance ratios were governed by the equation

$$\frac{R2}{R_1 + R_2} = \frac{V_1 - V_o}{V_B + V_1} \qquad - 17\text{-}8$$

$$= \frac{17}{70} = 0.24$$

The value of Vo is given by

$$Vo = V_1 - 0.24\,(V_B + V_1) \qquad - 18\text{-}8$$

When Vo is zero the above eqn. can be written as

$$0 = V_1' - 0.24\,(V_B + V_1') \qquad - 19\text{-}8$$

where $V_1' < V_1$. With V_B equal to 50V then, the value of V_1' will be,

$$V_1' = \frac{V_B \cdot (0.24)}{(1-0.24)} \qquad - 20\text{-}8$$

$$V_1' = 15.79V$$

The circuit should give an output voltage of zero when V_1 is 17V and using eqn. 17-8 again then the ratio value will be,

$$\frac{V_1}{V_B + V_1} = \frac{17}{67} = 0.254 \qquad - 21\text{-}8$$

This new ratio will modify eqns. 18-8, 19-8 and 20-8.

From eqn. 18-8

$$Vo = V_1 - 0.254\,(V_B + V_1) \qquad - 22\text{-}8$$

With V_1 having a value of - 20V as before and using the above equation Vo was set to - 2.22V.

From Eqn. 19-8

$$0 = V_1' - 0.254\,(V_B + V_1') \qquad - 23\text{-}8$$

Subtracting eqn. 23-8 from eqn. 22-8

$$Vo = (V_1 - V_1') - 0.254\,(V_1 - V_1')$$

or $$Vo = 0.746\,(V_1 - V_1') \qquad - 24\text{-}8$$

Therefore, when the diode D1 is conducting the relationship between the output (Vo) and the effective input $(V_1 - V_1')$ is

$$\frac{Vo}{(V_1 - V_1')} = 0.746 \qquad - 25\text{-}8$$

In this case, with V_B at + 50V, the effective input was - 3 volts and this should have given an output of - 3 volts instead of - 2.22 V. To correct this the output of the circuit was amplified by a factor of x 1.35.

Modifying eqn. 20-8, V_1' can be expressed as,

$$V_1' = \frac{V_B\,(0.254)}{(1-0.254)} \qquad - 26\text{-}8$$

or $$V_1' = 0.34\,V_B \qquad - 27\text{-}8$$

Fig. 8.6 illustrates the values of Vo for changing values of V_1' with three settings of V_B; the potentiometer resistance ratio (eqn. 17-8) remaining at 0.254.

Bearing in mind the attenuation caused by the dead zone circuit an extra potentiometer was required (PA5) to amplify the circuit output. This would save altering the value of PC6 which was solely related to the system stiffness K.

The circuit representing eqn. 13-8 is shown in Fig. (8.7). The dead zone circuit was set up as outlined previously except that when V_1 was $\pm$ 20V, then Vo was set to $\pm$ 2.5V, for a V_B value of $\pm$ 50V. The output voltage was checked for various values of V_B, in order to establish compliance with the circuit characteristics established theoretically in Fig. (8.6). It can be seen that the fixed potentiometer PA5 has been introduced (together with an input gain of x 10 on A4) to eliminate the attenuation caused by the dead zone circuit. It should be noted that due to a change in the force scaling factor the maximum value of X_1 in physical terms will be 0.254 mm($\equiv$ 10V). To demonstrate the effectiveness of this circuit the transient responses of Xo are illustrated in Fig. (8.8), for a linear condition when Fs is zero (V_B = o) and a non-linear condition when Fs is 771N (V_B = 50V). A step input of 0.127mm has been applied. The

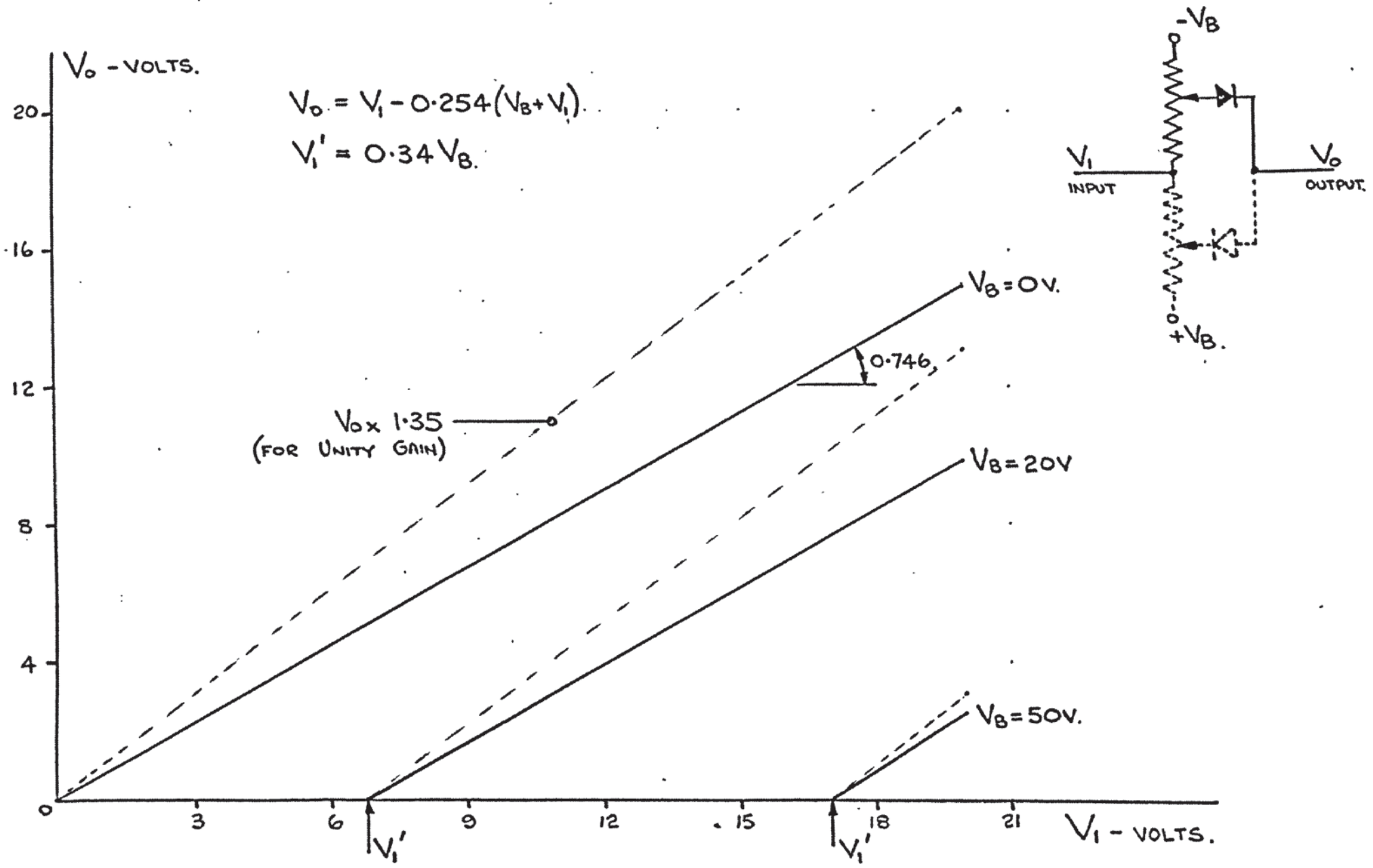

FIG. 8·6. CHARACTERISTICS OF DEAD ZONE CIRCUIT.

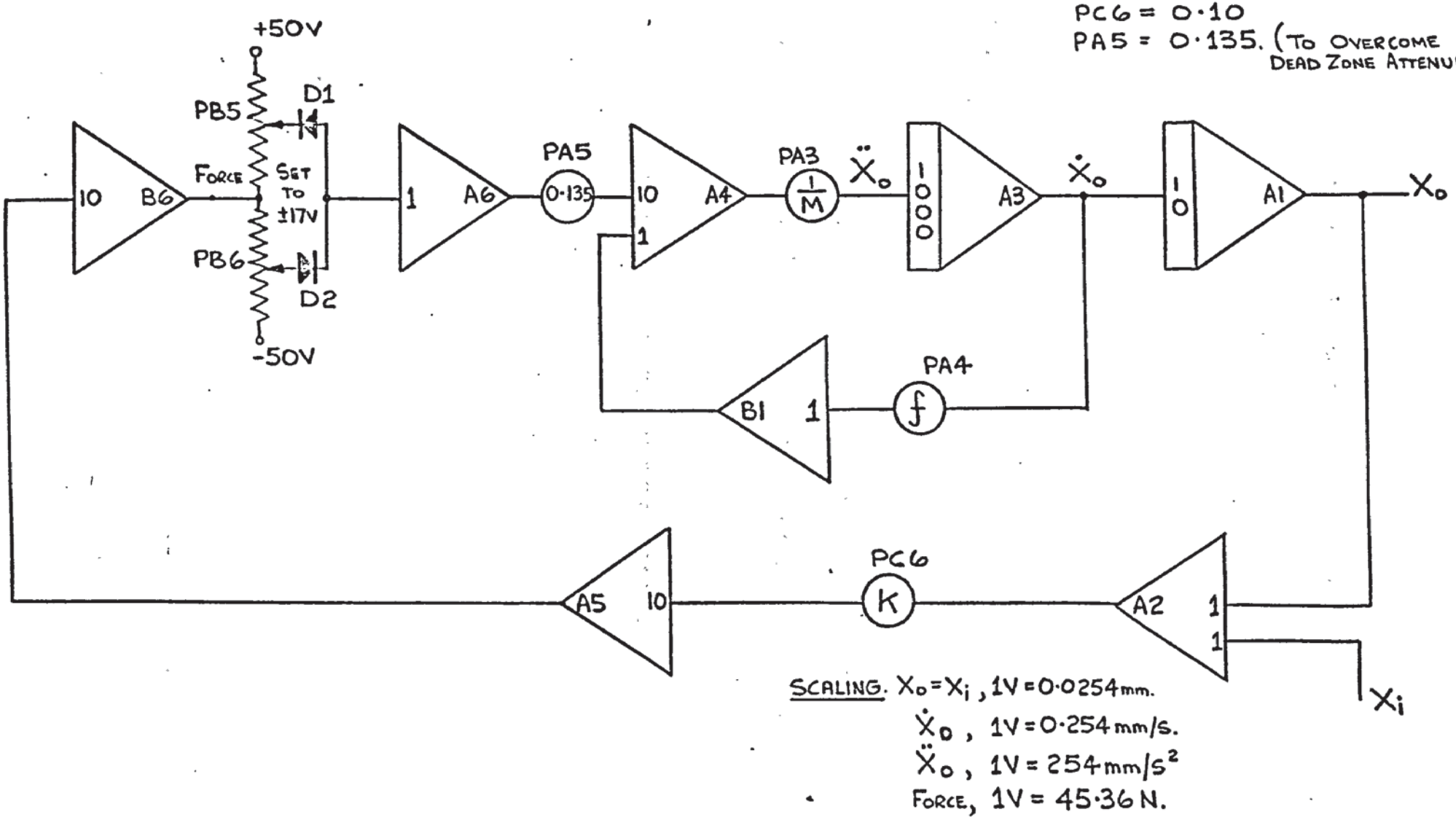

FIG. 8·7. SIMULATION DIAGRAM WITH SIMPLE NON-LINEARITY.

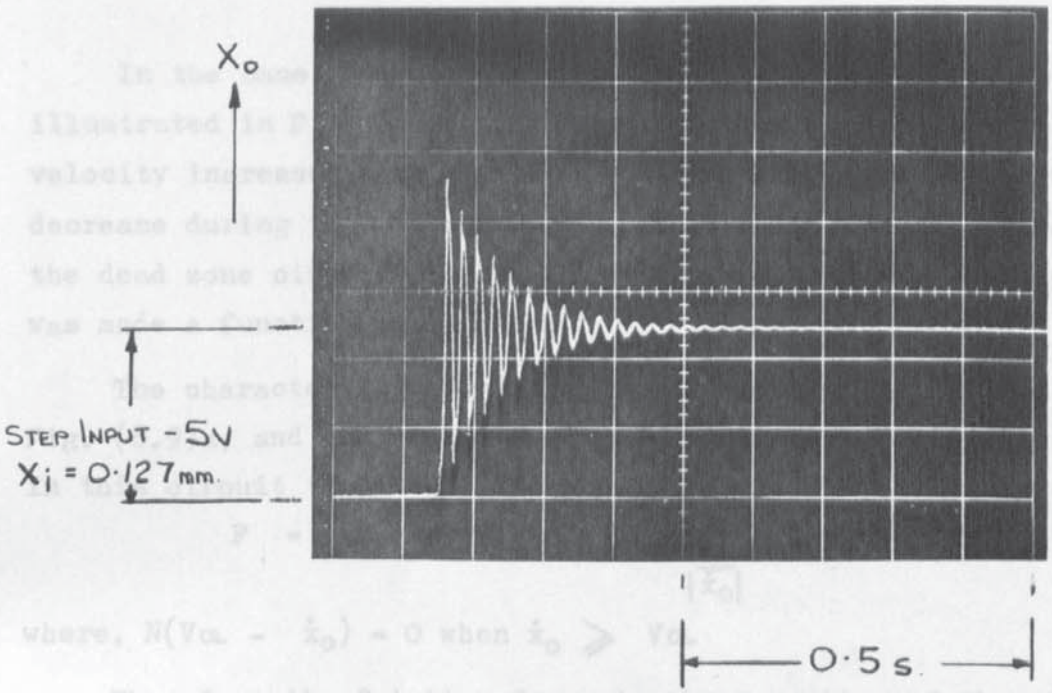

a) POSITION RESPONSE OF LINEAR SYSTEM. (FIG 8·4).

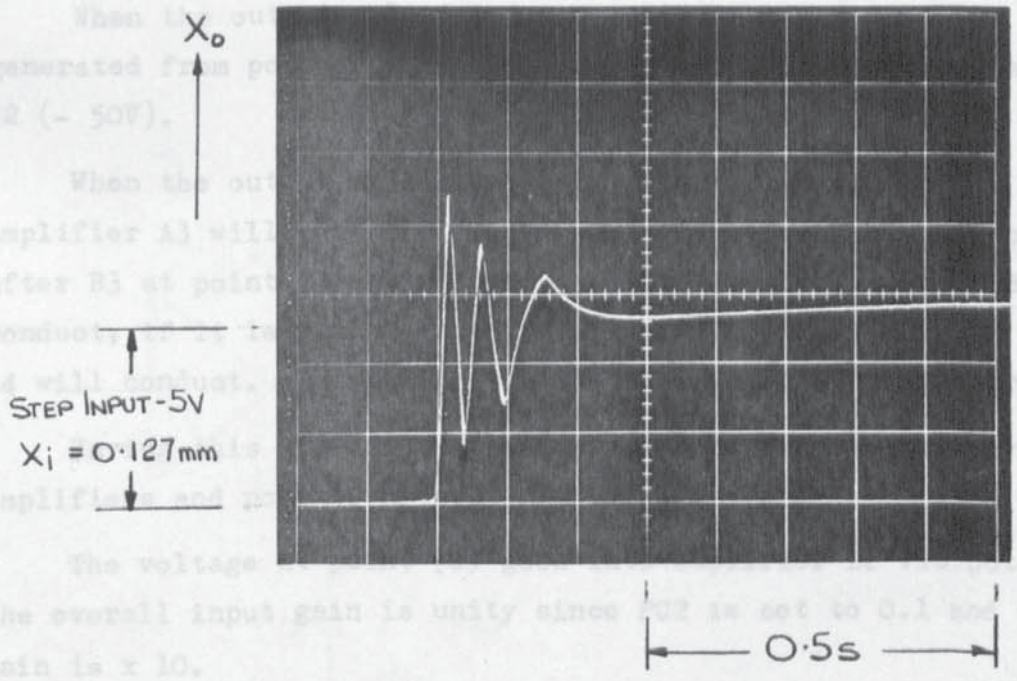

b) RESPONSE WITH DEAD ZONE CIRCUIT. (FIG. 8·7).

FIG. 8·8. SYSTEM TRANSIENT RESPONSES.

responses obtained are comparable with those that have been observed by other authors (25) (109).

In the case of the usual slideway friction characteristic such as that illustrated in Fig. 7.33, the friction force decreases initially as the velocity increases from zero. The steady state inputforce will also decrease during this stage. To accomplish this on the analogue computer, the dead zone circuit of Fig. (8.5) was modified such that the voltage V_B was made a function of velocity.

The characteristics relating V_B and V_F to velocity are shown in Fig. (8.9)a, and the required circuit modifications in Fig. (8.9)b. In this circuit the total friction force will be,

$$F = f\dot{x}_o + N(V_{cL} - \dot{x}_o)\frac{\dot{x}_o}{|\dot{x}_o|} \qquad - 28\text{-}8$$

where, $N(V_{cL} - \dot{x}_o) = 0$ when $\dot{x}_o \geqslant V_{cL}$

Therefore the friction force is the summation of the viscous and non-linear terms in the form of straight line approximations.

To describe this circuit let V_{cL} be 2.54 mm/s, the other parameters remaining the same as before.

When the output velocity is zero then V_B must be ± 50V which is generated from potentiometer PC1, amplifier X1 (+ 50V) and amplifier X2 (- 50V).

When the output velocity is ± 2.54 mm/s the voltage at the output of amplifier A3 will be ± 10V, and this is converted to a uni-polarity voltage after B3 at point (U). If the output of A3 is negative diode D3 will conduct, if it is positive its polarity will change through B3 and diode D4 will conduct. Thus at point (U) the voltage will be approximately -10V.

Having this element in the circuit reduces considerably the number of amplifiers and potentiometers.

The voltage at point (U) goes into amplifier B2 via potentiometer PC2. The overall input gain is unity since PC2 is set to 0.1 and the amplifier gain is x 10.

Amplifier B2 is set to saturate to give a maximum output of + 10V using a uni-directional saturation circuit consisting of PB2 and D5, such

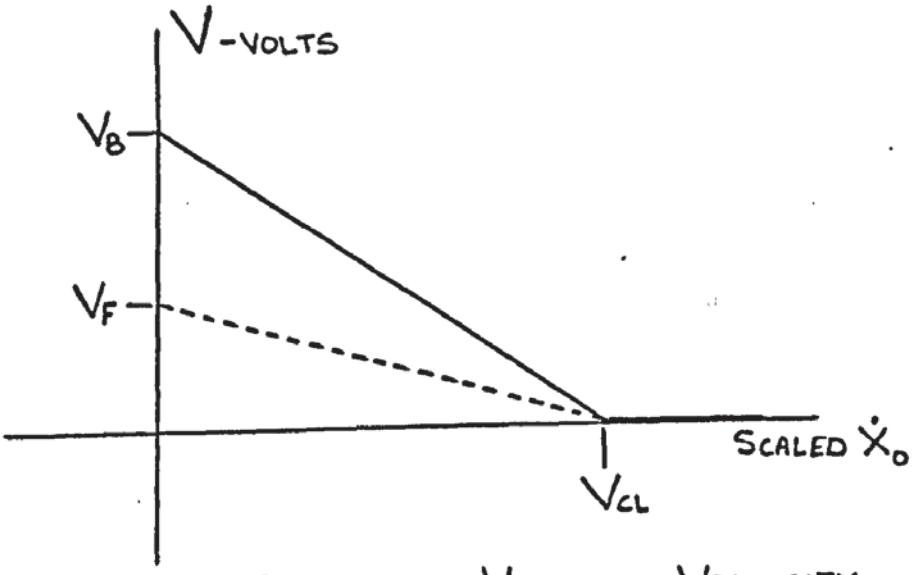

(a) CHANGES IN V_B WITH VELOCITY.

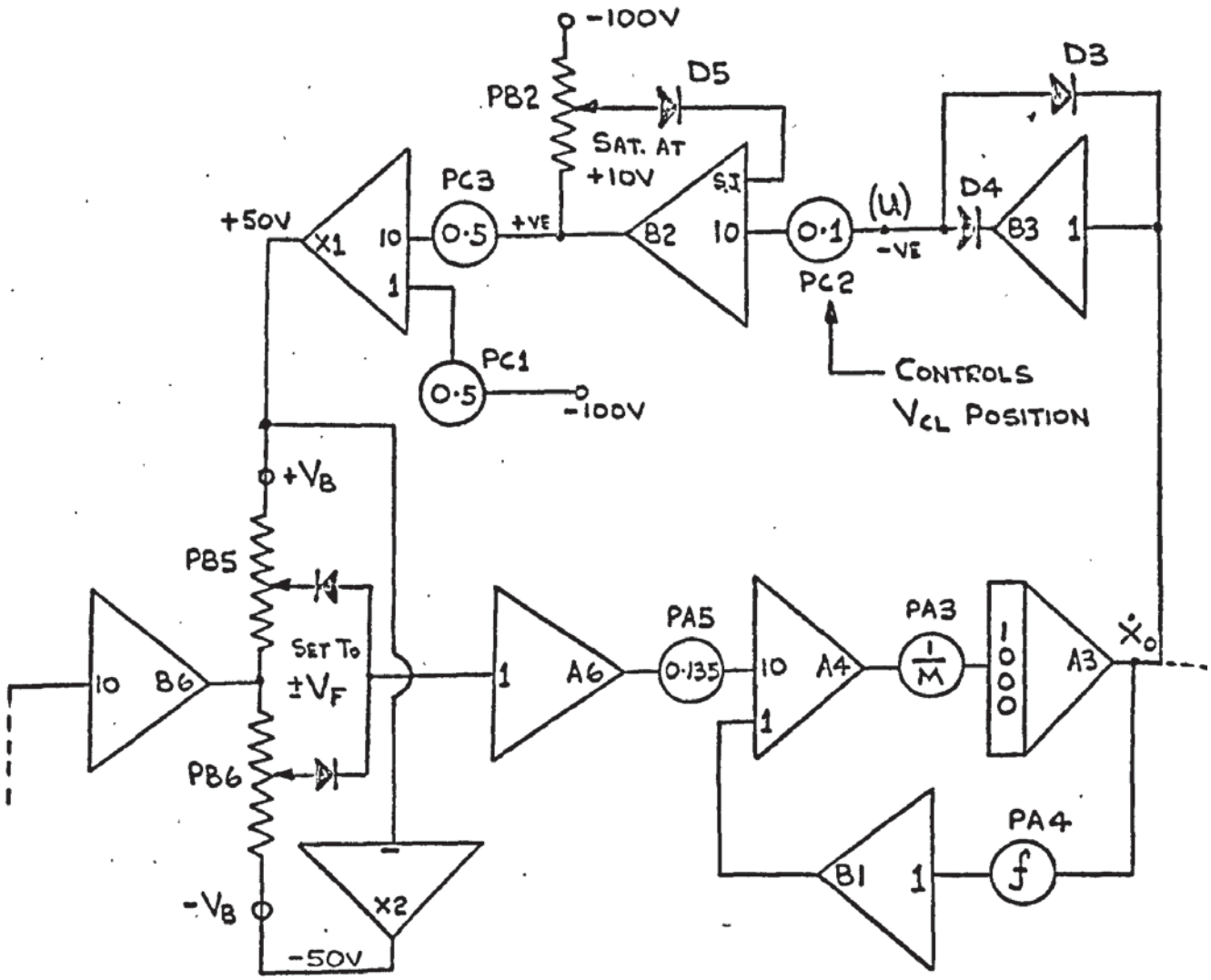

b) CIRCUIT TO PRODUCE CHARACTERISTIC IN FIG 8·9(a) ABOVE.

FIG. 8·9. DEAD ZONE CIRCUIT CONTROLLED BY VELOCITY.

an arrangement is known as a soft limiter (111). The output of B2 is set at + 10V, when the voltage output of A3 is ± 15 volts.

The output of B2 is fed into X1 via PC2, giving an overall input gain of x 5. Therefore when B2 saturates the "input" to X1 will be + 50V, As there is also a constant input of - 50V the output of X1 and X2 should be zero.

To ensure correct operation the outputs of X1 and X2 were checked when the output of A3 was ± 10V and ± 30V. In the former condition the outputs should be zero and in the latter condition the outputs should be slightly negative (approx. - 0.5V). Any necessary adjustment was made by making small changes to the setting of PC2.

When V_{CL} was 2.54 mm/s the value of PC2 was 0.1. If V_{CL} was to be 5.08 mm/s (output of A3, - 20V), then PC2 is adjusted to a setting of 0.05, and for a V_{CL} value of 1.27 mm/s PC2 is 0.2.

The setting of PC2 affects the velocity at which V_B becomes zero, and its setting can be derived from the following eqn.

$$\text{PC2 Setting} = \frac{V_{CL}}{10 \times 2.54} \qquad - 29\text{-}8$$

The complete steady state friction characteristic is shown in Fig. 8.10(a), with a plot of $K(x_i - x_o)$ against velocity $\dot{x}_o$ for three values of V_{CL} taken from the simulation, Fig. 8.10 (b)

The complete circuit shown in Fig. 8.11 was patched up with settings as shown in the diagram.

At low velocity inputs, less than V_{CL} , the simulation did exhibit 'stick- slip' motion. Fig. 8.12 shows the output position, velocity and acceleration for a ramp position input of ± 0.12mm/s (± 5V). All relevant data is also detailed in this figure.

A ramp velocity input was applied through a second input to amplifier B3. This had a value of ± 1.2 mm s^{-1}/s and the peak velocity amplitude was 10.16 mm/s (± 40V). Fig. 8.13 (a) shows the resulting S.V.P, the input velocity rising from zero.

Fig. 8.13 (b) illustrates the positional error and output velocity during "stick-slip" recorded on a base of time for a constant velocity input. It can be seen from these recordings that the simulation behaviour is very similar to that of the experimental equipment used by researchers such as Bell (46), and their recordings exhibit the same features.

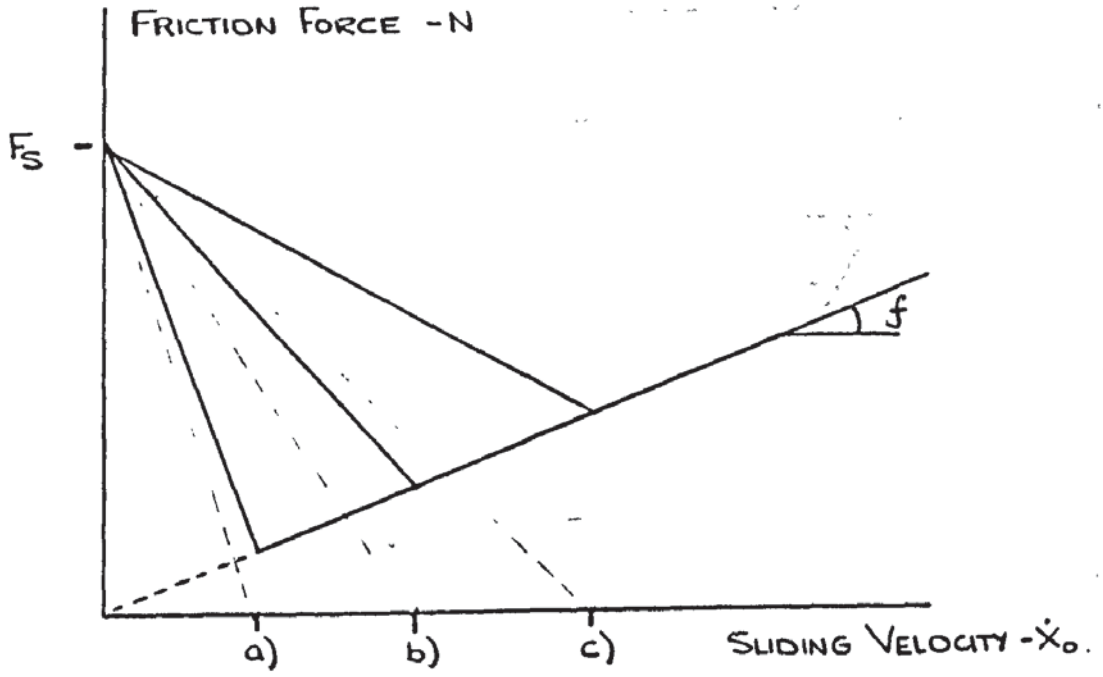

a) - V_{CL} = 1·27 mm/s.
b) - V_{CL} = 2·54 mm/s.
c) - V_{CL} = 3·81 mm/s.

SYSTEM FRICTION CHARACTERISTIC USING STRAIGHT LINES.

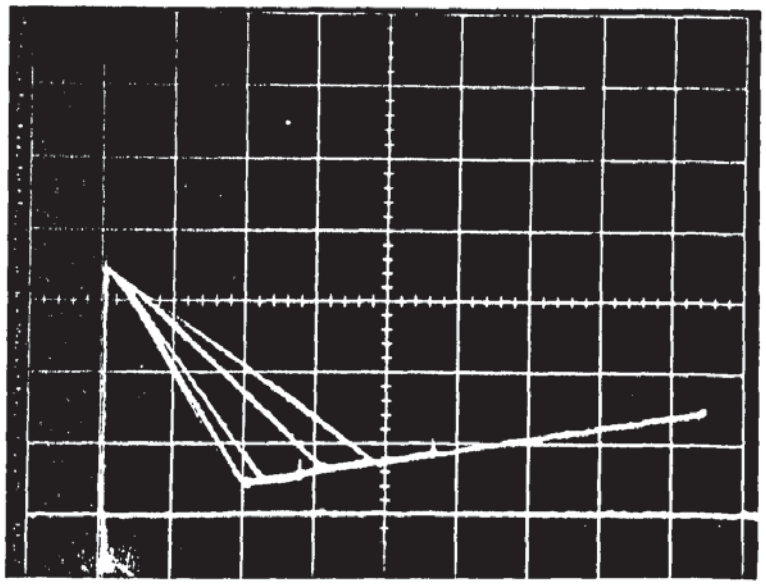

DEAD ZONE - 17V.

F_S = 771 N.

f = 35·7 Ns/mm

10V
(2·54 mm/s).

$\dot{X}_o$

SIMULATION CHARACTERISTIC (Fig 8·9)

FIG 8·10. STRAIGHT LINE FRICTION NON-LINEARITY.

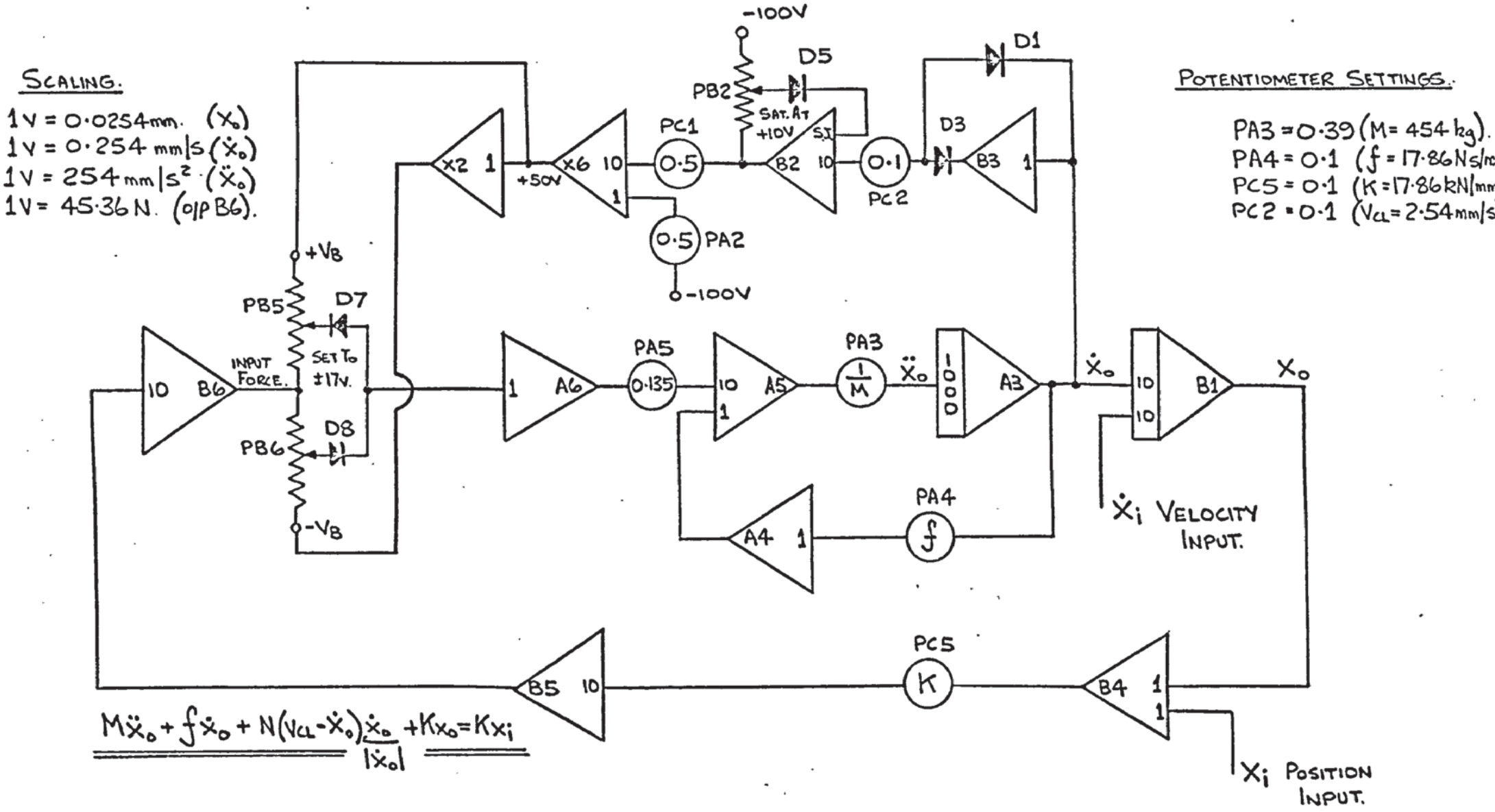

FIG. 8·11. SIMULATION CIRCUIT OF SECOND ORDER SYSTEM WITH NON-LINEAR FRICTION.

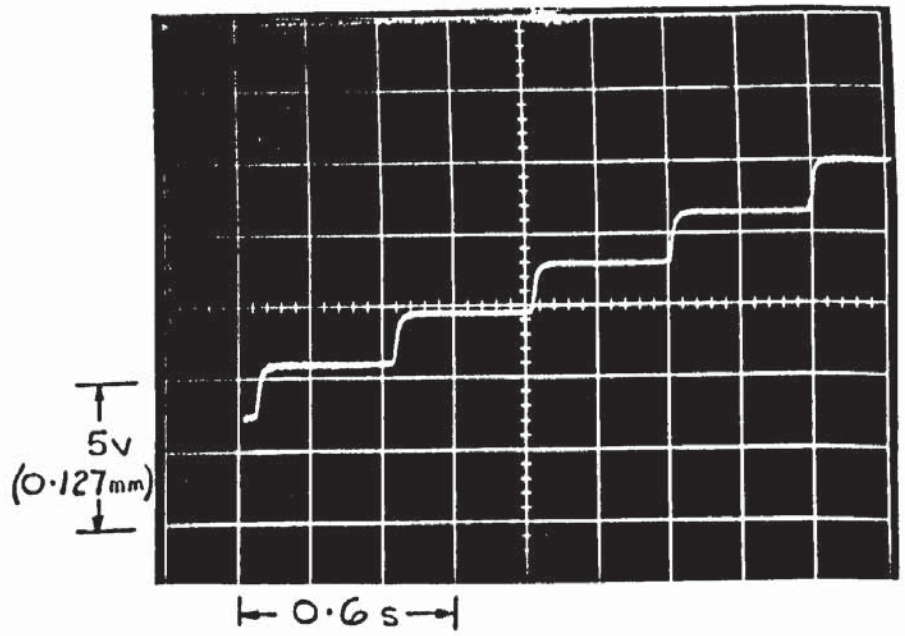

a) Output Position X_o.

V_{CL} = 2·54 mm/s

$\dot{X}_i$ = 0·12 mm/s.

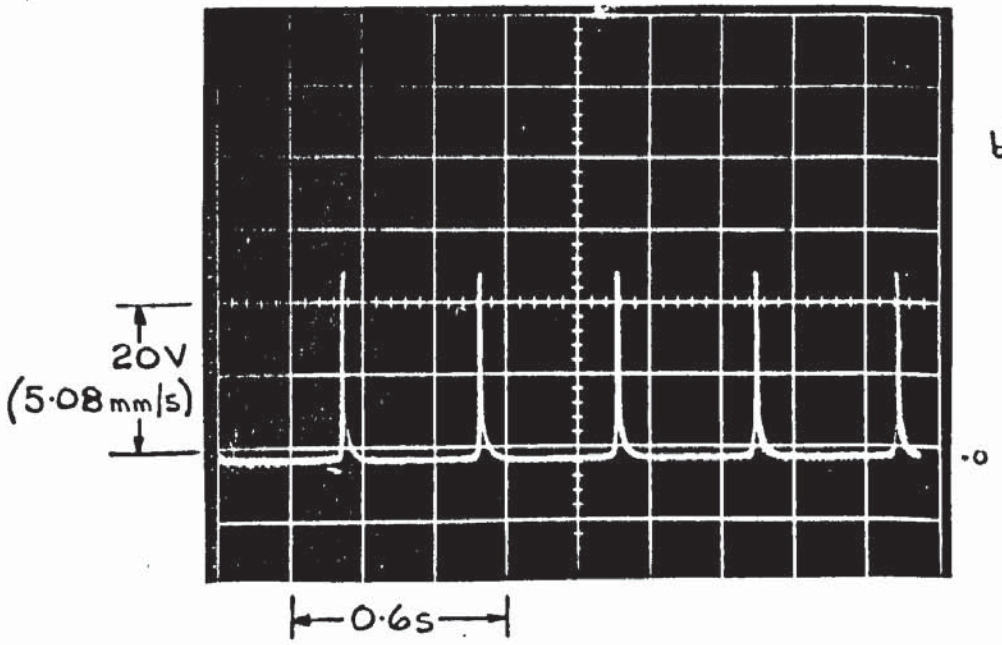

b) Output Velocity $\dot{X}_o$

V_{CL} = 2·54 mm/s.

$\dot{X}_i$ = 0·12 mm/s.

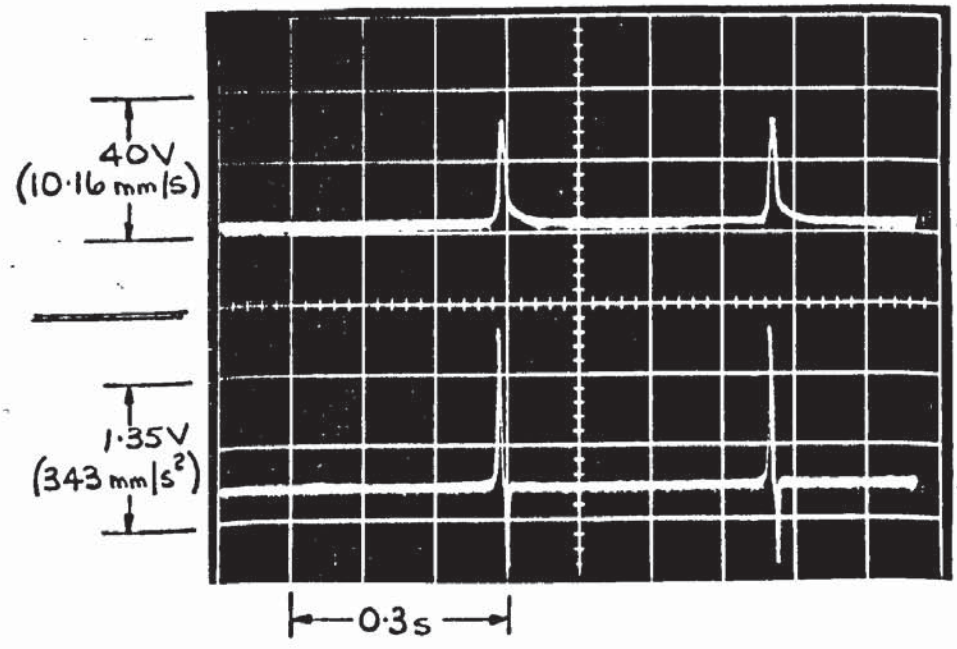

c)i Output Velocity $\dot{X}_o$

V_{CL} = 2·54 mm/s

$\dot{X}_i$ = 0·12 mm/s.

c)ii Output Acceln. $\ddot{X}_o$

Fig. 8·12. Recordings from Simulation Circuit (Fig 8·11).

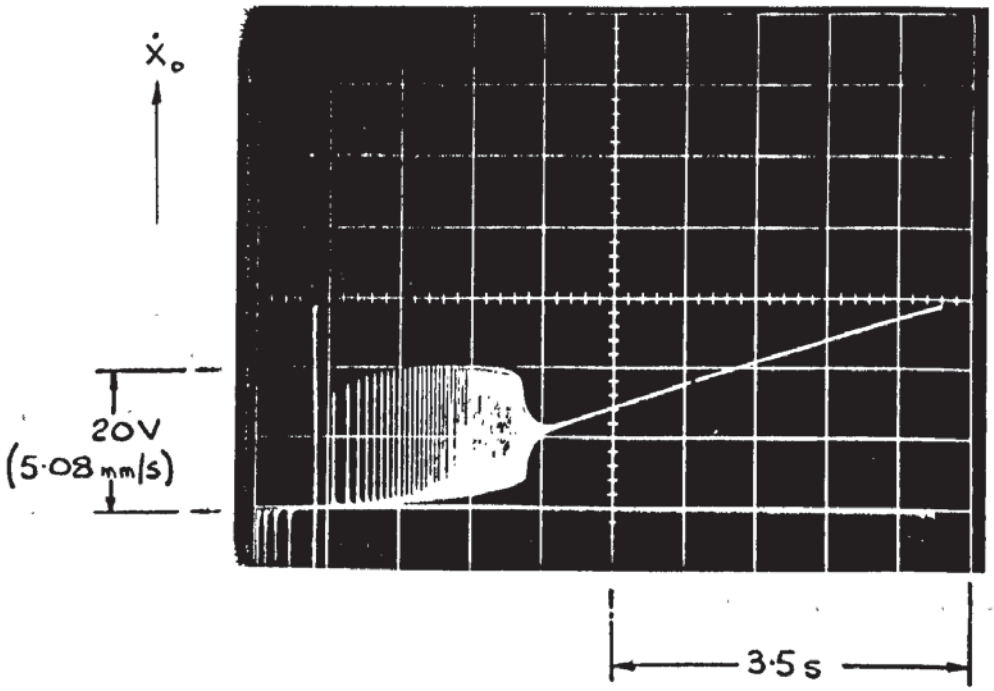

$V_{CL} = 2{\cdot}54$ mm/s.
$\dot{X}_i = 1{\cdot}21$ mm s^{-1}/s.

a) System Velocity Profile.

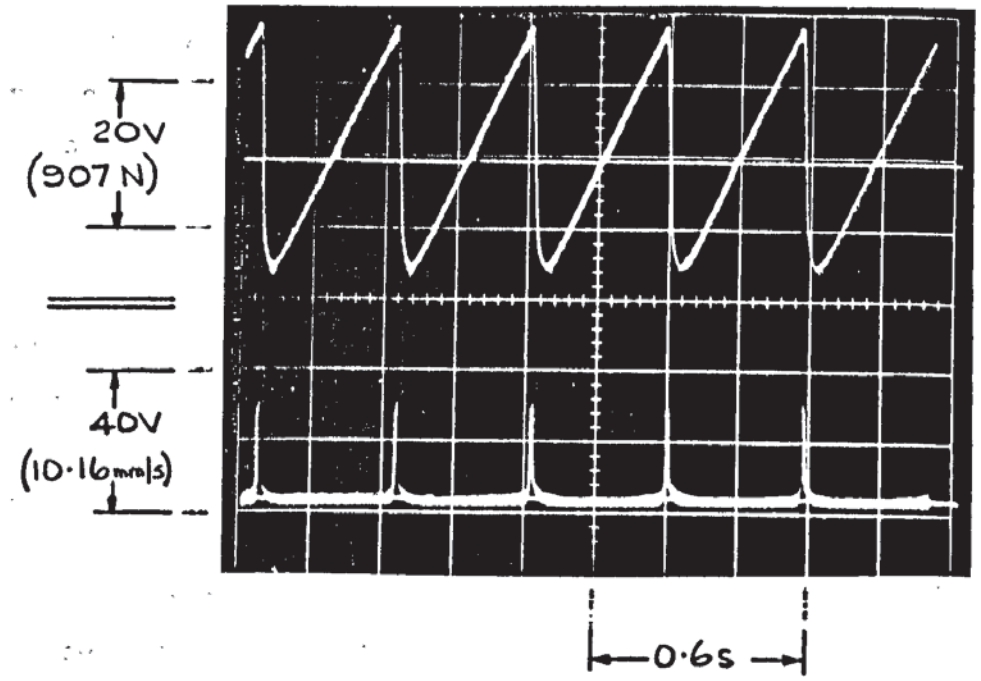

Error Force
(o/p B.6).

$V_{CL} = 2{\cdot}54$ mm/s

$\dot{X}_i = 0{\cdot}22$ mm/s.

Output Velocity
$\dot{X}_o$

b) Error Force and Output Velocity.

Fig. 8·13. Recordings from Simulation Circuit (Fig. 8·11)

As stated at the beginning of this chapter most of the simulation work was carried out before the analysis of chapter 7, and some parameter values had to be estimated. Typically these were V_{CL}, the viscous damping coefficient (f) and the static coefficient of friction. It has happened that the selected values appear to be satisfactory.

Some of the S.V.P.'s recorded practically by Britton (47) could be reproduced very closely by altering the position of the V_{CL} velocity and changing the coefficient (f), having set up the appropriate value of mass and subsequent static friction force. It is interesting to note that the critical velocity (Vc) at which oscillations would cease was always equal to the velocity V_{CL}, in other words at the velocity when the steady state friction characteristic changed from a negative slope to a positive slope. The work carried out by Bell et al (46) did not necessarily suggest this and it was difficult to see how the changes in simulation parameters could be related to his experimental changes in oil viscosity.

The development of the final simulation circuit was based upon the assumptions listed below.

1) The system simulated in Fig. 8.11 had a basically meaningful circuit and therefore the bulk of the circuit should remain.

2) The way V_B and hence the non-linear friction force (F) changes with velocity is obviously not linear. It was decided to select a square law relationship as this could be quite easily simulated.

3) If the sliding mass and drive system remained constant it was known (47) that the critical velocity reduced as the lubricant viscosity increased. It was reasoned that for a given mass the friction characteristic would not alter very much, especially the non-linear part. Therefore another mechanism must be influencing the point of critical velocity and so a first order circuit was introduced to enable a lag to occur between rapidly changing velocity and the equivalent level change in non-linear friction.

It was anticipated that these modifications would enable simulation velocity profiles to be produced which were in very good agreement with those experimentally recorded.

8.3 FINAL SIMULATION CIRCUIT

The non-linear friction force was to be related to sliding velocity through a square law relationship, (from eqn. 181-7).

$$F(\text{solid}) = N\,(V_{CL} - \dot{x}_o)^2 \qquad - 30\text{-}8$$

and $F(\text{solid}) = 0$ when $\dot{x}_o \geqslant V_{CL}$

Equation 28-8 describing the original total friction force can be rewritten as,

$$F = f\dot{x}_o + N(V_{CL} - \dot{x}_o)^2 \frac{\dot{x}_o}{|\dot{x}_o|} \qquad - 31\text{-}8$$

To achieve this type of reduction in F(solid), use is made of a multiplier (110) whose output will control the value of V_B. The circuit is shown in Fig. 8.14(a), in which a quarter squares multiplier (111) in a selected mode will give,

$$\text{Q.S.M. output} = \frac{+A^2 + B^2}{100} \text{ Volts} \qquad - 32\text{-}8$$

where A and B are the input voltages. In this mode the input voltage must be positive and the output will be positive. For negative inputs the output is zero. The output has a scaling factor of 0.01 so that if A is 100V (B = 0) then the output will be 100V. In the situation shown in Fig. 8.14 (a) input A is used and B is connected to signal ground (zero volts). V_B is to remain at 50V when $\dot{x}_o$ is zero and if this is the output voltage of the multiplier then the input at A must be 70.7V. As $\dot{x}_o$ increases the input will reduce from 70.7V and therefore V_B will reduce as a function of the square of this value. Fig. 8.14 (a) also shows a typical characteristic in which V_B will go to zero when $\dot{x}_o$ is equal to V_{CL} and the input to (A) is zero volts.

In use this multiplier is placed into the functional circuit shown in Fig. 8.14 (b). This entails minor modifications to the circuit shown in Fig. 8.9 (b). The operation is as follows,

1) When $\dot{x}_o$ is zero the output of A3 is zero, as also are the outputs of B3 and B2.

2) The output of B2 goes into amplifier X1 with an input gain of x 10. The other input to this amplifier is - 100V at unity gain. In the condition specified above the output of X1 will be + 100V.

3) This signal is attenuated by potentiometer PC1 to 70.7 volts before entering the multiplier on input (A).

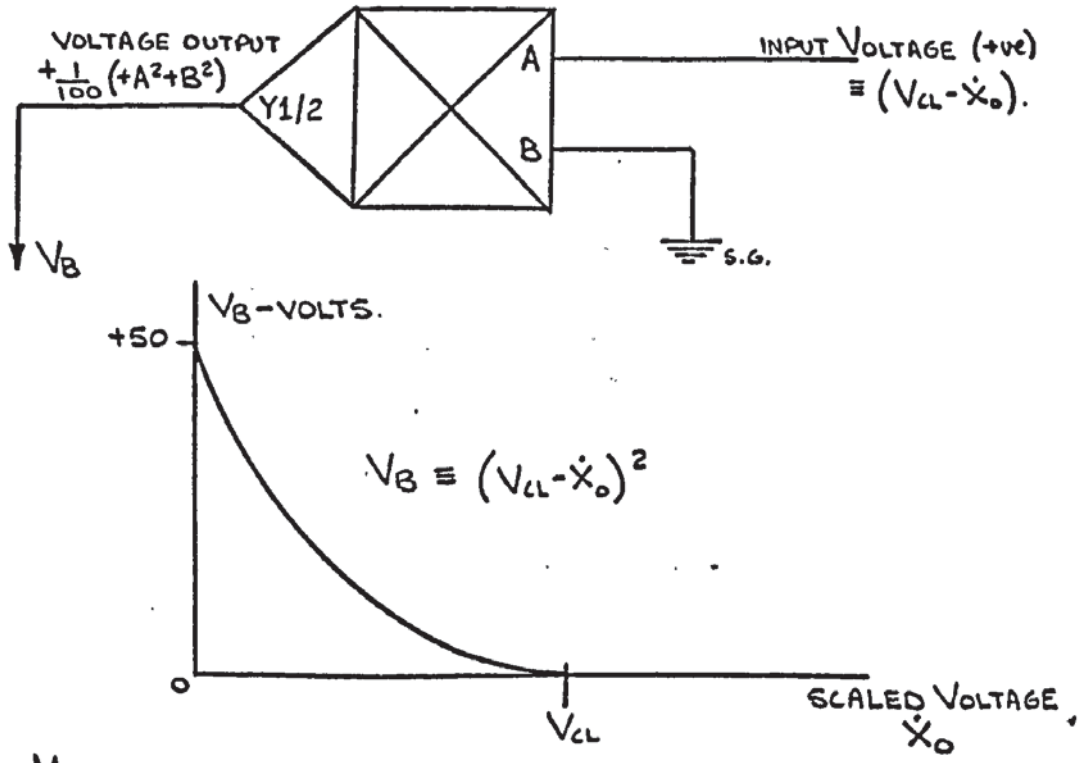

a) MULTIPLIER FUNCTION AND CHARACTERISTIC.

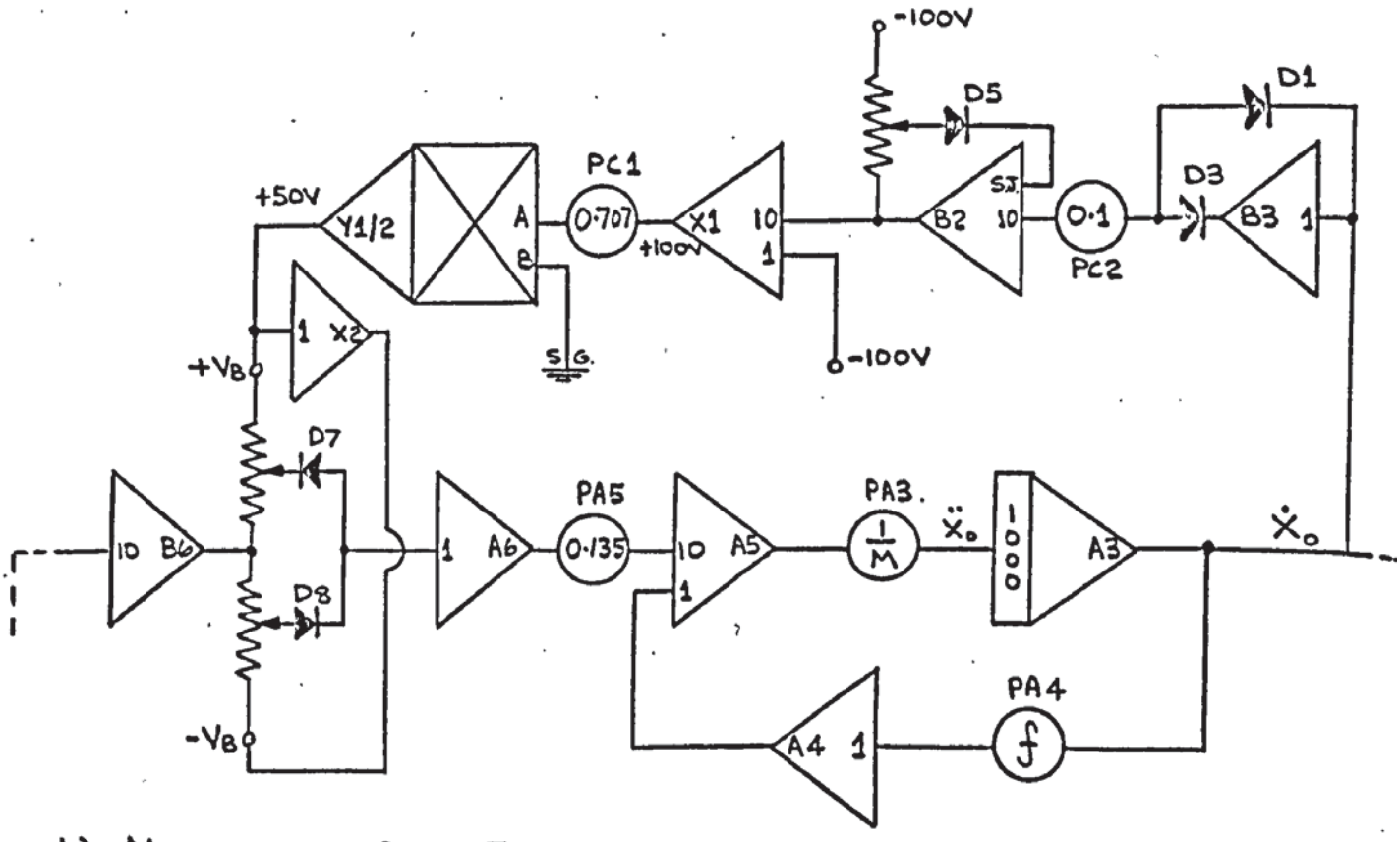

b) MULTIPLIER IN DEAD ZONE CIRCUIT.

FIG. 8·14. DEAD ZONE CONTROLLED BY SQUARE OF VELOCITY.

4) PC1 is normally set to give an output of + 50V on the multiplier. This is done by monitoring the output and adjusting PC1 in the computer problem check mode. This setting up procedure eliminates any slight errors in the multiplier. Obviously the potentiometer setting is very close to 0.7071.

5) When $\dot{x}_o$ is equal to Vcl the output of B2 will be + 10V and go into amplifier X1 to become + 100V. Therefore the output of X1 will be zero and so will the output of the multiplier.

6) B2 is set to saturate at + 10V and PC2 is set to 0.1 when Vcl is ± 2.54 mm/s (± 10V). The output of the multiplier is monitored so that when the output of A3 is ± 10V, PC2 may need to be slightly adjusted to give a multiplier output of zero.

A first order lag circuit can be introduced by replacing amplifier X1. This circuit is shown in Fig. 8.15 together with its signal flow diagram (20) and transfer function.

The transfer function has the form,

$$\frac{\text{Output}}{\text{Input}} = \frac{1}{1 + TcS} \qquad - 33\text{-}8$$

and for a given value of Tc the setting of PA1 will be,

$$\text{PA1 (setting)} = \frac{0.001}{Tc} \qquad - 34\text{-}8$$

If the setting value is below 0.05 (Tc = 0.02) then the integrator A1 must have an input gain of x 100 instead of x 1000, in which case,

$$\text{PA1 (setting)} = \frac{0.01}{Tc} \qquad - 35\text{-}8$$

where $Tc > 0.02$

There are two inputs to the network.

1) From + 100V terminal via a keyswitch and potentiometer PA2. The keyswitch was put into the line to isolate this input, and PA2 could be used to adjust the output of the network during setting up. The potentiometer was set at 0.1 and the outgoing signal was connected to an input gain on A2 of x 10. Effectively this input is made equal and opposite to the maximum value of the second input.

2) From the saturated amplifier B2 via amplifier X3 having an input gain of x 10. This meant that when the output of B2 reached its saturation level of + 10V the output of X3 would be - 100V. This signal was connected to the unity input on A2.

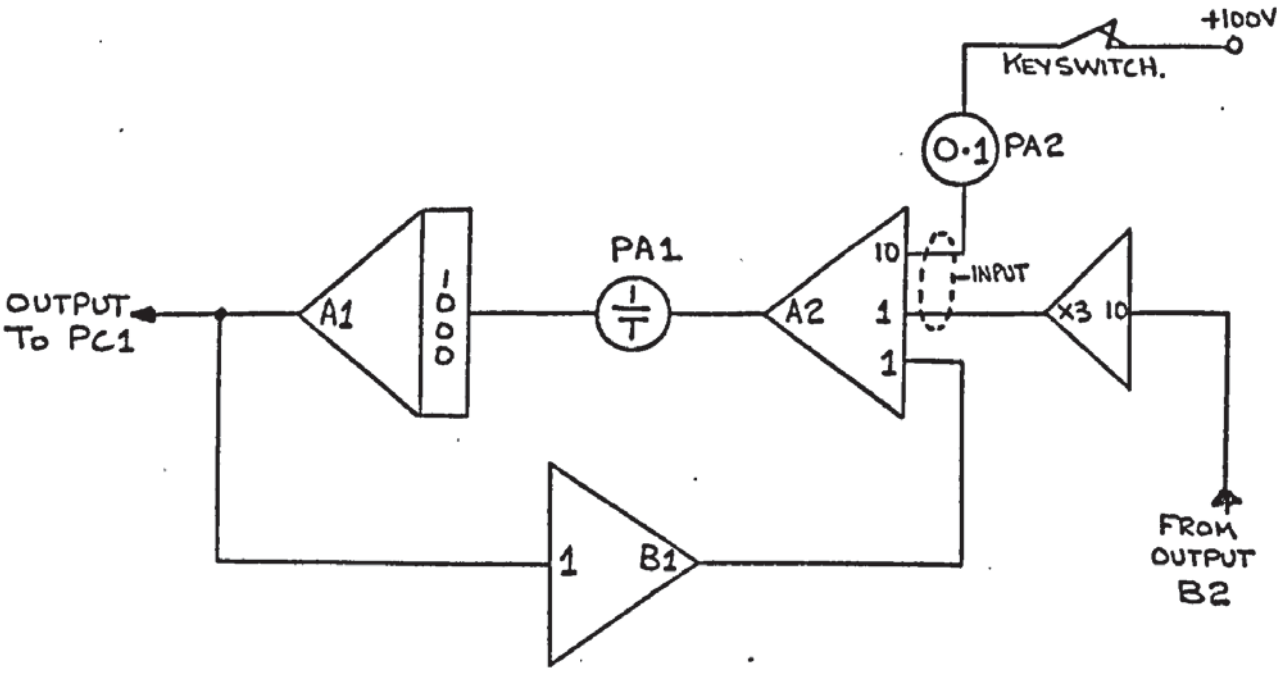

a) SIMULATION CIRCUIT FOR FIRST ORDER LAG.

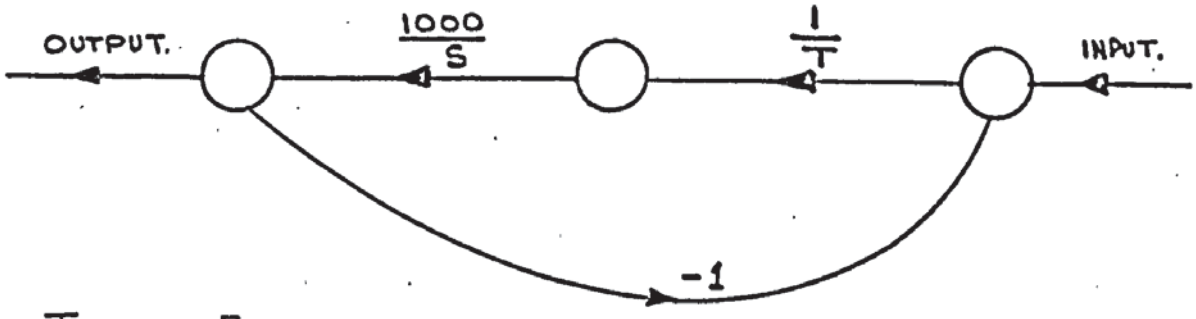

CIRCUIT TRANSFER FUNCTION
(IN LAPLACE OPERATOR)

b) SIGNAL FLOW DIAGRAM.

$$\text{OUTPUT} = \frac{\text{INPUT} \times \frac{1}{T} \times \frac{1000}{S}}{1 + \frac{1}{T} \times \frac{1000}{S} \times 1}$$

$$\frac{\text{OUTPUT}}{\text{INPUT}} = \frac{1000}{1000 + Ts} = \frac{1}{1 + T_c . S.}$$

IF PA1 = 0·1 , T = 10 AND T_c = 0·01 SECONDS. $\quad PA1 = \frac{0.001}{T_c}$.

FIG. 8·15. FIRST ORDER LAG NETWORK.

When the velocity signal was zero the output of X3 would also be zero and the output of the closed loop circuit comprising A2, A1 and B1 would be + 100V.

The effective input was the voltage difference between the two inputs mentioned above and was taken from A2 to PA1 and integrator A1. The gain of A1 and the setting of PA1 produced the effective forward path gain which could be regulated by the setting of this potentiometer. The output of A1 was fed back at unity gain via B1 to A2. In the steady state the output of the circuit would be equal in magnitude to the difference between the two inputs, i.e. a zero output from A2.

For a rapidly changing voltage input from X3 there would be a changing output of A1 lagging the input. The amount of lag, or phase shift and the degree of attenuation would depend upon the forward path gain, or the circuit time constant Tc as specified in the first order equation in 33-8.

As an example let the output of X3 be - 50V with a superimposed sinusoidally varying signal of 10V amplitude at $\frac{1}{Tc}$ radians per second. This is the system corner frequency (20) and in this condition the output of A1 will consist of a standing d.c. voltage of + 50V (100V - 50V) superimposed with a sinusoidal signal at the input frequency. The amplitude of this changing signal will be reduced to ± 7.07V (- 3dB attenuation) and there will be a lag in terms of phase shift of 45 degrees. For a particular value of Tc, the amount of attenuation and phase shift will depend upon the frequency or rate of change of the input signal.

The complete final circuit is shown in Fig. 8.16 and was used on the analogue computer to obtain all of the following results. A modification was tried by placing the lag circuit after the multiplier but this did not affect the simulation results at all. The circuit in Fig. 8.16 can be drawn in simple block diagram form as shown in Fig. 8.17 and is very similar to that suggested by Nakashima et al (54) with regard to their simulation study. However, some comments about features of their circuit and differences in capability can be made:-

a) Nakashima's circuit contains at least twice as many amplifiers which may cause added discrepancies due to amplifier drifting and changes in amplifier gain.

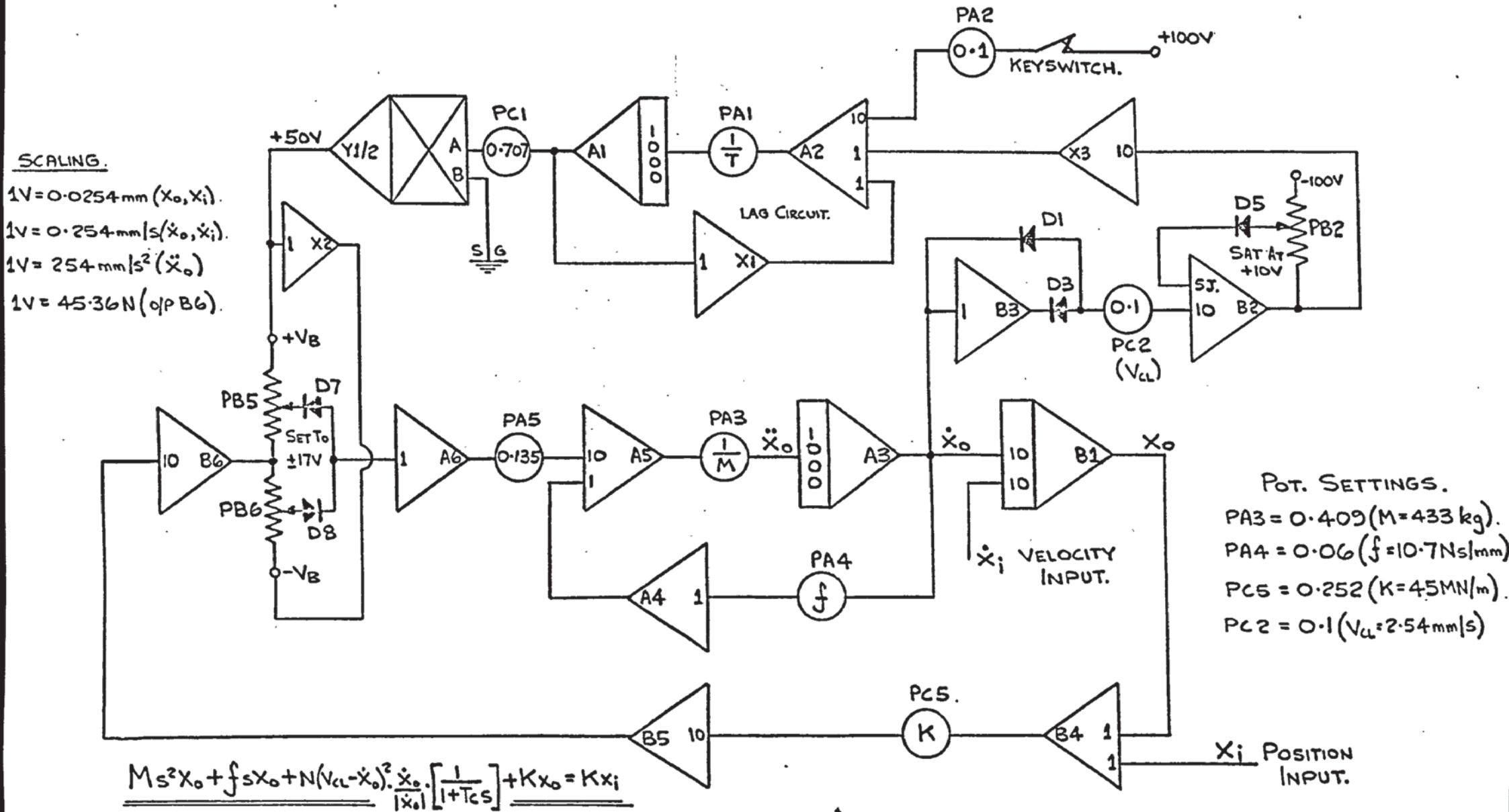

FIG. 8·16. FINAL SIMULATION CIRCUIT.

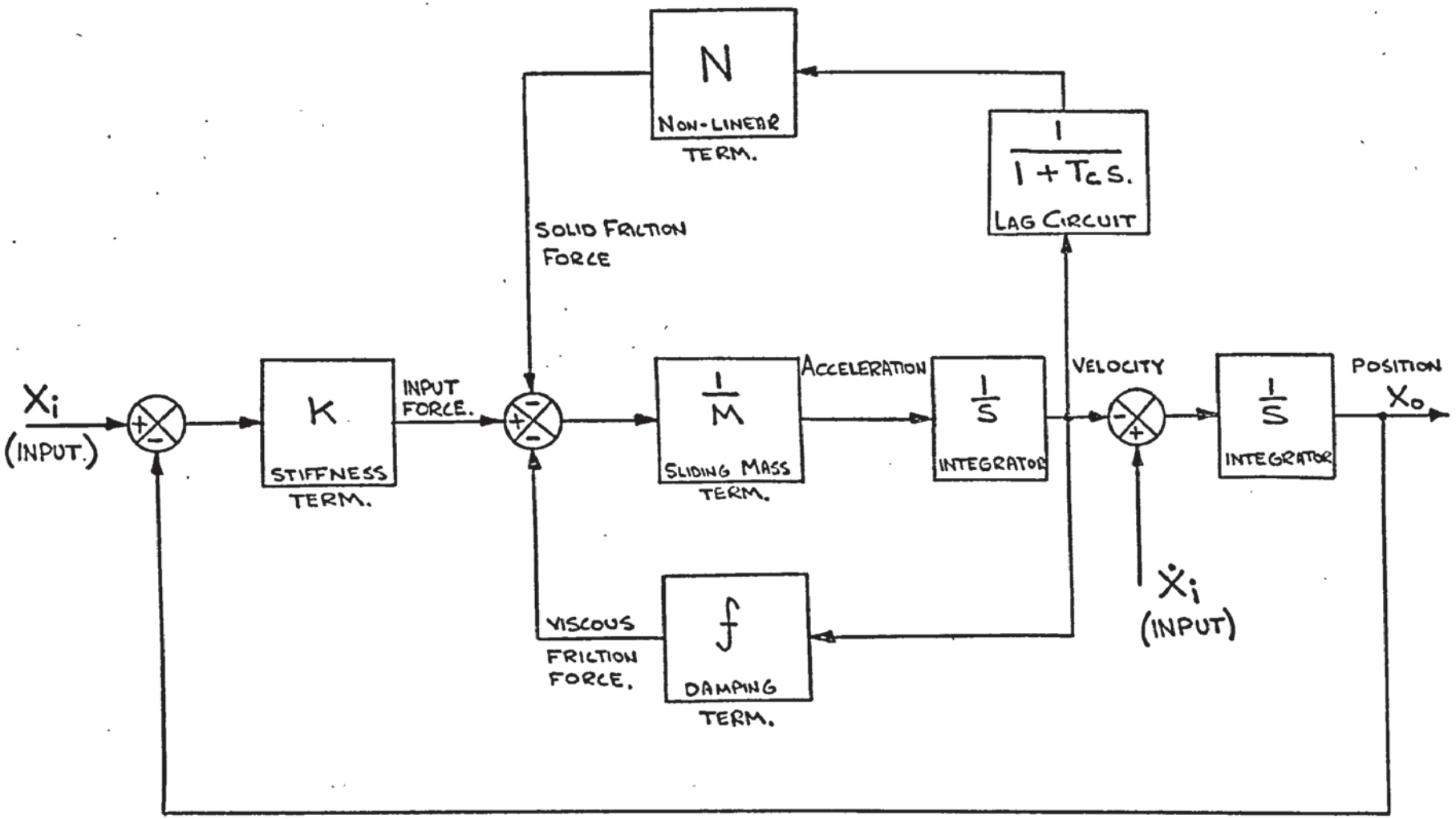

FIG. 8·17. BLOCK DIAGRAM REPRESENTING THE FINAL CIRCUIT.

b) The circuit used several multipliers as "electronic potentiometers" (111) which will lead to inaccuracies, especially under high frequency dynamic conditions.

c) Negative values of $\dot{x}_o$ cannot be simulated (A unidirectional sliding system is simulated).

d) There are multiple inputs on his circuit for system variables such as $\dot{x}_o$ and f.

e) His main output is the total coefficient of friction for the system.

f) "Stick-slip" motion at only one set velocity can be recorded. It is not possible to have a ramp velocity input.

g) There is not a positional input (x_i)or positional output (x_o).

h) The greatest difference is the way in which the non-linear friction is applied to the rest of the system. Nakashima used five relays to do this, and in the author's opinion this is not good simulation technique. The use of relays in simulation work is outdated and as his computer has a voltage range of ± 10V these could have been replaced by digital cos/mos analogue switches (114) which have extremely high frequency response and are free from hysteresis problems.

Both circuits entail the breakdown of the friction into two parts, the linear and non-linear. The application of the non-linear friction in the author's circuit is done through the use of a dead zone circuit and whilst admitting that this is a compromise, the circuit in Fig. 8.16 is representative of a complete slideway system. One limitation is that slideway movement for a position input is severely restricted.

8.4 BASIC SIMULATION RESULTS

The recordings shown in this section are similar to those that have been experimentally recorded by researchers mentioned in chapter 2.

Most of these recordings were taken with some of the system parameters set at the values listed below. Where these are varied due attention will be drawn.

SETTING FOR SIMULATION RECORDINGS

M = 433kg PA3 = 0.408

K = 45 KN/mm PC5 = 0.252

f = 10.7 N.s./mm PA4 = 0.06

Fs = 771N (μs = 0.178), V_B = 17V ($\dot{x}_o$ = o)

V_{CL} varies from 1.27 mm/s to 25.4 mm/s

Tc varies from 0.025s to 0.006s

Fig. 8.18 illustrates the steady state friction characteristic for very slow changes in input velocity. This was recorded for a very high value of Tc of 0.5s. Also shown are the variations in characteristic with changes in the position of V_{CL}.

The stick-slip motion is shown in Fig. 8.19 in terms of output position and velocity and in Fig. 8.20 of velocity and acceleration. The input velocity and values of V_{CL} and Tc are stated with the illustrations.

The positional error against time is illustrated in Fig. 8.21 using the same settings of the parameters as the previous illustrations.

Usually the dynamic friction characteristic is done by plotting the error force or input force against output velocity, and this is illustrated in Fig. 8.22 under stick-slip conditions. Superimposed on this curve is the steady state friction characteristic. Fig. 8.23 illustrates the same characteristic but this time under quasi-harmonic conditions which occur at a higher output velocity.

A system velocity profile is shown in Fig. 8.24 for an increasing input velocity of 1.2 mm s^{-1}/s and Fig. 8.25 illustrates the changes in input force over the same input velocity range. It can be seen from this recording that the oscillation ceases whilst the friction characteristic is still on the negative gradient.

Finally Fig. 8.26 illustrates the "frequency" of slideway oscillations plotted against input velocity for the same parameter settings as Figs. 8.24 and 8.25. In previous work (12) (54) the "frequency" has always been determined from the periodic changes in positional error or input force and in Fig. 8.26 the latter variable has been used.

It can be seen from all the results illustrated that they are in very good agreement with the practical data recorded by other researchers. In particular Fig. 8.24 is comparable with the recordings made by Britton (47)

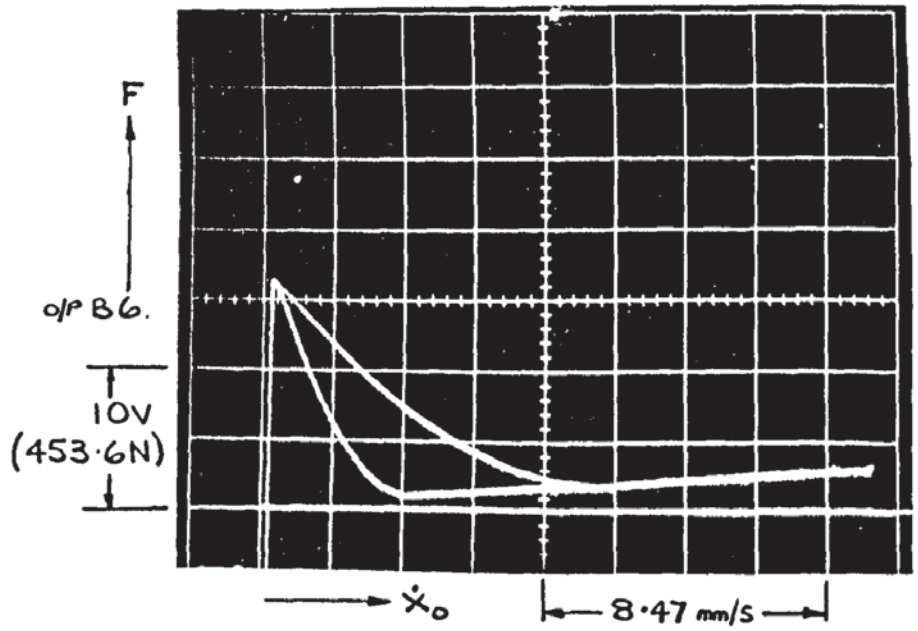

FIG. 8·18. FRICTION CHARACTERISTICS.

T_c = 0·5s
f = 10·7Ns/mm.
F_s = 771 N.

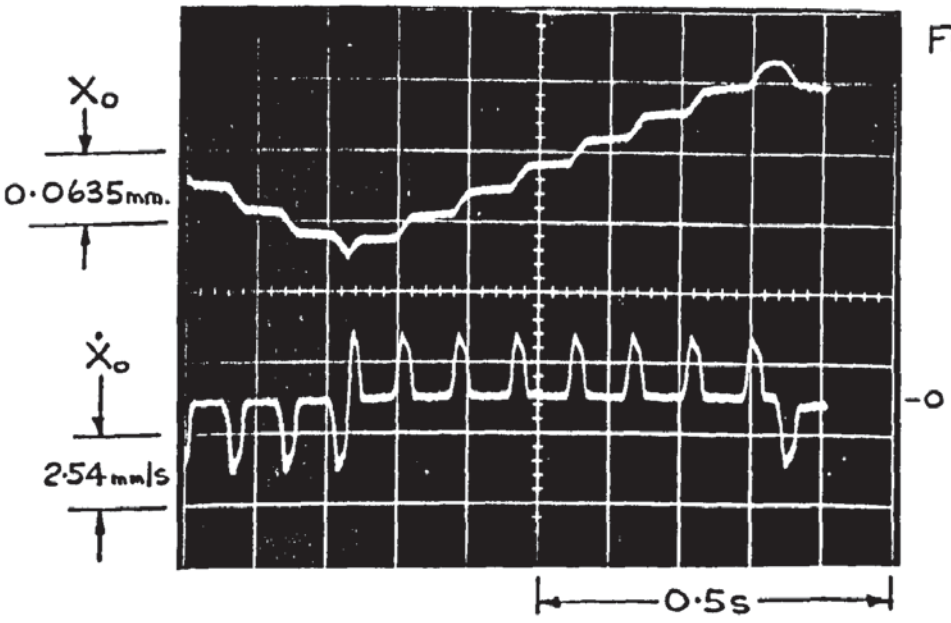

FIG 8·19. STICK-SLIP MOTION.

V_{CL} = 2·54 mm/s
T_c = 0·0125 s.
$\dot{x}_i$ = 0·13 mm/s.

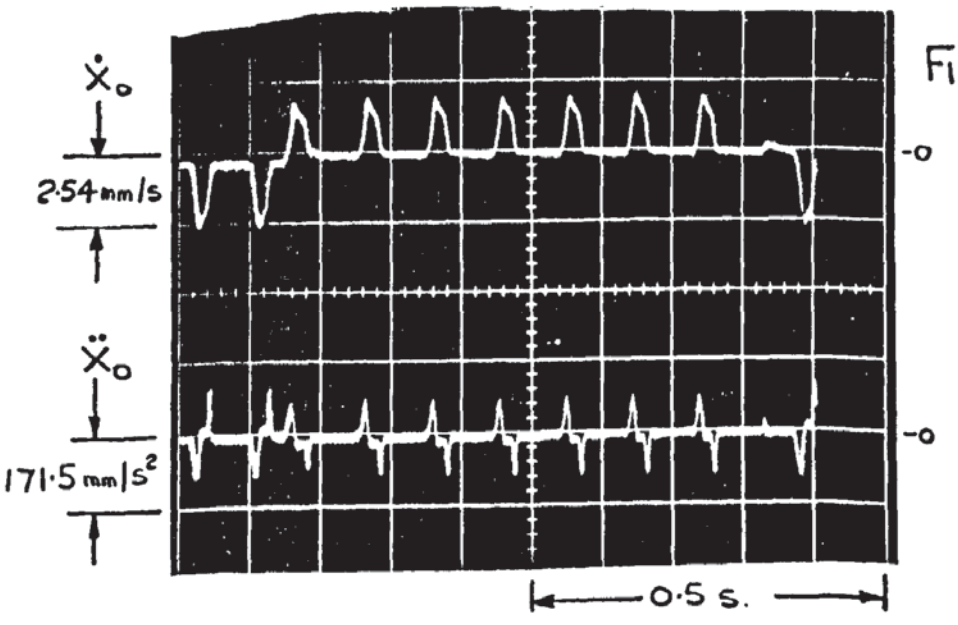

FIG. 8·20. STICK-SLIP MOTION.

V_{CL} = 2·54 mm/s.
T_c = 0·0125 s.
$\dot{x}_i$ = 0·13 mm/s.

RECORD FINAL SIMULATION CIRCUIT (FIG 8·16).

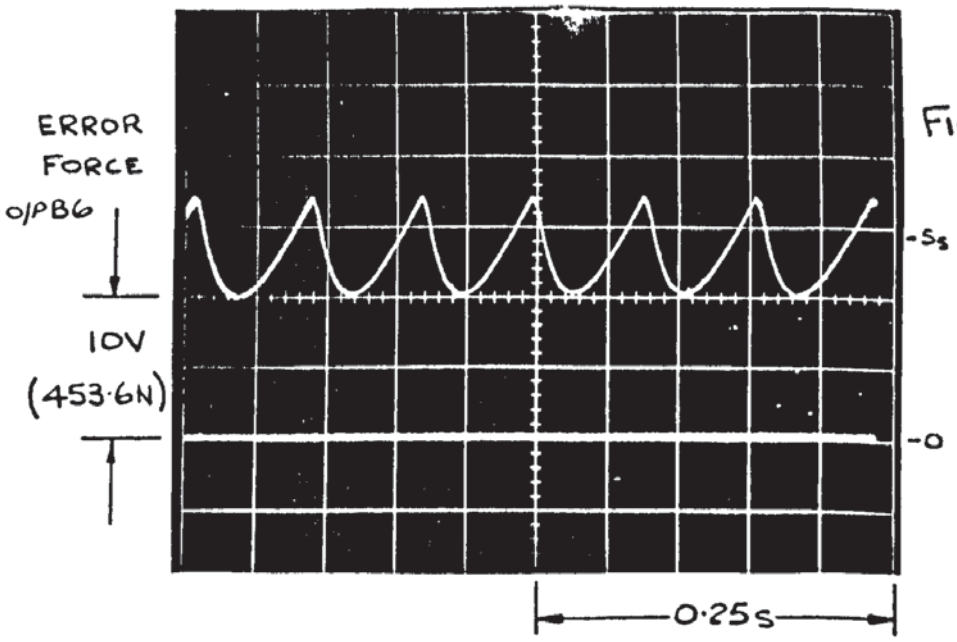

FIG. 8·21. STICK-SLIP MOTION

V_{CL} = 2·54
T_c = 0·0125s
$\dot{x}_i$ = 0·13mm/s.

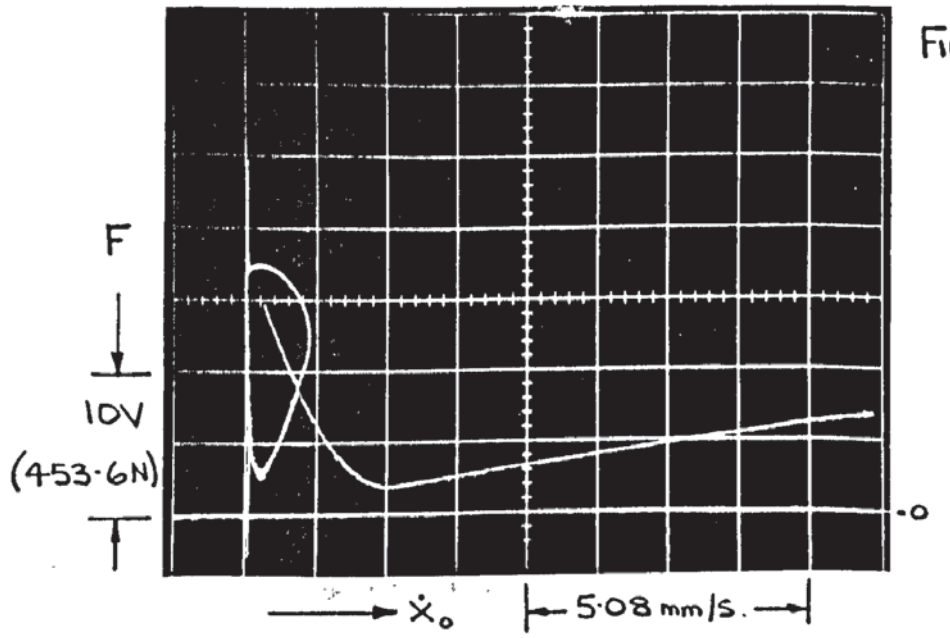

FIG. 8·22. STICK SLIP MOTION.

V_{CL} = 2·54mm/s
T_c = 0·0125s
$\dot{x}_i$ = 0·17mm/s.

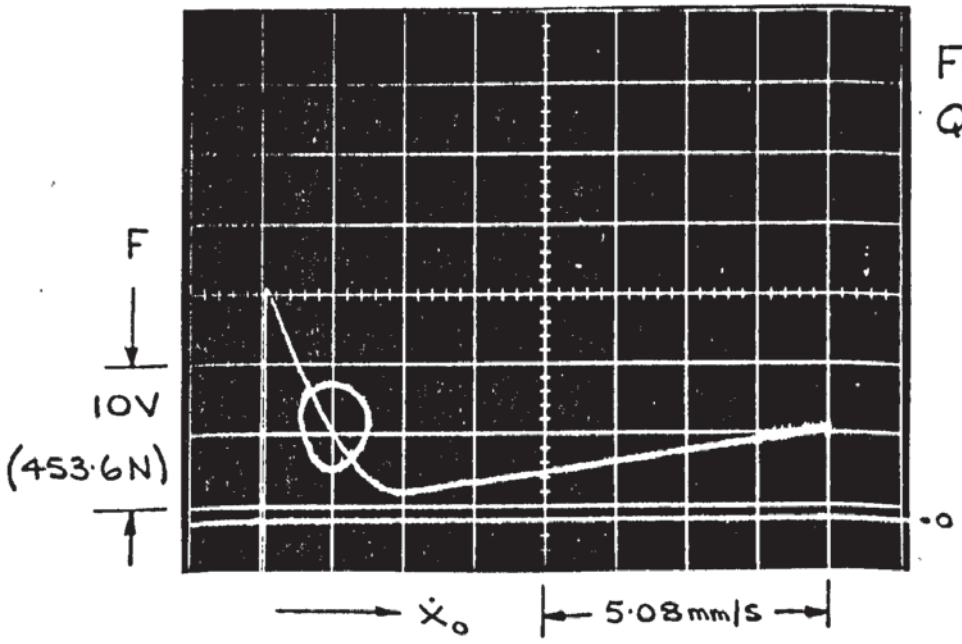

FIG 8·23.
QUASI-HARMONIC MOTION.

V_{CL} = 2·54mm/s.
T_c = 0·014s.
$\dot{x}_i$ = 1·26mm/s.

RECORDIN[illegible] FINAL SIMULATION CIRCUIT (FIG. 8·16).

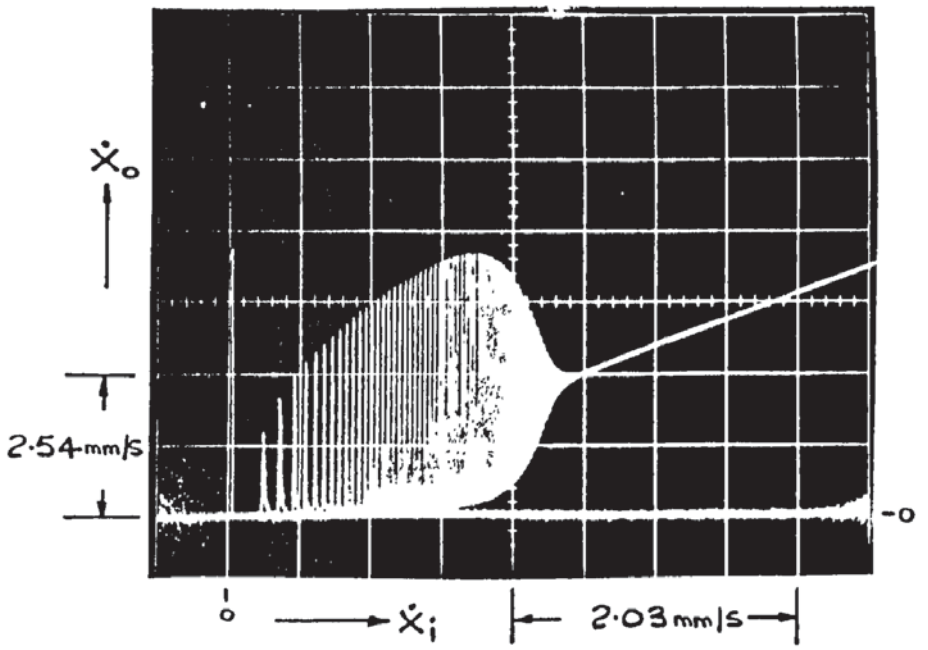

FIG 8·24. A SYSTEM VELOCITY PROFILE FROM FINAL CIRCUIT (FIG. 8·16)

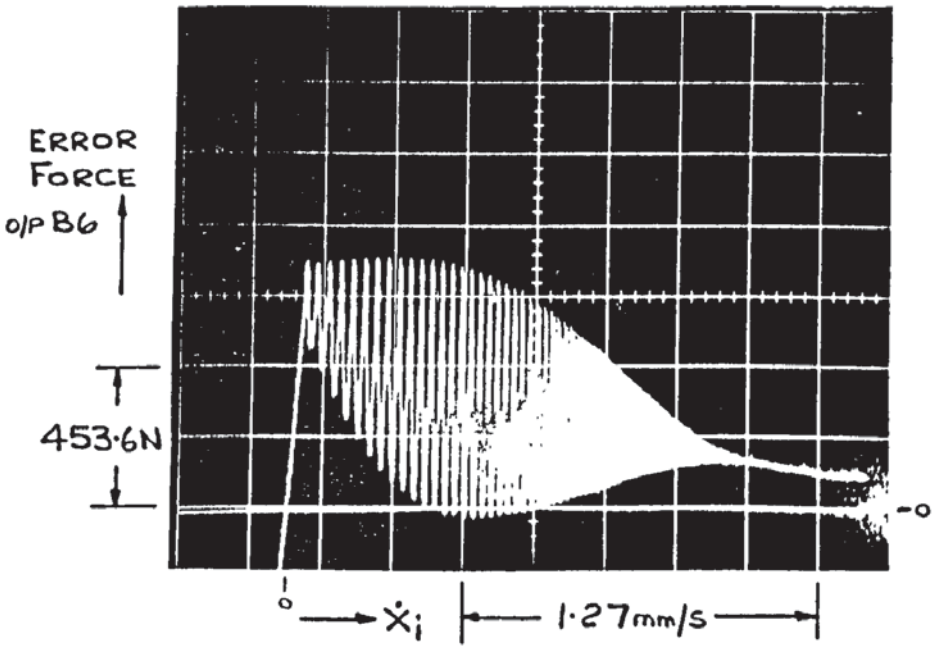

FIG. 8·25. ERROR FORCE VERSUS OUTPUT VELOCITY. FROM FINAL CIRCUIT (FIG 8·16)

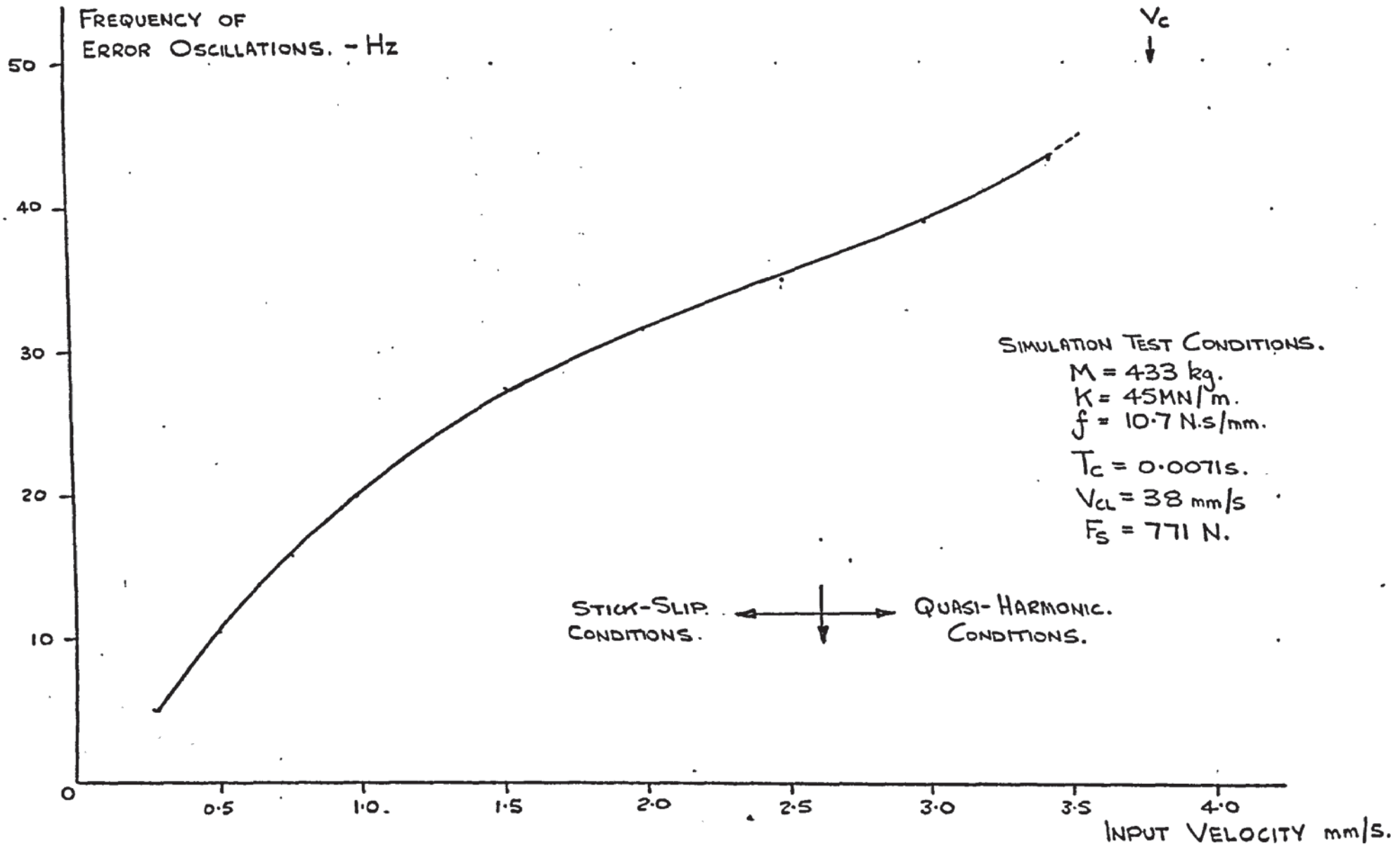

FIG 8·26. FREQUENCY OF SYSTEM OSCILLATIONS WITH CHANGES IN VELOCITY.

157.N.

of system velocity profiles. His recordings were made with a velocity sweep starting at zero to some maximum velocity. An S.V.P. for a reducing velocity input terminating at zero could not be made because of limitations in test rig size. But such a profile can be recorded from the simulation and is shown in Fig. 8.27 together with the increasing input velocity S.V.P. It can be seen that the upper critical velocity Vc is greater with increasing input velocity and is suppressed to Vc′ as the input velocity reduces to zero. This observation is new and important with respect to machine tool slideways, especially those on numerically controlled machines, where both acceleration and deceleration are controlled automatically.

The degree of change between Vc and Vc′ is due to an effect of the load mass on the system. In the reducing velocity condition it provides an inertia force which will aid the system in maintaining stable sliding conditions. In addition, the values of V_{CL} , f and Tc affect the difference between these two velocities but it was not possible on the simulation to obtain a value of Vc′ greater than Vc.

Finally it can be noted that for very small values of Tc the critical velocity always occurred near to the zero slope on the steady state friction characteristic. The introduction of this time constant into the circuit, coupled with the fact that the non-linear friction had a square law relationship with velocity, gave great flexibility in controlling the shape of the S.V.P. and the critical velocity Vc, the other variables remaining constant.

8.5 FURTHER SIMULATION RESULTS

This section deals in particular with the effect of changes in Tc and V_{CL} on the critical velocity (Vc) for increasing command velocity and a study of quasi-harmonic motion (24) especially near to the critical velocity.

The critical velocity Vc is not particularly easy to determine from the S.V.P. as some transient effects are carried forward beyond the true point for Vc giving slightly larger values. The simulation shows that, for a particular system, the point at which oscillations cease depends upon the rate of change of input velocity. Fig. 8.28 illustrates this point with a recording of S.V.P.'s from the same system as that for the recordings in Fig. 8.27 but with an input velocity rate of 2.4 $mm.s^{-1}/s$.

a) Increasing Velocity Input.

b) Reducing Velocity Input.

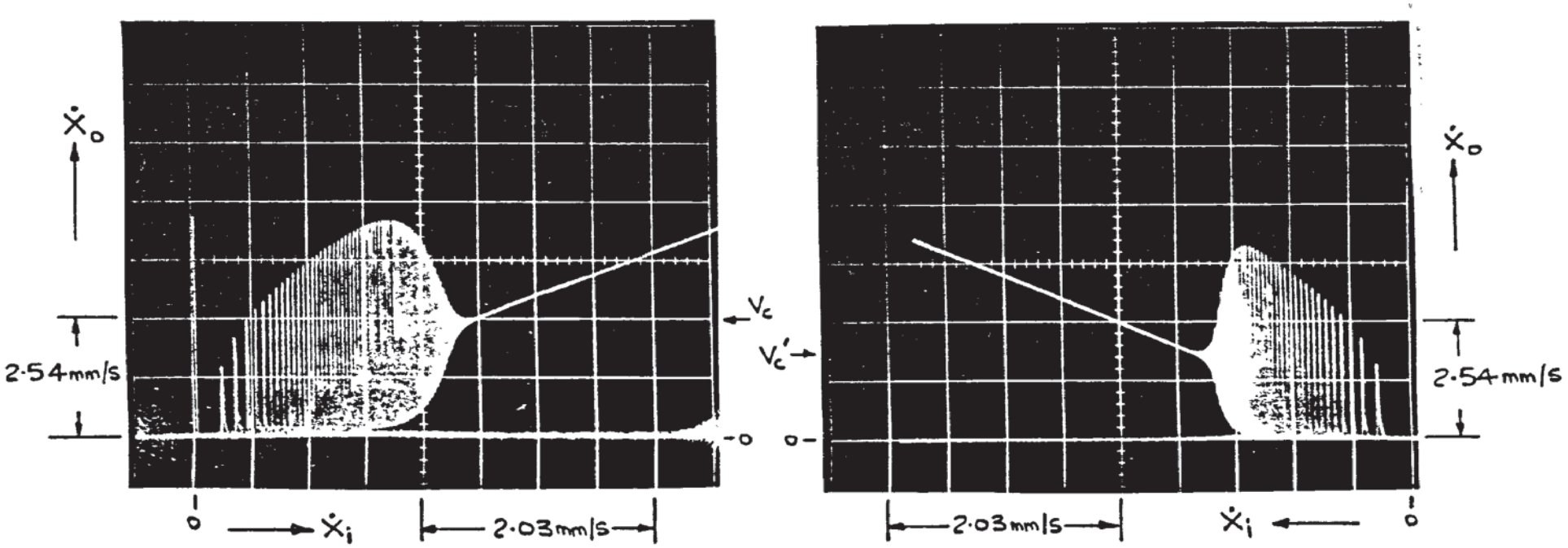

$V_{CL} = 2{\cdot}54$ mm/s.
$T_c = 0{\cdot}0065$ s.
$\ddot{X}_i = 1{\cdot}21$ mm.s^{-1}/s.

Fig. 8·27. Changes in S.V.P and V_c with Increasing and Decreasing Input Commands.

a) Increasing Velocity Input.

b) Reducing Velocity Input.

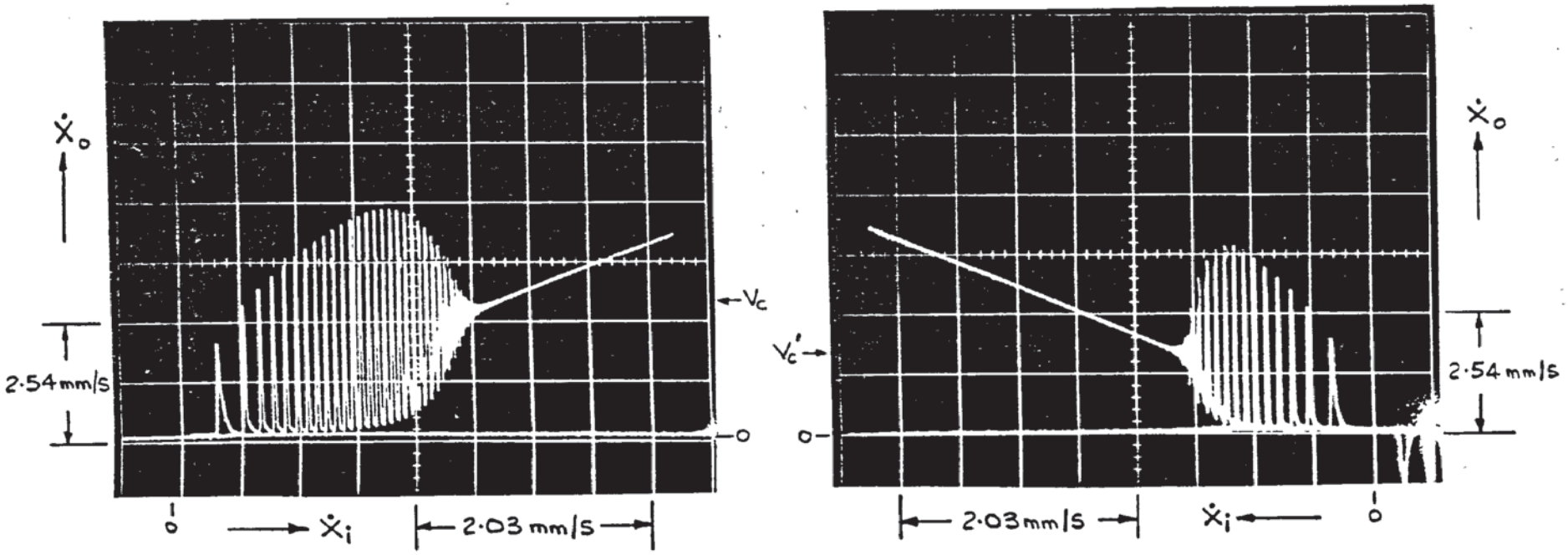

$V_{CL} = 2{\cdot}54\ \text{mm/s}$

$T_c = 0{\cdot}0065\ \text{s}$.

$\underline{\dot{X}_i = 2{\cdot}4\ \text{mm s}^{-1}/\text{s}}$

Fig 8·28. Changes in S.V.P. due to increase in rate of Input Velocity Command.

158.ii

Comparison between these two illustrations indicates that an increase in the velocity rate does give a rise in apparent critical velocity Vc. In the case of reducing velocity input Fig. 8.28b shows a greater reduction in Vc. The general shape of the S.V.P.'s change as the magnitude of ramp velocity increases.

If the velocity command rate is reduced below 1.2 mm s^{-1}/s smaller changes still occur but they are less easy to distinguish on the simulation recordings. These observations are important to note since any critical velocities established by experimental techniques depend upon the rate of velocity command. Even though a system does not exhibit oscillatory motion at one particular input, it may show oscillatory behaviour if the input rate is increased. Such a situation is illustrated in Fig. 8.29.

The effect of changes in Tc and V_{cL} on system behaviour with respect to Vc were studied for a rising velocity input of 1.2 mm.s^{-1}/s. The values of this upper critical velocity were estimated from the recordings and two sets of graphs were drawn. The first set shown in Fig. 8.30 are drawn for the selected values of Tc. However, in taking the results and checking by calculation, it was further observed that the critical velocity had occurred at the same value of slope on the solid friction curve.

The slope of the curve can be obtained from eqn. 30.8,

$$F(\text{solid}) = N(V_{cL} - V)^2$$

$$\text{and } N = \frac{Fs}{(V_{cL})^2} \qquad - 36\text{-}8$$

differentiating F(solid) with respect to V,

$$\frac{d\,F(\text{solid})}{dV} = -2N\,(V_{cL} - V) \qquad - 37\text{-}8$$

$$\text{Let} \qquad Cn = -\frac{dF}{dV} \qquad - 38\text{-}8$$

When V is equal to the critical velocity Vc,

$$Cn = 2N\,(V_{cL} - Vc) \qquad - 39\text{-}8$$

and substituting eqn. 36-8

$$Cn = \frac{2\,Fs}{(V_{cL})^2}\,(V_{cL} - Vc) \qquad - 40\text{-}8$$

It can be seen from these results that for a particular value of Tc the critical velocity (Vc) will occur at a point on any non-linear solid

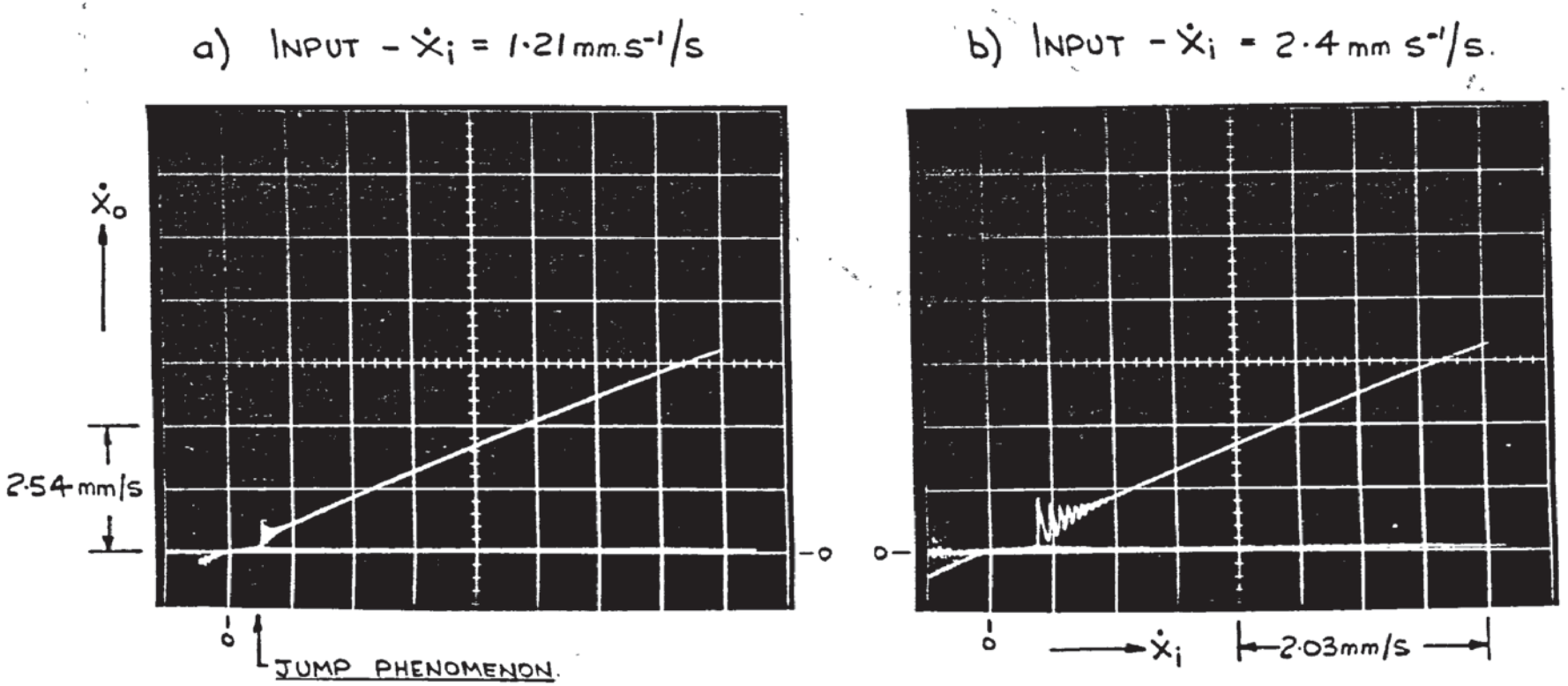

V_{CL} = 2·54 mm/s

T_c = 0·025 s.

FIG. 8·29. CHANGES IN S.V.P. DUE TO INCREASE IN RATE OF INPUT VELOCITY.

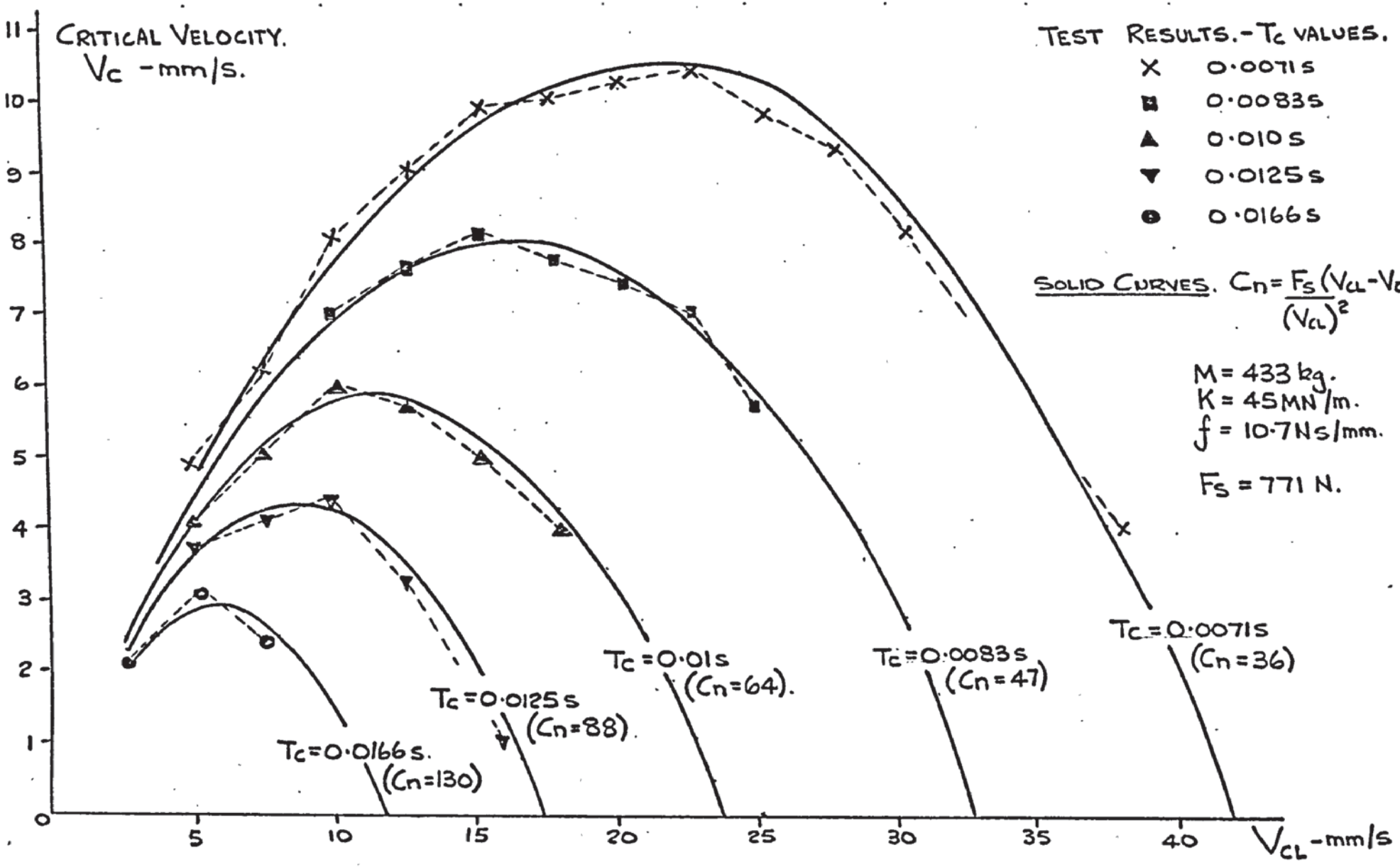

FIG. 8·30. VALUES OF V_C FOR CHANGES IN V_{CL} AND TIME CONSTANT T_C.

159.11.

friction/velocity curve where the slope Cn is the same. The value of Cn increases as Tc increases indicating that as the friction/velocity lag increases the critical velocity occurs at a steeper point on the negative friction characteristic.

For any particular value of Tc the value of Vc is dependent upon the slope of the F(solid) curve , in this case the simulation value of V_{cL} since Fs is a fixed quantity. The maximum value of Vc can be obtained by differentiating Vc with respect to V_{cL} and equating to zero.

From eqn. 40-8

$$Vc = V_{cL} - \frac{Cn(V_{cL})^2}{2Fs} \qquad - 41\text{-}8$$

$$\frac{dVc}{dV_{cL}} = 1 - \frac{CnVc}{Fs} \qquad - 42\text{-}8$$

substituting for Cn using eqn. 40-8,

$$\frac{dVc}{dV_{cL}} = 1 - \frac{2(V_{cL} - Vc)}{V_{cL}} \qquad - 43\text{-}8$$

equating eqn. 43-8 to zero then,

$$(Vc)\ max. = \frac{V_{cL}}{2} \qquad - 44\text{-}8$$

By rearranging eqn. 42-8 when it is equated to zero, then the maximum critical velocity value will occur when,

$$V_{cL} = \frac{Fs}{Cn} \qquad - 45\text{-}8$$

Therefore, with a constant value of Fs, as Tc increases so will Cn and the maximum critical velocity will reduce as shown in Fig. 8.30.

The second set of results are illustrated in Fig. 8.31. As the value of Tc reduces then it can be seen that Vc will become asymptotic to the value of V_{cL} . The mathematical expression in this figure is taken from chapter 9 and has been used to plot the curves.

If we assume that the limiting case will occur when the velocity is at a value giving zero slope on the total friction curve, by differentiating eqn. 31.8,

$$\frac{dF}{dV} = -2N(V_{cL} - V) + f \qquad - 46\text{-}8$$

Equating to zero and rearranging for V,

$$V = V_{cL} - \frac{f}{2N} \qquad - 47\text{-}8$$

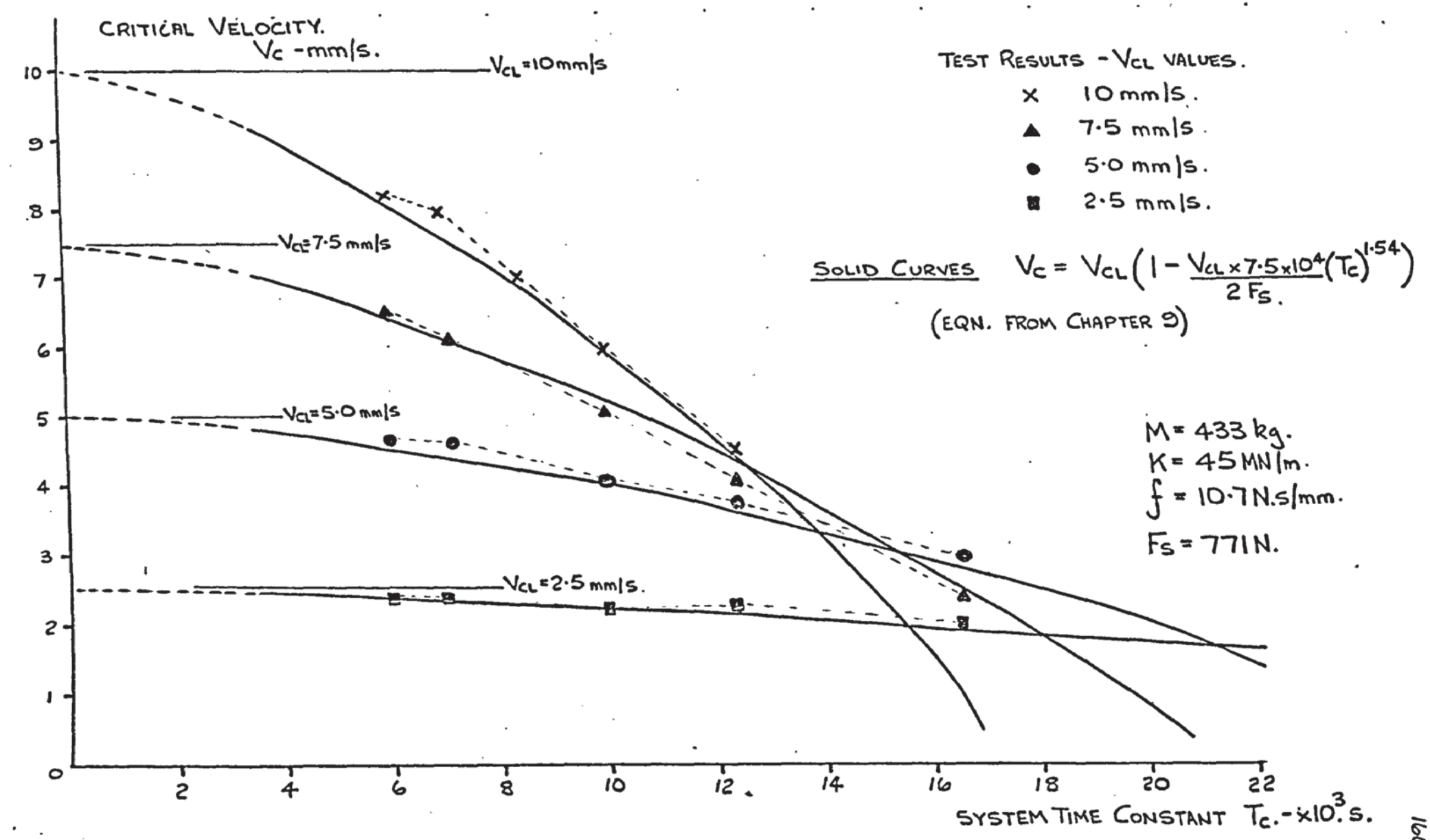

FIG 8·31. VALUES OF V_c FOR CHANGES IN T_c AND VALUES OF V_{CL}.

This value of velocity can be rewritten, by substituting for N (eqn.36-8) as

$$V = V_{cL}\left(1 - \frac{fV_{cL}}{2F_s}\right) \qquad - 48\text{-}8$$

For the given simulation parameters then

$$V = V_{cL}\left(1 - 0.00694V_{cL}\right) \qquad - 49\text{-}8$$

This velocity is the limiting value of Vc which will only occur when Tc is very close to a zero value and so is Cn.

It can be seen from these curves that Vc will have a zero value for a particular Tc and V_{cL} combination. If we look at equation 40-8 then for Vc to be zero

$$C_n = \frac{2F_s}{V_{cL}} \qquad - 50\text{-}8$$

and

$$V_{cL} = \frac{2F_s}{C_n} \qquad - 51\text{-}8$$

In order to include Tc there must be some relationship between Cn and Tc, and this point is dealt with in the following chapter.

The quasi-harmonic motion which is exhibited on the simulation recordings is now reviewed. In some conditions stick-slip will occur followed by periodic oscillations of output velocity between two non-zero values. (quasi-harmonic motion). In other cases only the latter type of oscillations will occur. The recordings taken by Britton (47) indicate that both can occur in practice. Fig. 8.32 shows the two cases recorded from the simulation.

The characteristic jump phenomenon at the start of output motion can be clearly seen, followed later by a cigar shaped profile leading to the critical velocity and stable motion. At input velocities near but below the critical velocity the oscillatory output motion is considered to be sinusoidal with equal excursions on both half cycles. This is shown in Fig. 8.33 for the conditions appertaining to Fig. 8.32a and 8.32b. The frequencies of these oscillations are very nearly equal to their system natural frequencies. The on-set of this type of motion is difficult to estimate from simulation recordings, especially if it is preceded by stick-slip motion. It is suggested at this point that it is related to the value of dF/dV (eqn. 46-8), the time constant Tc and the system natural frequency ωn.

a) System with Stick-Slip Motion.

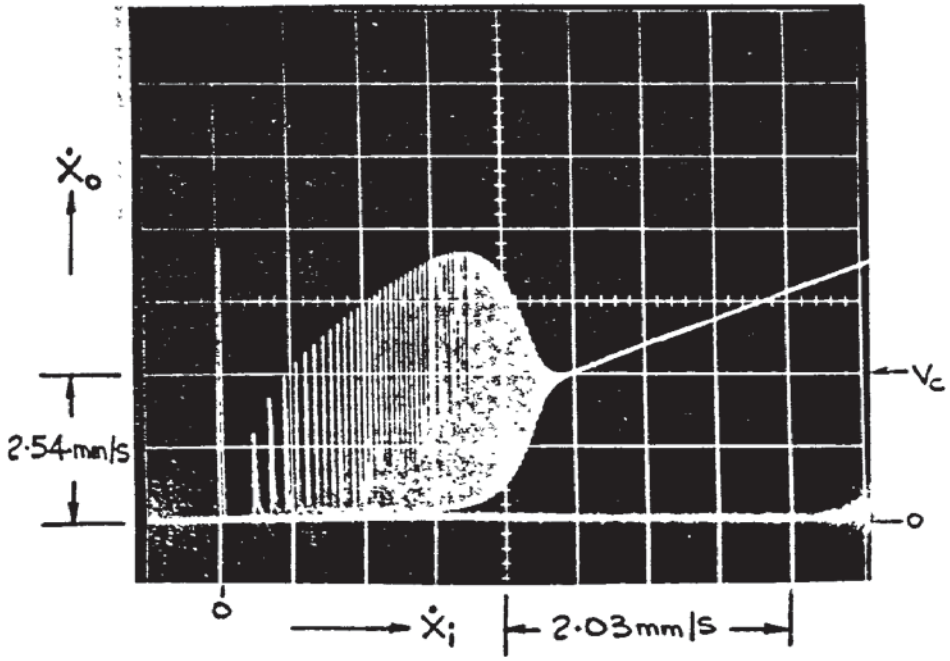

V_{cL} = 2·54 mm/s
T_c = 0·0065 s.
$\dot{X}_i$ = 1·21 mm s^{-1}/s
K = 45 MN/m.
$-f$ = 10·7 Ns/mm

b) System with Quasi-Harmonic Motion only.

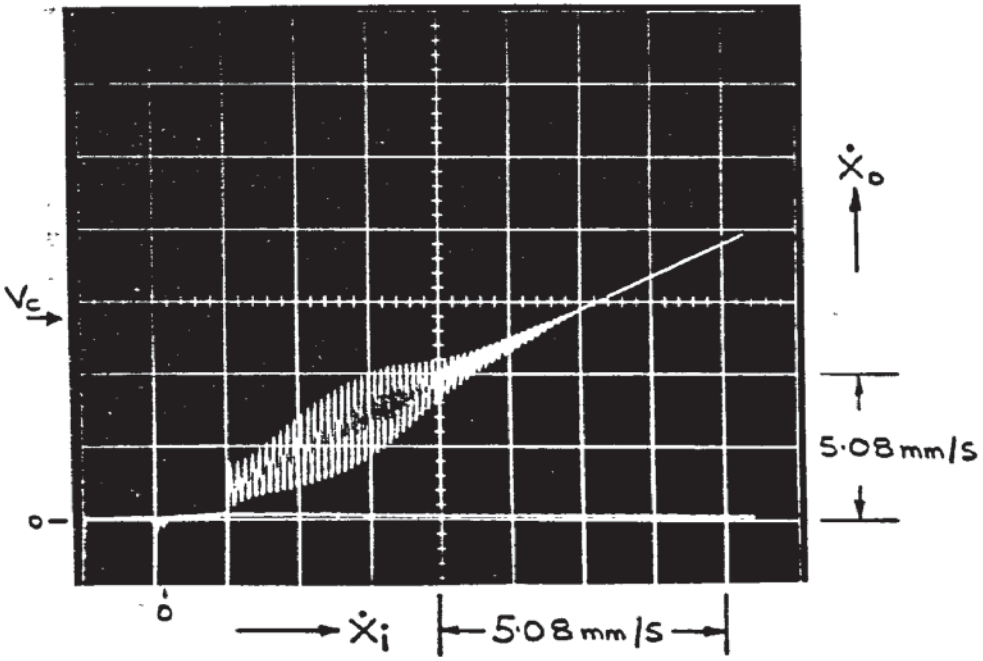

V_{cL} = 20 mm/s
T_c = 0·0083 s
$\dot{X}_i$ = 1·21 mm.s^{-1}/s
K = 2·4 MN/m.
$-f$ = 21·4 Ns/mm

FIG. 8·32 System Velocity Profiles.

a) System (Fig 8·32a.) $\omega_n = 51{\cdot}9\,Hz$

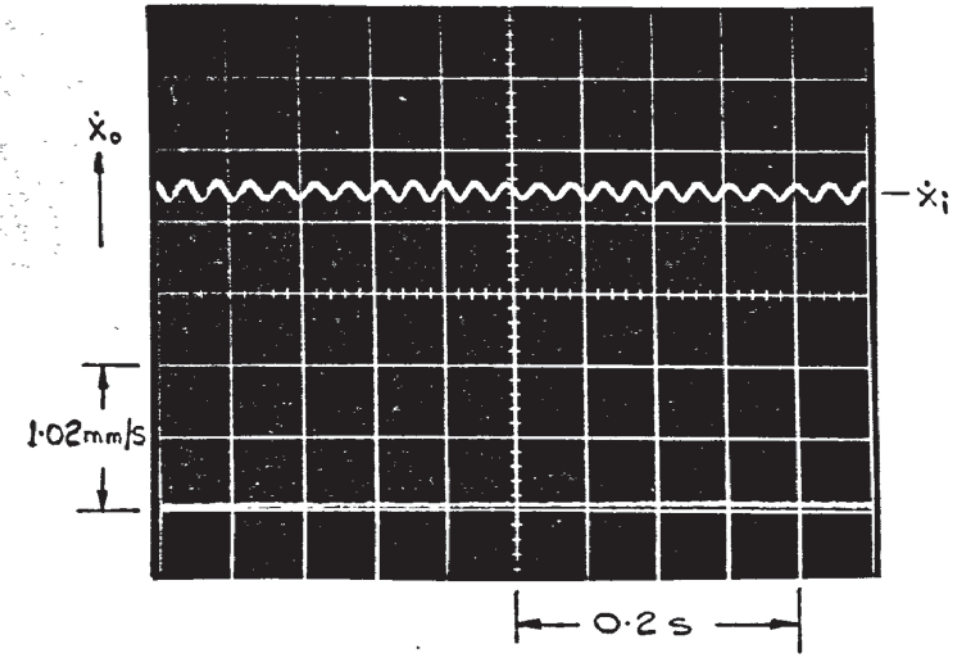

Recorded Frequency - 45 Hz

$\dot{X}_i = 2{\cdot}24$ mm/s
$V_{cl} = 2{\cdot}54$ mm/s
$T_c = 0{\cdot}0065$ s
$V_c = 2{\cdot}4$ mm/s

b) System (Fig 8·32.b) $\omega_n = 11{\cdot}85\,Hz$

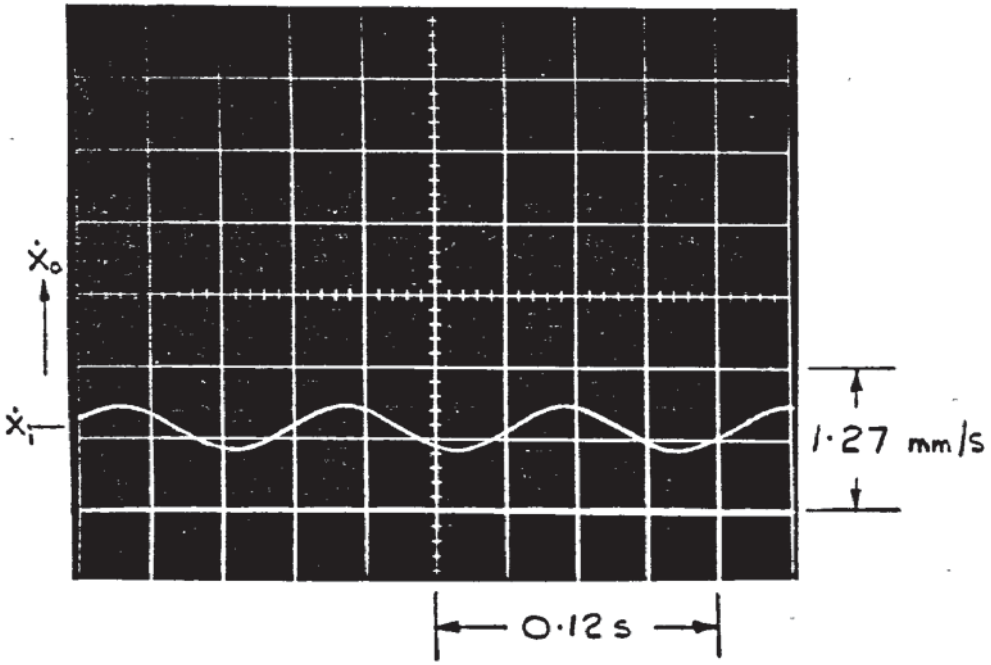

Recorded Frequency 11·1 Hz

$\dot{X}_i = 5{\cdot}08$ mm/s.
$V_{cl} = 20$ mm/s
$T_c = 0{\cdot}0083$ s.
$V_c = 5{\cdot}2$ mm/s.

Fig. 8·33. Quasi-Harmonic Motion near System Critical Velocity.

Simulation recordings show that the wave_form of the oscillatory motion, just following stick-slip, is not completely sinusoidal and there are not equal excursions either side of the "steady state" output velocity. An example of this type of wave_form is shown in Fig. 8.34 for the same system whose S.V.P. is illustrated in Fig. 8.32a.

Finally several authors (24), (47), (54), have commented on the fact that slideway critical velocity (Vc) can be reduced by increasing the drive stiffness, and therefore the undamped natural frequency. Simulation tests were carried out for changes in K only, other system parameters remaining as follows,

$M = 433kg$
$f = 10.7\ N.s/mm$
$Fs = 771N$
$Vcl = 40\ mm/s$
$Tc = 0.0071\ s$

The resulting values of Vc against K are plotted in Fig. 8.35. It can be seen that the stiffness does influence the critical velocity in the same way as experimental observations have indicated. Moreover, it was evident during the simulation that stick-slip did not occur in every case but that the slideway system did exhibit some form of indigenous oscillatory motion before stable conditions prevailed.

8.6 CONCLUSIONS

An attempt has been made to simulate a machine tool slideway system with non-linear friction. The author feels that the results compare favourably with experimental data so far recorded. Although the theoretical friction/velocity curves derived in chapter 7 have not been used due to factors mentioned earlier, the values selected are considered to be reasonable.

A theoretical analysis is made in chapter 9 with a view to relating the work of the previous chapter to the conditions of non-linear sliding motion observed here. It can be seen that there are many system variables that affect slideway motion, some of which are also parameters determining the friction/velocity characteristic.

One general observation that can be made, is that the value of a possible critical velocity will depend upon rate of change of the input

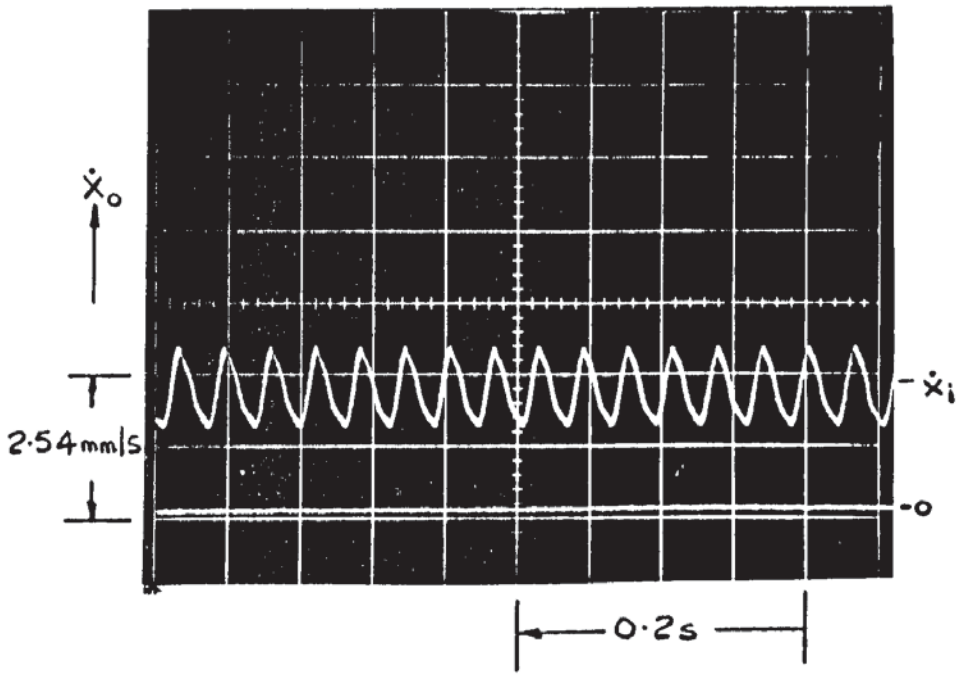

RECORDED FREQUENCY - 33Hz

SYSTEM AS FIG 8·32a.

V_{CL} = 2·54 mm/s
T_c = 0·0065s
$\dot{x}_i$ = 2·13 mm/s
K = 45MN/m
ω_n = 51·9 Hz

FIG. 8·34. QUASI-HARMONIC MOTION JUST FOLLOWING STICK-SLIP.

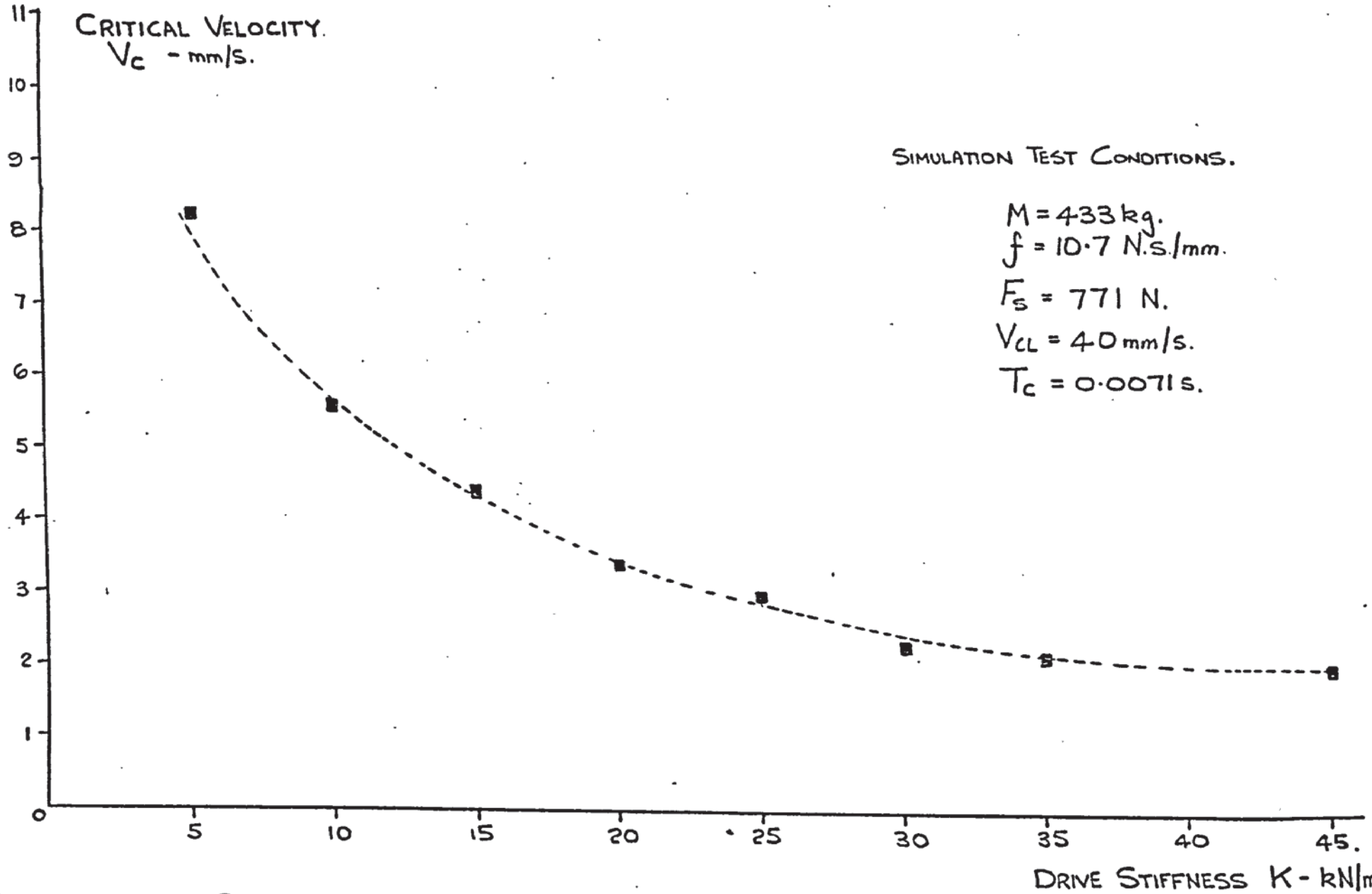

FIG. 8·35. SYSTEM CRITICAL VELOCITY WITH CHANGES IN DRIVE STIFFNESS.

force counterbalancing the rate of change of the non-linear friction force. After such a balance has been accomplished stable motion will occur. This of course will mean that oscillatory motion may start at some relatively high velocity due to the steady state friction characteristic having a slightly positive gradient at small velocities before becoming progressively negative. This oscillatory starting velocity has been called the lower critical velocity (24) and the author is of the opinion that this condition is not worth considering from a machine tool point of view as only the suppression of the "upper critical velocity" or Vc is of importance.

Finally, the non-linear motion is affected by the system "viscous" damping term. It is likely that the simulation value of (f) has an association with the solid friction behaviour. In practice such a term may be difficult to measure.

CHAPTER 9

A THEORETICAL ANALYSIS OF NON-LINEAR FRICTION BEHAVIOUR

9.1 INTRODUCTION

The simulation results together with mathematical relationships established in chapter 7 will be used to try and establish as complete a picture as possible of a friction system appertaining to a machine tool slideway. In particular the activities that take place at slow sliding speeds causing non-linear motion of the moving table.

The upper critical velocity, above which stable motion occurs, is considered to be most important. Its calculation in terms of the other system parameters will aid the engineer in the design of slideway systems.

One outstanding feature to be resolved here is the relationship between some surface parameters, including lubricant properties and the simulation time constant (Tc). Once such a relationship can be found an equation for the critical velocity can be attempted.

It has been shown in this thesis that the drive stiffness has a major effect upon the S.V.P. and the critical velocity. The drive stiffness has a unique position in the slideway system. It is completely independent of all other parameters and does not affect the friction characteristic. In contrast the sliding weight has a major influence on the friction characteristic as well as an effect on the system natural frequency. It is suggested here that, to a great extent, these effects counterbalance one another and there is an indication that although the sliding weight affects the S.V.P., it has only a minor influence on the value of the critical velocity. (This particular observation has also been made by Bell (47)).

For a given slideway configuration with fixed values of drive stiffness, mass and surface finish, the only other affecting parameter is the lubricant. Experimental work (47) has shown that as its viscosity increases the critical velocity reduces. The lubricant is likely to have two spheres of influence, one in changing the shape of the friction characteristics and the other in modifying the surface time constant. It is suggested here that

the former has greater importance. Similarly the addition of polar additives will cause marked changes in slideway friction.

The chapter starts with the analysis of results obtained from the simulation work. This gives rise to fairly simple mathematical relationships governing system performance. Data from chapter 7 is then used to provide a realistic mathematical interpretation of the non-linear behaviour. The resulting equations, although complex, could be useful to the design engineer by showing the relationship between measureable parameters.
Note. The analysis is presented in S.I. units. Where data has been taken from other sources it is quoted in its original units.

9.2 ANALYSIS OF SIMULATION DATA

The values of critical velocity for changes in V_{cL} and Tc are plotted in Fig. 8.30. For a particular value of time constant Tc the critical velocity always occurs at the same value of slope on the steady-state dry friction characteristic (Cn).

The relationship between Tc and Cn is illustrated in Fig. 9.1. A straight line drawn through these points yields the following relationship,

$$Cn = 7.5 \times 10^4 \, (Tc)^{1.54} \quad N.s/mm \qquad - \ 1.9$$

It should be noted that this relationship exists for a particular value of drive stiffness and table weight.

The value of Cn is given by eqn. 40.8 in terms of other system parameters,

$$Cn = \frac{2\,Fs}{(V_{cL})^2} \, (V_{cL} - Vc)$$

For complete system stability, then Vc must be zero and therefore this equation will reduce to

$$Cn = \frac{2\,Fs}{V_{cL}} \qquad - \ 2.9$$

If we rewrite this equation in terms of V_{cL} and substituting eqn. 1.9 then

$$V_{cL} = \frac{2\,Fs}{7.5 \times 10^4 (Tc)^{1.54}} \qquad - \ 3.9$$

This relationship is plotted in Fig. 9.2 and the curve marks the division between the unstable region where some oscillatory motion will occur, and the stable region where Vc will be zero.

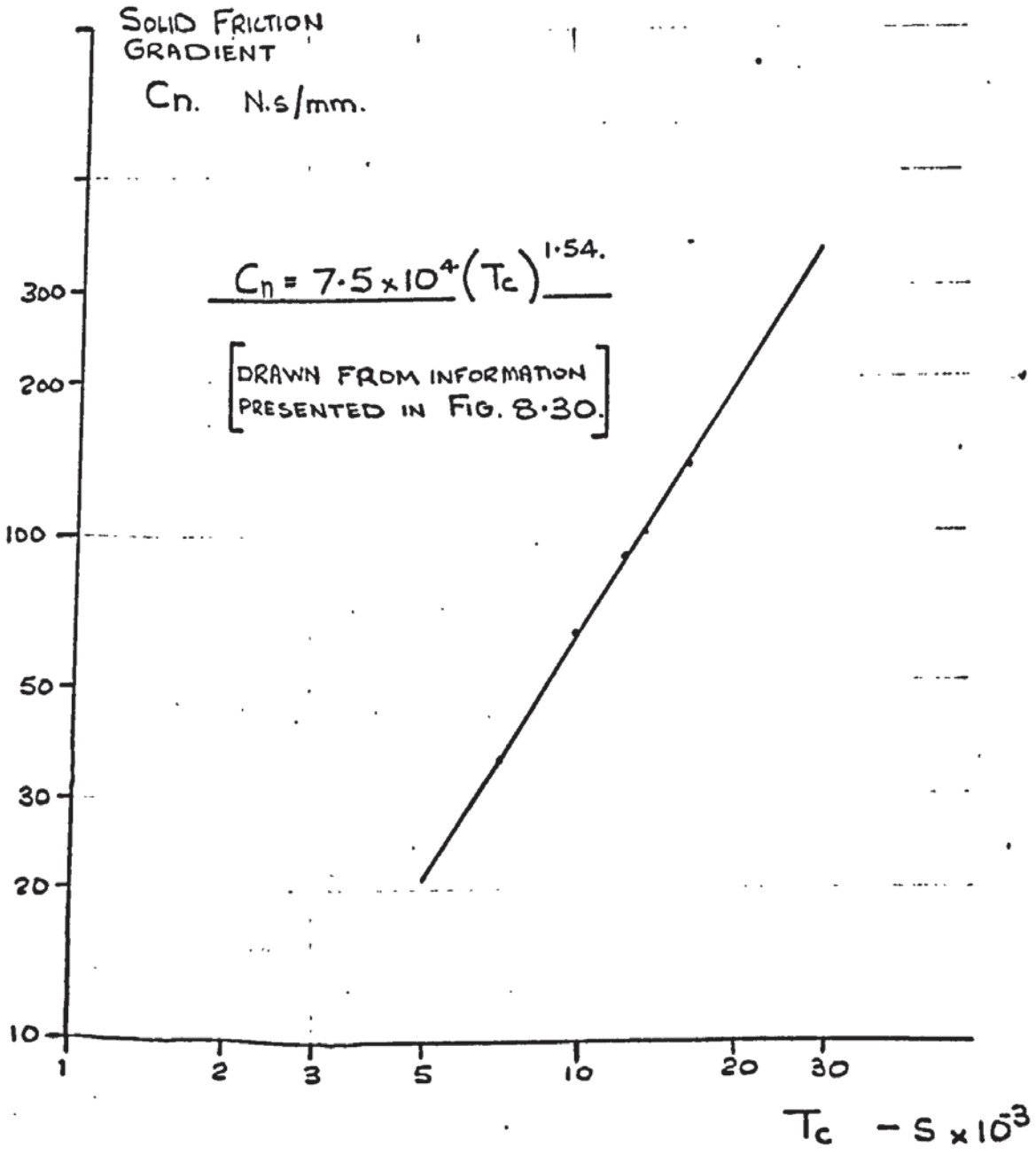

FIG. 9·1. RELATIONSHIP BETWEEN C_n AND T_c. - FROM SIMULATION RESULTS.

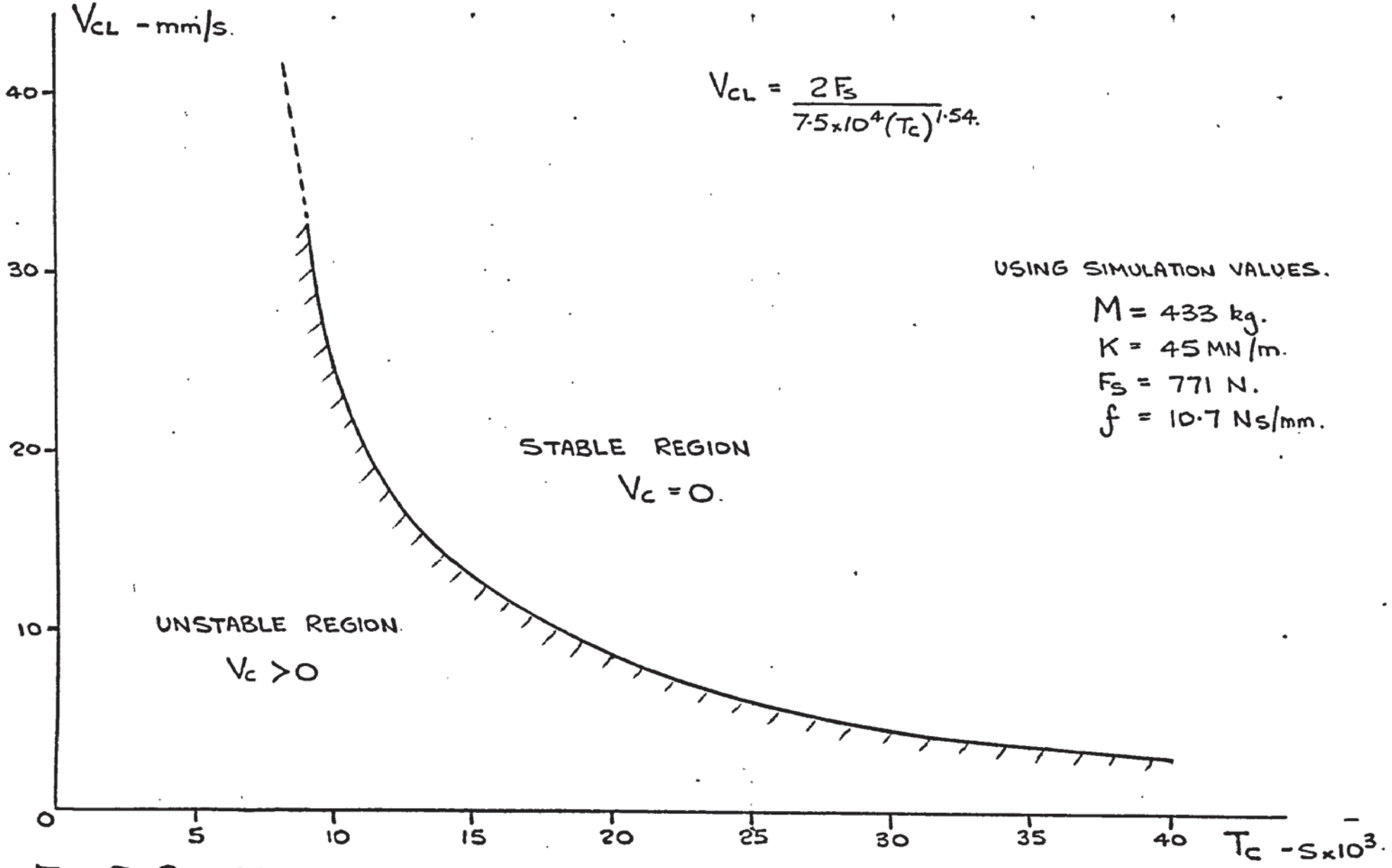

FIG. 9.2. VALUES OF V_{CL} AND T_c FOR STABLE SLIDING. - FROM SIMULATION RESULTS.

If we assume that a value of Tc has been established and oscillatory motion does occur, then by transposing eqn. 40.8 and introducing eqn. 1.9 the critical velocity can be expressed as,

$$Vc = Vc_L - \frac{(Vc_L)^2}{2\,Fs}\ 7.5 \times 10^4 (Tc)^{1.54} \qquad - 4.9$$

It can be seen from this expression that Vc can go to zero if the value of static friction (Fs) is reduced or the value of Tc is increased.

Eqn. 4.9 has been used to construct the curves shown in Fig. 8.31. These curves indicate that in the limiting condition, when Tc is zero, the critical velocity will be equal to Vc_L where Cn will also be zero.

The effect of changing the drive stiffness on the value of Vc is shown in Fig. 8.35. In this case we have fixed values of Vc_L and Tc. A plot of the corresponding Cn values against K is illustrated in Fig. 9.3. Again a straight line can be drawn through the experimental points to yield the following equation,

$$Cn = 16\ (K)^{0.077} \qquad - 5\text{-}9$$

where the units of K are N/mm.

We now have two expressions for Cn; in eqn. 1-9 the coefficient must contain the value of K (45 kN/mm) and in eqn. 5-9 the coefficient contains Tc(0.0071s). Testing these two equations yields a common coefficient of 3.3×10^4, thus Cn can be expressed in terms of Tc and K as,

$$Cn = 3.3 \times 10^4\ (Tc)^{1.54}\ (K)^{0.077} \qquad - 6\text{-}9$$

This equation has been obtained using particular simulation conditions. It has been shown to have reasonable validity with other limited data available and provides a means of taking the analysis further. It indicates that the value of Tc has the greater effect on the value of Cn. Equation 4-9 can now be rewritten to include the new expression for Cn giving,

$$Vc = Vc_L - \frac{(Vc_L)^2}{2\,Fs} \cdot 3.3 \times 10^4 (Tc)^{1.54} (K)^{0.077} \qquad - 7\text{-}9$$

It has been deliberate policy here to neglect the effect of the sliding weight and the simulation viscous friction quantity f. As stated earlier the weight will affect Vc and Fs; for example a moderate increase in weight will increase Vc_L and to a lesser extent Fs, as a consequence the value of Vc will increase.

From the slideway model analysis described in chapter 7 any viscous friction term is likely to be very small and therefore will play little part in the calculation of Vc. The simulation parameter f must be related to the

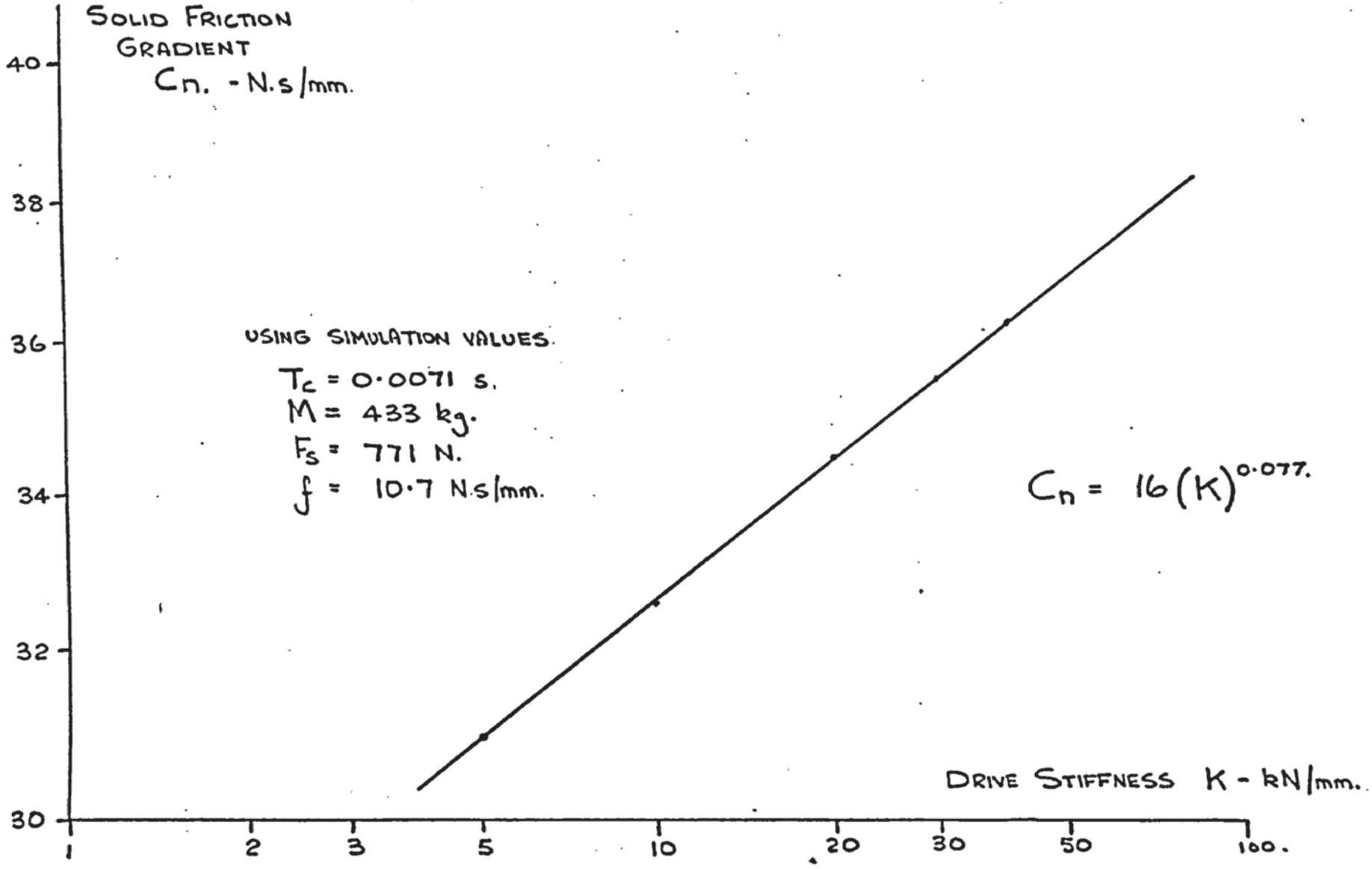

FIG 9·3 VALUES OF C_n AT CRITICAL VELOCITY FOR CHANGES IN DRIVE STIFFNESS.

166.1.

physical system in some complex way as stated in chapter 8 but it is felt that it is not directly comparable to the viscous damping coefficient usually associated with a linear physical slideway system.

9.3 THE RELATIONSHIP BETWEEN Tc AND OIL VISCOSITY

This analysis is carried out for non-polar oils because,

i) Relevant experimental results are available (47)

ii) The affect of polar additives will mainly result in the reduction of the static friction force and produce very little change in bulk oil viscosity.

The V_{CL} velocity has been described in eqn. 166-7 and 167-7, for two oil viscosities. The general form of these eqns. is,

$$V_{CL} = \left[\frac{P_w (H_o + h_d)^{2.478}}{K_L . \eta} \right]^m \qquad - 8\text{-}9$$

The constant (m) changes very little over a viscosity range greater than 10 to 1, therefore an average value has been taken.

$$m = 1.515 \qquad - 9\text{-}9$$

The other coefficient K_L does have a wide range and a logarithmic plot of this value against viscosity yields the relationship,

$$K_L = 18.7 (\eta)^{-0.819} \qquad - 10\text{-}9$$

Substituting eqn. 9-9 and 10-9 into 8-9 gives a general equation,

$$V_{CL} = \left[\frac{P_w (H_o + h_d)^{2.478}}{18.7 (\eta)^{0.181}} \right]^{1.515} \text{ - cm/s} \qquad - 11\text{-}9$$

The static friction force (Fs) can be determined using eqn. 164-7 in which $\alpha = 1$ and $K_{LP} = 22.8$ (non-polar coefficient, see eqn. 163-7).

Equation 165-7 gives the friction force per unit area (cm^2) and therefore the static friction force for the slideway model will be,

$$F_s = 10 A_A . \left[0.009705 (P_w)^{0.82} . (K_{LP}) + P_w \tan\Theta \right] \text{ -N.} \qquad - 12\text{-}9$$

as $A_A = 697\ cm^2$ and $\tan\Theta = 0.05$,

$$F_s = \left[1541.7 (P_w)^{0.82} + 348.4 (P_w) \right] \qquad - 13\text{-}9$$

In the work of Britton and Bell (47) two table weights were used and in this analysis the lower value has been selected since it is approximately the same as the simulation value, i.e. 450 kgf. giving a load per unit area

of 0.615 kgf/cm^2 (Pw). Applying eqn. 13-9 this gives a static friction force of 1249N.

Assuming their surface topology to be the same as the model then from eqn. 11-9, V_{cL} can be expressed in terms of viscosity only. In this case Ho = 4.64 μm (eqn. 140-7) and hd = 0.84 μm (eqn. 94-7), so that

$$V_{cL} = 10.\left[\frac{2.23}{(\eta)^{0.181}}\right]^{1.515} \text{ - mm/s} \qquad \text{- 14-9}$$

For convenience the following table has been constructed using Britton's (47) results, taking four viscosity values.

TABLE T9-1 VALUES OF V_{cL}, Vc and Cn for changes in viscosity and Drive stiffness

Viscosity η (P)	V_{cL} mm/s	K = 45000 N/mm		K = 27600 N/mm		K = 11000 N/mm	
		Vc mm/s	Cn.Ns/mm	Vc mm/s	Cn.Ns/mm	Vc mm/s	Cn.Ns/mm
0.13	59.0	5.5	38.4	12	33.7	↑ >15	↓ <31.6
0.34	45.3	4.2	50.0	7.0	46.6	7.8	45.65
0.455	41.83	2.7	55.86	5.0	52.58	6.0	51.15
0.595	38.9	2.0	60.9	3.3	58.77	5.0	55.96

where $Cn = \frac{2\,Fs}{(V_{cL})^2} \cdot (V_{cL} - Vc)$ (from eqn. 40.8)

Having values of V_{cL}, Vc and K enables eqn. 7-9 to be used to relate Tc to viscosity.

Rearranging eqn. 7-9

$$Tc = \left[\frac{(V_{cL} - Vc)}{(V_{cL})^2} \cdot \frac{2\,Fs}{3.3 \times 10^4 \times (K)^{0.077}}\right]^{0.649} \text{ -s} \qquad \text{- 15-9}$$

For the values set out in table T.9-1 the relevant value of Tc is calculated for the various drive system stiffnesses. These results are tabulated in Table T.9-2.

TABLE T.9-2 Values of Tc for changes in viscosity and drive stiffness

Viscosity η(P)	K = 45000N/mm Tc s	K = 27600N/mm Tc s	K = 11000N/mm Tc s
0.13	0.00720	0.00690	0.00690 (Vc = 16)
0.34	0.00860	0.00850	0.00870
0.455	0.00920	0.00910	0.00930
0.595	0.00980	0.00980	0.0099

In the above table the calculated time constant quantities show very consistent values for each viscosity value even though there is an appreciable change in stiffness.

In order to produce a mathematical relationship between Tc and viscosity these values are plotted using logarithmic scales as shown in Fig. 9.4. A straight line can easily be drawn through these points to yield the following relationships,

$$\eta = 36 \times 10^{-6} (Tc)^{4.238} \text{ -P.} \quad - 16\text{-}9$$

$$Tc = 11.16 (\eta)^{0.236} \text{ -mS.} \quad - 17\text{-}9$$

In these two equations Tc is expressed in milli-seconds.
Using eqn. 17-9 in eqn. 7-9 then the critical velocity can be expressed as,

$$Vc = Vc_L - \frac{(Vc_L)^2}{2\,Fs} 32.5 (\eta)^{0.363} (K)^{0.077} \quad - 18\text{-}9$$

This expression has been used to calculate Vc for changes in viscosity and drive stiffness using the data listed in table T9.1. These values are plotted against viscosity in Fig. 9.5 together with all of Britton's (47) experimental results for the same sliding mass.

The theoretical curves are in good agreement with the experimental observations made by Britton et al (47), and therefore the form of equation 18-9 would appear to have some validity.

The same procedure was adopted using the same experimental results (47) for a table weight of 850 kgf (Pw = 1.18 kgf/cm^2). The resulting time constants (using eqn. 15-9) were again plotted against the same viscosity values. Their relationship is also shown in Fig. 9.4 and the following equations can be formed,

$$\eta = 9 \times 10^{-6} (Tc)^{5.47} \text{ -P.} \quad - 19\text{-}9$$

$$Tc = 8.3 (\eta)^{0.183} \text{ -mS} \quad - 20\text{-}9$$

Using eqn. 20-9 in eqn. 7-9 then the critical velocity can be expressed as,

$$Vc = Vc_L - \frac{(Vc_L)^2}{2\,Fs} 20.6 (\eta)^{0.282} (K)^{0.077} \quad - 21\text{-}9$$

This equation has been used to calculate Vc for changes in viscosity and drive stiffness and the resulting curves are shown in Fig. 9.6 together with experimental data.

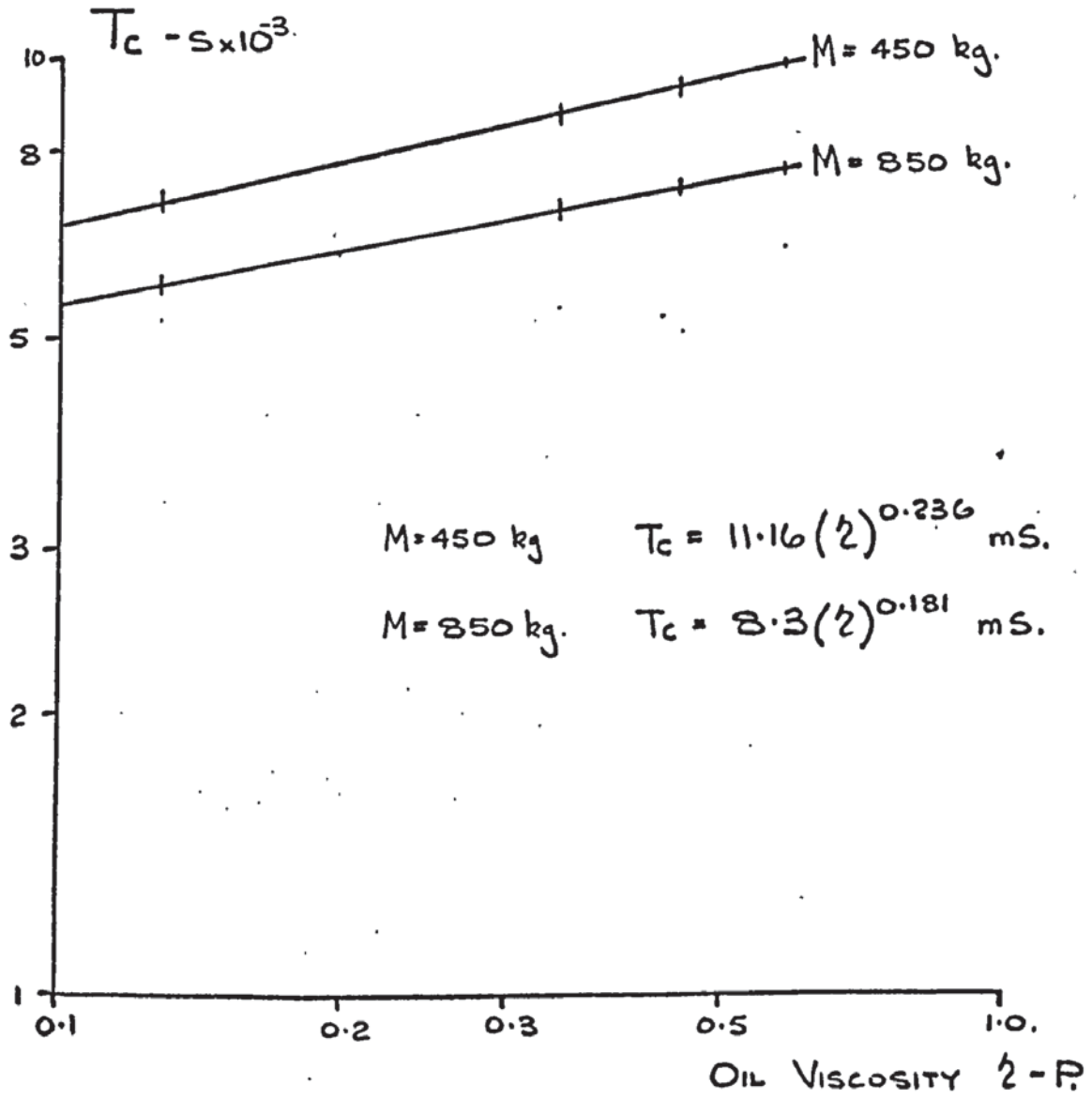

FIG. 9·4. RELATIONSHIP BETWEEN T_c AND OIL VISCOSITY.

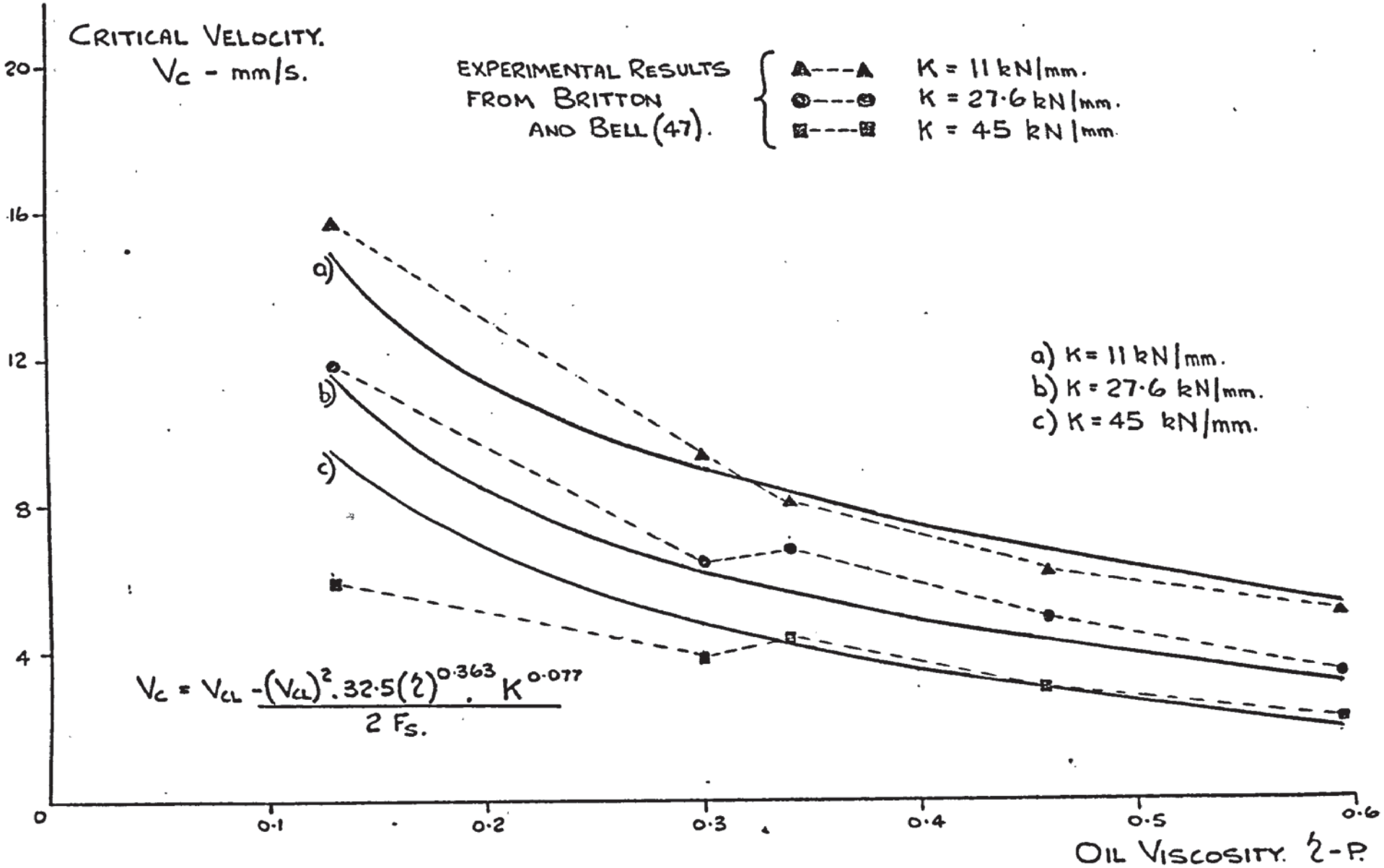

FIG 9·5. V_c VERSUS OIL VISCOSITY FOR CHANGES IN DRIVE STIFFNESS. (W = 450 kgf).

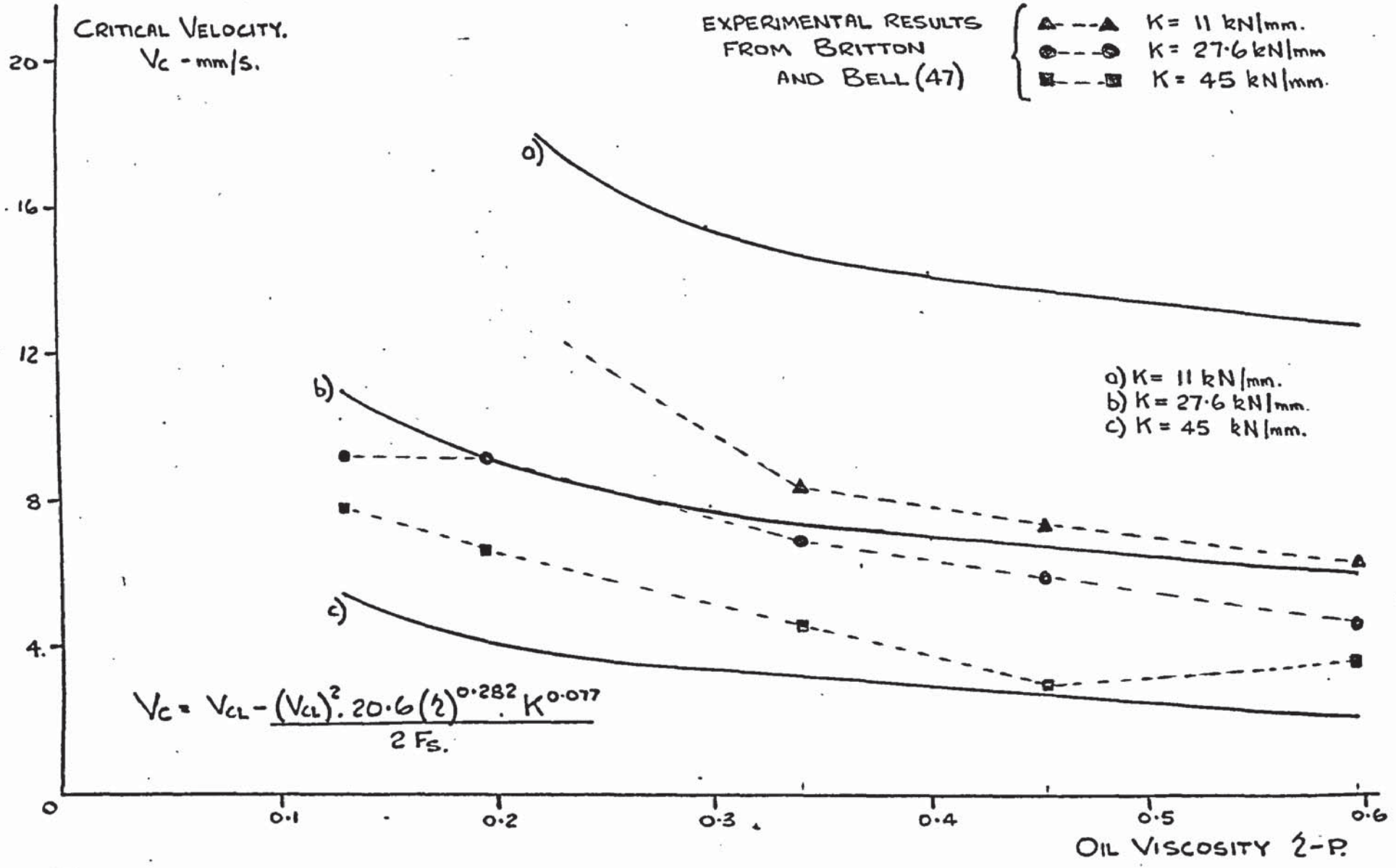

FIG. 9·6. V_c VERSUS OIL VISCOSITY FOR CHANGES IN DRIVE STIFFNESS. (W = 850 kgf).

The theoretical curves for drive stiffnesses of 45 MN/m and 27.6 MN/m are in reasonable agreement with the experimental data from Britton (47) but for a drive stiffness of 11 MN/m the data and theoretical curve show a large discrepancy. Nevertheless the author feels that the simulation results have provided a mathematical relationship enabling the critical velocity to be calculated, bearing in mind the assumptions that have been made between the slideway model data, experimental data and simulation results.

Equations 18-9 and 21-9 do have discrepancies in the form of a change in the value of a coefficient and the index for the viscosity. These are better illustrated by considering eqn. 6-9 and substituting the relevant values for Tc, thus,

For W = 450 kgf (Pw = 0.615 kgf/cm^2)

$$Cn = 32.5 \left(\dot{\zeta}\right)^{0.363} (K)^{0.077} \quad - 22\text{-}9$$

For W = 850 kgf (Pw = 1.18 kgf/cm^2)

$$Cn = 20.6 \left(\dot{\zeta}\right)^{0.282} (K)^{0.077} \quad - 23\text{-}9$$

These equations again indicate that as the sliding weight increases, the value of Cn reduces, thus the critical velocity increases. This same observation is made later in section 9-4 deduced by mathematical analysis of the system.

It has not been possible to simplify these equations but the general expression for Cn is of the form,

$$Cn = m \left(\dot{\zeta}\right)^{n} (K)^{0.077} \quad \text{-Ns/mm} \quad - 24\text{-}9$$

where m and n are variables mainly dependent upon the table weight. Both values decrease as the weight is increased.

W = kgf	m	n
450	32.5	0.363
850	20.6	0.282

A similar expression is possible for the relationship between the simulation time constant and viscosity.

$$Tc = a. \left(\dot{\zeta}\right)^{b} \quad \text{-mS} \quad - 25\text{-}9$$

The variables (a) and (b) again reduce with increased table weight as indicated below.

W - kgf	a	b
450	11.16	0.236
850	8.30	0.183

9.4 A MATHEMATICAL ANALYSIS OF THE FRICTION SYSTEM

9.4 (i) Routh-Hurwitz, Stability Criteron

A useful starting point for the analysis involves the Routh Hurwitz Stability technique (20) on the closed loop system. Fig. 9.7 illustrates the signal flow diagram and is drawn from Fig. 8.17 for a positional input. The closed loop transfer function is similar to that of Nakashima et al (54)

$$\frac{X_o}{X_i} = \frac{K(1 + Tcs)}{MTcs^3 + (M + fTc)s^2 + (KTc + f + N)s + K} \quad - 26\text{-}9$$

Using Routh-Hurwitz on the denominator the system stability condition occurs when,

$$(M + fTc)(KTc + f + N) \geqslant MKTc \quad - 27\text{-}9$$

Considering an input at the critical velocity i.e.

$$X_1 = Vc.t \quad - 28\text{-}9$$

for small perturbations about this point the non-linear term N is effectively the slope of the solid friction curve (Cn).

Putting

$$N = Cn \quad - 29\text{-}9$$

eqn. 27-9 reduces to the form,

$$(M + fTc)(f + Cn) + fKT_c^2 \geqslant 0 \quad - 30\text{-}9$$

or

$$Cn \geqslant -f - \frac{fKTc^2}{M + fTc} \quad - 31\text{-}9$$

(N.B. Cn is negative).

At the critical velocity (Vc)

$$Cn = -f - \frac{fKTc^2}{M + fTc} \quad - 32\text{-}9$$

These equations show that system stability can be achieved even when the sliding occurs at a velocity within the region of the negative gradient friction characteristic.

Expressing eqn. 32-9 in a non-dimensional form as done by Nakashima (54),

$$A = \frac{KTc^2}{M} \quad - 33\text{-}9$$

$$B = \frac{CnTc}{M} \quad - 34\text{-}9$$

$$C = \frac{fTc}{M} \quad - 35\text{-}9$$

then

$$B = -C - \frac{A.C}{1 + C} \quad - 36\text{-}9$$

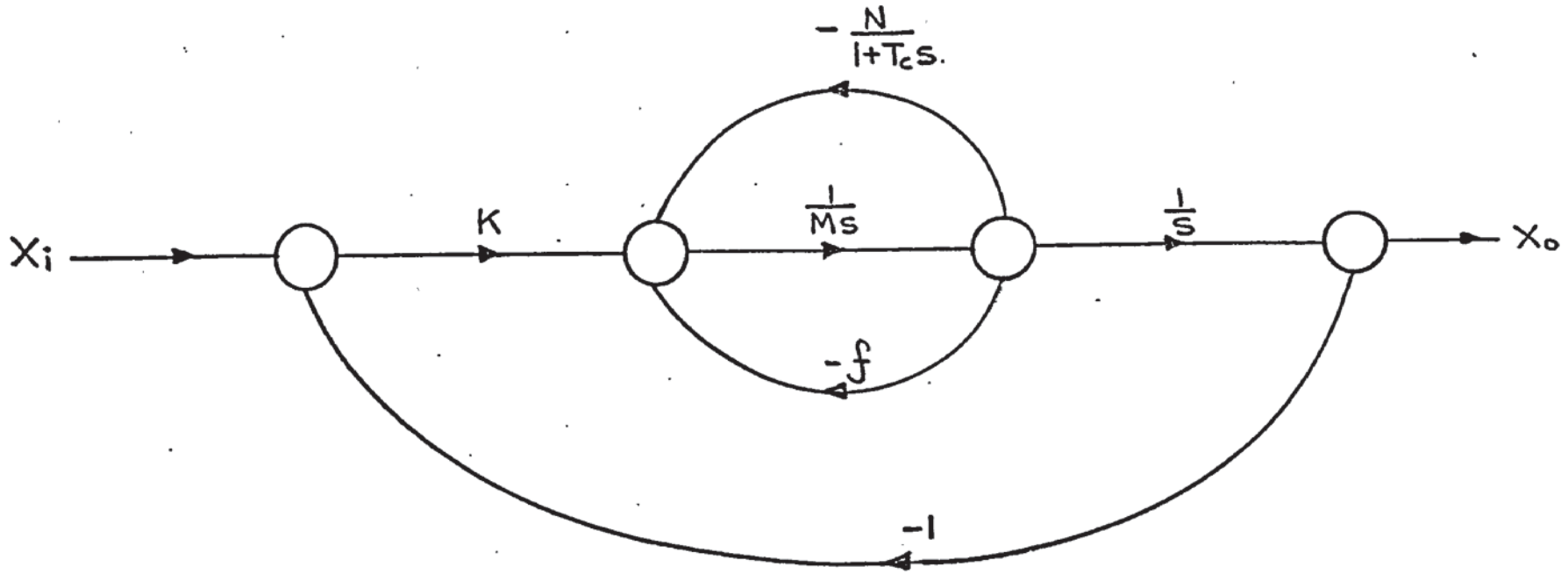

$$\frac{X_o}{X_i} = \frac{K/Ms^2}{1 + K/Ms^2 + f/Ms + \frac{N}{Ms(1+T_c s)}}$$

$$\frac{X_o}{X_i} = \frac{K(1+T_c s)}{MT_c s^3 + (M+fT_c)s^2 + (KT_c + f + N)s + K.}$$

FIG. 9·7. SIGNAL FLOW DIAGRAM FOR SLIDEWAY SYSTEM.

Fig. 9.8 illustrates the relationships between the factors of this equation. The curves indicate clearly that for a particular value of f the value of Cn increases negatively as the drive stiffness (K) increases. Stability is generally improved by increases in Tc and reductions in M. The greatest improvement is by changing Tc. This is also indicated in the earlier simulation analysis by eqn. 6.9.

Using eqn. 32-9 and the simulation time constants then an alternative relationship between Cn and Tc can be found.
The resulting formula is,

for, $W = 433$ kgf

$K = 45$ kN/mm

$f = 10.71$ Ns/mm

$$Cn = 12.95 \times 10^4 \ (Tc)^{1.55} \qquad - 37\text{-}9$$

This equation can be compared with eqn. 1.9, obtained using only simulation results. It is apparent that the Cn values will be greater using eqn. 37-9. The index for Tc in both these equations is practically the same.

Similarly a relationship between Cn and K can be made and this yields the following equation.

for, $W = 433$ kgf

$f = 10.71$ Ns/mm

$Tc = 0.0071$ s

$$Cn = 0.0385 \ (K)^{0.685} \qquad - 38\text{-}9$$

This formula does not compare favourably with the simulation equation 5-9. Equations 37-9 and 38-9 are combined to produce a composite equation for Cn,

$$Cn = 82.5 \ (Tc)^{1.55} \ (K)^{0.685} \qquad - 39\text{-}9$$

The simulation results yielded a quite different equation (6-9) which is repeated here for comparison,
From simulation results:

$$Cn = 3.3 \times 10^4 \ (Tc)^{1.54} \ (K)^{0.077}$$

Although there are major differences in these two equations, the simulation work and this analysis do have some common points. These are listed in order of importance.

1) The value of Cn, which determines the critical velocity, will change with the time constant Tc. As Tc increases so does Cn therefore reducing the critical velocity value.

2) As Cn is constant for a value of Tc, the critical velocity can be found if Fs and V_{cL} are known, using eqn. 40-8.

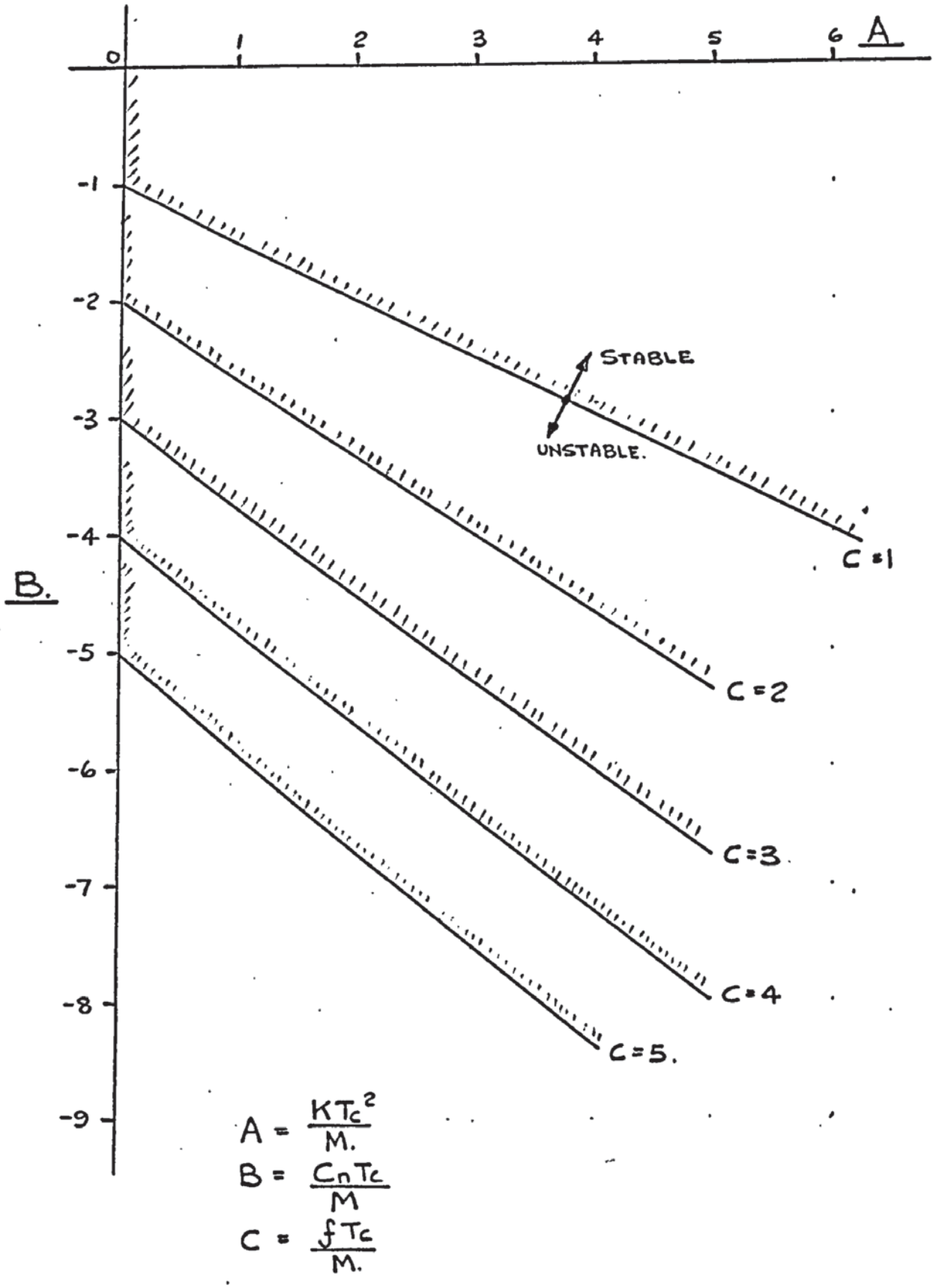

$$A = \frac{KT_c^2}{M.}$$

$$B = \frac{C_n T_c}{M}$$

$$C = \frac{f T_c}{M.}$$

FIG. 9·8. SYSTEM STABILITY USING ROUTH-HURWITZ FACTORS.

3) The value of Tc has the dominating influence on the parameter Cn.

4) As the value of drive stiffness (K) reduces Cn reduces, thus increasing the critical velocity. Its effect is not as great as that of Tc.

5) As the system approaches its critical velocity, the simulation indicates that the frequency of oscillations is very close to its undamped natural frequency. From the Routh-Hurwitz analysis this can be determined as

$$\omega = \left(\frac{K}{(M + fTc)} \right)^{0.5} \text{ -rad/s} \qquad - 40\text{-}9$$

An interesting parameter is f - the viscous damping term. This quantity is built into the simulation circuit and has rather a large value. It has an important role in that it has a stabilising influence on the system. In a physical system the "viscous" damping term will usually have a very low value and therefore the author feels that this linear term has very little influence. If this is the case, although Routh-Hurwitz provides some interesting pointers it is not suitable for obtaining mathematical confirmation of the physical or simulation data.

The simulation data does provide a formula that appears to be useful in obtaining a mathematical relationship describing the physical behaviour. A positive damping coefficient similar to the "f" value used in the computer work must also be present in the physical system and it is most likely that it is related to the solid friction characteristic.

In order to investigate further the interrelation of system parameters, the technique of Describing Functions (109) has been employed to handle this system non-linearity.

9.4 (ii) DESCRIBING FUNCTION TECHNIQUE

For the diagram in Fig. 9.9 the system transfer function will be,

$$\frac{x_i}{x_o} = \frac{N_E . G(s)}{1 + N_E . G(s)} \qquad - 41\text{-}9$$

The limiting condition for stability of the system is set by considering the denominator thus,

$$1 + N_E . G(s) = 0 \qquad - 42\text{-}9$$

and

$$G(s) = \frac{-1}{N_E} \qquad - 43\text{-}9$$

where N_E is a linearised description of the non-linear term. This

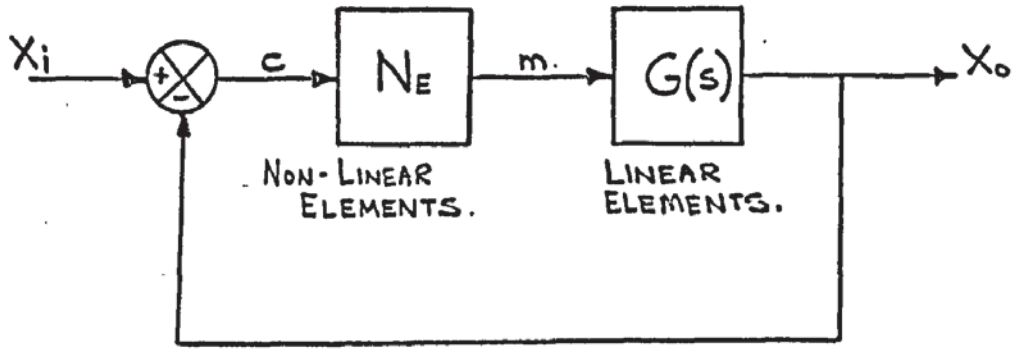

$$\frac{X_i}{X_o} = \frac{N_E G(s)}{1 + N_E G(s)}.$$

a) Division of System into Linear and Non-Linear Terms.

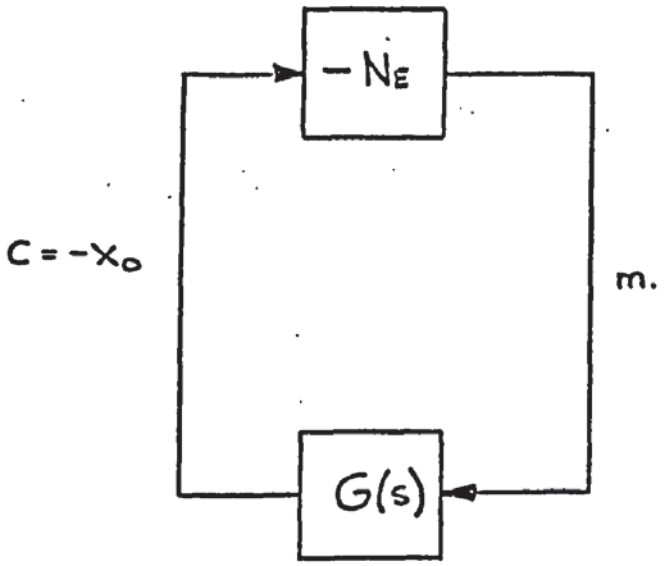

$m = -N_E . c.$

$\frac{c}{m} = G(s).$

$G(s) = \frac{1}{-N_E}.$

b) Control Theory Representation for Autonomous System.

Fig. 9.9. A Non-Linear System.

linearisation is done by Describing Functions. Further analysis using a form of eqn. 43-9 is then carried out in the frequency domain. The latter part is much akin to the Nyquist Stability technique (20), but the Nyquist point is replaced by some form of line described by the term $1/N_E$. Any intersection of the loci of the two plots indicates a critically stable condition under which the system will oscillate at some frequency and amplitude. The frequency quantity is taken from the plot $G(j\omega)$ and the amplitude from the curve $\left(\frac{1}{N_E}\right)$.

In the frequency domain the open loop transfer function (G) is related to the describing function, from eqn. 43-9 as,

$$G(j\omega) = \frac{-1}{N_E} \qquad - 44\text{-}9$$

All signals are taken to be sinusoidal and the attenuation of (G) is frequency dependent. The attenuation of the non-linear term is amplitude dependent. In general the "gain" of the non-linear term is given by,

$$N_E = g(E) + jb(E) \qquad - 45\text{-}9$$

where $$g(E) = \frac{1}{\pi E}\int_0^{2\pi} f(E.\sin\theta).\sin\theta.d\theta \qquad - 46\text{-}9$$

and $$b(E) = \frac{1}{\pi E}\int_0^{2\pi} f(E\sin\theta).\cos\theta.d\theta \qquad - 47\text{-}9$$

The difficulty with this technique is the establishment of the terms $g(E)$ and $b(E)$, they can become complex and unwieldy. Nevertheless the form of eqn. 45-9 can be established and it must then be expressed in polar form,

$$|N_E| \angle \gamma \qquad - 48\text{-}9$$

where $$|N_E| = \left[(b(E))^2 + (g(E))^2\right]^{0.5} \qquad - 49\text{-}9$$

and $$\gamma = \tan^{-1}\left[\frac{b(E)}{g(E)}\right] \qquad - 50\text{-}9$$

A polar plot is then made of $-1/|N_E|$ and γ ; usually for various values of (E), the input amplitude.

For single-valued non-linearities there will be no phase shift between the input fundamental and the output, thus b(E) will be zero. In the case of a non-linearity with memory, often called a double valued function, there will be a phase shift, γ. ($b(E) \neq 0$).

The most important step is the establishment of the non-linear relationship between input and output. In this case the analogue simulation circuit indicates the possibility of obtaining the function in terms of force.

Consider first of all Fig. 9.10(a) where, in a steady state velocity condition ($\dot{x}_o = \dot{x}_i$), the input force to the system would be (F). This is generated by the drive stiffness giving

$$K.(\text{error}) = F \qquad - \quad 51\text{-}9$$

If the error quantity increases there will be some "useful" force available,

$$\text{useful force} = K.(\text{error}) - F \qquad - \quad 52\text{-}9$$

which may be used to accelerate the moving mass. On the other hand if the error quantity reduces no "useful" force will be available. If we describe this function in terms of input forces then Fig. 9.10(b) can be drawn. This is a single valued non-linearity and would describe the element (N_ε) of Fig. 9.9.

It should be noted that the value of F does not change with velocity and it can be shown that $|N_\varepsilon|$ will tend towards unity as the input force sinusoid increases in amplitude or as the value of F decreases. Fig. 9.10(c) shows the effect of changing amplitude.

Fig. 9.11(a) shows a typical slideway friction curve in its decomposed form. For a value of $\dot{x}_o$ there will be a value of (F) the solid friction force and a value of viscous force (a). The viscous friction coefficient (f) is a linear term and is therefore related to the function (G). Considering only the solid friction characteristic as being non-linear, then if the input force for a steady value of $\dot{x}_i$ is K(error) the useful output force will be reduced to

$$a = f.\dot{x}_o$$

since this is required to overcome the linear term.

The output of the non-linearity will be,

$$a = f.\dot{x}_o = K(\text{error}) - F \qquad - \quad 53\text{-}9$$

This equation is depicted in Fig. 9.11(b). In this case both (F) and (a) are functions of velocity $\dot{x}_o$. If a sinusoidal force is impressed upon the standing error force the resulting output force is shown in Fig. 9.11 (c).

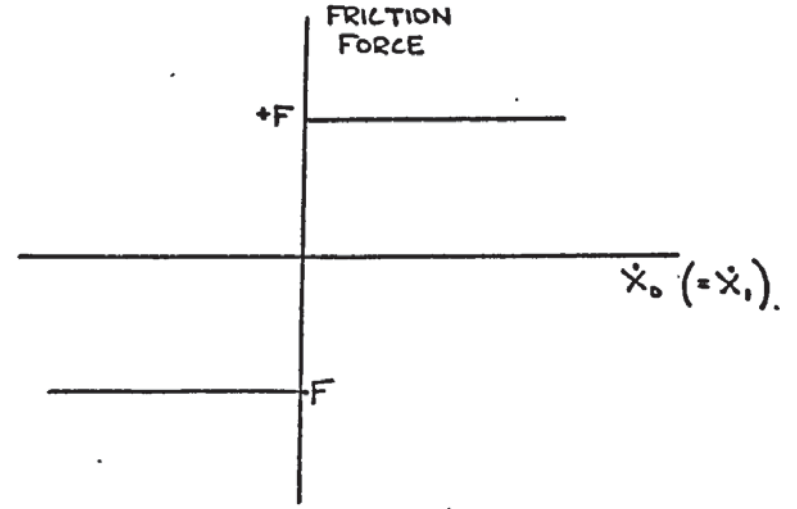

a) STEADY STATE FRICTION CHARACTERISTIC.

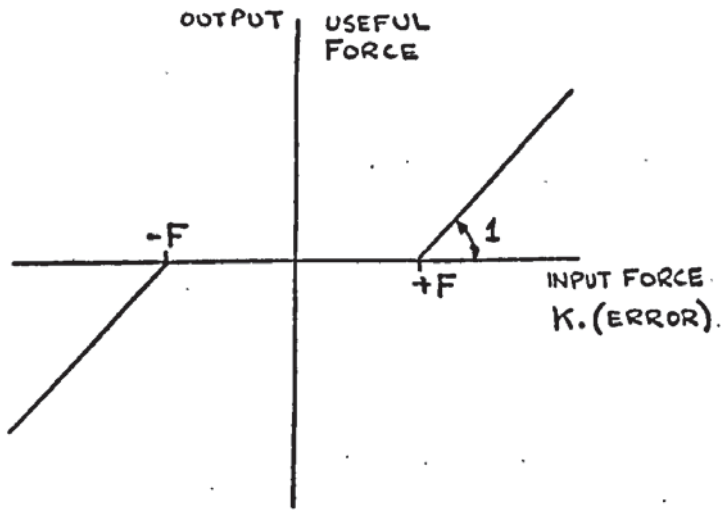

b) CHARACTERISTIC IN TERMS OF SYSTEM FORCES.

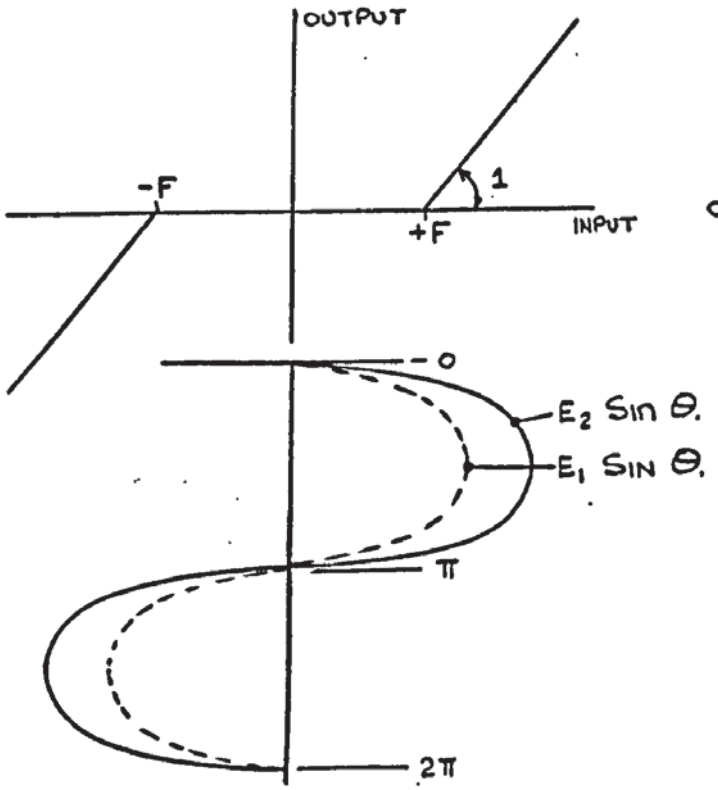

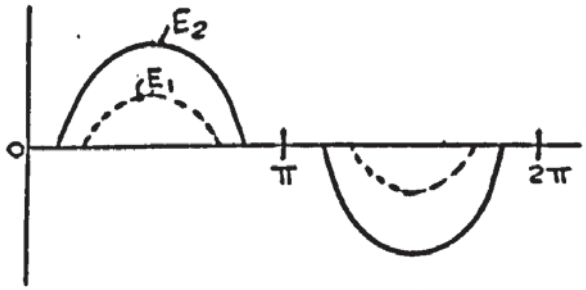

c). NON-LINEAR OUTPUTS DEPENDINT UPON INPUT AMPLITUDE AND VALUE OF F.

FIG. 9·10. DESCRIBING FUNCTION FOR FRICTION NON-LINEARITY.

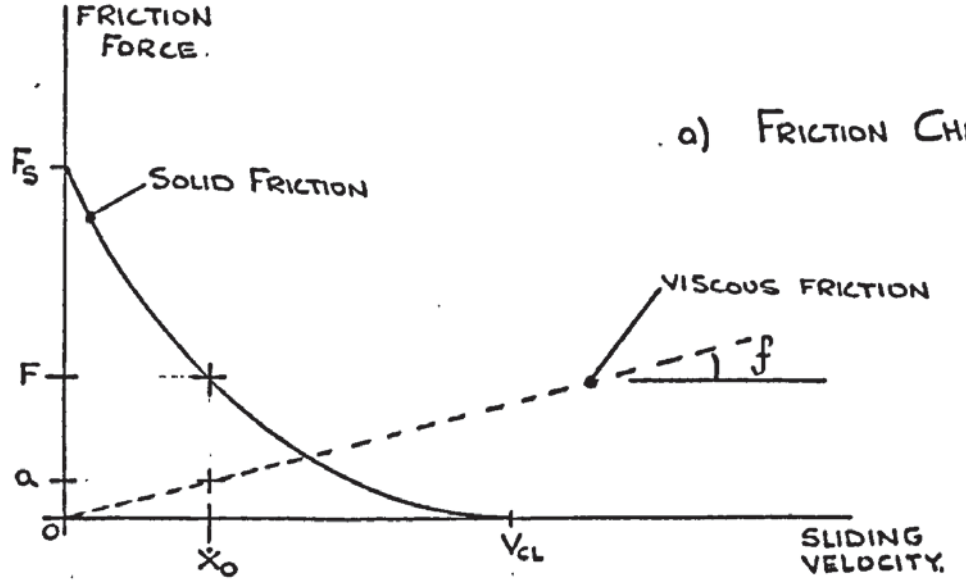

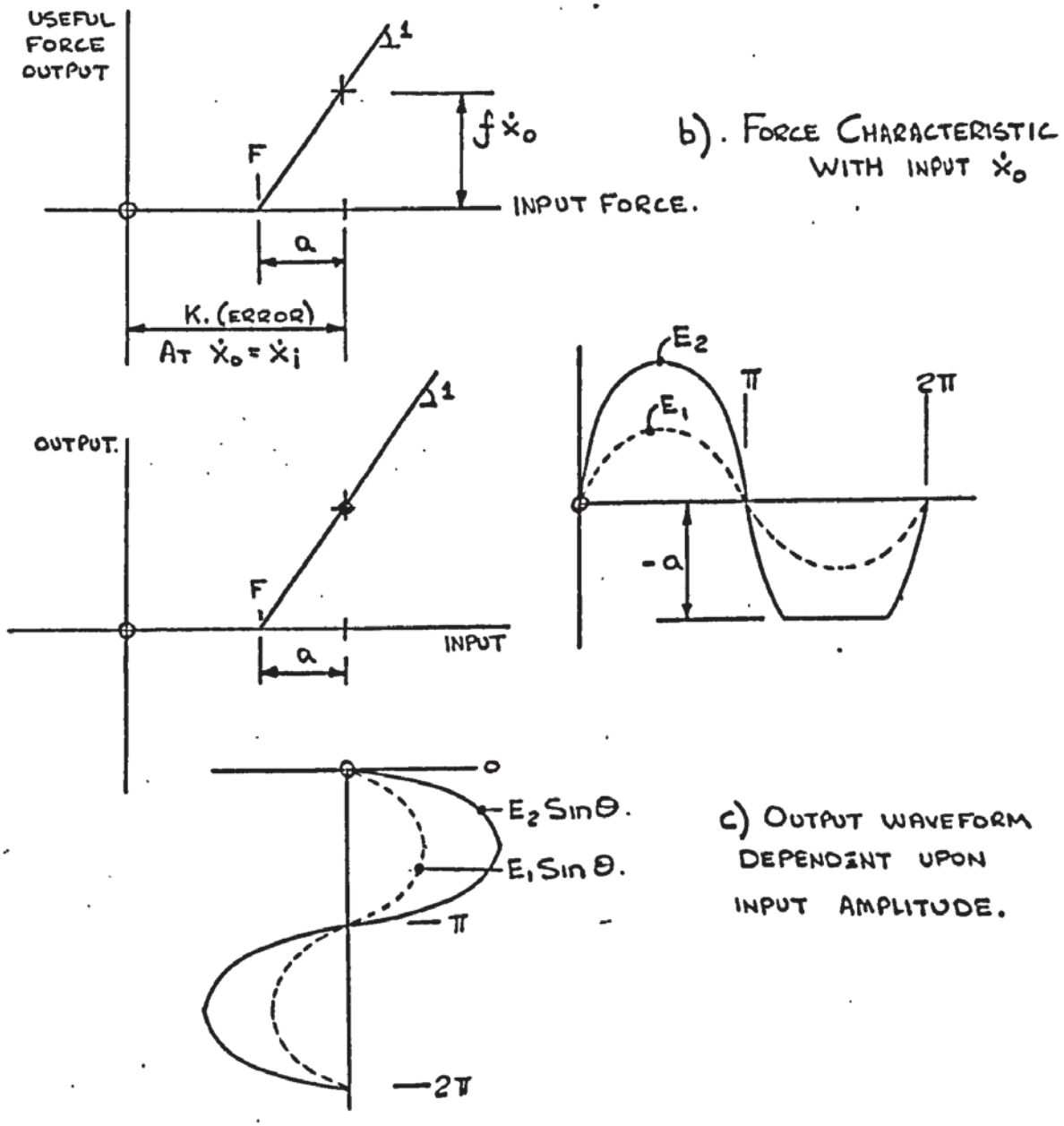

FIG. 9·11. DESCRIBING FUNCTION FOR SLIDEWAY FRICTION

In the case of oscillatory motion on a slideway it could be considered that the impressed force oscillation was due to this. Moreover it leads to the idea of making the standing force position the input axis for investigating the motion. The oscillations are taking place about a steady state condition $\dot{x}_o = \dot{x}_i$. With a transposition of the input axis it is apparent that an assumption has to be made that any input force oscillation is symmetrical about this axis. This assumption is well justified in a quasi-harmonic condition, but it may not be necessarily so in the stick-slip situation.

If we consider the input waveforms as in Fig. 9.11(c) for $E_1 < a$ the output waveform is complete and will be $E_1 . \text{Sin}\,\theta$. This will mean that the describing function (N_E) will have a value of unity. In other words the system gain has no attenuation and the system is performing in a linear fashion. If this is so, then due to the viscous damping remaining the oscillations will decay in time to zero giving a completely stable situation.

For $E_2 > a$, the output wave form is non-linear. This will give a describing function value which is less than unity and cause system attenuation. This will effectively reduce the value of the system gain K giving a reduction in the frequency of any system oscillations.

For a fixed value of input amplitude (E), the degree of attenuation will depend upon the magnitude of (a) which is a function of both f and $\dot{x}_o$. If the viscous damping term is also constant then system attenuation is a function only of velocity $\dot{x}_o$.

Let us consider the conditions appertaining to Fig. 9.11(c) in greater detail and obtain the describing function for this single valued non-linearity. Fig. 9.12 depicts the usual layout for describing function work. It can be seen that no phase-shifting exists and therefore b(E) will be zero.

Using eqn. 46.9,

$$g(E) = \frac{1}{\pi E}\int_{o}^{\pi+\theta_1}(E\text{Sin}\theta).\text{Sin}\theta.d\theta + \frac{1}{\pi E}\int_{\pi+\theta_1}^{2\pi-\theta_1}(-a)\text{Sin}\theta.d\theta + \frac{1}{\pi E}\int_{2\pi-\theta_1}^{2\pi}(E\text{Sin}\theta).\text{Sin}\theta.d\theta. \qquad - 54\text{-}9$$

and after integration and substitution,

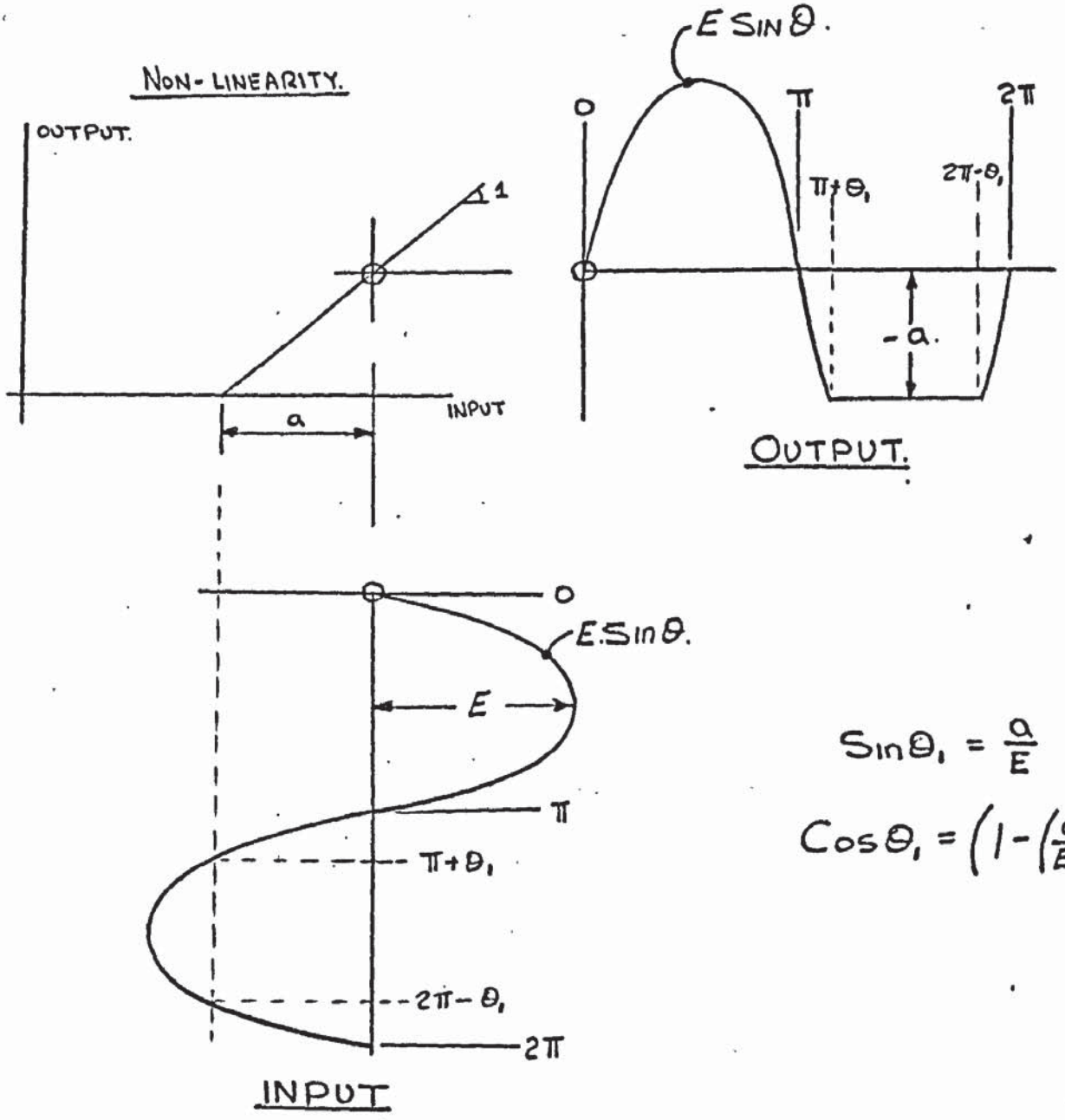

$$\text{Sin}\theta_1 = \frac{a}{E}$$

$$\text{Cos}\theta_1 = \left(1 - \left(\frac{a}{E}\right)^2\right)^{0.5}$$

$$g(E) = \frac{1}{2} + \frac{\theta_1}{\pi} + \frac{a}{\pi E}\left(1 - \left(\frac{a}{E}\right)^2\right)^{0.5}.$$

$$b(E) = 0.$$

FIG 9·12. DESCRIBING FUNCTION LAYOUT.

$$g(E) = \frac{1}{2} + \frac{\theta_1}{\pi} - \frac{\sin 2\theta_1}{2\pi} + \frac{2a.\cos\theta_1}{\pi E} \qquad - 55\text{-}9$$

The Sine and Cosine function can be expressed in terms of (a) and (E) (see Fig. 9.12) to yield

$$g(E) = \frac{1}{2} + \frac{\theta_1}{\pi} + \frac{a}{\pi E}\left[1 - \left(\frac{a}{E}\right)^2\right]^{0.5} \qquad - 56\text{-}9$$

The limiting conditions for this equation are,

$a = 0$, whence $\theta_1 = 0$ and $g(E) = \frac{1}{2}$

to

$a = E$, $\theta_1 = \pi/2$ and $g(E) = 1$

Usually g(E) is calculated in terms of ratios of (E) and (a) and this approach has been used in producing the table T9-3 below. It should be noted that in this case,

$$N_E = g(E) \quad \text{(from eqn. 45-9)}$$

and $$\frac{-1}{N_E} = \frac{-1}{g(E)}$$

Table T.9-3

E/a	g(E)	N_E	$-1/N_E$
1	1	1	-1
5	0.627	0.627	- 1.596
20	0.532	0.532	- 1.88
∞	0.5	0.5	- 2

$\gamma = 0$

These values for $-1/N_E$ are plotted on the Nyquist diagram Fig. 9.13 and form a straight line running along the negative real axis.

Although N_E has been established using a non-linear function in terms of forces the same results would be achieved if the non-linearity (Fig.9.12) was in terms of positional quantities by dividing both axis values by K. This will allow K to then form part of the linear function (G). The model system is second order and,

$$G(s) = \frac{K}{s(Ms + f)} \qquad - 57\text{-}9$$

In the frequency domain (G) can be expressed in polar form as,

$$G(j\omega) \quad \frac{K}{\left[(M\omega^2)^2 + (f\omega)^2\right]^{0.5}} \qquad - 58\text{-}9$$

$$\text{Tan } \phi = \frac{f}{M\omega} \qquad - 59\text{-}9$$

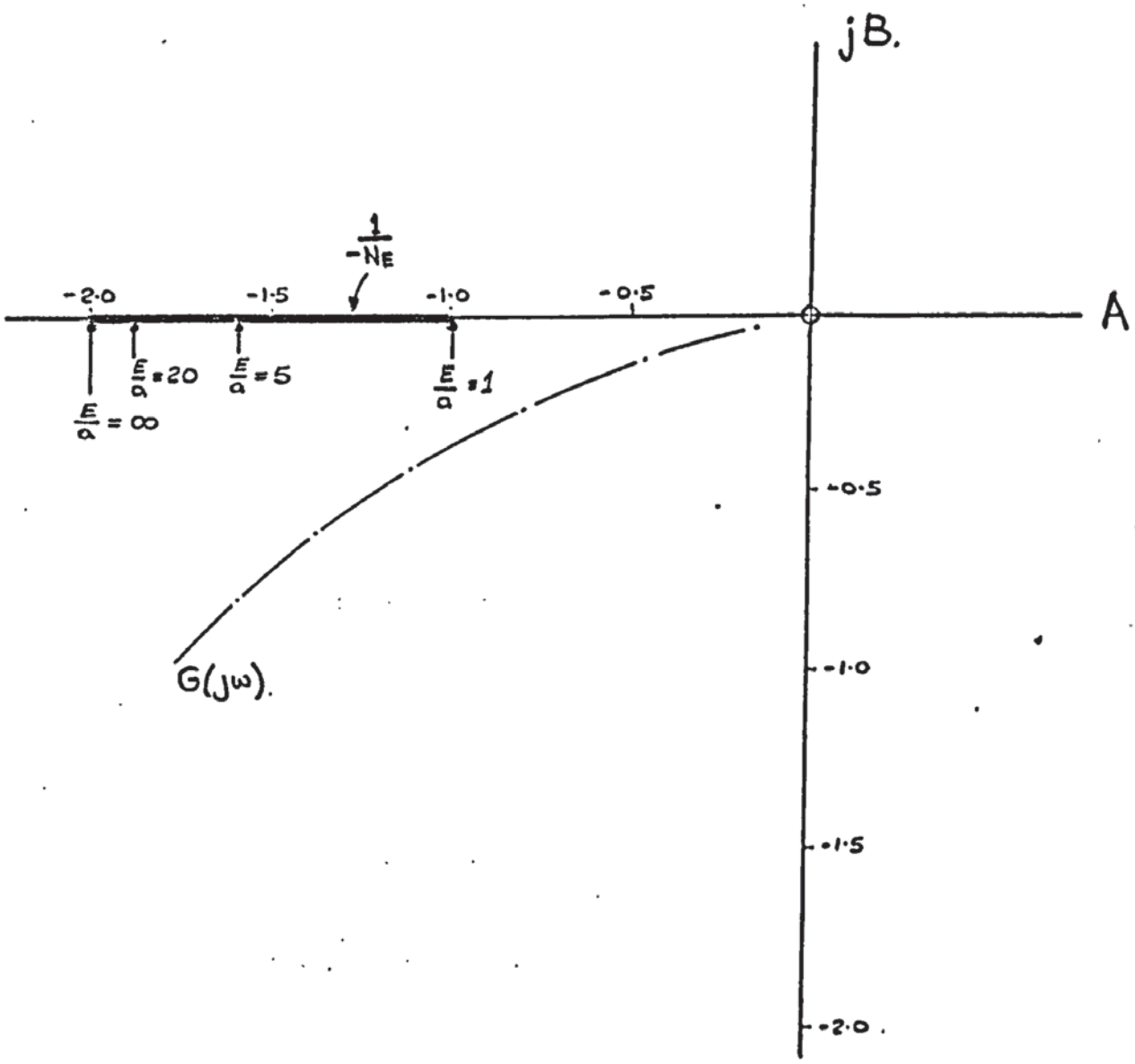

FIG 9·13. NYQUIST DIAGRAM INDICATING POSITION OF DESCRIBING FUNCTION.

As an example, such a polar plot has been sketched on the Nyquist diagram of Fig. 9.13. It is obvious that no interaction will occur and therefore the system will not exhibit oscillatory behaviour.

To enable system limit-cycling to occur, the diagram shown in Fig.9.12 has to be modified. We know that system oscillations will occur on the input force quantity, as already outlined, but they will also occur about the steady velocity $\dot{x}_o$. Consequently oscillations will be present about the standing value of F. Let

$$\text{input force} = K(\text{error}) + E.\sin\theta. \qquad - 60\text{-}9$$

$$\text{velocity} = \dot{x}_o - v\cos\theta. \qquad - 61\text{-}9$$

$$\text{Force at F} = F + n.\cos\theta. \qquad - 62\text{-}9$$

The parameter (n) has the linearised form,

$$n = -Cn.\ v. \qquad - 63\text{-}9$$

where Cn is the slope of the solid friction curve at velocity $\dot{x}_o$ and from eqn. 40-8,

$$Cn = \frac{2\,Fs}{(V_{CL})^2}.(V_{CL} - \dot{x}_o) \qquad - 64\text{-}9$$

Fig. 9.14 illustrates the modified describing function diagram and this will be used to demonstrate how this technique can be applied to solve the different types of non-linear motion.

Besides the terms (a) and (E) the size of (n) determines the type of output motion. Fig. 9.14(a) illustrates the output waveform when $n < a$ and Fig. 9.14(b) $n > a$. In both cases it is clear that some phase shift has taken place relative to the fundamental input.

For Fig. 9.14(a) $n < a$,

$$g(E) = \frac{1}{\pi.E}\int_0^{\pi+\theta_3}(E\sin\theta - n.\cos\theta).\sin\theta.d\theta + \frac{1}{\pi.E}\int_{\pi+\theta_3}^{2\pi-\theta_4}(-a).\sin\theta.d\theta + \frac{1}{\pi.E}\int_{2\pi-\theta_4}^{2\pi}(E\sin\theta - n.\cos\theta).\sin\theta.d\theta \qquad - 65\text{-}9$$

$$\text{and } b(E) = \frac{1}{\pi.E}\int_0^{\pi+\theta_3}(E\sin\theta - n.\cos\theta).\cos\theta.d\theta + \frac{1}{\pi.E}\int_{\pi+\theta_3}^{2\pi-\theta_4}(-a).\cos\theta.d\theta + \frac{1}{\pi.E}\int_{2\pi-\theta_4}^{2\pi}(E\sin\theta - n.\cos\theta).\cos\theta\,d\theta \qquad - 66\text{-}9$$

Solving for g(E) and b(E),

$$g(E) = \frac{1}{2}.\left(1 + \frac{\theta_3 + \theta_4}{\pi}\right) + \frac{a}{\pi}.\frac{(n^2 + E^2 - a^2)^{0.5}}{(n^2 + E^2)} \qquad - 67\text{-}9$$

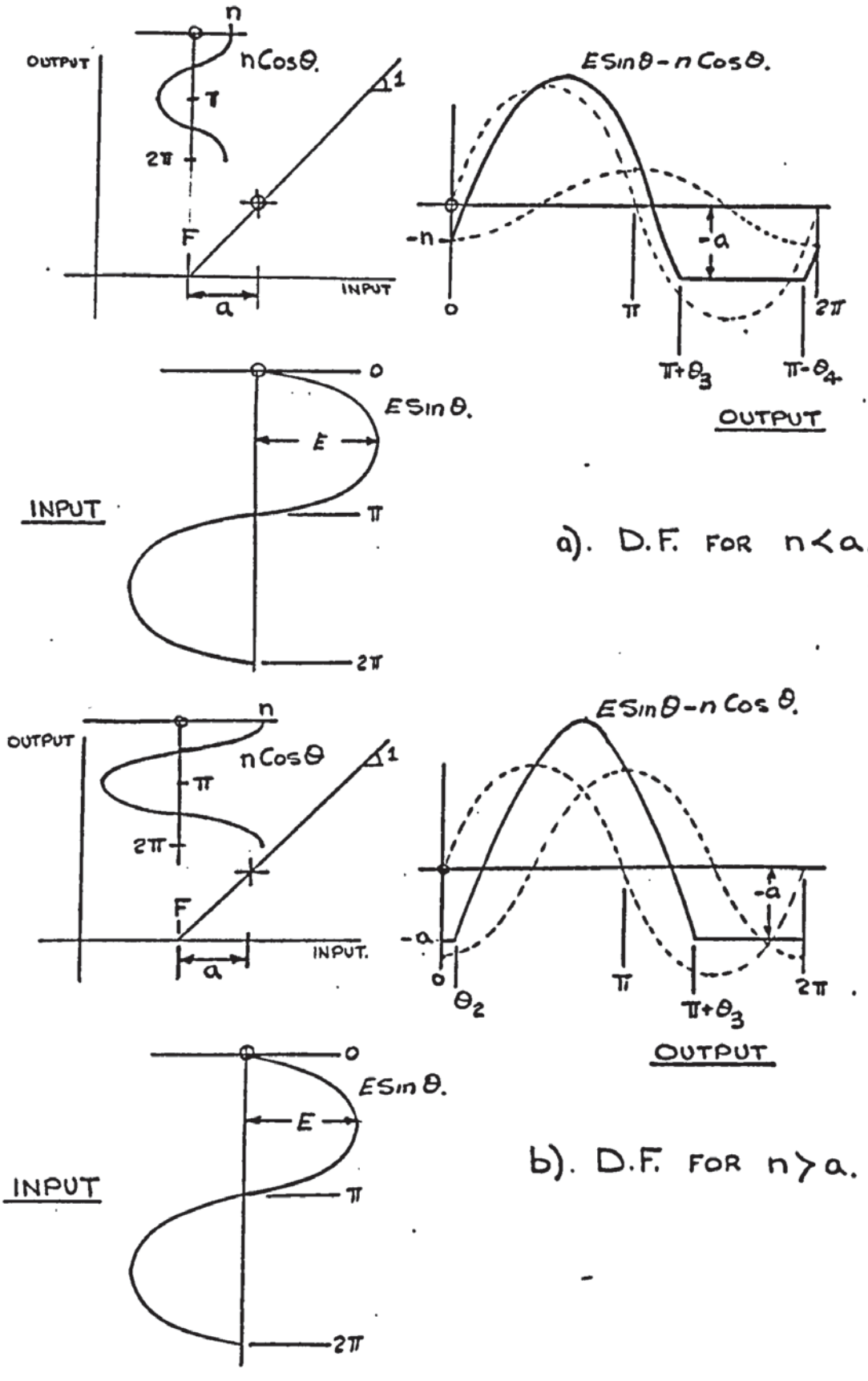

FIG 9·14. DESCRIBING FUNCTION FOR COMPLEX NON-LINEARITY.

$$b(E) = -\frac{n}{E}\cdot\left[\frac{1}{2}\cdot\left(1+\frac{\theta_3+\theta_4}{\pi}\right)+\frac{a}{\pi}\cdot\frac{(n^2+E^2-a^2)^{0.5}}{(n^2+E^2)}\right] \quad - 68\text{-}9$$

where, $\cos\theta_3 = \dfrac{E(n^2+E^2-a^2)^{0.5}-an}{(n^2+E^2)}$ - 69-9

$$\cos\theta_4 = \frac{E(n^2+E^2-a^2)^{0.5}+an}{(n^2+E^2)} \quad - 70\text{-}9$$

and $\tan\gamma = -\dfrac{n}{E}$ - 71-9

$$|N_E| = g(E)\cdot\left[1+\left(\frac{n}{E}\right)^2\right]^{0.5} \quad - 72\text{-}9$$

We now have to consider three parameters (E), (a) and (n) and for convenience ratios of $\left(\frac{E}{a}\right)$ have been selected together with ratios of $\left(\frac{n}{a}\right)$ in order to determine N_E and γ.

For Fig. 9.14(b) $n > a$, similar equations have been produced.

$$g(E) = \frac{1}{\pi E}\cdot\int_0^{\theta_2}(-a)\cdot\sin\theta\cdot d\theta + \frac{1}{\pi E}\cdot\int_{\theta_2}^{\pi+\theta_3}(E\sin\theta - n\cdot\cos\theta)\cdot\sin\theta\cdot d\theta + \frac{1}{\pi E}\cdot\int_{\pi+\theta_3}^{2\pi}(-a)\sin\theta\cdot d\theta \quad - 73\text{-}9$$

$$b(E) = \frac{1}{\pi E}\cdot\int_0^{\theta_2}(-a)\cdot\cos\theta\cdot d\theta + \frac{1}{\pi E}\cdot\int_{\theta_2}^{\pi+\theta_3}(E\sin\theta - n\cdot\cos\theta)\cdot\cos\theta\cdot d\theta + \frac{1}{\pi E}\int_{\pi+\theta_3}^{2\pi}(-a)\cos\theta\cdot d\theta \quad - 74\text{-}9$$

Solving for g(E) and b(E) in this case,

$$g(E) = \frac{1}{2}\cdot\left(1+\frac{\theta_3-\theta_2}{\pi}\right)+\frac{a}{\pi}\cdot\frac{(n^2+E^2-a^2)^{0.5}}{(n^2+E^2)} \quad - 75\text{-}9$$

$$b(E) = -\frac{n}{E}\cdot\left[\frac{1}{2}\cdot\left(1+\frac{\theta_3-\theta_2}{\pi}\right)+\frac{a}{\pi}\cdot\frac{(n^2+E^2-a^2)^{0.5}}{(n^2+E^2)}\right] \quad - 76\text{-}9$$

where

$$\cos\theta_3 = \frac{E(n^2+E^2-a^2)^{0.5}-an}{(n^2+E^2)} \quad - 77\text{-}9$$

$$\cos\theta_2 = \frac{E(n^2+E^2-a^2)^{0.5}+an}{(n^2+E^2)} \quad - 78\text{-}9$$

and $\tan\gamma = -\dfrac{n}{E}$ - 79-9

$$|N_E| = g(E)\cdot\left[1+\left(\frac{n}{E}\right)^2\right]^{0.5} \quad - 80\text{-}9$$

It should be noted that when $\left(\frac{E}{a}\right)$ and $\left(\frac{n}{a}\right)$ are unity then eqn. 67 is equal to eqn. 75-9 and eqn. 68 is equal to eqn. 76-9. In addition, when the term

(n) is zero eqn. 67 and 75-9 will have the same expression as eqn. 56-9. Although the reader may find the truth of these remarks rather obvious, it has been the author's experience that the usefulness of such inter-relationships is not always realised. It is quite easy to make mistakes during mathematical processing and if simple conditions can be applied the validity of the solutions can be checked.

The resulting data is shown below in table T.9-4.

Table T.9-4

E/a	20		5		1	
n/a	$1/N_E$	γ°	$1/N_E$	γ°	$1/N_E$	γ°
0	1.88	0	1.60	0	1.0	0
0.1	1.88	0.286	1.597	1.145	0.997	5.71
0.4	1.88	1.146	1.59	4.57	0.94	21.8
0.6	1.88	1.72	1.586	6.84	0.886	30.9
1.0	1.88	2.86	1.57	11.3	0.778	45.0
2	1.87	5.71	1.50	21.8	0.58	63.4
4	1.85	11.3	1.30	38.66	0.37	75.9
5	1.83	14.0	1.2	45.0	0.31	78.7
10	1.69	26.6	0.8	63.4	0.18	84.3

Using eqn. 58 and 59.9 two sets of results were calculated for the linear transfer function to demonstrate the effect of changing the drive stiffness K. The parameter values were the same as those used in the simulation. For completeness these results are tabulated below in table T.9-5.

Table T.9-5

K = 45MN/m	M = 433kg	f = 10.7 KN.s/m	K=22.5MN/m	M=433kg	f = 10.7KNs/m
ω. rad/s	$G(j\omega)$	ϕ°	ω.rad/s	$G(j\omega)$	ϕ°
100	10.09	13.9	150	2.28	9.36
200	2.58	7.04	180	1.57	7.77
250	1.654	5.65	227.95(ωn)	0.994	6.19
322.4(ωn)	0.997	4.383	300	0.574	4.71
400	0.65	3.54			

The resulting plots are drawn to scale in Fig. 9.15. In particular it should be noted that the curves describing the non-linear term, drawn for a set value of (E/a), now move away from the negative real axis as the ratio

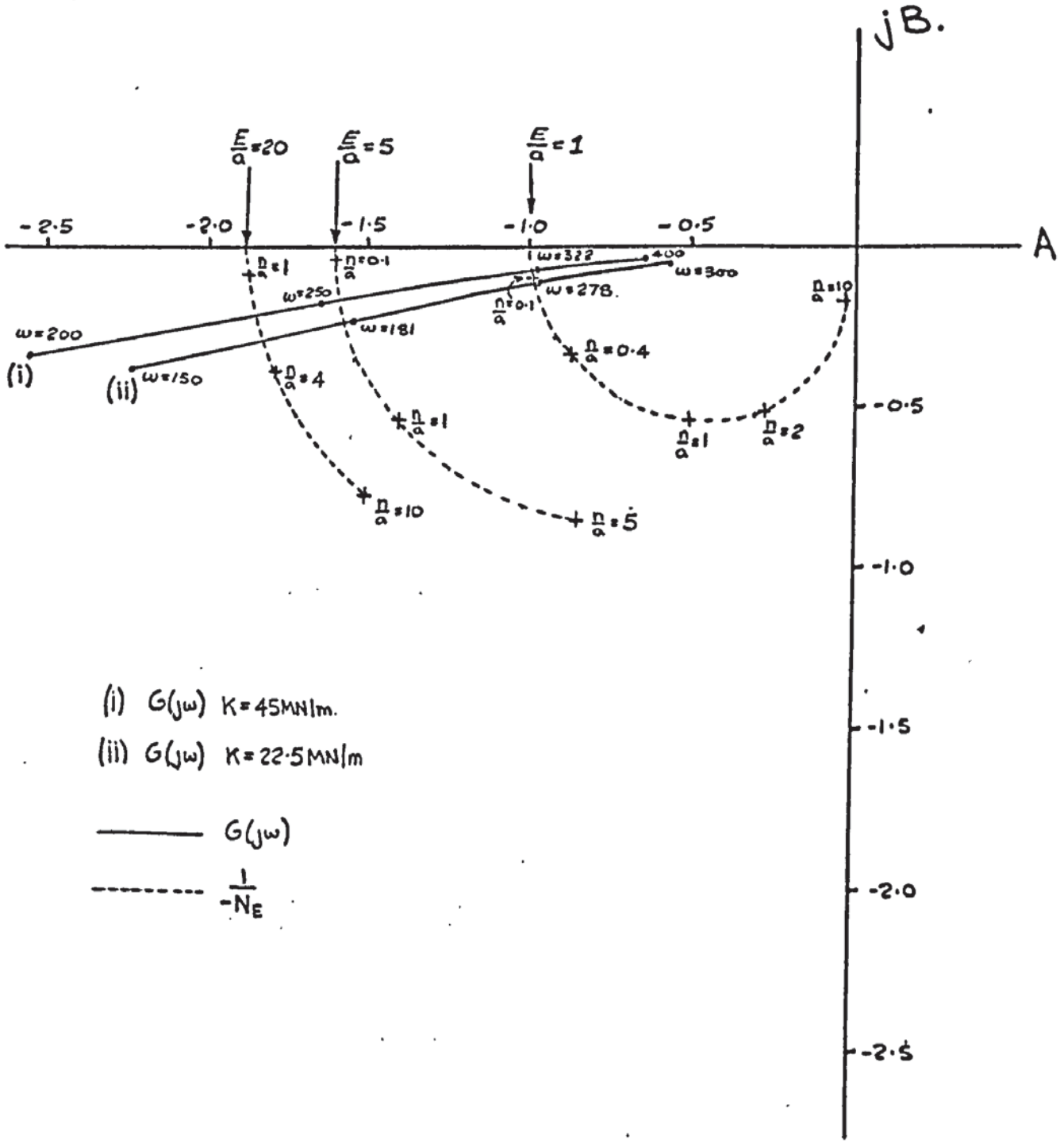

FIG. 9·15. NYQUIST DIAGRAM SHOWING INTERSECTIONS OF LINEAR PLOTS AND DESCRIBING FUNCTIONS.

(n/a) increases.

It can be seen that intersections will take place between the curves for the linear and non-linear elements. At such points the system will exhibit stable limit cycle conditions. Oscillations of a fixed amplitude and frequency will be maintained.

To interpret the results of Fig. 9.15 the following observations are made, considering the effects of various conditions in turn.

If (E) retains a constant value, and as (a) is given by,

$$a = f.\dot{x}_o \qquad - 81\text{-}9$$

then

$$\left(\frac{E}{a}\right) = \frac{\text{Constant}}{f.\dot{x}_o} \qquad - 82\text{-}9$$

As $\dot{x}_o$ is the steady sliding velocity about which oscillations take place, the ratio $\left(\frac{E}{a}\right)$ will increase as this velocity reduces.

For a constant value of (a) and using eqn. 63-9,

$$\left(\frac{n}{a}\right) = \frac{Cn \,.\, v}{\text{Constant}} \qquad - 83\text{-}9$$

The ratio (n/a) will increase as the amplitude (v) of the velocity oscillations increases.

For any of the $G(j\omega)$ curves then it can be seen that as $\left(\frac{E}{a}\right)$ increases, intersections take place at increasing values of $\left(\frac{n}{a}\right)$ and these occur at lower system frequencies. This means that as the command velocity reduces ($\dot{x}_o = \dot{x}_i$),

1) the amplitude of velocity oscillations increases.
2) the frequency of oscillations reduces.

Bearing these points in mind, it can now be seen that as the drive stiffness (K) reduces the ratio (n/a) increases at the intersections. Consequently velocity oscillations will increase in amplitude, for the same steady state velocity and their frequency will be reduced.

It can be visualised that the system velocity profile will tend to increase in size as (K) reduces. There will be increases in the critical velocity and the velocity at which stick-slip motion is replaced by quasi-harmonic oscillations.

The values of (n/a) are difficult to establish from Fig. 9.15 and so the data is re-presented in Fig 9.16. This time, the magnitudes $|G(j\omega)|$ and $1/N_E$ are plotted against phase angles ϕ and γ respectively. At the intersections the common phase angles are recorded, then from eqn. 59-9 the frequency can be calculated and from eqn. 71-9 the ratio $\left(\frac{n}{E}\right)$ can be established. It is then a simple matter to determine $\left(\frac{n}{a}\right)$ as the product of $\left(\frac{n}{E}\right)$ and the appropriate value of $\left(\frac{E}{a}\right)$ at the intersection.

K = 45MN/m				K = 22.5MN/m			
E/a	1	5	20	E/a	1	5	20
ϕ/γ	4.39°	5.53°	6.0°	ϕ/γ	6.19°	7.8°	8.47°
ω.rad/s	322.2	255	235	ω.rad/s	227.7	180	166
(n/E)	0.0768	0.0968	0.1051	(n/E)	0.1085	0.1370	0.1490
(n/a)	0.0768	0.484	2.10	(n/a)	0.1085	0.685	0.298

In order to find Cn let (e) be the amplitude of the error signal oscillation which will be related tothe velocity signal (v) by frequency (ω).

$$v = e.\omega. \qquad - 84\text{-}9$$

Now, $$\frac{n}{E} = \frac{Cn\ v}{K.e}$$

and substituting the above eqn.

$$\frac{n}{E} = \frac{Cn.\omega}{K} \qquad - 85\text{-}9$$

As Cn has the relationship (from eqn. 40-8)

$$Cn = \frac{2.Fs}{(V_{CL})^2} . (V_{CL} - \dot{x}_o)$$

the steady sliding velocity $(\dot{x}_o)$ can be found. With this information, the term (a) can be established and hence the value of (E) and subsequently (e).

$$E = \left(\frac{E}{a}\right) \times a = Ke.$$

$$e = \frac{\left(\frac{E}{a}\right) \times a}{K} = \frac{\left(\frac{E}{a}\right) \times f\dot{x}_o}{K} \qquad - 86\text{-}9$$

Using eqn. 84-9,(v) can be calculated.
These values are listed in table T9.6

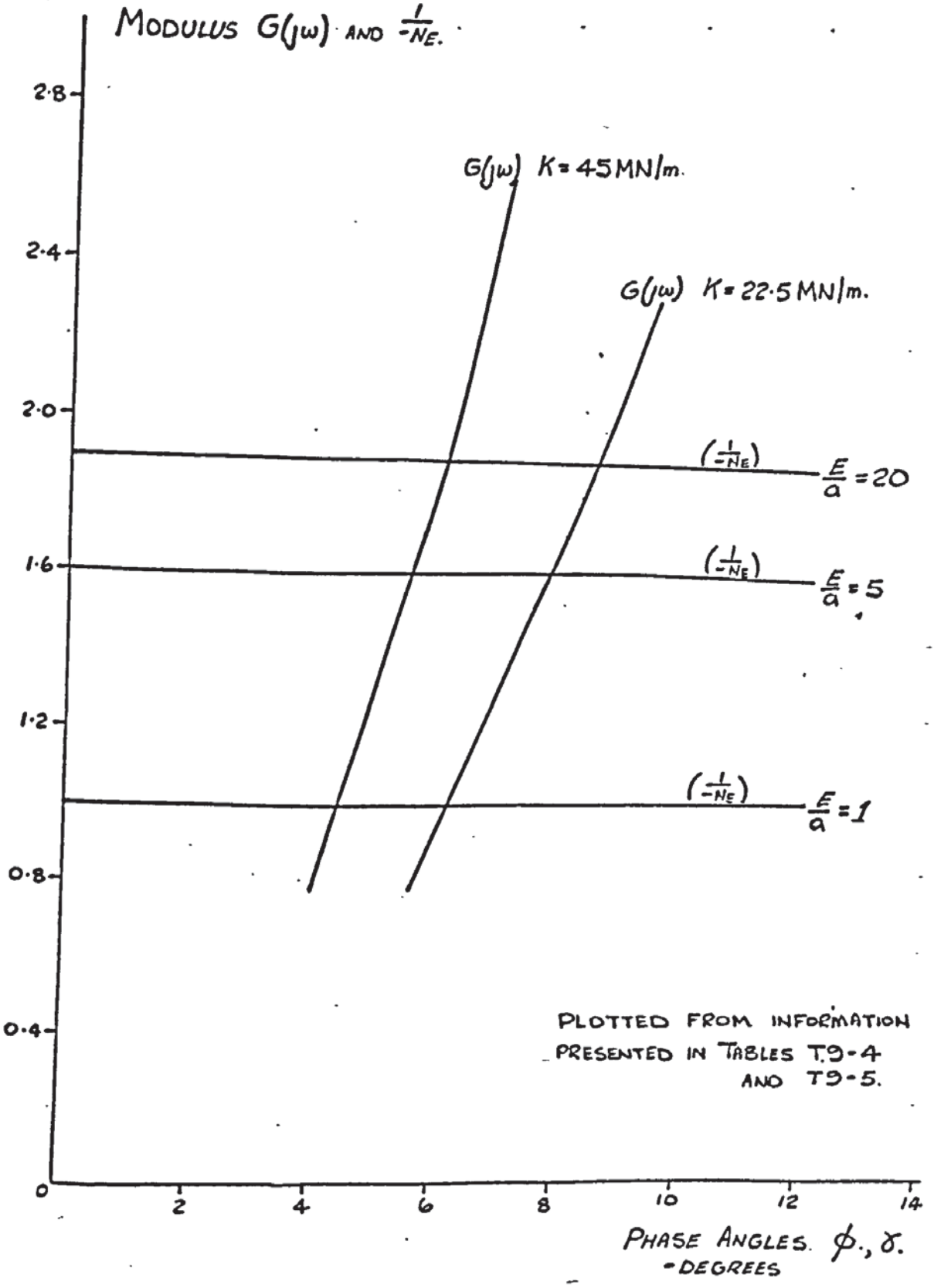

FIG. 9.16 MODULUS VERSUS PHASE ANGLE FOR LINEAR AND NON-LINEAR ELEMENTS.

Table T.9-6

K = 45 MN/m				K = 22.5 MN/m			
E/a	1	5	20	E/a	1	5	20
Cn	10.71	17.1	20.13	Cn	10.71	17.1	20.15
$\dot{X}_o$ mm/s	28.89	22.26	19.1	$\dot{X}_o$ mm/s	28.89	22.26	19.1
e. mm	0.00687	0.0255	0.091	e.mm	0.01374	0.0529	0.1818
v.mm/s	2.213	6.757	21.36	v.mm/s	3.122	9.528	30.18
ω.rad/s	322.2	255	235	ω.rad/s	227.7	180	166

This table shows that Cn (and hence $\dot{x}_o$) is related to the ratio (E/a) and the same values occur for both values of drive stiffness. Other comments are as follows,

1) When the ratio (E/a) is unity Cn has the same value as the simulated "viscous" friction. The frequency of oscillation is practically the same as the undamped natural frequency (ωn). As angle ϕ is equal to angle γ then,

$$\frac{n}{E} = \frac{f}{M(\omega n)} \qquad - 87\text{-}9$$

substituting eqn. 85-9

$$\frac{Cn(\omega n)}{K} = \frac{f}{M(\omega n)} \qquad - 88\text{-}9$$

and as

$$\omega n^2 = \frac{K}{M} \qquad - 89\text{-}9$$

then by transposing eqn. 88-9

$$Cn = f \qquad - 90\text{-}9$$

2) As $\dot{x}_o$ reduces, the amplitudes of oscillation of both position and velocity increase. In particular when (E/a) is equal to 20 the amplitude of the velocity signal (v) is greater than $\dot{x}_o$ in both cases. Therefore this must mean that "stick-slip" motion will occur. At the lower values of (E/a) the value of (v) is less than $\dot{x}_o$ and quasi-harmonic oscillations will be present.

3) A reduction in drive stiffness increases the amplitude of the oscillations. It is interesting to see that when the drive stiffness is reduced by 50% the velocity amplitudes (v) are increased by approximately 50%.

4) An attempt has been made to draw an S.V.P. for both values of K using the information presented in table T.9-6. This is shown in Fig. 9.17

Although the velocity scales are not of the same magnitude as the simulation results, the shape produced is consistent with those in the later section of the recorded S.V.P.s

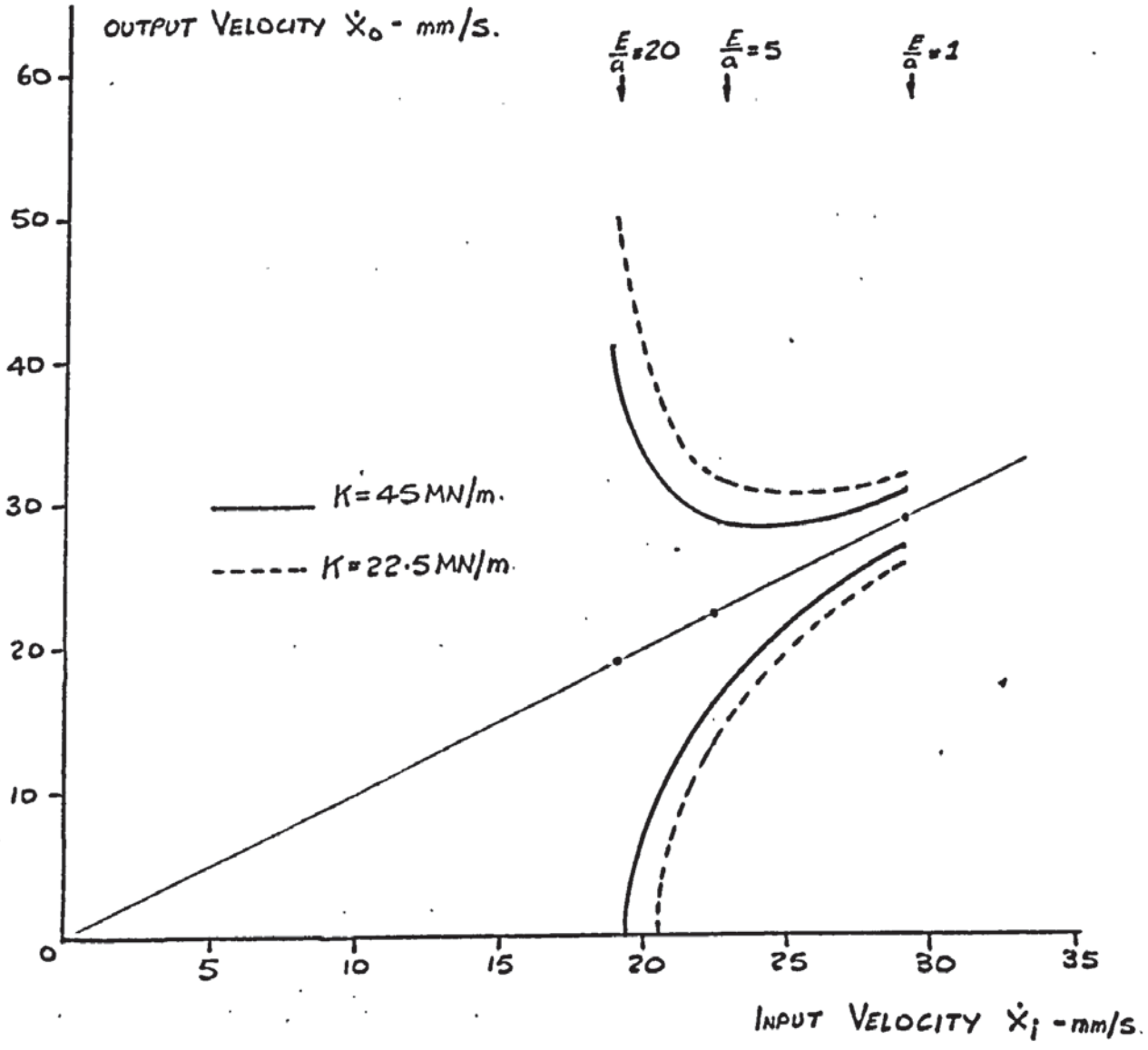

FIG 9·17. A SYSTEM VELOCITY PROFILE - USING DATA OBTAINED FROM DESCRIBING FUNCTION ANALYSIS OF FRICTION SYSTEM.

To conclude this section on describing functions, the author feels it is clear that this technique does have a superiority over other forms of analysis. In particular the mode of oscillation and their magnitude can be estimated for a particular mean sliding velocity. An attempt has been made to show that oscillations, especially in quasi-harmonic conditions can be sustained.

The critical velocity condition is not so easy to visualise. From the information presented in table T.9-6 the system will oscillate at a frequency very close to its ωn value when (E/a) is unity. Observations made in chapter 8 indicate that at the critical velocity, system oscillations are also at frequency ωn. Therefore it is suggested that for this particular describing function (Fig.9.14) the critical velocity will occur when (E/a) is unity. This means that the magnitude of Cn is the same as that for the "viscous" damping value f. (eqn. 90-9).

If this relationship gives the true value of Vc then the observed value obtained by applying a ramp velocity input, will definitely be larger. This can be appreciated by considering Fig. 9.17 since a fixed amplitude (v) is present at the velocity for which (E/a) is unity. It is suggested that this amplitude would reduce to zero with further velocity increases, probably following a linear exponential decay.

The effect of the solid friction time constant (Tc) has not been considered here although it was present in the simulation study. The describing function curves will change their positions if this term is included. The added complexity means the use of a digital computer would be essential to handle the calculations.

Although a great deal of further work is required the author feels that it is by describing function techniques that a satisfactory analytical solution can be established.

9.5 CONCLUSIONS

The analysis of a slideway system is made complicated by the non-linear friction behaviour. Mathematical analysis is not easy and only one technique, that of Describing Functions, is worthy of concentrated study. Nevertheless oscillatory problems associated with low sliding speeds can be analysed using simulation techniques. The problem in this case is the degree of sophistication to be built into the simulation circuit.

The answers provided by the simulation used here have allowed equations to be formed that do give comparable results with those obtained from machine tool slideways (eqn. 22-9 and 23-9).

To provide a guide to design engineers, eqn. 22-9 can be expanded to include data derived in chapter 7. Using eqn. 18-9 (W = 450 kgf) and rearranging in terms of Vc,

$$Vc = Vc_L \left[1 - Vc_L \left(\frac{32.5 \cdot \eta^{0.363} \cdot K^{0.077}}{2\,Fs} \right) \right] \qquad - 92\text{-}9$$

Substituting for Vc_L and Fs using eqn. 11-9 and 12-9 with the following changes

i) Pw replaced by $\frac{W}{A_A}$

ii) Pw.Tan θ approximated to $(Pw)^{0.82}$. Tan θ for simplification.

$$Vc = \frac{W^{1.515} \cdot (Ho + hd)^{3.754}}{8.45\,(A_A)^{1.515} \cdot \eta^{0.274}} \cdot \left[1 - \frac{19.8(W)^{0.695} \cdot (Ho+hd)^{3.754} K^{0.077} \cdot \eta^{0.12}}{(A_A)^{1.695} \cdot (K_{LP} + 103.Tan\,\theta)} \right] \text{-mm/s} \qquad -93\text{-}9$$

Several observations can now be made about ways to reduce Vc.

a) Oil viscosity (η) should increase.

b) Load (W) must reduce.

c) Stiffness (K) must increase.

d) The term (K_{LP}) must reduce - this is most easily done by the inclusion of polar additives in the lubricant.

e) The term (Ho + hd) should increase. This means that the general surface waviness over one centimetre intervals should be larger. This could be done by scraping the sliding surface, which would provide a better lifting action.

f) Tan θ should decrease making the asperity wedge base angle smaller, producing a "smoother" local surface condition. Again, scraping the surface may produce this.

g) The apparent contact area (A_A) should decrease, and could be done by making small slots on the sliding surface. This rather unusual result comes about from the fact that although a reduction in area will increase Vc_L it will have a greater affect on reducing the value of (Fs). Therefore the bracketed term of eqn. 92-9 will reduce by a greater amount than the quantity Vc_L will increase, thus reducing the critical velocity.

If it is possible to apply eqn. 93-9 down to the limit when the critical velocity is zero,

$$\frac{19.8(W)^{0.695}.(Ho + hd)^{3.754}.K^{0.077}.\zeta^{0.12}}{(A_A)^{1.695}.(K_{LP} + 103.\text{Tan}\,\theta)} = 1 \qquad - 94\text{-}9$$

or

$$(A_A)^{1.695}.(K_{LP} + 103.\text{Tan}\,\theta) = 19.8(W)^{0.695}.(Ho+hd)^{3.754}.K^{0.077}.\zeta^{0.12} \qquad - 95\text{-}9$$

In practice, the left hand side is always the larger. On a particular machine with fixed values for Tan θ, A_A, K, (Ho + hd) and W the relationship between K_{LP} and ζ becomes very important. The equality of eqn. 95-9 could be achieved by extremely large increases in bulk oil viscosity, but the author feels that it is far more convenient to reduce K_{LP}. This can be done easily by including polar additives in the bulk lubricant.

In conclusion it should be pointed out that all the parameters in eqn. 93-9 could quite easily be found with the exception of K_{LP}. This will prove a difficulty until further studies are made. Meanwhile it is suggested that the values found in chapter 7 could be used for cast iron slideways.

For Polar Oils $K_{LP} = 7.87$ kgf/mm^2

For Non-Polar Oils $K_{LP} = 23.0$ kgf/mm^2

The remaining parameters in eqn. 93-9 have the following units, W - kgf, (Ho + hd) - μm, ζ - P, K - N/mm, A_A - cm^2. These can be available for the design engineer, but the author suggests that, from the work carried out in chapters 5 and 7, the values of Tan θ and (Ho + hd) could be taken to be the same for all ground cast iron surfaces.

CHAPTER 10
CONCLUSIONS AND RECOMMENDATIONS

This study has brought together physical and mathematical considerations using a control system approach to the overall analysis.

The non-linear friction characteristic of machine tool slideways is dependent upon many variables. As stated in the introduction some of these variables have not been proven. It has been shown that two new parameters (K_o) and (K_{LP}) will help to provide a better understanding of oil behaviour in a friction model. Available data about the effect of oil on lubricated surfaces is not yet sufficient to express these independently, like properties such as surface finish and viscosity.

The way in which the friction characteristic falls with increasing velocity is an extremely important mechanism. An engineering solution depends upon an understanding of the physical interaction between the surfaces.

The detailed work undertaken regarding surface conditions does give as complete a picture as possible, in particular the determination of the static friction level (F_s) and the velocity at which 'solid' friction ceases (V_{cL}). These two enable a solution to the problem to be initiated, and are used to form the equation for solid friction gradient.

$$C_n = \frac{2F_s}{(V_{cL})^2} (V_{cL} - \dot{X}_o)$$

In many cases they could be measured quite easily on a machine tool slideway, especially as the viscous friction quantity is small.

This is not the complete picture, for the friction/velocity relationship is time dependent. It must have a system transfer function of its own. In this work a first order equation has been used.

$$F(\text{solid}) = \frac{F_s}{(V_{cL})^2} (V_{cL} - \dot{X}_o)^2 \cdot \left(\frac{1}{1 + T_c.S} \right)$$

The value of T_c has been difficult to establish from studies of the system in terms of its physical parameters. The simulation study has provided the only way of doing this. The value of C_n at the critical velocity will depend upon the value of T_c, and as C_n can be expressed in terms of the physical parameters it has been possible to relate T_c to oil viscosity.

$$Tc = 5.3 (\eta)^{0.183} \text{ -ms}$$

It would be dangerous to presume that Tc is a function of bulk oil viscosity alone. It is more likely that this constant is a function of metal damping within the asperities, coupled with some additional effect of the lubricant. Even in a dry condition Tc would have some value and could be effectively equated to some minimum "viscosity" value.

Concerning the oscillatory motion, of the mathematical analysis carried out only the Describing Function technique has proved of value. It is a cumbersome technique but does provide the necessary confirmation of observed results. The answers obtained depend upon the sophistication of the describing function equations, and in this work a successful way has been explored and is capable of further development.

For the present the Analogue computer gives excellent results and now that some relationship between (Tc) and (η) has been established its usefulness can be extended. By keeping the circuit simple only a few design parameter values are required. Apart from the sliding mass and drive stiffness, the values of V_{cL} , Fs and f can be obtained from the equations produced in chapter 7. From an engineering point of view the value of Tc must be established which will suppress the critical velocity to a value below the normal operating range of velocity.

The simulation will give a direct recording of the S.V.P. In most cases the shape will be of little importance. If stick-slip motion is exhibited efforts should be made to eliminate this. It is possible that under "quasi-harmonic" conditions only, the system can be stabilised by conventional control techniques; these would not operate satisfactorily under 'stick-slip' conditions. From simulation studies a complete quasi-harmonic regime can be established by increasing the value of V_{cL} only.

From a purely friction point of view the best characteristic to achieve is one in which the coefficient remains constant at all velocities. This would be difficult to obtain under dry surface conditions, and anyway would incur high friction forces. Oil lubrication can make sliding stability more uncertain since it accentuates the normal dry friction characteristic, causing the friction coefficient to reduce by a much larger factor over a greater velocity range. The important point here is the degree of change in friction level. What is required is the suppression of the static friction level and this can only be achieved with oil lubricants

by the use of polar material. What seems to be the best situation is to have a low viscosity oil (say 0.2P) containing long chain polar material. This will suppress the value of Fs and increase the magnitude of V_{cL}, producing a very shallow friction characteristic.

Considering now the wear conditions and changes in surface topography. Obviously we must discount the operation of a slideway system under dry conditions. It has been shown in chapter 5 from the model tests that a very low wear rate prevails after a period we would normally call "running-in". What has happened is that the actual contact area has been increased and consequently individual asperity loading has reduced. This is a condition that a slideway system should maintain over its working life. Unfortunately only in a dry situation can the wear rate be estimated. With the addition of lubrication the time taken to reach a steady "higher contact area" condition is prolonged and any"constant" wear rate would be difficult to assess. Measurements have demonstrated that a steady state surface topographical condition is reached ultimately on cast iron slideways and it is suggested that this will occur regardless of the initial surface conditions. In other words it is inherent in a slideway system to produce a condition of least wear and perhaps least resistance. The understanding of such a mechanism is essential in order to aid and sustain such a condition.

Eventually oil lubrication as we know it will be finished and it is becoming important to make good use of available lubricants and reduce waste. It is suggested that cast iron slideways should continue to be used and radical changes should be made in the forms of 'lubricant'. All that is required on a slideway is some form of protection from chemical and atmospheric attack and reduction in the static friction level, moreover these effects must be maintained.

Some intimations of further work have been made but are now listed in what the author feels to be the order of importance.

1) A study of the mechanism by which oil polar additives reduce the coefficient of friction at very low sliding speeds

2) A study of the mechanism by which slideway surfaces reach a steady state topographical condition, both when dry and lubricated.

3) A study into alternative forms of lubricant and methods of lubricating cast iron slideways

4) The establishment of a physical means of determining the surface time constant (Tc), needed in the friction/velocity transfer function.

5) The development of the Describing Function technique for the analysis of slideway oscillatory motion due to friction.

6) An expansion of slideway system simulation techniques both analogue and digital. It seems certain that these techniques will present the best picture of performance related to friction behaviour.

7) The suppression of oscillatory motion on slideways by the use of control system techniques, especially on automated machine tools.

Complex answers to rather complex problems are not conducive to increases in machine tool sales. As far as slideways are concerned some frictional problems can be analysed quite easily by the findings presented here. In addition data has been assembled so that the effects of parameter changes can be predicted.

APPENDIX 1

The Scanning Electron Microscope

The scanning electron microscope Fig. A.1 enables surfaces to be examined over a wide range of magnification (x 20 to x 50,000) with a greater depth of focus, without the elaborate and costly specimen preparation, than can be achieved by other methods of microscopy. The specimen can be manoeuvred in five different planes about the x, y and z axes, and can be accurately positioned in any of these planes from a given datum. To obtain a stereoscopic effect, pairs of photomicrographs can be obtained by movement of one of the five positioning devices and insertion of this pair in a suitable viewing unit produces the three dimensional effect.

The principle of the S.E.M. in that an electron beam is directed down an evacuated chamber containing electro-magnetic lenses which reduce the diameter of the beam. Scanning coils are used to raster the beam across the specimen surface being viewed. Fast reflected primary and slower secondary electrons are emitted from the specimen. A proportion of both types of electrons strike a layer of aluminium, approximately 700 Å thick, which is coated on the end of a perspex rod which causes fluorescence. This light energy is converted to an electrical signal by a photomultiplier which provides the major part of the amplification of the signal required. This amplified signal is recorded as a pulse on a cathode ray tube, and by scanning the electron beam in synchronism with the raster on the cathode ray tube, an image of the surface topography of the specimen is built-up, which is similar to a television picture. In applying a voltage to a collector grid positioned between the specimen and the scintillator the slower secondary electrons can be made to contribute to the C.R.T. image and as the applied voltage is increased so the number of secondary electrons attracted increases. The electron image is produced on two separate C.R.T.s, one with long persistence for visual examination and the other with no persistance for photographic recording.

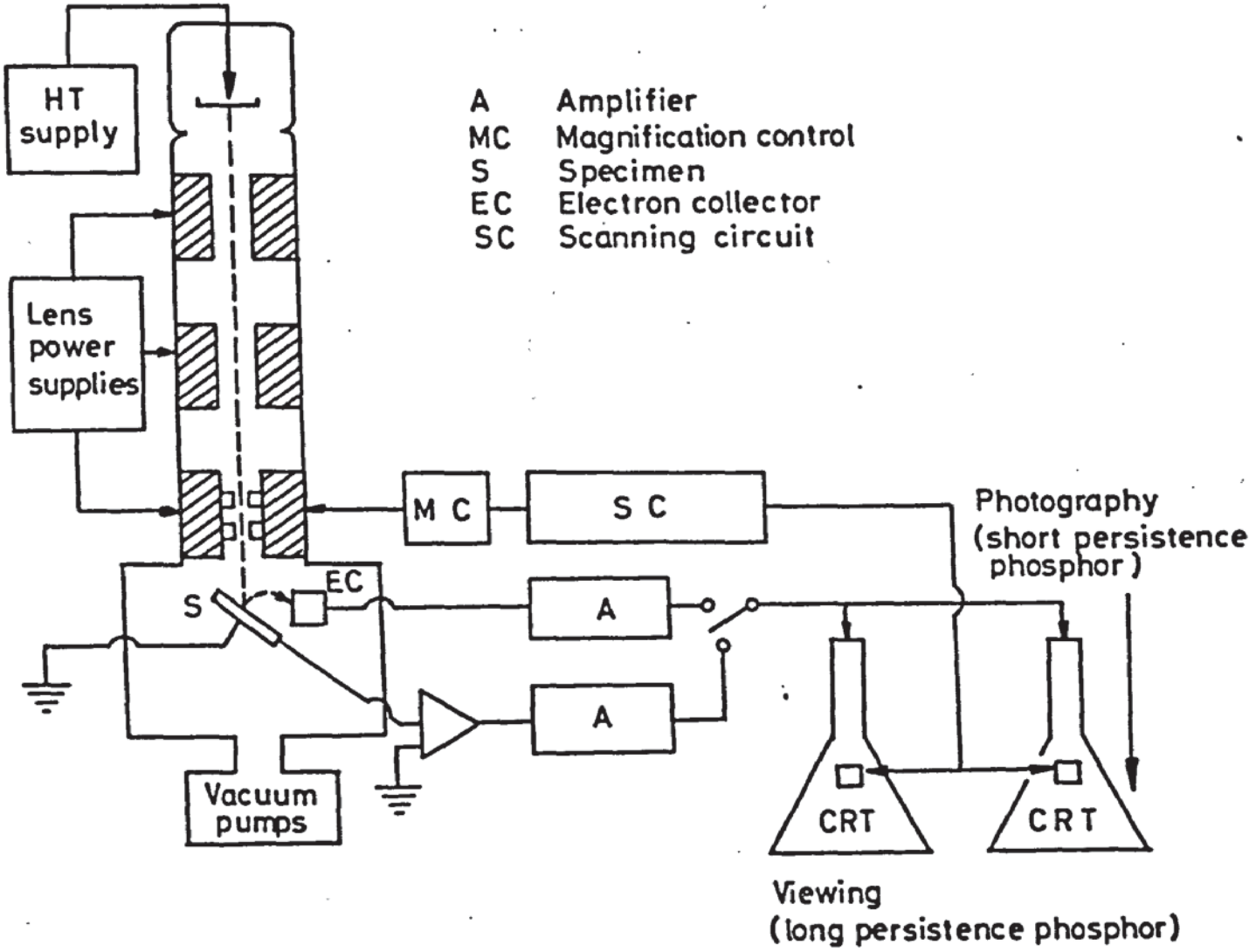

FIG. A.1. SIMPLIFIED BLOCK DIAGRAM OF A SCANNING ELECTRON MICROSCOPE.

High density (high atomic number) materials reflect more primary electrons than low density (low atomic number) materials. Hence in a multi-phase region of a specimen the densest phase is brightest on the screen. Surfaces orientated favourably reflect electrons towards the scintillator which appear bright on the screen while the areas reflecting electrons away from the scintillator attracts these electrons, which are deflected away from the scintillator, so that the interior features of holes can be observed. The electrons attracted by the grid are referred to as secondary electrons, and these are also produced as a result of collision between high energy electrons of the beam and the atoms of the specimen. The original electrons loose their energy but orbital electrons are ejected from the atoms of the target material and these possess sufficient energy to cause reproduction of the process. This process continues until the ejected electrons have insufficient energy to cause further liberation of electrons from target atoms or until the ejected electrons leave the surface of the specimen as secondary electrons.

Projections usually appear brighter than the rest of the surface since there is less possibility of secondary electron emission. Secondary electrons usually give a larger total signal and consequently a more advantageous signal to 'noise' ratio. Non-conducting particles, such as oxide, which are on the specimen surface become charged to a high voltage by the beam so that primary electrons are repelled, and those that travel towards the collector produce a stronger signal. Low density materials therefore can appear as the brightest area of the image produced on the C.R.T. due to this emission.

The limitation of the S.E.M. are factors which affect the resolution of the C.R.T. image. They are principally, the diameter of the electron beam, the wavelength of the electrons, (the higher the accelerating voltage the smaller the wavelength) and the 'noise' resulting from the electronic circuitry of the instrument.

The size of specimen for maximum specimen manoeuvrability must be limited to 12.7 mm diameter by 10 mm length.

Conducting specimens need no special preparation; the specimen is cut to size and mounted on a specimen holder, using an adhesive, before mounting into the instrument. If a non-conducting adhesive is used then electrical contact is made by painting the junction between specimen and holder with silver 'dag'. Non-conducting specimens can only be examined if the surface is first coated with an evaporated conducting film.

Scanning electron microscopy gives the best results when examining small areas of machined surfaces since the nature of metal removal and the surface deformation caused through the machining can be examined in detail, in a manner not possible by optical microscopy or surface profile investigation.

BIBLIOGRAPHY

(1) FRICTION - SELECTED REPRINTS
Published for the American Association of Physics Teachers by the American Institute of Physics. 1967

(2) BOWDEN F.P. and TABOR D.
The friction and lubrication of solids
Oxford University Press. Pub: 1950 2nd Edition: 1964

(3) PALMER F.
What about Friction?
American Journal of Physics. 1949 pp.181-187 and pp 327-342
Vol. 17

(4) KRAGALSKII I.V.
Friction and Wear
Butterworths, London 1965

(5) NICA A.
Theory and Practice of Lubrication Systems
Scientific Publications (G.B.) 1970

(6) TOMLINSON G.A.
A molecular theory of Friction
Philosophical Magazine and Journal of Science
Vol. 7 No.46 1929 pp. 905-939

(7) BOWDEN F.P. and LEBEN L.
The Nature of Sliding and the Analysis of Friction
Proc. Royal Society, London
Vol. A. 169 1939 pp.371-391

(8) KRAGALSKII I.V.
Calculation of Dry Friction Force
Proc. Conf. Lub. and Wear. I.MECH.E. Paper 75 1957 pp. 302-307

(9) SCHNURMAN R. and WARLOW-DAVIES E.
The electrostatic component of the force of sliding friction
Physical Society Proceedings. Vol. 54 1942 pp. 14-27

(10) SAMPSON J.B., MORGAN F., REED D.W., MUSKET M.
Friction behaviour during the slip portion of the stick-slip process
Journal of Applied Physics. Vol.14 Dec.1943 pp.689-700

(11) RABINOWICZ. E.
The nature of the Static and Kinetic Coefficients of friction
Journal of Applied Physics. Vol.22 No.11 1951 pp.1373-1379

(12) RABINOWICZ E.
The intrinsic variables affecting the stick-slip process
Proc. Physics Society London Vol.71 1958 pp.668-675

(13) RABINOWICZ E.
Practical Uses of the Surface Energy Criterion
Mechanisms of Solid Friction. Pub. Elsevier, 1964, pp 9-22
(Papers presented at a conference held at the Midwest Research Institute, Missouri, U.S.A. in 1963)

(14) Proceedings of the Conference on Lubrication and Wear
Institution of Mechanical Engineers, London 1957

(15) JOHNSON K.L.
Recent Developments in the Theory of Elastic Contact Stresses; their Significance in the study of surface breakdown
Proc. Con. Lub. and Wear, 1957
I. MECH. E. London Paper 24

(16) KRAGHELSKII I.V. and SABELINIKOV V.P.
Experimental check of Elementary Laws of Friction: dry friction
Proc. Con. Lub. and Wear 1957
I.MECH.E. London Paper 7

(17) ARCHARD J.F.
From Discussion of Conference Papers - Session 3
Proc. Con. Lub. and Wear 1957
I. MECH. E. London

(18) ARCHARD J.F.
Contact and Rubbing of Flat Surfaces
Journal of Applied Physics. Vol. 24 1953 p.981

(19) DERJAGUIN B.V. TOLSTOI D.M. and PUSH V.E.
A Theory of stick-slip sliding of Solids
Proc. Con. Lub. and Wear 1957
I. MECH. E. London Paper 13

(20) HARRISON H.L. and BOLLINGER J.G.
Introduction of Automatic Control
Internation Textbook Company 1963

(21) BROCKLEY C.A., POTTER A.F. and CAMERON R.
Friction Induced Vibrations
Trans. A.S.M.E. Journal of Lubrication Technology
Vol. 89 April 1967 pp 101 - 108

(22) BROCKLEY C.A. and DAVIES H.R.
The time-dependence of static friction
Trans. A.S.M.E. Journal of Lubrication Technology
Vol. 90, January 1968, pp. 35-41

(23) BROCKLEY C.A. and KO P.L.
The measurement of Friction and Friction Induced Vibrations
Trans. A.S.M.E. Journal of Lubrication Technology
Vol. 92, October 1970, pp. 543-549

(24) BROCKLEY C.A. and KO P.L.
Quasi-harmonic Friction-induced Vibration
Trans. A.S.M.E. Journal of Lubrication Technology
Vol. 92 October 1970 pp.550-556

(25) MINORSKY N.
Introduction to Non-linear Mechanics
Pub. Edwards Brothers Inc. Michigan 1947

(26) BELL R. and BURDEKIN M.
Dynamic Behaviour of Plain Slideways
Proc. of the Inst. Mech. Eng.
Vol. 181 No.8 1966/67 pp 169-184

(27) JOHANNES V.I., BROCKLEY C.A. and GREEN M.A.
The Role of the Rate of Application of the Tangential Force in determining the Static Friction Coefficient
Wear. Vol. 24 1973 pp. 381-385

(28) TAKANO E. and ISHIBASHI T.
Oscillation Caused by Solid Friction (Part 3 and 4)
Bulletin of the J.S.M.E.
Vol. 16, No.98 1973 pp 1153-1175

(29) PAVELESCU D.
Dependence of Friction and Stick-slip on the Main Wear Factors
Rev. Roumaine des Sciences Techniques series de Mechanique Applique. Vol. 13 No.1 1968 pp 61-77

(30) PAVELESCU D. and DIMITROV B.
Wear under Stick-slip Conditions
Rev. Roum. Sci. Tech. - Mech. Appl.
Vol. 14, No.3, 1969. pp 673-682

(31) PEKLENIK J.
New Developments in Surface Characterisation and Measurements by means of Random Process Analysis
Proc. Inst. Mech. Eng. Vol. 182, PT.3K 1967-68 pp 108-126

(32) KIMURA Y.
Estimation of the Number and the Mean Area of Real Contact Points on the basis of Surface Profiles
Wear. Vol. 15, 1970 pp 47-55

(33) TSUKIZOE T. and HISAKADO T.
The Influence of Surface Roughness on the Mechanism of Friction
Trans. A.S.M.E. Journal of Lubrication Technology
Vol. 92, April 1970. pp. 264-273

(34) GUPTA P.K. and COOK N.H.
Junction Deformation Models for Asperities in Sliding Interaction
Wear. Vol. 20, 1972 pp. 73-87

(35) CHIVERS T.C., MITCHELL L.A. and ROWE M.D.
The Variation of Real Contact Area between Surfaces with Contact Pressure and Hardness
Wear Vol.28, No.2 1974 pp 171-185

(36) TSUKADA T. and ANNO Y.
An Analysis of the Elasticand Plastic Deformations of Machined Surfaces in Contact (3 reports)
Bulletin J.S.M.E. Vol. 17, No.105 1975 pp 376-400

(37) HISAKADO T.
Effect of Surface Roughness on Contact Between Solid Surfaces.
Wear. Vol. 28, No.2 1974 pp 217-234

(38) TOLSTOI D.M.
Significance of the Normal Degree of Freedom and Natural Normal Vibrations in Contact Friction
Wear. Vol. 10, 1967 pp 199-213

(39) TAKAHASHI N. and OKADA K.
Electron Microscope study of the Intermittent Motion of Friction.
Wear Vol. 28 No.3 1974 pp 285-298

(40) QUINN T.F.J.
Physical Techniques for examining surfaces
Tribology No.3 November 1970 pp. 198-205

(41) MATSUZAKI A. and HASHIMOTO S.
Theoretical and Experimental Analysis of Stick-slip in Hydraulic Driving Mechanisms
Bulletin J.S.M.E. Vol. 6 No.23 1963 pp. 449-458

(42) MATSUZAKI A.
The Vibration of a Hydraulically Driven Table in Milling
Bulletin J.S.M.E. Vol.9 No.33 1966 pp. 67-76

(43) STEWART D.G. and HUNT J.B.
Relaxation Oscillations on a Machine Tool Slideway
Proc. Instn. Mech. Engrs. Vol.184 Pt. 3L 1969/70 pp 33-39

(44) BELL R. and BURDEKIN M.
The Frictional Damping of Plain Slideways for Small Fluctuations of the Velocity of Sliding
Proc. 8th International M.T.D.R.Conference 1967 pp 1107-1126

(45) BELL R. and BURDEKIN M.
An investigation into the Steady-State Characteristics of Plain Slideways
Proc. Instn. Mech. Engrs. Vol.184 (Pt.1 No.59) 1969/70

(46) BELL R. and BURDEKIN M.
A Study of Stick-Slip Motion of Machine Tool Feed Drives
Proc. Inst. Mech.Engrs. Vol.184 (Pt.1 No.30) 1969/70 pp 54-560

(47) BRITTON D.R. and BELL R.
The Influence of Design Parameters on the Stability of Sliding Motion of Machine Tool Feed Drives
Proc. 12th International M.T.D.R. Conference 1971

(48) MATSUZAKI A.
Methods of Preventing Stick-Slip
Bulletin J.S.M.E. Vol. 13 No.55 1970 pp 34-42

(49) LENKIEWICZ. W.
The Sliding Friction Process - Effect of External Vibrations
Wear Vol.13 1969 pp 99-108

(50) KATO S., YAMAGUCHI K., and MATSUBAYASHI T.
On the Dynamic Behavior of Machine Tool Slideway
(2nd Report. Characteristics of Kinetic Friction in Stick-Slip Motion).
Bulletin J.S.M.E. Vol. 13 No.55 1970 pp.180-188

(51) KATO S., SATO N. and MATSUBAYASHI T.
Some Considerations on Characteristics of Static Friction of Machine Tool Slideway
Trans. A.S.M.E. Journal of Lubrication Technology
Vol. 94 No.3 1972 pp. 234-247

(52) SINGH B.R.
Study of Critical Velocity of Stick-slip Sliding
Trans. A.S.M.E.Journal of Engineering for Industry
Vol. 82 Series B. 1960 pp. 393-398

(53) BANERJEE A.K.
Influence of Kinetic Friction on the Critical Velocity of Stick-Slip Motion
Wear Vol.12 1968 pp. 107-116

(54) NAKASHIMA K., TAKATO M. and MORITA Y.
Study on Machine Tool Slideway
(Analysis of Sliding Motion by Simulation)
Bulletin J.S.M.E. Vol. 16 No.99 1973 pp. 1457-1466

(55) WITTGENSTEIN L.
Philosophical Investigations
Oxford Press 1972

(56) NEALE M.J.
Selection of Bearing Types (Section A1)
Tribology Handbook
Pub. in association with the Committee on Tribology of the Department of Trade and Industry 1973

(57) STANSFIELD T.M. and YOUNG A.G.
Sliding Bearings - Selection and Design (Section A.28)
Tribology Handbook
Pub. in Association with the Committee on Tribology of the Dept. of Trade and Industry 1973

(58) LEVIT G.A. and LUR'E B.G.
Application of Various Types of Slideway
Machines and Tooling Vol. 37 No.1 1966 pp 4-10

(59) M.T.I.R.A.
Machine Tool Slideways - A Bibliography
Published March 1973

(60) KATO S., MATSUBAYASHI T. and MORI N.
On the Dynamic Behaviour of Machine Tool Slideway
(3rd Report, Pitching and Yawing Motion of Moving
Element caused by Stick-Slip)
Bulletin J.S.M.E. Vol. 13 No.64 1970 pp. 1255-1263

(61) ELLIS E.G.
Fundamentals of Lubrication
Scientific Publications (G.B.) Ltd. 1968

(62) SHELL INTERNATIONAL PETROLEUM CO.LTD. LONDON
Metallurgy and Lubrication
Shell Report No.386F Nov. 1968

(63) BURDEKIN M., COWLEY A. and HEMMINGWAY P.
Wear of Slideways
Tribology. February 1971 pp. 15-20

(64) LAPIDUS A.S.
Research on Machine Tool Slideway Wear
Advances in M.T. Design and Research
Proc. 8th Int. M.T.D.R.Conf. University of Manchester 1967
pp 1139-1154

(65) P.E.R.A.
Slideway Wiper Performance Tests - A Guide to Basic Design
P.E.R.A.Report No.124 1964

(66) M.T.I.R.A.
Machine Tool Slideways, Pt. 7, Covers for Slideways
Machine Tool Research Vol.5, No.4 1966 pp 105-107

(67) HOCKE H.
Wear Resistant Parts - Material Selection (Section A41)
Tribology Handbook
Pub. in association with the Committee on Tribology of the
Dept. of Trade and Industry - Butterworths, London 1973

(68) SEIFERT W.W. and WESTCOTT V.C.
A method for the Study of Wear Particles in Lubricating Oil
Wear Vol.21 No.1 1972 pp 27-42

(69) M.T.I.R.A.
Friction and Wear of Materials for Machine Tool Slideways
Research Report No.47 1972

(70) MORGAN H.L.
Surface Hardening of Cast Iron by Induction and
Flame Hardening Processes
B.C.I.R.A. Journal Sept. 1971 pp 107-116

(71) B.C.I.R.A.
Engineering Data on Grey Cast Irons
B.C.I.R.A. 1968

(72) H.W.WARD & CO.LTD.
Machine Tool Manufactures
Blackpole Worcester

(73) M.T.I.R.A.
Plastics for Machine Tool Slides
Research Report No.43 1971

(74) PRODUCTION ENGINEER
A report on the use of Plastic Coated Slides on a large Machine Tool
Journal Inst. Prod. Engrs. Vol.53 No.11 1974 p.470

(75) BACK N., BURDEKIN M. and COWLEY A.
Review of the Research on Fixed and Sliding Joints
Proc. 12th M.T.D.R. Conference University of Manchester 1971 (Paper No.96)

(76) FOX D.G.
Hydraulic Feedrate on the "Autoward" - Investigation and Redesign.
MSc Thesis. The University of Aston in Birmingham 1967

(77) DOLBEY M. P.
The Normal Dynamic Characteristics of Machine Tool Slideways
Ph.D. Thesis U.M.I.S.T. 1969

(78) YOKOYAMA Y ., OKABE S. and ISHIKAWA K.
Reduction of Kinetic Friction by Harmonic Vibration in an Arbitary Direction
Bulletin J.S.M.E. Vol. 14 No.68 1971 pp. 139-146

(79) REASON R.E.
Surface Specification (Section F.2)
Tribology Handbook
Pub. in Association with the Committee on Tribology of the Dept. of Trade and Industry - Butterworths, London 1973

(80) FREY H. and FELLER H.G.
Investigations of Wear with the Scanning Electron Microscope
Prakt. Metallographie Vol.9 No.4 1972 pp. 187-197

(81) GRIEVE D.J., KALIZER H. and ROWE G.W.
A "normal wear" process examined by measurements of Surface Topography
C.I.R.P. Annuals Vol.18 1970 pp.585-592

(82) DENNIS J.K. and FUGGLE J.J.
Surface Damage resulting from a Talysurf Stylus
Trans. Inst. Metal Finishing Vol.47 1969 pp.177-178

(83) GUERRERO J.L. and BLACK J.T.
Stylus Tracer Resolution and Surface Damage as determined by Scanning Electron Microscopy
Journ. of Engineering for Industry A.S.M.E. Vol.9 Series B. No.4 1972 pp. 1087-1093

(84) EYRE T.S.
Wear Characteristics of Grey Iron
Foundry Trade Journal December 1970 pp. 931-936

(85) EYRE T.S. and MAYNARD D.
Surface Aspects of Unlubricated Metal-to-Metal Wear
Wear Vol. 18 No.4 1971 pp. 301-310

(86) ENDO K., FUKUDA Y. and TAKAMIYA O.
Wear Behaviours of Metals under Lubricated Conditions and the effect of Small Electric Potential
Bulleting J.S.M.E. Vol. 14 Pt.78 1971 pp.1281-1288

(87) GRUNDY J.R.
An intra-oral Replica Technique for use with the Scanning Electron Microscope
British Dental Journal Vol. 130 No.3 1971 pp. 113-117

(88) FINKIN E.
Surface Roughness in Wear
Wear Vol.6 1963 pp. 293-302

(89) KAWAI N., KONDO K. and NAKAMURA T.
The Frictional Mechanism of Surface of Metals Plastically Deformed
Bulletin J.S.M.E. Vol. 17 No.108 1974 pp. 803-809

(90) LANDSDOWN A.R.
Lubrication (Section P1)
Tribology Handbook
Pub. in association with the Committee of Tribology of the Dept. of Trade and Industry - Butterworths, London 1973

(91) CINCINNATI MACHINE TOOL CO.LTD.
Kingsbury Road
Birmingham 35

(92) FOWLE T.I.
Lubrication (Section B2)
Tribology Handbook
Pub. in association with the Committee of Tribology of the Dept. of Trade and Industry - Butterworths, London 1973

(93) GODFREY D.
Boundary Lubrication
Proc. Int. Symposium on Lubrication and Wear 1963
Pub. McCutchan Pub. Corp. 1965 pp 285-292

(94) DOWSON D.
Fluid film Lubrication (Section F5)
Tribology Handbook
Pub. in association with the Committee of Tribology of the Dept. of Trade and Industry 1973 Butterworths, London

(95) CLAYFIELD E.J. and CALVIN G.D.
Surface Chemistry in Lubrication and Wear
Proc. Instn. Mech. Eng. Vol. 183 Pt. 3P 1968-69 pp 150-163

(96) ELIN L.V.
Mutual Intrusion of the Surface Layers of Metal as one of the causes of wear during Imperfect Lubrication.
Friction and Wear in Machinery
Pub. A.S.M.E. Vol. 13 1961 pp 44-55

(97) FULLER D.D.
Theory and Practice of Lubrication for Engineers
Pub. John Wiley and Sons Inc. 1966

(98) RABINOWICZ E.
Friction and Wear of Materials
Pub. Wiley, New York 1965

(99) KAYE G.W.C. and LABY T.H.
Tables of Physical and Chemical Constants
Pub. Longmans 1962

(100) TIMOSHENKO S.P. and GOODIER J.N.
Theory of Elasticity (3rd Ed.)
McGraw - Hill Pub. Co. 1964

(101) GREENWOOD J.A. and WILLIAMSON J.B.P.
Contact of Nominally Flat Surfaces
Proc. of the Royal Society (London) Vol.295 1966 pp. 300-319

(102) ARCHARD J.F.
Single Contacts and Multiple Encounters
Journ. of Applied Physics Vol.32 1961 p. 1420

(103) MIKIC B.
Analytical Studies of Contact of Nominally Flat Surfaces;
Effect of Previous Loading
A.S.M.E. Journ. Lub. Tech. Vol.93 Pt.4 1971 pp.451-456

(104) AKHMATOV A.S.
Molecular Physics of Boundary Lubrication.
Israel Program for Scientific Translations 1966
Distributed by H.A.Humphrey Ltd. London

(105) BLAND D.R.
The Theory of Linear Viscoelasticity
Pergamon Press 1960

(106) MOORE D.F.
On the Decrease in Contact Area for Spheres and Cylinders
Rolling on a Viscoelastic Plane
Wear Vol. 21 1972 pp. 179-194

(107) GILMAN J.J.
Micromechanics of Flow of Solids
McGraw - Hill Book Co. 1969

(108) CHRISTENSEN H. and TONDER K.
The Hydrodynamic Lubrication of Rough Bearing Surfaces
of Finite Width
Trans. A.S.M.E. Journ. Lub. Tech. Vol.93 Pt.3 1971 pp 324-329

(109) GIBSON J.E.
Non-Linear Automatic Control
McGraw - Hill Book Co.
International Student Edition 1963

(110) SOLARTRON
TY.1451 System Analogue Computer
The Solartron Electronics Group Ltd.
Farnborough
Hampshire, England

(111) CHARLESWORTH A.S. and FLETCHER J.R.
Systematic Analogue Computer Programming
Pub. Pitman 1972

(112) JACKSON A.S.
Analog Computation
McGraw - Hill Book Co. 1960

(113) LEWIS E.E. and STERN H.
Design of Hydraulic Control Circuits
McGraw - Hill Book Co. 1962

(114) R.C.A.
Cos/Mos Integrated Circuits
Book SSD - 203C pp. 86-93

(115) SHCHEDROV V.
On Preliminary Displacement
Proc. Conf. Lub. and Wear I.Mech E. Paper 76 1957
pp 308-313